In situ Degradation of Trichloroethylene in Soil and Groundwater with Stabilized Zero Valent Iron Nanoparticles and Catalytic Hydrodechlorination with Supported Palladium Nanoparticles

by

Man Zhang

A dissertation submitted to the Graduate Faculty of
Auburn University
in partial fulfillment of the
requirements for the Degree of
Doctor of Philosophy

Auburn, Alabama
May 7, 2012

Keywords: Dechlorination, Zero valent iron, Nanoparticles, Palladium, In-situ remediation, Hydrodechlorination

Approved by

Dongye Zhao, Chair, Huff Professor of Civil Engineering
T. Prabhakar Clement, Professor of Civil Engineering
Ahjeong Son, Assistant Professor of Civil Engineering
Christopher B. Roberts, Professor of Chemical Engineering
German Mills, Associate Professor of Chemistry

Abstract

Chlorinated solvents, such as trichloroethylene (TCE), are potent carcinogens and have been found in soil and groundwater at thousands of National Priorities List sites in the U.S. To facilitate in-situ chlorinated solvents remediation, a new class of stabilized zero valent iron nanoparticles was prepared using carboxymethyl cellulose (CMC) as a stabilizer.

This study reported that CMC stabilized Fe-Pd nanoparticles could effectively degrade TCE sorbed on two model soils. Soil sorption can limit the rate and extent of the dechlorination reaction especially for organic matter-rich soils. Dissolved orgaic matter (DOM) can inhibit the degradation rate. Anionic surfactant SDS could aid in overcoming these limitations, however, its effectiveness would depend on soil type and dosage.

The transport behavior of CMC-stabilized ZVI was investigated. CMC-stabilized ZVI nanoparticles can be delivered into porous media even with 200 mg/L Ca^{2+}. The presence of 40~80 mg/L DOM as total organic carbon (TOC) had insignificant effect on breakthrough profiles of the nanoparticles, whereas metal oxides on sand grains (4.1 mg-Fe/g and 3.6 mg-Al/g) increased particle deposition by approximately 10%. A revised transport model was developed to simulate the breakthrough profiles and to evaluate the respective effects of adsorption and filtration on transport of ZVI nanoparticles.

A field test of the in-situ remediation technology was conducted at the Hill Air Force Base site in Utah. The results confirmed the soil deliverability and dechlorination

reactivity of CMC-stabilized Fe-Pd nanoparticles. The nanoparticles were able to be delivered at least five feet down-gradient of the injection well. Following the nanoparticles injection, rapid TCE degradation and elevated degradation products, such as ethane and ethene, were observed in the groundwater.

To facilitate application of nanoscale Pd catalysts for water treatment uses, we developed and characterized a new class of supported Pd catalyst by immobilizing CMC-stabilized Pd nanoparticles on three support materials (alumina, Ambersorb 572 and Titanium-Silicalite (TS-1)). The alumina-supported Pd nanoparticles could facilitate rapid and complete hydrodechlorination of TCE. The strong adsorption of TCE and carbon contamination on Ambersorb-572 resulted in much diminished activity. TS-1 could offer superior catalytic performance, suggesting that a support of modest hydrophobicity is in favor of TCE hydrodechlorination.

.

.

Acknowledgments

I would like to express my deepest gratitude to my advisor Dr. Dongye Zhao, the Elton Z. and Lois G. Huff Professor in the Department of Civil Engineering at Auburn University, for his guidance, patience and support in completion of the research and dissertation. He enlightened me with his immense knowledge and taught me the logical way of thinking. I gratefully acknowledge all the members of my committee, Dr. T. Prabhakar Clement, Dr. Ahjeong Son, Dr. Christopher B. Roberts and Dr. German Mills for their insightful comments and constructive advice throughout this work. Sincere appreciation is also extended to Dr. Yucheng Feng, who served as the outside reader. She helped me on the DLS analysis and soil mapping and has provided invaluable advice.

Best regards to all members of Dr. Zhao's research group for their friendship and help. I gratefully acknowledge Dr. Clifford Lange and Mr. Jinling Zhuang for their generous help on Gas Chromatograph analysis and analytical instrumentation in the lab. In addition, I wish to thank Dr. Deborah Bacik for her help with preparation and characterization of supported-Pd nanoparticle catalysts. The results are partially presented in Chapter 4. I deeply appreciate my friends for their care and belief in me.

Finally, and most importantly, I would like to thank my parents for their endless patience and encouragement to help me succeed in finishing all the research work. Their continuous love and support made this dissertation possible.

Table of Contents

List of Tables

List of Figures

CHAPTER 1 General Introduction

1.1 Chlorination solvents contamination in groundwater and soil

The widespread contamination of chlorinated solvents in the environment has become a significant concern of public health and environmental safety in the United States and other industrialized countries over the past 60 years (Bartsch et al., 1979; Lyne and McLachlan, 1949; McCarty, 1997). These chlorinated solvents were widely used in metal and plastic degreasing, fabric cleaning, chemical extraction and some other industries due to their high volatility and non-flammability (Fauvarque, 1996). However, these past massive usages and improper disposal /release of these chlorinated solvents have resulted in enormous contaminations of soil and groundwater (Jackson, 1998; Moran et al., 2007). Trichloroethylene (TCE) is one of the most commonly chlorinated contaminants found in the environment and was ranked at the 16th most commonly found contaminant on the priority list of hazardous substances in 2011 (Agency for toxic substances and Disease Registry, 2011b).

According to the US Environmental Protection Agency Toxic Release Inventory, in the year of 2008 total on-and off-site release of TCE was about 3.6 million pounds (U.S. EPA, 2008). In 2011, TCE was found at 291 National Priorities List sites and 405 ATSDR's (Agency for Toxic Substances and Disease Registry CEP (Completed Exposure Pathway) sites (Agency for toxic substances and Disease Registry, 2011a). TCE was found associated with strong acute health effect on central nervous system depression, cardiac arrhythmias and dermal problems (Dobrev et al., 2002; Page and

Arthur, 1978). The long-term exposure of TCE could also induce tumors in animals' kidney, liver, cervix, and lymphatic systems as a result of the production of highly reactive metabolite trichloroethylene epoxies during the metabolism of TCE. To reduce its potential health hazard, the United States Environmental Protection Agency (U.S. EPA) proposed a maximum contaminant level (MCL) of 5μg/L for TCE in drinking water (U.S. EPA, 2009).

TCE is often categorized as a dense non-aqueous phase liquid (DNAPL) contaminant due to its low aqueous solubility of 1100mg/L at 25°C and high liquid density of 1.464g/cm^3. Once released into the ground, it tends to migrate downward through the soil until it pools on top of sediments with low permeability, such as a layer of clay. A fraction of TCE is trapped and retained under the capillary forces during its transport in the soil pores (Jackson, 1998). The contaminant could spread with groundwater flows due to dissolution of the DNAPL plume and/or TCE vapors in the unsaturated zone. TCE could also be sorbed on the soil media, which may be on the same order or even greater than the dissolved mass (Mackay and Cherry, 1989). In general, the goal of TCE remediation in groundwater is to remove the whole organic mass, including TCE dissolved in water, sorbed in a soil matrix, trapped in the soil pores, as well as isolated as DNAPL pools because they all serve as long-term persistent contamination sources.

1.2 Current remediation methods for chlorinated solvent cleanup

1.2.1 Pump and Treat

Pump and treat is one of the most widely used technologies for groundwater remediation, which is designed to hydraulically prevent the contaminant migration and

remove the significant amount of the contaminant mass (Travis and Doty, 1990). Between 1982 and 1992, 73% of the remediation agreements at superfund sites were using the pump-and-treat technology for groundwater remediation (National Research Council, 1994). The pump and treat system is usually operated by extracting the contaminated groundwater from the subsurface and recharging clean water back into the subsurface. The injected water is normally taken from the uncontaminated aquifer nearby or the cleaned extracted water treated by traditional water and wastewater treatment technologies. Air stripping and granular activated carbon are the commonly used methods to remove the organic contaminants. Basically, the standard pump-treat system is using the water as the main carrier to remove the contaminants from the aquifer. The efficiency of this technology strongly relies on the physic-chemical properties of the contaminants of interest and the complex properties of the site (Voudrias, 2001).

In the past decades it has been found that the complete aquifer restoration by pump and treatment to the drinking water standards is essentially impossible, especially for the sites contaminated with DNAPLs (Mackay and Cherry, 1989; National Research Council, 1994; Travis and Doty, 1990; Voudrias, 2001). “Tailing” and “rebound” were often observed at pump and treat sites (Cohen et al., 1994). “Tailing” refers to the gradually slower rate of extracted contaminant concentration decrease over the long-term operation of a pump-and-treat system. Studies have indicated that although the initial reduction of the contaminant concentrations is rapid and significant, it is usually followed by a slow, steady reduction in removal rate in a long term (Mackay and Cherry, 1989; Nyer and Morello, 1993). “Rebound” means the dissolved contaminant concentration step back to a high level if the pumping process stops. The common explanations for the

tailing and rebound phenomenon are slow non-aqueous phase liquid dissolution, contaminant desorption from the soil media, precipitate dissolution for inorganic contaminants, groundwater velocity variation and diffusion of contaminant into the less permeable media (Cohen et al., 1994). Another reasons may include the groundwater table being lowered below the most contaminated zone during extraction or the contaminant concentration being diluted by the less contaminated groundwater drawn from the neighbor area (Nyer and Morello, 1993).

To improve the efficiency of this technology, some strategies have been explored such as periodically turning off the pump or slowing down the extraction flow rate to allow some slow mass-transfer processes to reach equilibrium. Some examples of the mass-transfer process include the NAPLs dissolution to the groundwater, diffusive transfer of contaminant in low-permeability zones and desorption of contaminants from the soil media (Harvey et al., 1994). Mackay et al. (2000) reported a field evaluation of the continuous vs pulsed pump-and-treat remediation in Dover, DE. Pulsed-pumping was more efficient than the continuous pumping, which is attributed to the enhanced diffusion of the contaminant from low-permeability zones.

1.2.2 Thermal treatment

Thermal remediation is designed to deliver the heat energy to the saturated and unsaturated contaminated subsurface by hot water/air injection, steam injection, thermal conductive heating, electrical resistive heating, electromagnetic heating and etc. (Davis, 1997). The increased subsurface temperature would significantly change the physic-chemical properties of the chlorinated solvents and, therefore, alter the distribution of organic contaminants between the solid, liquid and gas phase.

At an elevated temperature, the density of organic contaminants and its sorption onto solid phase could decrease, while its vapor pressure and molecular diffusion in the aqueous /gas phase increase. The viscosity of liquid could also decrease along with temperature, which in turn enhances the movement of the heated flow. All in all, these changes with temperature could help the mobilization of contaminants from the subsurface as well as the contaminant diffusion from the low permeable zone.

Steam injection is employed by injecting the hot steam to dissolve, vaporize and mobilize the contaminants and then collecting the mobilized contaminants using vapor or liquid extraction equipment in a recovery well for further aboveground treatment (Hunt et al., 1988). Compared to the hot air and hot water, the steam has larger heating capacity and would provide more heat input to the subsurface. Steam injection is more effective for contaminated zones of moderate or high permeability (U.S. EPA, 2004). Heron et al. (2000) conducted a field demonstration of steam stripping remediation of TCE in a DOE site in Ohio, and about 830lb of TCE was removed from the contaminated subsurface. In a low permeable soil layer, the high capillary pressures in small soil pores could result in a low evaporation rate of contaminants (Heron et al., 1998).

Electrical resistive heating provides the heat by applying the electrical current between electrodes installed underground. The volatilized contaminants are captured by the vapor extraction system. Hot steam is formed in saturated zones to mobilize the contaminants. In the unsaturated zones, organic contaminants vaporize as a result of an increase in Henry's constant. Compared to the steam injection, electrical resistive heating can be applied to the lower permeable zone and/or higher organic content zone where the affinity of chlorinated solvents is strong. Heron et al. (1998) reported that 99.8% of TCE

was removed in the silty soil after 37 days of heating by electrical currents in a 2-D laboratory tank. Newmark et al. (1999) applied the thermal remediation for two DNAPLs-contaminated sites using combined steam injection and electric current. In the LLNL gasoline spill site, more than 7600 gallons of trapped gasoline were removed in 21 weeks, and in the other Visalia pole yard site, 300,000 pounds of contaminants were removed or destroyed in six weeks.

Thermal conductive heating is designed to directly heat the subsurface soils using an array of direct vertical heater and vacuum wells, which could increase the subsurface temperature to 800 °C (Baston et al., 2010). It does not rely on steam or water as a carrier so that preferential flow and bypassing of low permeable area is not a limiting process. As the subsurface zone is heated, contaminants would be removed via evaporation, steam distillation, boiling, oxidation and pyrolysis (Baker and Heron, 2004).

Hydrothermal oxidation of contaminants would be facilitated after heat injection. Laboratory tests have shown at the temperature of 100~120 °C, TCE, PCE (tetrachloroethylene), TCA (trichloroethane) could be degraded to carbon dioxide, water, hydrogen ion and chloride ion in the presence of sufficient oxygen (Knauss et al., 2000). After thermal treatment, the reaction zone usually stays hot due to the large heat capacity of soils and further promotes the following chemical or biological degradation. Heron et al. (2000) observed that in a DOE site, following stream stripping, the concentration of carbon dioxide, which is the product of chemical oxidation of TCE, increased from 330 ppmv to 1400~2000 ppmv after injecting air. Newmark et al. (1999) also reported that in a Visalia Pole Yard site, about 800 lb/day of contaminants were degraded when air was

injected after the initial steam injection. About 18% of the total contaminants were removed via hydrous pyrolysis/oxidation.

1.2.3 Surfactant flushing

It is widely recognized that the pump-and-treat method is not very effective nor cost-efficient. It requires a very long time to meet the cleanup goals for NAPLs remediation (Mackay and Cherry, 1989). The kinetic limitation was attributed to low solubility in water, slow desorption of contaminants from the aquifer solids, slow diffusion from lower permeable layers and geological complexity of contaminated aquifers.

Using aqueous surfactant solutions has been proposed to enhance the efficiency of NAPLs removal. Surfactants are amphiphilic compounds with both hydrophobic and hydrophilic moieties. When the concentration increases, they could self-assemble into "micelles" in the aqueous phase, which have their hydrophobic tails sequestered in the center while orienting their hydrophilic heads outside. The concentration at which micelles are formed is called critical micellar concentration (cmc). The organic interior of micelles could serve as an organic sorbent to enhance the apparent solubility of organic contaminants in the aqueous phase. Experimental work has been carried out on the solubility behavior of hydrophobic organic contaminants in the presence of various surfactants (Li et al., 2007; Schaerlaekens et al., 2000). At a low concentration, the presence of surfactants could also mobilize the residual NAPLs in water by lowering the NAPL-water interfacial tension. However, the risk of migration of free-phase organic substances or expansion of the contaminant plumes to a less accessible area may exist (Fountain et al., 1991).

Surfactant flushing has been widely used to facilitate the removal of chlorinates solvents from the subsurface aquifer. Pennell et al. (1994) observed that 90% and 97% of the residual PCE could be removed from 20-30 and 40-120 mesh Ottawa sand, respectively, by injecting 4% polyoxyethylene sorbitan monooleate. Dwarakanath et al. (1999) demonstrated that up to 99.9% of the contaminants were removed by surfactant flushing from a Hill AFB field soil. Field demonstrations have also been performed. Knox et al. (1997) built vertical circulation wells for surfactant flushing in a site located in Michigan. By injecting 540 gallons of 3.6% Dowfax 8390 surfactant, the mass of PCE extracted increased by 40-fold. Childs and his coworkers (2006) reported that at a Dover National Test Site, about 65% of PCE was removed after applying 10 pore volumes of surfactant flooding and the residual PCE saturation decreased from 0.7% to 0.2%.

However, in order to design a successful flushing, surfactant sorption and precipitation should be taken into account because they decrease the active concentration of surfactants. Sorption of surfactants could also increase the organic carbon content of the soil and sequentially increase the sorption of hydrophobic contaminants (Ko et al., 1998). Usually the surfactant sorption on soils depends on the structure of surfactants and the properties of soils, such as soil organic matter, clay fraction content and clay mineralogy (Ozdemir et al., 2007; Rodriguez-Cruz et al., 2005).

To avoid the tendency of surfactant precipitation, mixed surfactants were proposed, rather than a single type of surfactant. Stellner and Scamehorn (1989) reported that the addition of nonionic surfactants and sodium chloride into solutions of anionic surfactant prevented their precipitation with calcium, which is commonly present in the soil matrix and groundwater. The mixture of anionic and nonionic surfactants can thereby

increase the apparent solubility of contaminants and enhance the contaminant desorption efficiency in the soil-water system. Yang et al. (2006) found that the mixed anionic surfactant SDBS and nonionic TX100 exhibited the highest contaminant desorption, as a result of the low sorption loss of surfactants to soil. Zhao et al. (2006) observed that the solubilization of TCE was enhanced by adding a mixture of nonionic TX100 and anionic SDBS surfactants, because of a decreased loss of TX100 to the DNAPL phase in presence of SDBS.

1.2.4 Bioremediation

Reductive biodegradation of TCE/PCE is an effective and promising remediation technology for chlorinated aliphatic contaminants. Considerable studies have demonstrated that under anaerobic conditions, TCE and PCE could be sequentially degraded to less chlorinated compounds such as three dichloroethylene isomers (DCE) and vinyl chloride (VC), or even to non-chlorinated products such as ethene and ethane (Gantzer and Wackett, 1991; MaymoGatell et al., 1997).

$$Cl_2C = CCl_2 \rightarrow ClHC = CCl_2 \rightarrow ClHC = CHCl \rightarrow H_2C = CHCl \rightarrow H_2C = CH_2 \qquad (1\text{-}1)$$

Generally, the efficiency of biodegradation of chloroethenes is dependent on the number of chlorine substitutes (Niven, 2006). The most chlorinated compounds undergo faster dechlorination processes than those less chlorinated molecules. Haston and McCarty (1999) investigated the maximum degradation rates for chloroethenes with different degrees of chlorination on an anaerobic mixed culture seeded with aquifer material from a PCE-contaminated site. It was found that at ambient room temperature the maximum dechlorination rate decreased from 77 μM/day for PCE to13 μM/day for VC with 38 mg/L of volatile suspended solids. Magnuson et al. (1998) observed that the

degradation rates of trans-DCE and VC were about 2 orders of magnitude lower than those of PCE and TCE in an anaerobic microbial enrichment culture. In this way, the slow dechlorination rates of DCE and VC result in an accumulation of these reduced intermediates, which are more toxic than their parent compounds.

The sequential degradation process could proceed in a cometabolic way. For example, the dechlorination of PCE and TCE by *methanogenic, homoacetogenic* and *sulfate-reducing* bacteria would be mediated by another organic material as the primary source of energy, such as methanol. Some biomolecules such as bacterial transition-metal coenzymes vitamin B_{12} (Co), coenzyme F_{430} (Ni) and hematin (Fe), could effectively catalyze the reductive biodegradation of PCE to small chlorinated compounds like VC or ethylene (Gantzer and Wackett, 1991).

Fathepure and Boyd (1988) investigated the biological dechlorination activity of *Methanosarcina sp. strain* DCM for PCE in a pure culture. They found that dechlorination of PCE to TCE was observed during the methanogenesis process and the dechlorination rate was strongly coupled with the rate of methane production. No dechlorination by strain DCM occurred in the presence of other carbon substrates such as acetate or methanol, implying that a cometabolic relationship existing between PCE and strain DCM.

PCE was observed being sequentially reduced to TCE and DCE, with the cell extracts of a sulfate-reducing bacterium, *Desulfomonile tiedjei* grown on pyruvate and 3-chlorobenzoate (Townsend and Suflita, 1996). The dechlorination rates of PCE and TCE were 0.396 and 0.004 nmol/min/g when using hydrogen as the electron donor and methyl

viologen as an electron carrier. The dechlorination of PCE in *D. tiedjei* was mediated by meta-halobenzoate which is a dehalogenase in *D. tiedjei* for 3-chlorobenzenes.

Rather than cometabolism, a number of bacteria have been found to make use of chlorinated solvents as terminal electron acceptors to obtain energy for cell growth. This process is called as chlororespiration or dehalorespiration.

Dehalobacter restrictus strain PER-K23 is the first reported dehalorespiration bacterium which is dependent on PCE/TCE as catabolic electron acceptors and hydrogen as electron donor (Holliger et al., 1993). This gram-negative anaerobic bacterium could derive energy from the reductive biodegradation of PCE to TCE and cis-1,2-DCE to support self-growth, but not from the degradation of DCE and VC, resulting in a final accumulation of even more toxic byproducts.

A gram-positive, curved rod-shaped *Desulfitobacterium frappieri* strain TCE1 was isolated from a PCE-dechlorinating mixed culture in a chemostat and was found to use PCE and TCE as electron acceptors for reductive dehalogenation to cis- and trans-DCE and lactate as the electron donor. The dechlorination rates were 118 ± 8.1 nmol/min/mg protein for PCE to TCE and 50 ± 7.9 nmol/min/mg protein for TCE to cis-DCE (Gerritse et al., 1999). Different from the *Dehalobacter restrictus* strain PER-K23, this microorganism could utilize a range of compounds as electron acceptors such as sulfite and thiosulfate, nitrate and fumarate.

Dehalococcoids microorganisms were found able to obtain growth energy through converting DCE to VC and ethene. He et al. (2003) reported anaerobic disc-shaped *Dehalococcoids* isolate BAV1 could destruct DCE and VC to ethene at a rate of 134.2 ± 10 nmol/min/mg protein in a pure culture and derive its growth energy strictly on

this reductive dechlorination of VC with hydrogen at ambient temperature. However, PCE and TCE could only be cometabolically utilized with the growth-supporting chloroethenes such as DCE or VC. Cupples et al. (2003) examined the growth of *Dehalococcoids* strain VS by the means of a PCR assay targeting 16S ribosomal DNA. The *Dehalococcoids* microorganism growth rate was clearly correlated to the dehalogenation of VC and cis-DCE, when using hydrogen as an electron donor, suggesting a catabolic reaction of VC reduction in D. strain VS. Later, Cupples et al. (2004) further found that *Dehalococcoids* strain VS could also grow on TCE as terminal electron acceptor, but not on PCE. However, not all of *Dehalococcoids* strains could use VC as a catabolic electron acceptor. Muller et al. (2004) suggested using the expression of vcrAB gene sequence to determine the existence of a VC dehalorespiratory bacterium.

Dehalococcoides ethenogenes strain 195 is the only pure culture reported so far that is capable of respiratory dechlorination of PCE completely to ethene with hydrogen as electron donor. However, this microorganism could only derive energy from PCE, TCE and cis-DCE for growth. Trans-DCE and VC can only be dechlorinated co-metabolically and slowly after the depletion of PCE. PCE could be metabolized by a culture of strain 195 at a rate of 40 μmol/h/L medium (Maymo-Gatell et al., 1999; MaymoGatell et al., 1997). Magnuson et al. (1998) successfully identified a 51-kDa PCE-reductive dehalogenase (PCE-RDase) and a 61-kDa TCE-RDase from *Dehalococcoides ethenogenes* 195. PCE-RDase could exclusively dechlorinate PCE and TCE-RDase is capable of catalyzing all of chlorinated compounds except PCE.

In natural systems, anaerobic dehalogenator must compete with other bacteria in the vicinity to access electron donors, such as nitrate-reducing bacteria, Fe(III)-reducing

bacteria, sulfate-reducing bacteria, methanogens and homoacetogens (Bradley, 2003). Sulfite was observed to strongly inhibit the PCE dechlorination (Gerritse et al., 1999). Successful field tests have been reported for in-situ reductive bioremediation of chlorinated solvents. De Bruin et al. (1992) established a fixed-bed column with a mixture of anaerobic Rhine River sediment and granular sludge for PCE removal at 20 °C. About 95% or 98% of PCE was degraded to ethane after 300-day of steady-state operations, only slight amount of TCE, cis-DCE and VC were observed. Major et al. (2002) added one natural dechlorinating microbial consortium containing *Dehalococcoides ethenogenes* into a site at Kelly Air Force Base to stimulate the reductive dechlorination of PCE. Methanol and acetate were amended to provide a carbon source. Within 200 days, the concentration of PCE was dropped below 5 μg/L from the original 1mg/L and the concentration of other dechlorination intermediates such as TCE or cis-DCE were also lower than 5 μg/L. Complete dechlorination of PCE to ethene occurred.

1.2.5 Chemical oxidation

In situ chemical oxidation remediation refers to injecting oxidants and other amendments into the contaminant subsurface to react and convert contaminants to less or non-toxic substances such as carbon dioxide, water and inorganic ions (Interstate Technology and Regulatory Cooperation, 2001). Compared to the traditional pump-and-treat technology, in situ chemical oxidation could completely degrade the contaminant without generating a large volume of waste for further treatment. It has drawn significant attention because of the fast destruction rate of chlorinated solvents as well as the low long-term cost of field monitoring and maintenance. However, the hazards associated

with these oxidants during transport/handling and vigorous unselected reactions are issues of concern (Interstate Technology and Regulatory Cooperation, 2001). The commonly used oxidants are hydrogen peroxide, permanganate, persulfate, ozone, and etc.

Hydrogen peroxide is an effective liquid oxidizing agent. It serves as an oxygen donor for direct oxidation of contaminants. It is also known to react with iron salts or iron oxides to produce hydroxyl radicals which are strong nonselective oxidizing species, often referred to Fenton's process (Ravikumar and Gurol, 1994). The iron catalyst could be either added as soluble iron such as Fe^{2+} or in the form of the natural iron minerals such as iron oxyhydroxide. Ravikumar and Guraol (Ravikumar and Gurol, 1994) observed that 50% of TCE were readily oxidized by 1.68 mmol of hydrogen peroxide in the sand column and the addition of iron sulfate could effectively lower the oxidant requirement by increasing the reaction efficiency. Laboratory and fields tests have shown the effectiveness of hydrogen peroxide with chlorinated solvents. Gates and Siegrist (1995) injected hydrogen peroxide into clay soils contaminated with TCE in bench-scale slurry tests and about 98% of TCE was removed with 28 g H_2O_2/kg soil. Not only for the TCE dissolved in water or sorbed on the soil, Yeh et al. (2003) also suggested that the mineral-catalyzed Fenton reaction would directly oxidize TCE in the non-aqueous liquid form. The oxidation of TCE DNAPLs would decrease the size of DNAPL plume and in turn enhanced the dissolution of TCE into the aqueous phase. However, the injection of hydrogen peroxide would be retarded by interference of subsurface impurities such as soil containing carbonate and bicarbonate. Soil organic matter would compete for the oxidant agents and thereby hinder the success of the oxidative treatment (Amarante,

2000; Watts et al., 1990). When applying hydrogen peroxide in the subsurface, a significant increase in soil temperature would be observed, which is undesirable because it may cause soil sterilization, reactants instability or even a chemical explosion (Mecozzi et al., 2006). Fenton's reagent is toxic for indigenous bacteria and not compatible with bioremediation (Imlay et al., 1988).

Permanganate has been used in water and wastewater treatment for taste and odor control, color removal, biological disinfection and et al. Both laboratory and field experiments showed that permanganate is an effective oxidant for chlorinated solvents such as PCE and TCE (Lee et al., 2003). It could attack the double bonds of TCE, which is first oxidized to a cyclic hypomanganate ester and then decomposed to carboxylic acids until oxidized to CO_2 (Yan and Schwartz, 2000). Yan and Schwartz (1999) observed complete dechlorination of ~ 0.1 mM TCE by 1 mM potassium permanganate in a batch test and suggested that the oxidative rate increased with a decreasing number of chlorine substitutes on the ethylene. Huang et al. (2002) observed in column tests that permanganate could completely oxidize TCE with about 100% chloride recovery, no matter when TCE is dissolved in the aqueous phase or stays as a separate organic phase. However, the formation of MnO_2 precipitates and CO_2 gas would decrease the permeability of porous media. The pore space of the aquifer medium was reduced by 20% after permanganate flushing. Lee et al. (2003) suggested that the efficiency of permanganate flushing would decline with time because of the formation of low permeability zones near the TCE source, leaving a large amount of permanganate solution unreacted. Permanganate is a metal-oxo reagent (Gardner and Mayer, 1995), not relying on the formation of hydroxyl radicals for oxidative reactions. Therefore, the

presence of well-known radical scavengers such as carbonate and bicarbonate would not interfere with the oxidative effectiveness of permanganate flushing (Amarante, 2000; Ma and Graham, 2000).

Ozone is another common oxidant extensively applied in water treatment processes. However, its effectiveness for oxidation decreases with increasing chlorine substitution of chloroethenes. The reaction rate constants for TCE and PCE are quite low as compared with those of less chlorinates contaminants such as vinyl chloride and dichloroethylene (Dowideit and von Sonntag, 1998) . Some advanced oxidation strategies, such as combining ozone with hydrogen peroxide or ultraviolet radiation, are reported to enhance generation of reactive free hydroxyl radicals (Glaze and Kang, 1988). Clancy et al. (1996) reported that the addition of hydrogen peroxide to the ozonation system would significantly enhance the overall treatment of PCE and TCE in groundwater from one IBM site. High energy input from UV radiation could promote the formation of hydroxyl radicals from ozone and hence increase the reaction rate for elimination of chlorinated solvents, especially at low pH (Peyton et al., 1982; Prengle, 1983). However, similar to hydrogen peroxide, the presence of hydroxyl radical scavengers such as inorganic carbon will retard the oxidative reaction (Sunder and Hempel, 1997).

Persulfate is one of the strongest oxidants with a high standard oxidation reduction potential (ORP) of 2.1 V, although its oxidative reactivity towards TCE is relatively low (Liang et al., 2007). Similar to hydroxyl radicals formed with the Fenton's reagent, persulfate would produce sulfate radicals which are also strong oxidizing species with a standard redox potential of 2.6 V (Block et al., 2004). The activation of persulfate

to form sulfate free radicals would require the application of heat, transition metal catalysts such as ferrous ion or UV radiation. Waldemer et al. (2007) investigated the destruction of chloroethenes with heat-activated persulfate and suggested that reactivity decreased with lower degree of chlorine substitution, which is opposite to the reactivity order with permanganate. Liang et al. (2008) found that the presence of ferrous ion would facilitate the degradation of TCE during persulfate flushing in column tests. It is very important to maintain an appropriate molar ratio of persulfate/ferrous ion/TCE because excessive ferrous ion would result in rapid cannibalization of persulfate. A rapid conversion of ferrous iron to ferric would also limit the decomposition of persulfate. Dahmani et al. (2006) also demonstrated that sodium persulfate would effectively degrade PCE, TCE and cis-DCE in a soil from a Roosevelt Mills site. However, the interaction between the field soil and the added ferrous catalyst could reduce the catalytic effect on persulfate decomposition.

Although numerous studies have shown the effectiveness of in situ chemical oxidation for chlorinated solvent destruction in groundwater aquifer, incomplete removal of DNAPLs may still exist due to the presence of soil organic matter, radical scavengers, soil heterogeneities and declined soil permeability due to precipitation of byproducts. Biological mediated dehalogenation coupled with in-situ chemical oxidation was proposed for advanced remediation. Buyuksonmez et al. (1999) reported that PCE could be transformed to a biodegradable byproduct dichloroacetic acid by Fenton's reagents and the utilization of microorganism Xanthobacter flavus following oxidative remediation would increase the PCE mineralization by 10%. Considering that the oxidizing environment of soils would impair the dechlorination reactivity of anaerobic

microorganisms, biostimulation is required to establish reducing conditions for microbial activity. Hrapovic et al. (2005) reported that without bioaugmentation, reductive biodechlorination of TCE to cis-DCE was observed 290 days after permanganate flushing in column tests.

1.2.6 Chemical reductive dechlorination

In situ chemical reductive dechlorination is designed to reductively transform the contaminants in groundwater and soil to less toxic or even nontoxic compounds by chemical amendments. Abiotic reductive dehalogenation of chlorinated solvents in anaerobic environment has received significant attention in past decades. It has been reported that sulfide, transition metal sulfides such as iron sulfide, ferrous iron-bearing minerals and zero valent iron could effectively transform chlorinated ethanes and ethenes primarily to non-chlorinated products.

Studies have shown that sulfide can facilitate the reductive dechlorination of chlorinated contaminants as electron donor (Wolfe and Macalady, 1992) or a nucleophile (Bouwer et al., 1981). Curtis and Reinhard (1994) reported that TCE would be degraded at a rate of 0.028 day^{-1} in the presence of 250 µM HS^- . The disappearance rate would increase by a factor of 9 by adding 25 mg/L of IHSS humic acid as carbon, where natural organic matter might serve as an electron transfer mediator for dechlorination process. The presence of mineral surfaces could also enhance the transformation rate of chlorinated solvents by dissolved sulfide. Kriegman-Klng and Reinhard (1992) observed that CCl_4 could be degraded by 1 mM HS^- with a reaction rate constant of 0.02 day^{-1} and the transformation rate constant further increased to 0.08 day^{-1} and 0.12 day^{-1} in the presence of vermiculite and biotite, respectively.

Iron sulfide minerals such as pyrite, troilite, mackinawite have shown to reductively destroy halogenated compounds such as trichloroethylene, tetrachloroethylene and pentachloroethane in anaerobic environment (Butler and Hayes, 1999; Butler and Hayes, 2000; Kriegman-King and Reinhard, 1994). Acetylene was the major reaction product reported for reductive transformation of TCE and PCE. A minor fraction of VC and cis-DCE were observed as reaction byproducts for TCE and PCE, respectively (Butler and Hayes, 1999). Increasing the pH is not desirable because it may result in a decrease in the reduction potential of reactive surface species. The oxidation state of iron sulfide in the environment would significantly influence the potential for reductive remediation (Butler and Hayes, 2001). A deactivation of the iron sulfide mineral for reductive dechlorination was noticed after a 3-day aging period at 76 °C.

Research has been conducted to investigate the activity of iron oxide minerals for abiotic reductive dechlorination. It has been reported that magnetite and green rust could transform chlorinated contaminants (Lee and Batchelor, 2002a; Lee and Batchelor, 2002b). Green Rust showed greater reactivity towards TCE than pyrite, with acetylene as the main transformation product. The reductive dechlorination was enhanced at higher pH, which may be attributed to more reactive deprotonated species available on the mineral surface. The reaction by magnetite alone was much slower than other reactive iron bearing minerals. However, addition of Fe(II) to magnetite suspensions enhanced the dechlorination rates by nearly a factor of 10, which is probably due to the formation of reactive surface precipitates or surface clusters.

Because of its availability at low cost and high effectiveness, zero valent iron (ZVI) has drawn great interest for abiotic reductive dechlorination remediation. It is

known that zero valent iron is a strong reducing agent, with a standard redox potential of -0.44 V when ZVI is oxidized to Fe^{2+}. If the resultant oxidized iron is in the form of Fe_3O_4, the corresponding standard redox potential will be -0.4987 V at the pH of 7, which is thermodynamically more favorable (Liu and Lowry, 2006). Extensive laboratory research in the past decades has demonstrated that zero-valent iron could transform various kinds of organic, inorganic contaminants and some heavy metals into less or non-toxic or immobile species. Gillham and O'Hannesin (1994) examined the dehalogenation ability of zero-valent iron as a source of electrons for 14 chlorinated methanes, ethanes and ethenes, such as tetrachloromethane (CT), trichloromethane (TCM) and hexachloroethane (HCA). Substantial degradation rates were observed with 100-mesh electrolytic iron for all chlorinated compounds except dichloromethane (DCM). Schreier and Reinhard (Schreier and Reinhard, 1994) studied the stepwise reductive dehalogenation of tetrachloroethylene (PCE) with 100-200 mesh iron powder and the half life of PCE was only 20 days when using 4.1 g/L iron. Field installation of ZVI as permeable reactive barriers (PRBs) has shown great potential for contaminant remediation (Powell et al., 1998). In 1995 one 36 ft×20 ft×4 ft reactive wall with granular iron was installed at an industrial site in Sunnyvale, California and the volatile organic compounds (VOCs) were effectively degraded to non-detectable levels. In the same year at a United State Coast Guard (USCG) site a full scale demonstration of a PRB was installed, about 2 ft thick, 24 ft deep and 150 ft deep. The concentrations of chlorinated compound were found to decrease to less than regulatory levels after installation, except for one port where the solvent concentrations were highest. However, the operation of this remedial technology depends significantly on the subsurface hydrogeology and

contaminant distribution, to make sure that contaminants could flow passively through the reactive zone of PRBs. The effectiveness of PRBs for contaminated soil is limited unless contaminants could be rapidly desorbed into groundwater and move through the PRBs for treatment. In addition, the loss of permeability of PRBs over a long-term period may occur due to clogging and fouling by the transformation products or colloidal materials.

1.2.7 Catalytic hydrodechlorination

Catalytic reductive dechlorination is one of the emerging technologies for treatment of chlorinated contaminants using noble metals as catalysts and hydrogen gas as an electron donor. The common metal catalysts are palladium, platinum, ruthenium, nickel, and others (Barrabés et al., 2010; Kim and Allen, 1997; Schreier and Reinhard, 1995). They could catalyze the substitution of chlorine from the carbon chains with hydrogen atoms and the saturation of double bonds under mild or ambient conditions. Activated carbon, silica, aluminum are widely used as the support in metal catalysis (Marques et al., 1993).

Noble metal catalysts are effective for the destruction of chlorinated organic carbons at ambient conditions. Lowry and Reinhard (1999) suggested that palladium could effectively promote the rapid hydrodechlorination of nine small chlorinated organic carbons with little or no production of toxic chlorinated intermediates. Trichloroethylene would be converted directly to ethane without the formation of any detectable chlorinated intermediates such as vinyl chloride and dichloroethylene. The catalytic destruction of chlorinated aromatics and chlorinated olefins using hydrogen gas are also effective (Kim and Allen, 1997; Schuth and Reinhard, 1998).

Introduction of another metal to the monometallic catalyst to build a bimetallic system can improve the hydrodechlorination reactivity or selectivity due to electronic effects, geometric effects, the presence of mixed active sites, etc. (Coq and Figueras, 2001). The concurrent or subsequent addition of Yb to Pd enhanced the hydrogen uptake of the silica-supported catalyst due to the formation of YbH_2 and effectively increased the reactivity towards chlorobenzene (Jujjuri et al., 2006). Similarly, Nutt et al. (Nutt et al., 2005) reported that Pd doping of Au nanoparticles can improve more than 34 times the dechlorination activity for TCE as compared with that of monometallic Pd nanoparticles, especially for Au nanoparticles partially covered by Pd metal.

A field catalytic degradation of chlorinated hydrocarbon using a commercial Pd/Alumina catalyst was reported at a superfund site (McNab et al., 2000). The contaminated groundwater was extracted, mixed with hydrogen gas and then flowed through two fixed-bed Pd catalyst columns for reaction before the water discharged back to an adjacent water-bearing zone. The effluent TCE was reduced to less than 5 µg/L, as compared to an initial concentration of 3612 µg/L in the influent. Less-chlorinated byproducts were not observed, expect for trace levels of cis-1,2 DCE in the influent. However, under field conditions, catalyst deactivation is possible due to sulfur fouling and biological fouling such as growth of sulfate-reducing bacteria (Schuth et al., 2004). Potential competition for hydrogen gas from other electron acceptors such as nitrate could also decrease the dechlorination rate (Ilinitch et al., 2000). For in-situ application of catalytic hydrodechlorination technology, the cost of the noble metal catalysts should be considered. The Pd/Al_2O_3 used by McNab et al. (2000) was $270/kg. Therefore, the regeneration and stability of the catalyst is of vital importance.

1.2.8 Nanoscale zero valent iron nanoparticles

With the development of nanotechnology, ZVI nanoparticles have drawn increasing attention among environmental researchers for chlorinated solvent remediation. Its nanoscale size (1-100 nm) leads to a high specific surface area and provides more available surface sites for reductive reactions. Studies have shown that increasing the clean surface area of iron would greatly improve the dehalogenation rate (Matheson and Tratnyek, 1994). Compared with the fixed Permeable Reactive Barriers, nanoparticles could be delivered by pumping or gravity feeding directly to the targeted contaminated area and diffuse with the groundwater flow. ZVI nanoparticles are not only applied in groundwater and soil treatment in the form of a slurry, but they are also suitable for ex situ applications on surface water and wastewater treatment after immobilization, for example, on ionic exchange resins (Ponder et al., 2000).

However, these bare ZVI nanoparticles tend to agglomerate rapidly into larger flocs due to the attractive van der Waals and magnetic attractive forces. These ZVI aggregates barely migrate through the soil matrix or even sand columns and lose their mobility in the aquifer (Saleh et al., 2007). Surface modification with certain polysaccharides or polyelectrolytes has been successfully explored to prepare physically stable but chemical reactive ZVI nanoparticles, by introducing repulsive electrostatic or steric interaction among particles. It was found that starch-stabilized and CMC-stabilized nanoparticles are able to degrade TCE 3 times and 17 times faster than their non-stabilized counterparts (He and Zhao, 2005; He et al., 2007). Laboratory and field studies have confirmed the great deliverability and strong dechlorination reactivity of CMC-

stabilized iron nanoparticles in groundwater and sediments (Bennett et al., 2010; He et al., 2009b; He et al., 2010).

1.3 Research Objective

The overall goal of this research is to investigate the fate and transport of CMC-stabilized ZVI nanoparticles in the subsurface aquifer under both laboratory and field conditions and examine the catalytic hydrodechlorination of chlorinated solvents using CMC-stabilized novel metal nanoparticles. The specific objectives include:

- Investigate the effect of soil sorption on the dechlorination extent and reaction rate of CMC-stabilized Fe-Pd nanoparticles with two representative soils and TCE as a model contaminant. Different types of surfactants will be used to test their effects on TCE desorption and degradation rates.
- Examine the effect of different stabilizers, particle concentration and solution chemistry such as ionic strength, organic matter concentrations as well as metal oxides on transport of CMC-stabilized ZVI nanoparticles in porous media.
- Demonstrate the performance of CMC-stabilized ZVI nanoparticles for field remediation of chlorinated solvents in soil and groundwater.
- Characterize the catalytic capacity of CMC-stabilized Palladium nanoparticles loaded on support materials.
- Evaluate the reactivity of various metal nanoparticles to both vinyl polyhalides and alkyl polyhalides.

CHAPTER 2. Degradation of Soil-sorbed Trichloroethylene by Stabilized Zero Valent Iron Nanoparticles: Effects of Sorption, Surfactants, and Natural Organic Matter

2.1 Introduction

Over the past six decades or so, groundwater contamination of chlorinated solvents, such as trichloroethylene (TCE) and tetrachloroethylene (PCE), has been a major concern to public health and environmental safety (Bartsch et al., 1979; Lyne and McLachlan, 1949; Wu and Schaum, 2000). The past extensive uses and discharges of chlorinated hydrocarbons left a catastrophic legacy of widespread groundwater contamination in the U.S. as well as other major industrialized nations (Moran et al., 2007). From 2003 to 2011, trichloroethylene kept being ranked at the 16th most commonly found contaminant on the priority list of hazardous substances (Agency for toxic substances and Disease Registry, 2011b). By 2007, trichloroethylene was found at 301 of the 1689 National Priorities List sites and 391 of the 1444 ATSDR's (Agency for Toxic Substances and Disease Registry) CEP (Completed Exposure Pathway) sites(Agency for toxic substances and Disease Registry, 2007).

Chlorinated hydrocarbons including TCE are often categorized as dense non-aqueous phase liquid (DNAPL) for their low aqueous solubility and greater density than water. Once released into the subsurface environment, TCE will distribute between soil and water. Because of its low solubility and high adsorbability to soil organic matter (SOM), a large fraction of TCE tends to be retained in the solid phase. Yet, soil-sorbed

TCE can be slowly released back into groundwater (Burris et al., 1995; Mohammad and Kibbey, 2005). It is well known that soil sorption can inhibit or limit natural attenuation or bioavailability of TCE, rendering TCE a long-term threat to the environment and human health.

In situ dechlorination in the subsurface through injection of Zero Valent Iron (ZVI) nanoparticles is an innovative technology. Since it was first proposed by Wang and Zhang (1997), it has attracted extensive interests from academia, industries, and government agencies. Extensive bench-scale and pilot-scale studies have been carried out to demonstrate the technical effectiveness of this technology. For instance, ZVI particles have been found effective for rapid degradation of chlorinated solvents such as chlorinated methanes, ethanes and ethenes, chlorinated aromatic compounds, and pesticides that are dissolved in water (Arnold and Roberts, 2000; Joo and Zhao, 2008; Lien and Zhang, 2005; Lowry and Johnson, 2004; Matheson and Tratnyek, 1994; Schrick et al., 2002). Researchers also noticed that such abiotic reductive dechlorination processes could be greatly enhanced in the presence of trace amounts (typically 1% of ZVI) of a metal catalyst such as Pd (He and Zhao, 2005; Wang and Zhang, 1997).

To facilitate soil mobility of ZVI particles, various particle stabilization techniques have been reported (He and Zhao, 2005; Ponder et al., 2001; Ponder et al., 2000; Saleh et al., 2007; Schrick et al., 2002). These supports serve as dispersants and prevent iron particles from agglomeration through electrosteric interactions. Phenrat et al. (2008) reported that coatings of poly(styrene sulfonate) and polyaspartate would improve the transportability of ZVI particles. Zhan et al. (2009) presented a class of multifunctional colloidal particles by embedding carboxymethyl cellulose stabilized

bimetallic Fe-Pd nanoparticles in hydrophobic carbon microspheres. The presence of carbon microspheres was intended to enhance TCE removal from the aqueous phase via enhanced surface accumulation.

In recent years, Zhao and co-workers have developed and extensively studied a class of soil-injectable ZVI nanoparticles that were prepared using low-cost and "green" water soluble starches and celluloses. These resultant stabilized nanoparticles also displayed greater dechlorination reactivity compared to their non-stabilized ZVI counterparts. He and Zhao reported that starch-stabilized and CMC-stabilized ZVI nanoparticles were not only mobile in various porous media, but could degrade TCE 3 times and 17 times faster than non-stabilized counterparts, respectively (He et al., 2009b; He and Zhao, 2005; He et al., 2007). While non-stabilized ZVI nanoparticles could barely flow through saturated sand columns, CMC-stabilized ZVI have shown tremendously-enhanced mobility and might travel over 146 m under a flow rate of 61 m/day (He et al., 2009b; He et al., 2007; Schrick et al., 2004). A number of field tests have been reported to demonstrate the effectiveness of the in situ injection of ZVI nanoparticles. Elliott and Zhang (2001) reported that Fe-Pd nanoparticles of 100-200 nm were able to remove TCE by 1.5% to 96.5% at a contaminated site. Quinn et al. (2005) reported that injection of ZVI particles emulsified with a nonionic surfactant sorbitan trioleate at a NASA site decreased TCE concentrations in soil by 87%-99.5% in four of the 6 sampling borings in 90 days, and TCE concentration in groundwater was lowered by 57-100% at all depths in 5 months. He et al. (2010) successfully injected 0.2 g/L of CMC-stabilized Fe-Pd nanoparticles (CMC = 0.1 wt%, Pd/Fe = 0.1 wt%) into a secondary source zone of PCBs and chlorinated ethenes (TCE and PCE). They observed effective dechlorination within

two weeks, followed by a long-term (nearly two years) biotic dechlorination, which was boosted by the injected nanoparticles. However, due to the complexity of the subsurface environment, these pilot-tests have been largely limited to a "black-box" approach, i.e. the effectiveness has been quantified based on samples from limited monitoring wells without knowledge of detailed transport, distribution and reaction processes of the nanoparticles.

Although sorption/desorption and diffusion are known to limit the physical and biological availabilities of contaminants in porous media, the role of soil sorption on the degradation effectiveness of ZVI nanoparticles remains unknown. While numerous studies have revealed the effectiveness of ZVI nanoparticles for degradation of chlorinated hydrocarbons such as TCE and PCE in homogeneous systems, little is known on the effectiveness for degrading soil-sorbed contaminants. In addition, while dissolved natural organic matter (NOM) is known to interact with ZVI particles (Giasuddin et al., 2007; Tratnyek et al., 2001), the effect of dissolved NOM on the nanoparticle stability and dechlorination effectiveness remains unknown. In fact, lacking this critical information has often rendered results from various field tests inconclusive.

Surfactant-enhanced desorption have been widely studied for enhanced dissolution and removal of soil-sorbed hydrophobic contaminants in aquifers (Mayer et al., 2007; Park and Bielefeldt, 2005; West and Harwell, 1992). Due to their amphiphilic nature, surfactants are known to enhance the solubilization and mobilization of soil-sorbed contaminants. A cationic surfactant, HDTMA, was observed to enhance chlorinated solvent degradation with micro-sized ZVI powders at concentrations under its critical micelle concentration (cmc) due to increased TCE adsorption on ZVI

nanoparticles (Shin et al., 2008). Note that in this work, lower case cmc refers to critical micelle concentration and upper case CMC to carboxymethyl cellulose. When the surfactant concentrations are above the cmc value, soil sorption of TCE decreased as a result of competitive TCE partitioning into the surfactant micelles (Ayoub et al., 2008; Loraine, 2001). Li et al. (2006b) reported that amending granular ZVI particles with 2.5 mM HDTMA solution decreased TCE reduction by a factor of 2~3, and they attributed the inhibitive effect to the blockage of atomic hydrogen release from the surface of the ZVI particles. While various stabilizers (e.g. polyelectrolytes or polysaccharides) have been employed to enhance mobility and physical stability of ZVI nanoparticles, the combined effect of surfactants and these stabilizers is unknown. Also, while most of the reported studies have focused on dechlorination in the aqueous phase, information has been lacking pertaining to effect of surfactants on ZVI's degradation of soil-sorbed TCE.

This research aimed at investigating the effect of soil sorption on the effectiveness of CMC-stabilized ZVI nanoparticles and explore ways to overcome the sorption effect. The specific objectives were to: 1) investigate effect of soil sorption on the dechlorination extent and rate of CMC-stabilized Fe-Pd nanoparticles with two representative soils and using TCE as a model contaminant; 2) examine effect of water-soluble NOM on the reactivity of the nanoparticles; and 3) test the effectiveness of various surfactants for enhanced degradation of soil-sorbed TCE.

2.2 Materials and methods

2.2.1 Chemicals

The following chemicals (analytical grade or higher) were used as received: ferrous sulfate heptahydrate ($FeSO_4 \cdot 7H_2O$, Acros Organics, Morris Plains, NJ, USA), sodium carboxymethyl cellulose (NaCMC or CMC, M.W. = 90,000, Acros Organics), sodium borohydride ($NaBH_4$, ICN Biomedicals, Aurora, OH, USA); sodium tetrachloropalladate(II) trihydrate ($Na_2PdCl_4 \cdot 3H_2O$, 99%, Strem Chemicals, New Buryport, MA, USA), sodium azide (NaN_3, Fisher, Fairlawn, NJ, USA), hydrochloric acid (Fisher), methanol (Fisher), hexane (Fisher) and photometric grade trichloroethylene (Aldrich Chemical, Milwaukee, WI, USA).

Four commercially available surfactants were tested for their effects on desorption and degradation of soil-sorbed TCE, including two anionic surfactants known as sodium dodecyl sulfate (SDS) with a purity of > 98.5% (Sigma-Aldrich, St. Louis, MO, USA) and sodium dodecyl benzene sulfonate (SDBS) with a purity of > 88% (Acros Organics), a nonionic surfactant Polyoxyethylene (20) sorbitan monooleate (Tween80) (Aldrich) and a cationic surfactant hexadecyltrimethylammonium bromide (HDTMA) with a purity of ~99% (Sigma). **Table 2-1** provides selected properties of these surfactants. Two soils were tested in this study. A potting soil (HYPONEX®, OH, USA) purchased from a local Wal-Mart store (Auburn, AL, USA) was used to represent soils of relatively high organic content, whereas a top (0.5 m) loam soil obtained from a local farm (Smith Farm, Auburn, AL, USA) was used to represent soils lean of organic matter. Before use, the soils were sieved through a standard sieve of 2 mm openings, and washed with tap water to remove fine colloids and water-soluble materials. The washed soils can be completely separated from water through centrifugation at 400 g-force. Finally the soils were air-dried at room temperature and stored for use. Soil testing was performed by the Soil

Testing Laboratory at Auburn University. The soil textural analysis was conducted with sieve analysis and following the bouyoucos hydrometer method. The soil pH was measured via the Reference Soil Test Methods for the Southern Region of the United States: Southern Cooperative Series Bulletin 289 (1983). The total organic carbon and sulfur were analyzed with an Elementar Vario Macro CNS Analyzer (Elementar, Hanau, Germany) at 140 °C. The soil minerals were analyzed by Inductively Coupled Plasma Emission Spectroscopy (Varian Vista-MPX Axial Spectrometer, Varian, Walnut Creek, CA, USA) after acid digestion following EPA method 3230. Soil potassium, calcium, magnesium and sodium were determined by a Varian Vista-MPX Radial Spectrometer following Melich I extraction. The pH at point of zero charge (PZC) of the soil was determined following the potentiometric titration method (Marcano-Martinez and McBride, 1989). **Table 2-2** gives salient physical and chemical properties of the soils.

Table 2- 1. Selected properties of surfactants used

Surfactants	Ionic property	Molecular formula	Critical micellar concentration (cmc), mM	Molecular structure
Sodium dodecyl sulfate (SDS)	Anionic	$NaC_{12}H_{25}SO_4$	8.2 (Fillipi et al., 1999)	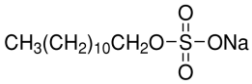
Sodium dodecylbenzene sulfonate (SDBS)	Anionic	$C_{12}H_{25}C_6H_4SO_3Na$	1.5 (Zhang et al., 2006)	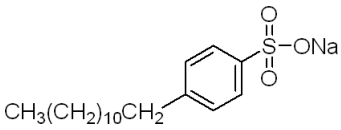
Polyoxyethylene (20) sorbitan monooleate (Tween 80)	Neutral	$C_{64}H_{124}O_{26}$	0.012 (Yeom et al., 1995)	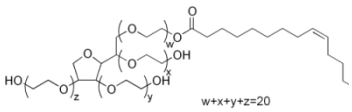
Hexadecyltrimethyl ammonium bromide (HDTMA)	Cationic	$C_{16}H_{33}N(Br)(CH_3)_3$	0.9 (Karapanagioti et al., 2005; Li, 2004)	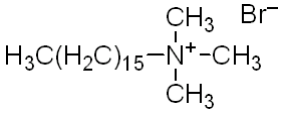

.

Table 2- 2. Physicochemical characteristics of potting soil and Smith Farm soil

Sample	Taxonomy	pH	H_2O	OM,%	S,%	CEC* Meq/100g
potting soil	Sandy loam	6.65	0.11	8.2	0.025	10.3
Smith farm soil	loam	6.60	0.14	0.7	0.022	1.4

Sample	Ca ppm	K ppm	Mg ppm	P ppm	Al ppm	B ppm	Cu ppm	Fe ppm	Mn ppm	N ppm	Zn ppm
potting soil	1834	153	365	42	77	0.4	11	95	62	81	19
Smith farm soil	172	17	49	3	34	<0.1	24	43	9	58	10

*CEC: Cation exchange capacity.

2.2.2 TCE sorption tests

TCE sorption to the two soils was tested through batch isotherm tests. A series of TCE solutions at concentrations of 50, 100, 200, 300, 500 and 600 mg/L, respectively, were prepared by adding a known mass of TCE, delivered in a small volume of methanol, into DI water. Total methanol content in the final solution was below 0.02% (v/v). To inhibit any possible biological activities during the sorption tests, 0.2 g/L of NaN_3 was included in the solutions. Sorption tests were then initiated by adding 12 g of each of the soils into ~63 mL of the respective TCE solution in 67 mL screw-capped glass vials sealed with PTFE-lined septa. The samples had virtually no head space to avoid volatilization loss of TCE, and the mixtures were mixed on a rotating shaker placed in an incubator at 21±1 °C. Based on separate sorption kinetic tests, the mixtures were equilibrated for 1 week for the potting soil and 2 weeks for the Smith Farm soil to ensure that equilibrium was established. Upon equilibration, the vials were centrifuged with a Fisher Marathon 21K/R Centrifuge (Fisher Scientific) at 400 g-force for 10min. Then, 100 mL of the supernatant was withdrawn using a 100 mL gastight glass-syringe and transferred to 1 mL of hexane in a 2 mL GC vial. Upon phase separation, TCE in hexane was analyzed using an HP 6890 GC (Hewlett Packard, Palo Alto, CA) equipped with an electron capture detector (ECD) following the method by He and Zhao (2005).

2.2.3 Effects of surfactants on TCE desorption

To examine the physical availability of soil-sorbed TCE, desorption kinetic tests were carried out with the same batch reactors and the soils that were pre-equilibrated as in the isothermal tests. Upon centrifuging, about 93% of the supernatant was pipetted out and replaced with soil amended water, which was prepared by mixing DI water and a

TCE-free soil at the same soil-to-water ratio as in the sorption tests. The amendment ensures that the background compositions (e.g. soil extrudates) during sorption and desorption remain identical. Again, 0.2 g/L of NaN_3 was maintained to minimize biological activity. The vials were resealed and mixed on the rotator at 21 ± 1°C. At selected timed intervals, the suspension was centrifuged and the supernatant was extracted with hexane and analyzed with GC-ECD following the same method as described before. The amount desorbed from the soils was obtained via mass balance calculations.

2.2.4 Effects of surfactants on TCE degradation in water

CMC-stabilized ZVI nanoparticles were prepared at 0.1 g/L as Fe following the approach of aqueous phase reduction with borohydride as described in our previous study (He and Zhao, 2007). Trace amounts (0.1% or 0.3 wt% of Fe) of Pd catalyst were added to the fresh ZVI particles by adding a known amount of Na_2PdCl_4 into the nanoparticle suspension. The addition of Pd was able to greatly enhance the dechlorination rate of TCE (He and Zhao, 2005).

Batch degradation tests were carried out using 43 mL amber glass vials with open-top screw caps and PTFE-lined septa. To test the effects of each surfactant, 1 mL of a surfactant stock solution was added into the Fe-Pd nanoparticle suspension to yield a desired concentration level. TCE degradation was then initiated by injecting 25 μL of a TCE stock solution, resulting in an initial TCE concentration of 10 mg/L for all cases. The mixture was then mixed using a rotary shaker (50 rpm) at room temperature. At selected time intervals, 100 μL of aqueous samples were taken, extracted with hexane, and analyzed via GC-ECD for TCE. Parallel control experiments were conducted with a

0.16% CMC solution but without the nanoparticles. Mass balance analyses of TCE in the control tests indicated that the mass loss was < 4% in all cases.

2.2.5 Effects of surfactants on soil-sorbed TCE

The same procedure was followed to pre-load TCE to the soils as in the sorption isotherm tests, except that no NaN_3 was added. Based on our separate experimental results (data not shown), the presence of NaN_3 inhibited the ZVI's reducing action, and there was no significant biological degradation of TCE during the loading. The equilibration time was 1 week for the potting soil and 2 weeks for the Smith Farm soil. Based on the TCE desorption and solution-phase TCE degradation tests, SDS displayed the greatest ability to enhance both TCE desorption and TCE degradation. Consequently, SDS was investigated further for its effect on the degradation of soil-sorbed TCE.

First, a stock suspension of Fe-Pd nanoparticles (1.0 g/L as Fe, Pd = 0.1% of Fe) was prepared with 0.8 wt% NaCMC. The suspension was diluted with nitrogen-purged DI water and/or nitrogen-purged SDS solution. The resultant nanoparticle concentration was 0.3 g/L as Fe. The tests were carried out at two levels of SDS, i.e. 1 and 5 times the cmc value. The degradation tests were then initiated by replacing 93% (58 mL) of the supernatant in each of the 62.5 mL soil suspensions with the same volume of the nanoparticle suspension. Thus, the final SDS concentration in the mixtures was 0.93 and 4.64 times the cmc value, respectively. For comparison, the degradation tests were also conducted in the absence of SDS. The mixtures were mixed using a rotary shaker at 21 ± 1°C. At selected time intervals, duplicated vials were centrifuged to separate soil and water, and TCE in the supernatant was extracted using hexane and analyzed via the GC-ECD method. To facilitate mass balance calculations, the TCE remaining in the soil was

extracted using 50 mL of methanol in a hot water bath for 48 hours at 70°C twice consecutively. Control tests were carried out in parallel in the absence of the nanoparticles, which indicated that the TCE mass balance was within 88-110%.

2.2.6 Effect of dissolved organic matter (DOM) on TCE degradation

To study effect of DOM on TCE degradation, batch kinetic tests were carried out in the 43 mL glass vials with a soil-amended background solution. The background solution was prepared by mixing 36 g of the potting soil with 63 mL of DI water for 3 days, and then collecting the supernatant upon centrifuging. The total organic carbon (TOC) in the resultant soil-amended solution was 860 mg/L (the TOC value for soil-amended solution with a soil-to-DI water ratio of 12 g: 63 mL was 42 mg/L). Then, 28.7 mL of 0.45 g/L CMC-ZVI nanoparticle suspension was mixed with a nitrogen-purged mixture of the background solution and distilled water in a 43 mL glass vial, which resulted in a total Fe concentration of 0.3 g/L and a TOC concentration of 40 mg/L and 350 mg/L, respectively. The reaction was then initiated by injecting a TCE stock solution into the mixtures, which resulted in an initial TCE concentration of ~100 mg/L. Control tests were conducted in the absence of soil supernatant but under otherwise identical conditions. At selected time intervals, samples (100 µL each) were taken from the vials and analyzed for remaining TCE.

2.2.7 Sorption of CMC-stabilized ZVI nanoparticles to soils

Batch tests were performed to examine the sorption behavior of the stabilized ZVI nanoparticles on the two soils. To be consistent with the procedures in the TCE degradation tests, 12 g of a soil was first mixed with 63 mL DI water and aged for 1 week for the potting soil and 2 weeks for the Smith Farm soil. Subsequently, the nanoparticle

sorption was initiated by replacing 93% of the supernatant in each vial with the same volume of the Fe-Pd nanoparticle suspension (Fe=0.3 g/L). The vials were placed on a rotator placed in an incubator at 21±1°C. Adsorption of ZVI from the aqueous phase to the soils was followed in duplicate for up to 70 hours. At selected time intervals, duplicate vials were centrifuged at 400 g -force for 10 min. Centrifugation was able to remove soil and soil-sorbed nanoparticles, but not free nanoparticles. Then, 1 mL of the supernatant was taken and digested with 4 mL of 12 M HCl to dissolve the suspended nanoparticles. The samples were then analyzed using a flame atomic-absorption spectrophotometer (AAS) (220FS, Varian, Palo Alto, CA). The ZVI nanoparticles remaining in the solid phase was quantified based on the total dissolved Fe concentration.

2.3 Results and discussion

2.3.1 TCE sorption and desorption

Figure 2-1 shows TCE sorption isotherms for the two soils. The classical Langmuir model (Eq. 2-1) was able to adequately interpret the non-linear isotherm data,

$$q = \frac{bQC}{1+bC} \tag{2-1}$$

where q is the equilibrium uptake of TCE in soil (mg/g); C is TCE concentration in the aqueous phase (mg/L); Q is the Langmuir maximum capacity (mg/g); and b is the Langmuir affinity constant (L/mg).

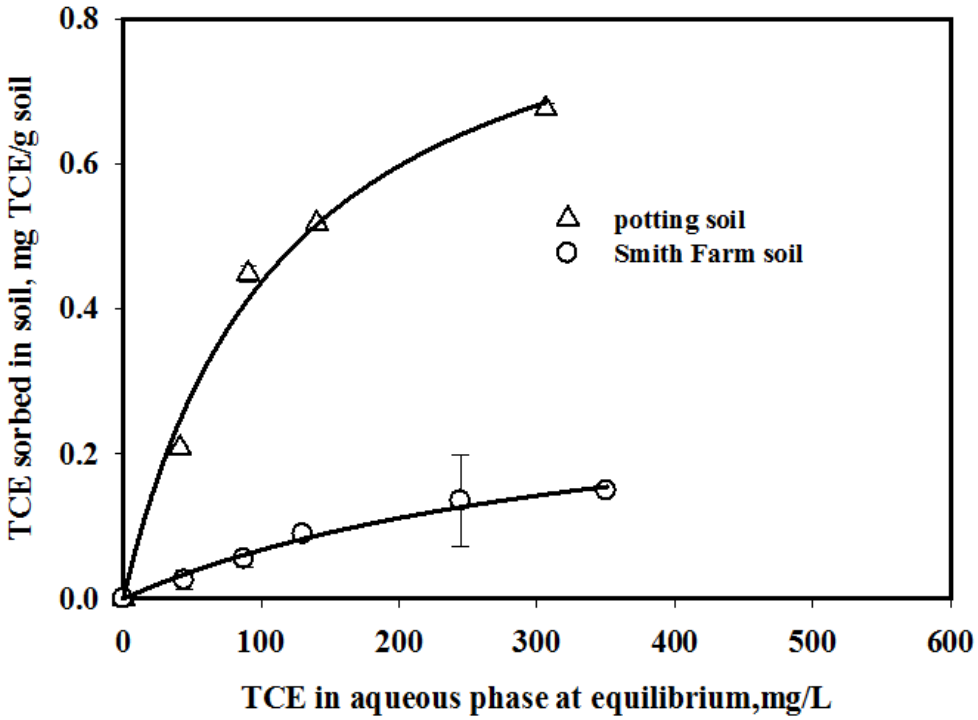

Figure 2- 1 Experimental (symbols) and Langmuir model fitted (lines) TCE sorption isotherms for a commercial potting soil (sandy loam) and a Smith Farm soil (loam). Data plotted as mean of duplicates, error bars indicate deviation from the mean.

As shown in **Table 2-1**, the SOM content for the potting soil was 8.2%, as compared to only 0.7% for the Smith Farm soil. Soil organic matter has been well known to be the primary sink for hydrophobic organic contaminants (Chiou et al., 1979; Ong and Lion, 1991; Zhao et al., 2001). As expected, the potting soil offered a much higher sorption capacity and affinity with a Langmuir Q value of 0.94 mg/g and b of 0.0080 L/mg, as compared to 0.32 mg/g and 0.0027 L/mg, respectively, for the Smith Farm soil.

Figure 2-2 shows desorption kinetic data of TCE in DI water in the presence of 0.2 g/L NaN_3. The TCE mass remaining in the soils was normalized to the mass of TCE initially loaded in the soils. Both soils displayed a rapid initial (< 3 h) desorption rate followed by a slow release over the test period of 120 h. The observed desorption profile agrees with the commonly known biphasic process: rapid desorption from the easily-accessible sites followed by slow desorption associated with slow diffusion in the SOM and in the micropores (Pavlostathis and Mathavan, 1992; Pignatello and Xing, 1996; Sahoo and Smith, 1997). However, the extent of equilibrium desorption differed substantially for the two soils. Approximately 78% of TCE was desorbed in the first 24 h for the Smith Farm soil, compared to 13% for the potting soil.

2.3.2 Degradation of soil-sorbed TCE and effect of DOM

Figure 2-3 compares degradation kinetic data of TCE that was pre-sorbed in the two soils and TCE dissolved in water solution. In the homogeneous system (i.e. in the absence of soil), complete TCE degradation was observed within 4 h. The degradation data can be interpreted using the pseudo-first-order reaction kinetics (He et al., 2007; Liu et al., 2007), and the reaction rate constant was determined to be 1.64 s^{-1}. In contrast, only 44% of TCE sorbed in the potting soil was degraded in 30 h and ~82% in the Smith Farm

soil was degraded in 27 h. It is evident from **Figure 2-3** that the degradation rate and extent were severely suppressed by soil sorption, especially for the soil of higher SOM content. Comparing the desorption (**Figure 2-2**) and degradation data (**Figure 2-3**) reveals that the degradation lowered the TCE remaining in the soil from 86% to 66% for the potting soil and from 22% to 18% for the Smith Farm soil. This is reasonable because the aqueous phase degradation of TCE enhances the desorption driving force, i.e., the chemical potential difference between the soil and solution phases. However, the fact that in both cases a relatively large fraction of TCE remained in the soils confirmed that sorption of TCE in the solid phase greatly reduced the availability and the overall extent of TCE degradation by the nanoparticles.

Given the relatively short reactive lifetime (days to a couple weeks) (He et al., 2007; He et al., 2010) of the stabilized ZVI nanoparticles, a rapid initial desorption rate is essential for making best use of the overall dechlorination potential of the nanoparticles.

In addition to the sorption limitation, we found that chemical compositions, especially soluble SOM, exuded from the soils can retard the ZVI's dechlorination power. **Figure 2-4** illustrates the aqueous-phase TCE degradation by the nanoparticles in the presence of various levels of exudates (measured as TOC) from the potting soil. The observed pseudo-first order rate constant was reduced from 1.22 h^{-1} with no soil exudates to 0.81 and 0.41 h^{-1}, respectively, when 40 mg/L and 350 mg/L of TOC were present.

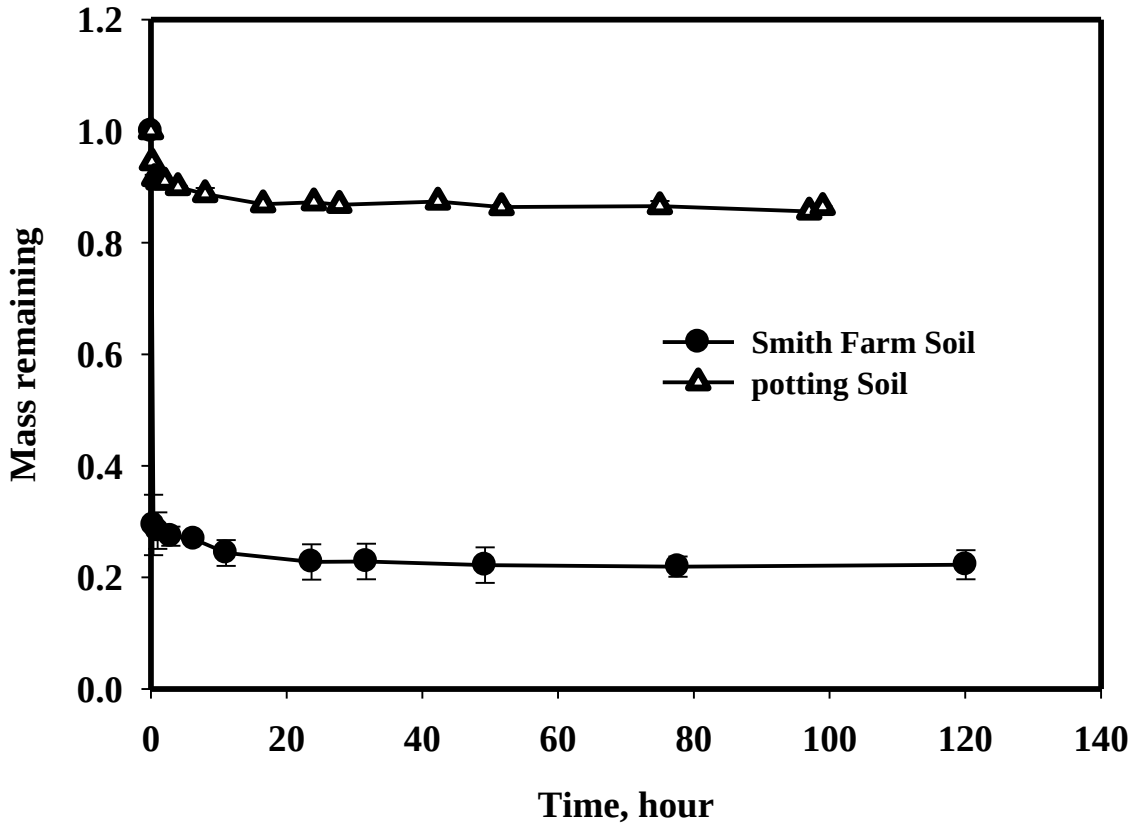

Figure 2- 2. Experimental data for desorption of TCE from potting soil and Smith Farm soil. Initial TCE in the potting soil and Smith Farm soil was 0.52 mg/g and 0.45 mg/g, respectively. Data plotted as mean of duplicates, error bars indicate deviation from the mean.

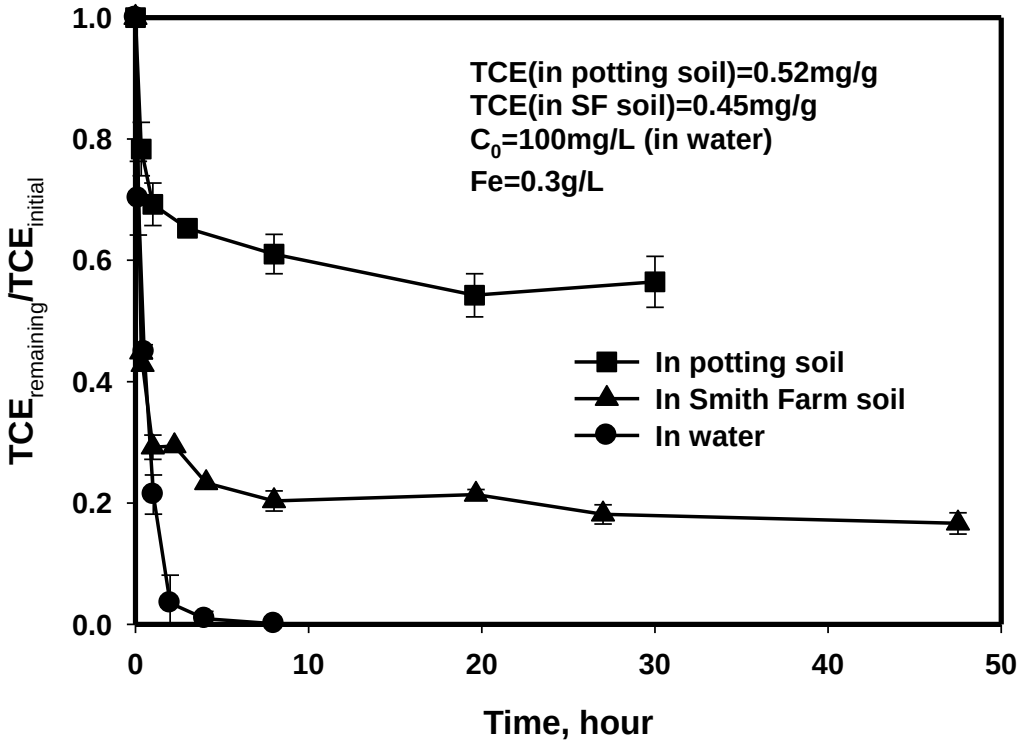

Figure 2- 3. Dechlorination of soil-sorbed and dissolved TCE with CMC-stabilized Fe/Pd nanoparticles with two model soils. Initial TCE in potting soil and Smith Farm soil was 0.52 mg/g and 0.45 mg/g, respectively; C_0 = 100 mg/L (initial TCE concentration in the solution only degradation tests); Fe = 0.3 g/L; Pd/Fe = 0.1 wt%; NaCMC = 0.24 wt%. ZVI to TCE mass ratio = 6.24:17.4 and 5.4:17.4 and 1:3 for the three systems, respectively. Data plotted as mean of duplicates, error bars indicate deviation from the mean.

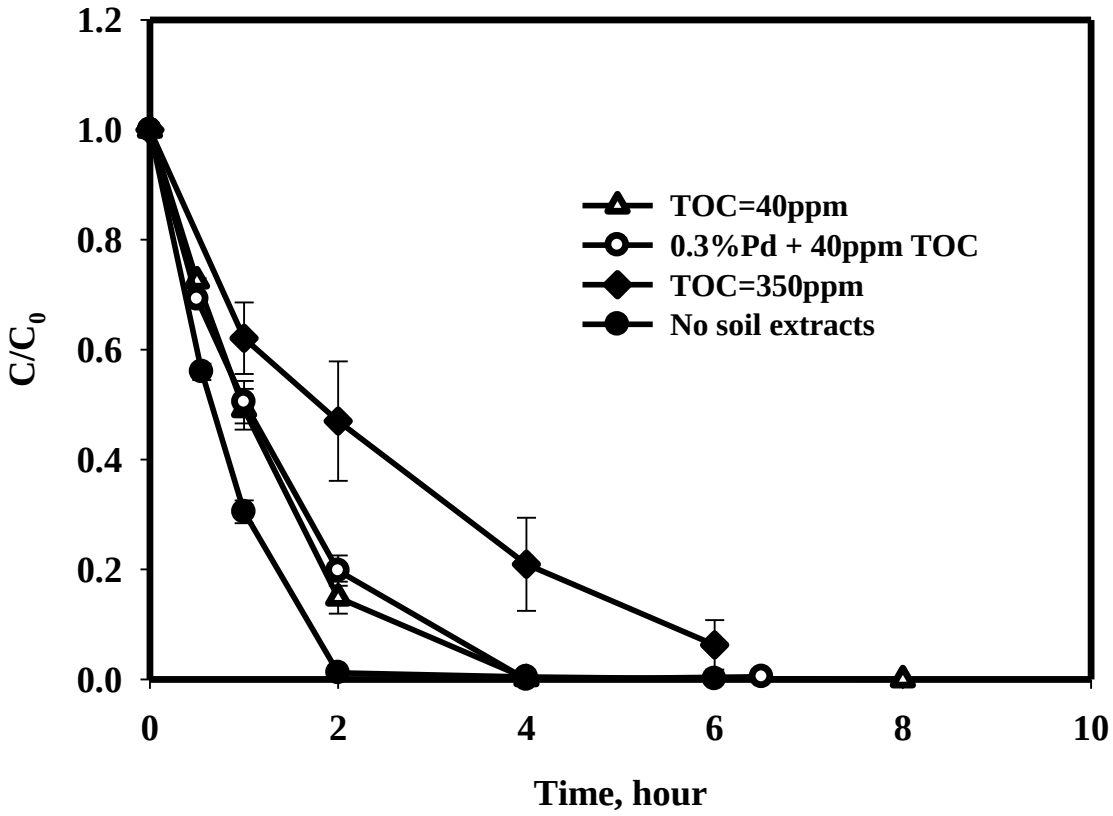

Figure 2- 4. Reductive dechlorination of TCE in water by CMC-stabilized ZVI nanoparticles with or without soil extracts. Initial TCE concentration is 100 mg/L, Fe = 0.3g/L, Pd = 0.1 wt% of Fe except for one case where Pd = 0.3 wt% of Fe. Soil exudates were quantified as TOC in the aqueous phase. Data plotted as mean of duplicates, error bars indicate deviation from the mean.

Similar retardation effects were reported by several researchers (Doong and Lai, 2005; Klausen et al., 2003; Tratnyek et al., 2001) on dechlorination effectiveness of granular or non-stabilized ZVI particles (which are typically present as micron-scale aggregates). For instances, Klausen et al. (2003) followed dechlorination of TCE using a granular ZVI for 100 days and observed that the presence of 2~ 20 mg/L humic acids or Great Dismal Swamp NOM reduced the pseudo-first-order rate constant by up to 50%. Doong and Lai (Doong and Lai, 2005) reported that the presence of 50 mg/L humic acid decreased the normalized surface reaction rate constant of PCE dechlorination by palladized iron powders by a factor of 20.

DOM can retard dechlorination in several ways. First, it may interfere with the particle stabilization by CMC, resulting in larger particles due to replacement of CMC molecules from the nanoparticle surface and/or direct coating of the DOM molecules on the nanoparticles. Based on dynamic light scattering (DLS) measurements, the mean particle size in the presence of the exudates from the potting soil (TOC = 350 mg/L) was 200 nm, as compared to 155 nm when no soil exudates were present. DOM is mainly composed of humic acid and fulvic acid, which are known to chelate with the iron oxides shell of the ZVI nanoparticles (Giasuddin et al., 2007). Such chelating effects will compete with the CMC molecules that are adsorbed on the particle surface, thereby diminishing the stabilizing effectiveness of CMC and inducing particle agglomeration. The DOM-nanoparticles interaction and the associated alteration of surface chemistry are evident from the change in the zeta potential. The presence of 350 mg/L TOC from the potting soil lowered the zeta potential of CMC-stabilized ZVI nanoparticles from -160 mV to -111 mV, which in turn lessens the electrostatic repulsion between the

nanoparticles. The sorption of DOM and an increase in particle size decreases the available reactive sites on the particle surface. Attachment of larger DOM molecules can also render the nanoparticles bulkier and less mobile, reducing the overall mass transfer rate. Second, the uptake of DOM molecules on the particle surface can result in a barrier to electron transfer that impedes the contact and reaction between TCE and the reactive sites of the nanoparticles. As a result, the dechlorination rates can be diminished (Feng et al., 2008; Giasuddin et al., 2007). The CMC molecules are macromolecules with a molecular weight of 90 kmol/g. Our prior work (He et al., 2007) indicated that CMC can strongly complex with the nanoparticle surface, stabilizing the nanoparticles through concurrent steric exclusion and electrostatic repulsion. Yet, the large molecular structure of CMC results in a relatively loose layer of sorbed molecules, which allow for a relatively easy mass transfer of TCE. However, when DOM molecules, especially those with smaller M.W., are adsorbed, the attached molecular barrier becomes much more compact, exerting a more profound mass transfer resistance to TCE. Tratnyek et al. (2001) investigated the DOM sorption effect on ZVI's TCE reduction kinetics, and reported that DOM could be sorbed more strongly to Fe^0 than TCE, resulting in reduced TCE degradation. Klausen et al. (2003) also observed that the TCE degradation rate by a granular iron column in the presence of 2 mg/L (as TOC) Great Dismal Swamp DOM decreased by about 50% after 100 days. They attributed the reactivity drop to the stronger NOM-iron interaction that competitively excluded the weakly bonded TCE-iron surface complex. Third, DOM might also be a competitive H_2 acceptor for dechlorination in the presence of Pd. Zhu et al. (2008) obtained UV-vis spectroscopic evidence showing the occurrence of a new π-π^* electron transition when 200 mg/L DOM was mixed with 0.83

g/L Fe-Pd particles. Therefore, NOM might compete with TCE for electrons generated from the iron oxidation. Fourth, DOM may affect the catalytic activity of Pd. Although Pd was present at only 0.1% of the Fe content, Pd plays a pivotal role in accelerating the dechlorination process (He and Zhao, 2008). The formation of galvanic couples between the iron and palladium greatly accelerates the electron flow among metals and thereby enhances the rate of reduction process (Schrick et al., 2002). Pd also acts as a catalyst and promotes formation of the highly reactive atomic hydrogen which is essential for the reductive dechlorination process (Cwiertny et al., 2007). However, natural organic matter would attach to the surface of the catalyst and consequently reduce the degradation rate of TCE, as Chaplin et al. (2006) observed during the catalytic nitrate reduction process with Pd-Au bimetallic catalyst. Ambonguilat et al. (2006) also reported a 98% decrease of nitrate reduction rate in a 20 mg C/L DOC solution with Pd-Sn/Al_2O_3 catalyst. To test the possible effect of NOM on the activity of Pd, TCE dechlorination rates were compared at two levels of Pd (0.1% and 0.3% of the Fe content) but at a fixed TOC concentration of 40 mg/L. **Figure 2-4** shows that the pseudo-first-order reaction rate constants were quite comparable: 0.81 h^{-1} at Pd = 0.1wt% Fe and 0.77 h^{-1} at Pd = 0.3wt% Fe. This observation suggests that DOM did not appear to diminish Pd's catalytic activity in our experiment, but rather the observed inhibiting effect of DOM is likely due to scavenging the atomic hydrogen in addition to the aforementioned effects.

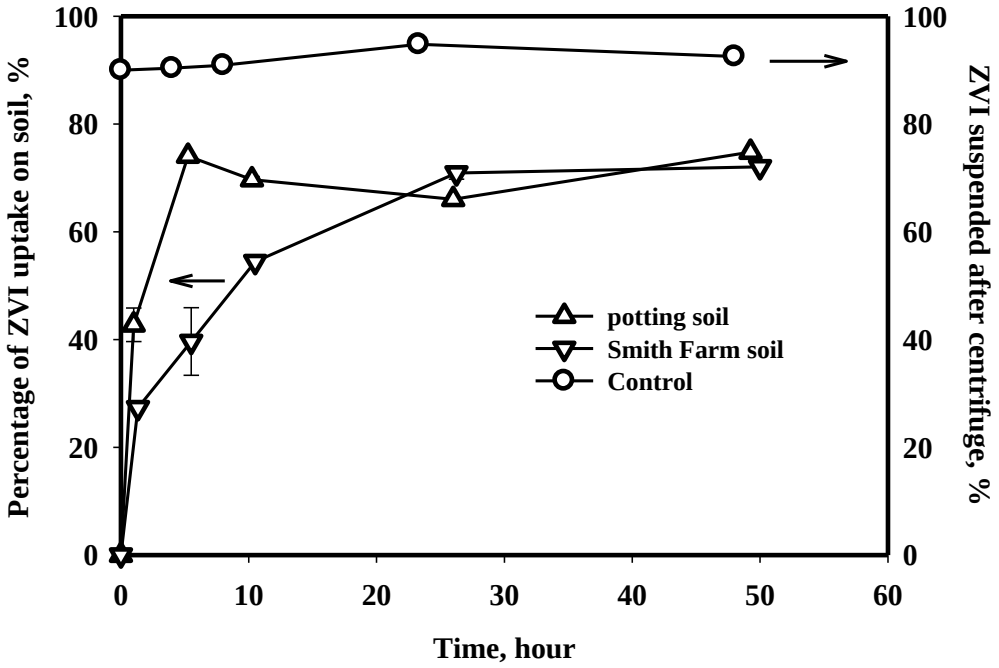

Figure 2- 5. Sorption kinetics of 0.3 g/L CMC-stabilized ZVI nanoparticles onto potting soil and Smith Farm soil. The soil-to-ZVI suspension ratio is 12g: 63 mL for both potting soil and Smith Farm soil. The experimental pH was in the range of 7.9 - 8.5 for both cases.

Lastly, strong adsorption of CMC-stabilized ZVI nanoparticles was observed for both of the soils as shown in **Figure 2-5**. One control test was conducted without any soil to quantify the removal of CMC-stabilized ZVI nanoparticles during centrifuging. Evidently, the centrifugal removal of ZVI nanoparticles in the absence of soil was fairly constant, which confirmed that ZVI nanoparticles remained stable during the experimental period.

In both cases, ~71% of the nanoparticles were associated with the soils, which can diminish the mobility of the nanoparticles, and thus, the collision and reaction rates between the nanoparticles and TCE. Based on the sorption kinetic data, it can be inferred that the slower degradation of TCE after 5 h in **Figure 2-3** was actually facilitated by the soil-sorbed nanoparticles. For in situ degradation, controlled mobility of the nanoparticles is of profound importance. The research findings here indicate that once delivered into the contaminant zone, most of the nanoparticles will be adsorbed on the soil matrices, forming a stationary reactive zone for degrading TCE.

2.3.3 Effects of surfactants on TCE desorption

Figure 2-6 (a) and **(b)** show the TCE desorption kinetic data for the potting soil in the presence of various surfactants at concentrations equal to, or at ~5 times the respective cmc values. In these tests, mass remaining is defined as the ratio of the total mass of TCE sorbed at time t to the initial mass of TCE in the soil. Control tests were performed to quantify any losses of TCE during the experiment and sample analysis. Mass balance results showed that the overall recovery of TCE was always within 90-105%. In all cases, the surfactants displayed various degrees of enhancement on TCE desorption, especially for the potting soil. For both soils, equilibrium was achieved within

60 h. In the previous TCE desorption test with soil-amended water (**Figure 2-2**), only 14% of TCE was released from the potting soil after 100 hours. **Figure 2-6** shows that the presence of 1 x cmc of SDS, SDBS, Tween 80 and HDTMA increased the amount of TCE desorbed to 19%, 17%, 15% and 17%, respectively. When the surfactant concentration was raised to 5 x cmc, the amount of released TCE went up to 22%, 17%, 18% and 16% for SDS, SDBS, Tween 80 and HDTMA, respectively. Apparently, the anionic surfactant SDS outperformed the other surfactants in both cases, whereas no marked differences were evident among HTDMA, Tween 80 and SDBS.

The presence of a surfactant can increase the solubility of TCE in the aqueous phase, thereby promoting the desorption process. On the other hand, a surfactant can be attached to soil, and thus, facilitate sorption of TCE via partitioning into the surfactant lamellae on the solid surface, which depends on surfactant type, properties of contaminants and porous media (Liu et al., 1992; Mata-Sandoval et al., 2002; Yuan et al., 2007). At a pH less than the PZSE of the soil, anionic surfactants (SDS and SDBS) could be chemisorbed through the electrical attraction with the positively charged groups such as NH_4^+ and OH_2^+ of the soil organic matter and soil Fe/Mn oxides (Rodriguez-Cruz et al., 2005; Yang et al., 2006; Yuan et al., 2007). However, sorption of the anionic surfactants was unfavorable at the prevailing experimental pH of ~8. Consequently, most of the surfactant molecules remain in the aqueous phase, resulting in greater desorption enhancement. In contrast, the nonionic surfactant Tween 80 and cationic surfactant HDTMA can be favorably adsorbed to the soil due to the electrostatic attraction (Deshpande et al., 1999; Rodriguez-Cruz et al., 2005), which potentially creates a sink for retaining more TCE in the soils. Because of soil sorption, the actual concentration of each

surfactant in the aqueous phase is expected to be below the initial level. Consequently, no aqueous phase micelles are expected for the case of 1 x cmc. As a result, the increase of desorption was only modest (maximum 5% for SDS). Grasso et al. (2001) observed that desorption of PAHs (polynuclear aromatic hydrocarbons) was negligible when the concentration of a nonionic surfactant, Alfonic 1412-7, was lower than its cmc.

When initial surfactant concentration was increased to ~5 x cmc, stable micelles are expected to be formed, which in turn would solubilize more TCE (Mata-Sandoval et al., 2002; Yang et al., 2006; Yuan et al., 2007). However, a 5 fold increase in surfactant dosage only increased the TCE desorption by 4% (from 19% to 22%) for SDS and even less for the other surfactants (**Figure 2-6**). This disproportionality lies in the fact that as the number of micelles in solution increased, attachment of the surfactants on the soils also rose (Liu et al., 1992), which counteracted any solubility enhancement.

Of the two anionic surfactants, SDS was more effective than SDBS for enhancing TCE desorption. This can be attributed to the differences in their molecular structures and associated physical and chemical characteristics such as the hydrophilic lipophilic balance (HLB) value. HLB is a measure of the hydrophilicity or lipophilicity of a surfactant. A higher HLB value indicates a surfactant's greater tendency to partition into the aqueous phase than in the oil phase. The HLB value was reported to be 40 for SDS and 11.7 for SDBS (Shen et al., 2007b; van Aken, 2003), suggesting a greater hydrophilicity for SDS. The stronger hydration ability of SDS resulted in greater TCE solubility. Li et al. (2007) reported that SDS could enhance the solubility of biphenyl A more effectively than CTAB and SDBS. Boving and Brusseau (2000) reported that SDS

was more effective for solubilization and removal of TCE from porous media, compared to DOWFAX 8390, hydroxypropyl-b-cyclodextrin and methyl-b-cyclo-dextrin.

Figure 2-6 (c) shows the TCE desorption rate from the Smith Farm soil in the presence of various surfactants at ~1 x cmc (initial concentration). Unlike the potting soil, the presence of the surfactants did not show any significant enhancement of TCE desorption. In all cases, equilibrium was rapidly reached in only 20 min, where almost 80% of adsorbed TCE was released, whereas desorption of the residual 20% TCE appears to be not feasible. This observation indicates that surfactants are much less effective for enhancing TCE desorption from SOM-deficit soils. Sanchez-Camazano et al. (2000) reported that atrazine desorption with SDS was more effective for desorbing SOM-sorbed atrazine.

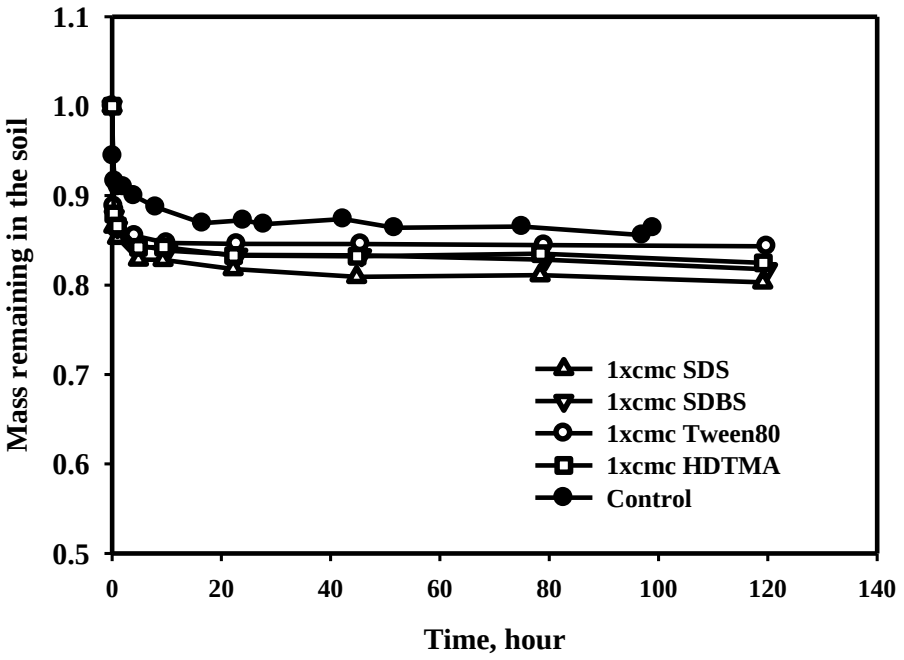
Mass remaining in the soil
1.1
1.0
0.9
0.8
0.7
0.6
0.5
0
20
40
60
80
100
120
140
Time, hour
1xcmc SDS
1xcmc SDBS
1xcmc Tween80
1xcmc HDTMA
Control

(a)

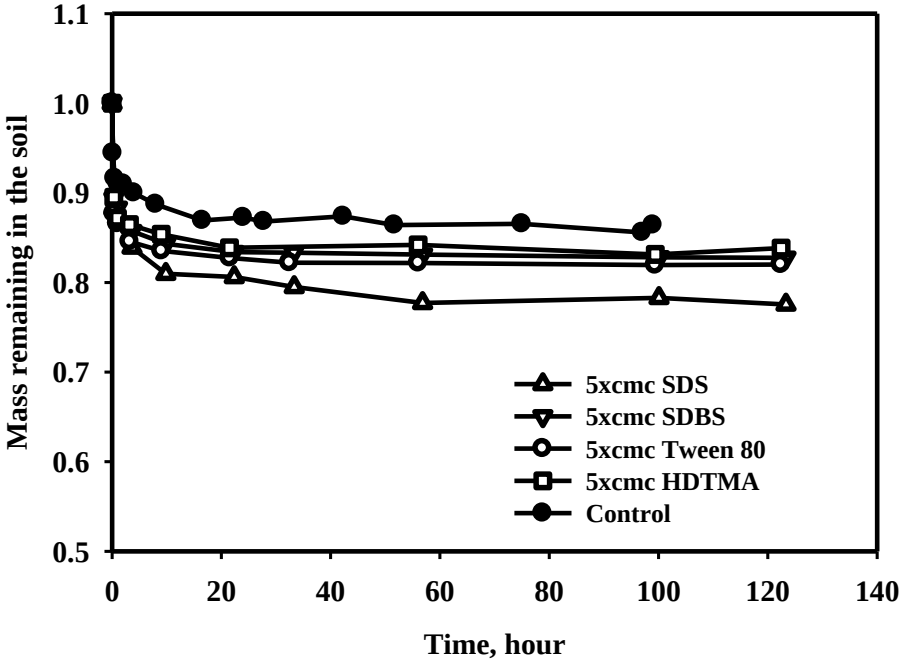
Mass remaining in the soil
1.1
1.0
0.9
0.8
0.7
0.6
0.5
0
20
40
60
80
100
120
140
Time, hour
5xcmc SDS
5xcmc SDBS
5xcmc Tween 80
5xcmc HDTMA
Control

(b)

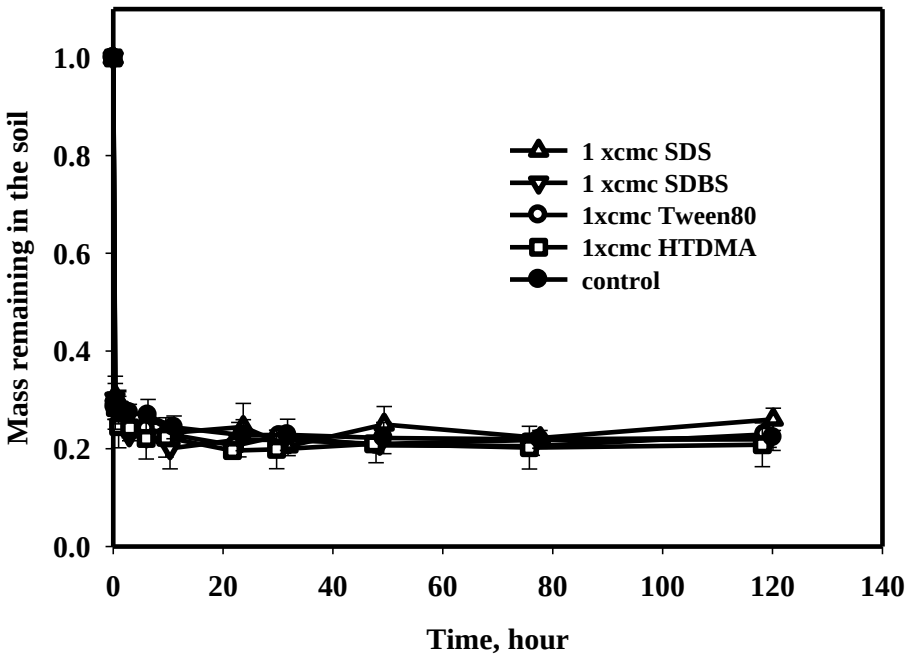

(c)

Figure 2- 6. (a) Effect of representative surfactants at 1 x cmc on desorption of TCE from potting soil. **(b)** Effect of various surfactants at 5 x cmc on desorption of TCE from potting soil. **(c)** Effect of various surfactants at 1xcmc on desorption of TCE from Smith Farm soil. Surfactant concentration is given as initial concentration. Initial concentration of TCE was 0.52 mg/g for potting soil and 0.45 mg/g for Smith Farm soil. Data plotted as mean of duplicates, and error bars represent deviation from mean of duplicates.

2.3.4 TCE degradation by ZVI nanoparticles in the presence of surfactants

Surfactants are known to interact with ZVI nanoparticles, and thus, may affect the reactivity of the nanoparticles. Sayles et al. (1997) reported that the dechlorination rate of DDT, DDD and DDE by ZVI was increased by ~ 1.8 times with a nonionic surfactant Triton X-114 at a concentration of 250 mg/L.

Aqueous TCE degradation in the presence of various surfactants at various concentrations (from sub- to supra-critical micelle concentration) was examined in batch tests of CMC-stabilized ZVI nanoparticles with 0.1 g/L as Fe. As shown in **Figure 2-7**, surfactants can either enhance or inhibit TCE degradation, depending on type and concentration of surfactant. To facilitate the rate comparison, the TCE degradation data are interpreted with a pseudo-first-order rate law. In the absence of a surfactant, the observed rate constant was approximately 0.063 min^{-1}. **Figure 2-7 (a)** shows that the presence of 1 x cmc SDS increased the rate constant by a factor of ~1.7 to 0.106 min^{-1}. However, when the SDS concentration was increased further to 5 x and 10 x cmc, the reaction rate constant was reduced to 0.087 min^{-1} and 0.074 min^{-1}, respectively, but still higher than that when no surfactant was present. Interestingly, the presence of the other anionic surfactant (SDBS) at concentrations of 1 x cmc and 5 x cmc clearly inhibited the reductive dechlorination of TCE (**Figure 2-7(b)**), whereas the nonionic Tween80 at concentrations of 1 x cmc, 5 x cmc and 10 x cmc did not show any appreciable effect on the degradation rate (**Figure 2-7(c)**). The degradation rate was also inhibited by the cationic surfactant (HDTMA) at 0.5 x cmc and 1 x cmc, where the rate constant was reduced to 0.025 min^{-1} and 0.031 min^{-1}, respectively.

Of the 4 surfactants, SDS appeared to be most promising to enhance degradation of soil-sorbed TCE for its ability to promote both desorption of soil-sorbed TCE and accelerate the aqueous-phase dechlorination. The presence of CMC-coating on the surface of Pd/Fe nanoparticles renders a negatively charged surface, as evidenced by the zeta potential of -160 mV. Consequently, the head groups of anionic surfactants are subjected to electrostatic repulsion from the particle surface. On the other hand, the amphiphilic nature of the surfactant tends to decrease the interfacial tension of the solution. As a result the tails of the surfactant molecules tend to be adsorbed to the particle surface, which favors the mass accumulation of TCE at the surface, and thus enhances the TCE degradation rate. However, when the surfactant concentration is so high that more micelles are formed in the aqueous phase, the micelles will tend to hold TCE in solution, resulting in reduced TCE accessibility to ZVI nanoparticles. Note that micelles may not be fully developed at lower surfactant dosages (e.g. 1 x cmc) due to sorption of the surfactants to the nanoparticles. However, TCE reduction was inhibited by the other anionic surfactant SDBS at 1 x cmc or higher. This can be attributed to the different molecular structures between SDS and SDBS. Although both surfactants carry the same sulfonic functional groups, SDBS contains a benzene ring at the head of the molecules, as compared to the linear chain structure of SDS (**Table 2-1**). As a result, SDBS is more hydrophobic than SDS, which is consistent with the much lower HLB value of SDBS. Consequently, TCE bound to SDBS in the solution phase tends to be less available for the nanoparticles. In addition, SDBS itself as a TCE carrier is likely subjected to a greater mass transfer resistance due to the benzene ring, which hinders the delivery of TCE to the nanoparticle surface. Compared to SDS, Tween 80 has a 4.5 times

greater M.W. and a much bulkier molecular structure. As a result, the CMC molecules on the particle surface may exert a greater barrier effect toward Tween 80 molecules, resulting in little enhancement in TCE delivery and degradation at concentrations less than 5 x cmc. When the surfactant dose was increased to 10 x cmc, more aqueous-phase micelles were formed, leading to an increased inhibition effect (**Figure 2-7(c)**).

The cationic surfactant displayed the most inhibitive effect on TCE degradation even at a 1 x cmc dosage. The positively charged heads of HDTMA interact with the negative charges of CMC on the ZVI surface. This interaction can lead to two important consequences. First, the surfactant molecules are sorbed on the CMC layer in a tail-outward mode, which will not promote TCE delivery toward the nanoparticles. Second, neutralization of the surface negative charges tends to destabilize the ZVI nanoparticles, which reduces the reactive surface area. In the experiments, the zeta potential of the Fe-Pd nanoparticle with 0.5 x cmc, 1 x cmc and 5 x cmc of HDTMA was measured to be -154 mV, -158 mV and -72 mV, respectively, compared to -160 mV when no HDTMA was present. The hydrodynamic diameter of the Fe-Pd nanoparticles increased with the addition of HDTMA, from 214 nm with no surfactant to 228 nm with 0.5 x cmc, 318 nm with 1 x cmc and 585 nm with 5 x cmc of HDTMA. Earlier, Shin et al. (2008) studied TCE degradation using non-stabilized ZVI aggregates and they observed that 3 cationic surfactants including CTAB were able to enhance TCE degradation at a concentration below the cmc level, while anionic and nonionic surfactants inhibited TCE dechlorination. The apparently contradicting results stem from the different surface properties of bare and CMC-coated ZVI particles, and reflect the important role of the CMC stabilizer. In the absence of a stabilizer, the bare ZVI particles were not only much

larger (up to 0.15 mm), but exhibited a nearly neutral surface (zeta potential = ~20 mV). When a cationic surfactant was added (e.g. cetylpyridinium chloride (CPC)), the surface charge was readily neutralized or reversed (e.g. zeta potential became ~ +3 mV at 1 x cmc and ~ +54 mV at 2 x cmc of CPC. This positive surface charge favors sorption of TCE to the nanoparticles due to its electrostatic interaction with the electronegative chloride group on TCE, and thus, boosting the reductive dechlorination process.

It is worth noting that in the case of SDS, the maximum dechlorination rate was observed at the 1 x cmc. A similar tendency was also observed by Zhu et al. (2008), who studied dechlorination of 1, 2, 4-trichlorobenzene by non-stabilized Fe-Pd nanoparticles. They claimed that the contact between the contaminant and Fe-Pd will be enhanced due to the augmented accumulation of the contaminant on the nanoparticles by the sorbed surfactants (Zhu et al., 2008). However, with elevated surfactant concentration, more micelles would form in the solution and compete for TCE, resulting in a decreased rate of contaminant degradation.

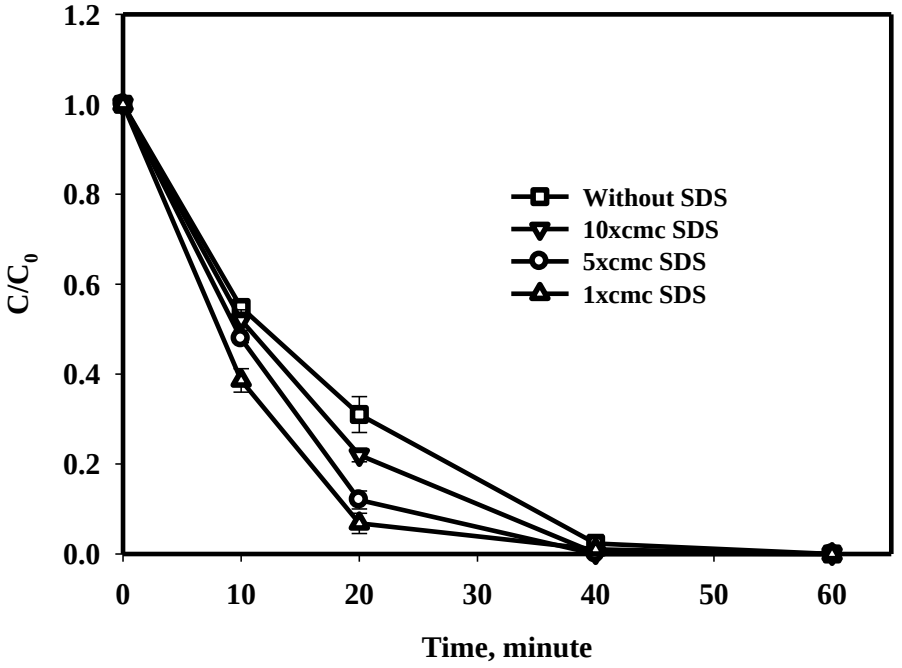
1.2
1.0
0.8
0.6
0.4
0.2
0.0
C/C0
0
10
20
30
40
50
60
Time, minute
Without SDS
10xcmc SDS
5xcmc SDS
1xcmc SDS

(a)

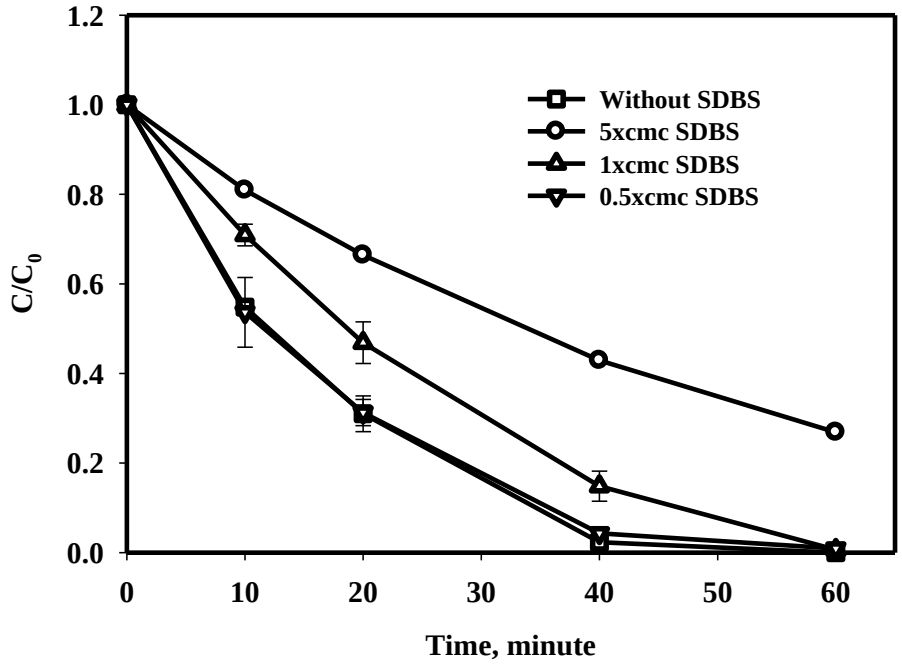
1.2
1.0
0.8
0.6
0.4
0.2
0.0
C/C0
0
10
20
30
40
50
60
Time, minute
Without SDBS
5xcmc SDBS
1xcmc SDBS
0.5xcmc SDBS

(b)

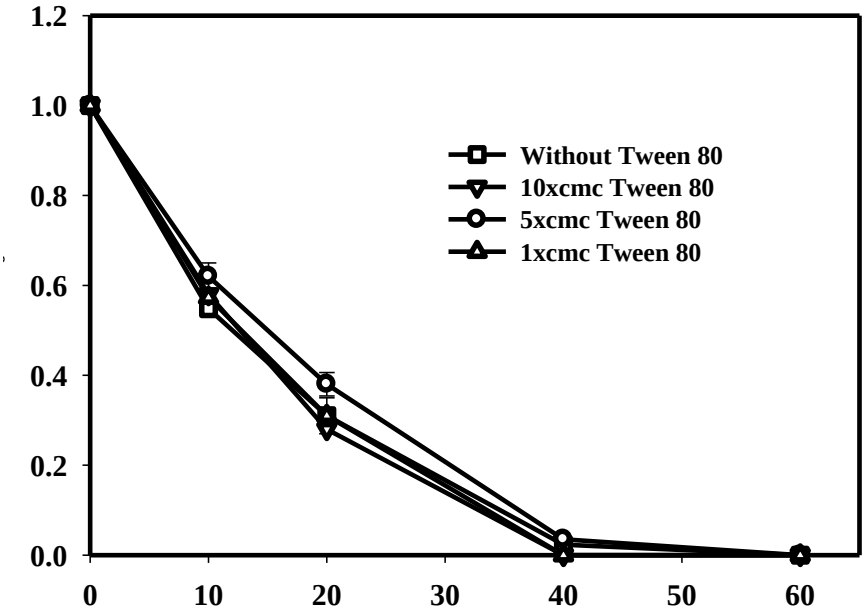

(c)

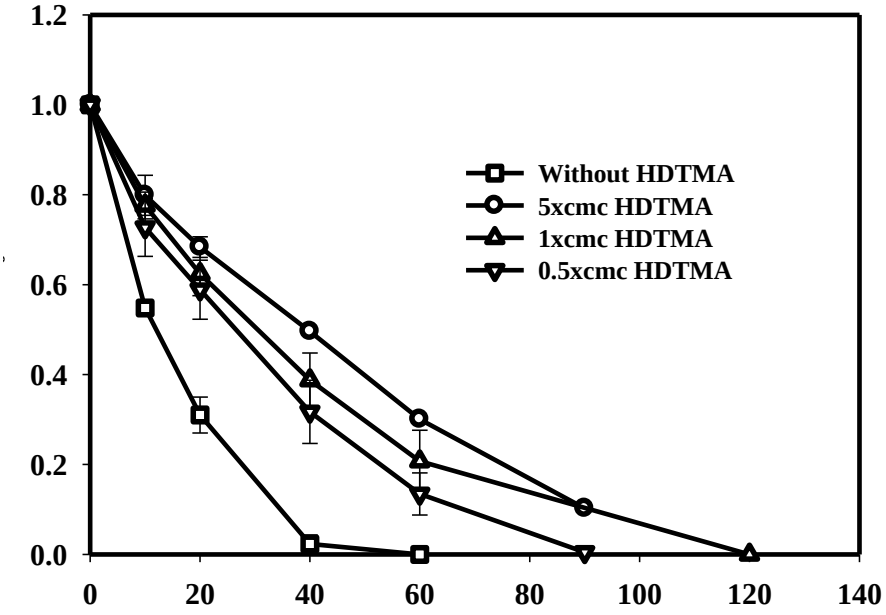

(d)

Figure 2- 7. TCE degradation by CMC-stabilized ZVI nanoparticles in the aqueous phase in the presence of various initial concentrations of: **(a)** SDS, **(b)** SDBS, **(c)** Tween 80, and **(d)** HDTMA. Fe=0.1g/L, Pd/Fe=0.1wt%, NaCMC= 0.2wt%, Initial TCE C_0=10mg/L. Data plotted as mean of duplicates and error bars refer to deviation from the mean.

2.3.5 Degradation of soil-sorbed TCE

The effect of SDS on the degradation of soil-sorbed TCE was further tested using CMC-stabilized Fe-Pd nanoparticles. **Figure 2-8** shows the total TCE remaining in the system as a function of reaction time. The experimental data displayed a two-stage rate profile, i.e., an initial rapid reaction in the first hour followed by a slower dechlorination rate. This clearly staged rate profile agrees with the biphasic desorption profile (**Figure 2-2**), revealing the profound limitation of desorption kinetics on the degradation rate of soil-sorbed TCE.

For the potting soil (**Figure 2-8 (a)**), 44% of sorbed TCE was degraded within 40 h when no surfactant was added. When SDS was added at 1 x cmc (initial concentration), however, only 39% of TCE was degraded. When SDS dosage was raised to 5 x cmc, TCE degradation was increased to 49%. Evidently, SDS was able to enhance the rate and extent of TCE degradation in the soil only at a sufficiently high concentration (e.g. 5 x cmc), and the presence of 1 x cmc SDS actually inhibited the TCE degradation rate by 5%. For the Smith Form soil (**Figure 2-8(b)**), however, SDS appeared much more effective at enhancing TCE degradation. In this case, nearly 80% of soil-sorbed TCE was degraded within 8 h, and finally 83% of total TCE was removed after 47.5 hours without surfactant addition. When 1 x cmc SDS was added, more than 90% of TCE was degraded in < 30 h.

The different surfactant effects on the two soils are attributed to their different SOM contents (**Table 2-2**). Given the fact that SDS enhances both desorption of TCE from the potting soil (**Figure 2-6**) and degradation of TCE (**Figure 2-7**), the observed inhibition of TCE degradation at 1 x cmc SDS (**Figure 2-8 (a)**) is somewhat

counterintuitive. This inhibition effect at the lower SDS dosage can be attributed to the inhibitive effect of the dissolved NOM, which results from the addition of SDS, as discussed above. In the presence of SDS, more organic matter in the soil phase was released into the solution phase. As measured, the TOC value for SDS concentrations of 1 x cmc and 5 x cmc is 422.5 mg/L and 2054.6 mg/L, respectively. After 1-day of mixing with Smith Farm soil at the same water-soil ratio as for the TCE degradation test, the TOC concentration in the aqueous phase decreased to 262.2 mg/L for the solution with 1 x cmc SDS, mainly due to the SDS sorption on soil. However, for the solution with 5 x cmc of SDS, the TOC in the aqueous phase increased to 2505.7 mg/L, which is probably due to the strong release of natural organic matter from soil matrix even though SDS sorption on soil was still undergoing. There was only 43 mg/L of TOC released from soil with DI water. Muroi et al. (2009) reported that formation of humic substance-surfactant complex at SDS concentrations below the cmc level and solubilization of humic substances into the surfactant micelles at SDS concentrations above the cmc level would increase the concentration of humic acid in the aqueous phase. Otto et al. (2003) also pointed out that SDS and humic substances can interact strongly through strong hydrophobic interactions. Sorouradin et al. (1993) reported that SDS could effectively enhance the desorption of humic substances from Amberlite ® XAD resins.

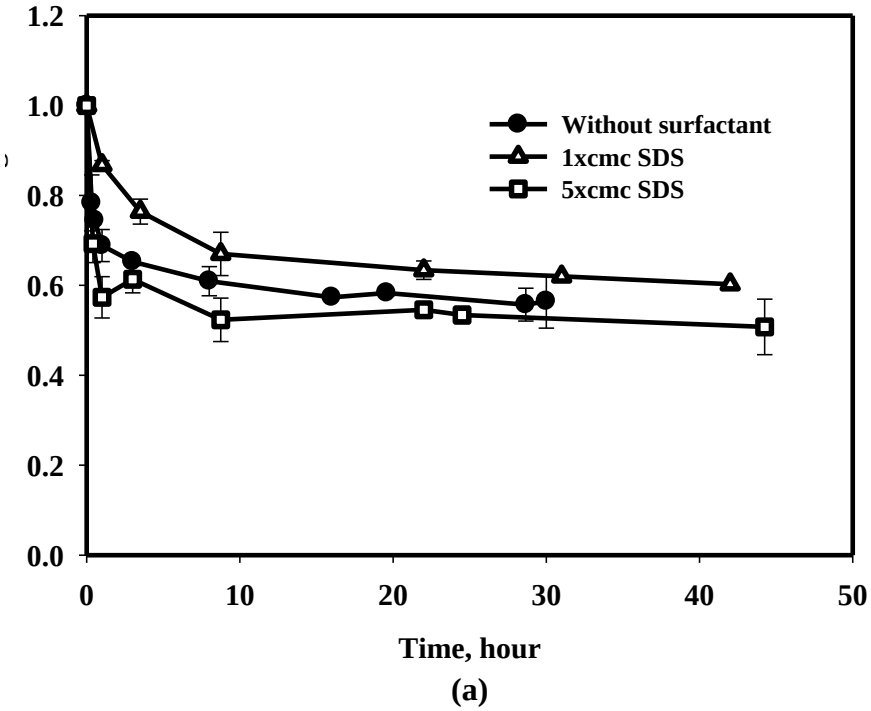

(a)

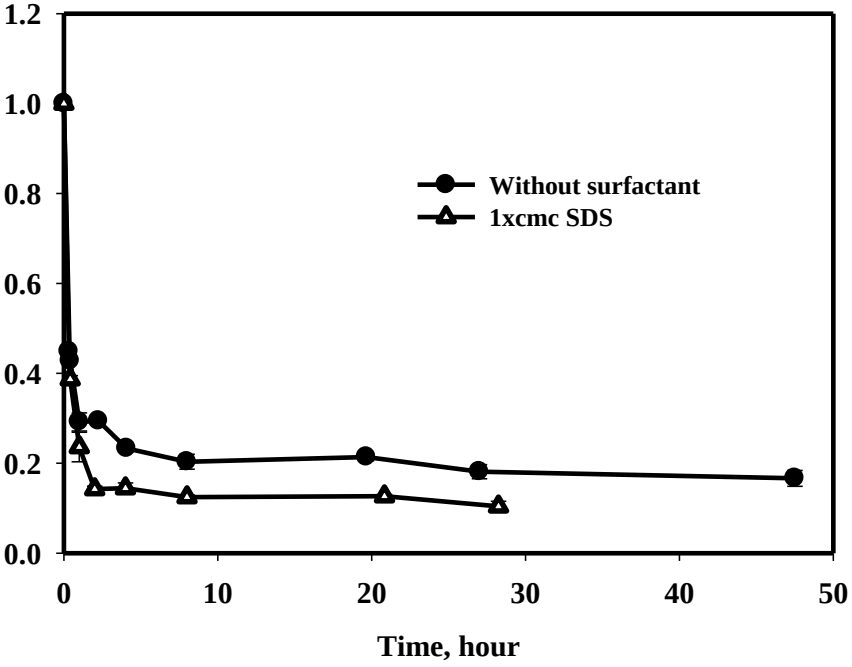

(b)

Figure 2- 8. Effect of SDS on degradation rate and extent of TCE by CMC-stabilized ZVI nanoparticles in potting soil **(a)** and Smith Farm soil **(b)** The initial amount of TCE in potting soil and Smith Farm soil was 0.52 mg/g and 0.45 mg/g, respectively. Fe = 0.3g/L, Pd/Fe = 0.1 wt%, NaCMC = 0.24 wt%. Data plotted as mean of duplicates and error bars indicate deviation from the mean.

At 1 x cmc SDS, the increased release of NOM competes with the desorbed TCE for the reactive sites on Fe-Pd nanoparticles, resulting in a decline of the overall degradation rate and extent of TCE. It is also possible that at the lower SDS concentrations, more NOM was dissolved than TCE from the soil. When the SDS dosage is further increased to 5 x cmc, SDS micelles are formed, which increase the partition of NOM into the hydrophobic interior of the SDS micelles. The outer micelle structure mitigates the sorption of dissolved NOM onto the particles and thereby lessens the inhibitory effect of NOM on TCE degradation, and the overall degradation of TCE was augmented.

For the Smith From soil, no NOM was leached during the reaction. Consequently, the interference of NOM on the TCE degradation was negligible, allowing for better use of the positive effect of SDS on TCE degradation. In fact, the SDS-enhanced degradation of TCE in the aqueous phase promotes further desorption of TCE, leading to the enhanced overall reaction rate. Therefore, the beneficiary effect of SDS is better utilized for soils lean of SOM.

2.4 Conclusions

The major findings from this study are summarized as follows:

1) CMC-stabilized Fe-Pd nanoparticles can effectively degrade soil-sorbed TCE. However, the TCE degradation rate can be strongly limited by desorption kinetics, especially for soils with a higher content of organic matter.

2) The presence of surfactants can impact TCE desorption and degradation with CMC-stabilized Fe-Pd nanoparticles. However, this impact depends on the physiochemical properties of surfactants and soil characteristics (especially the

SOM content). The anionic surfactant SDS was most effective at enhancing TCE desorption, and furthermore, was able to enhance TCE degradation in water at concentrations both at and above its critical micelle concentration. However cationic and nonionic surfactants were found to inhibit the TCE degradation. For soil-sorbed TCE, the addition of SDS appears more beneficial at lower SOM content. For SOM-rich soil, higher dosages (e.g. 5 x cmc) of SDS are required to achieve enhanced degradation of TCE.

3) The presence of soil soluble organic matter can severely inhibit TCE degradation by Fe-Pd nanoparticles.

4) Under batch mixing conditions, more than 71% of CMC-stabilized Fe-Pd nanoparticles became associated with the soil matrix, suggesting that after injected into the subsurface, the nanoparticles are very likely to become immobilized. Yet, even the immobilized Fe-Pd nanoparticles remain reactive for dechlorination.

The findings in this work indicate that while injection of suspensions of ZVI nanoparticles into the subsurface environmental system is a promising technology for in situ dechlorination, effects of sorption and soluble soil organic matter must be considered. Although some surfactants such as SDS may aid in overcoming the limitations, factors such as soil type, SOM content and surfactant type and dosage must be considered.

CHAPTER 3. Transport of Stabilized Iron Nanoparticles in Porous Media: Effect of Surface and Solution Chemistry

3.1 Introduction

Zero valent iron (ZVI) nanoparticles have received considerable attention as a promising in-situ environmental remediation technology in recent years (Elliott and Zhang, 2001; He et al., 2010; Quinn et al., 2005). The nano-scale ZVI particles have been proven to be technologically and economically effective to remove the halogenated organic compounds, pesticides, heavy metals, arsenic, nitrate and perchlorate in either laboratory studies or field demonstrations (Cheng et al., 1997; Joo and Zhao, 2008; Li and Zhang, 2007; Liu et al., 2005; Su and Puls, 2001). However, before the widespread use of this technology by delivering or emplacing the ZVI nanoparticles to the contamination sources in soil and groundwater, the fate and transport behavior of ZVI nanoparticles in the subsurface area should be well understood.

ZVI nanoparticles are known to exhibit a core-shell structure, with an iron oxide (Fe_3O_4 and Fe_2O_3) shell surrounding a zero valent iron core (Lin et al., 2010; Martin et al., 2008). In addition to the universal van der Waals attractive force, magnetic Fe^0 and iron oxide would induce dipole-dipole attractions and thereby result in a rapid agglomeration of these nanoscale particles into micro-scale aggregates and fractal, chain-like clusters (Cushing et al., 2004; Phenrat et al., 2007). Once aggregated, the nanoparticles would lose not only their chemical reactivity but also the mobility in the subsurface area due to straining and deposition (Hong et al., 2009). Studies have shown

that non-stabilized ZVI nanoparticles could not transport through porous media (He et al., 2007; Kanel et al., 2008; Saleh et al., 2007; Schrick et al., 2004). Even in sand columns, only about 1% of ZVI nanoparticles could break through (Saleh et al., 2008). Therefore, how to keep ZVI nanoparticles readily dispersible in water and delivered directly to the targeted contaminant source zone become a significant challenge for field applications of this technology.

To improve the ZVI stability and mobility, various strategies have been employed including immobilization of iron nanoparticles on colloidal supporting materials such as carbon microspheres or silica (Zhan et al., 2009; Zhan et al., 2008), or modification of the surface properties of iron using polymers, surfactants or even natural organic matter (Johnson et al., 2009). He et al. (2007) developed a new class of stabilized ZVI nanoparticles by using carboxymethyl cellulose as a stabilizer to enhance the intraparticle electrostatic repulsion and steric hindrance between particles. The CMC-stabilized ZVI nanoparticles could remain well dispersed in water for 9 days before been completely oxidized. A successful field test in Alabama demonstrated the improved reactivity and mobility of the ZVI nanoparticles for in-situ dechlorination remediation (He et al., 2010). Kim et al. (2009) used carboxymethyl cellulose to stabilize a commercial ZVI nanoparticles and found that more than 70% of the ZVI nanoparticles could be eluted from a sand column even after aging for 8 months.

Generally, the retention of colloids on porous media is inhibited by repulsive electrostatic forces and enhanced by adhesive forces between suspended colloids and collector grains. In the natural aquatic environment, some subsurface mineral constituents such as iron oxides and aluminum oxide usually carry a positive charge under neutral pH

conditions (Adamczyk et al., 2003; Johnson et al., 1996). Laboratory and field tests suggested that the iron oxide and aluminum oxide would play an important role in determining the underground transport and mobility of colloids (Abudalo et al., 2005; Kim et al., 2008; Ryan et al., 1999). Johnson et al. (1996) reported that the introduction of positively charge iron oxyhydroxide surface on the negatively charged quartz sand could significantly increase the retention of negatively charged silica colloids. Zhuang and Jin (2008) studied the transport of two bateriaophages in a goethite-coated sand column and suggested that the attachment of bateriophages was favored with the presence of the goethite on the sands, especially at a lower pH.

For the in-site remediation, different concentrations of ZVI nanoparticles were prepared and injected into groundwater under diverse field conditions (Elliott and Zhang, 2001; He et al., 2010; Wei et al., 2010). Especially after groundwater dilution the concentration of ZVI might vary significantly from place to place in subsurface area. Consequently, the transport behavior of ZVI may change with varied concentrations, considering that the transport of colloids would change with different colloid concentrations (Camesano and Logan, 1998; Liu et al., 1995). Camesano and his coworkers (Camesano and Logan, 1998; Camesano et al., 1999) found that the retention of *Burkholderia cepacia* G4 would decrease when increasing its inlet concentration because the available deposition sites on collector grains decreased due to continuous bacteria coverage, while increased retention of *Pseudomonas fluorescens* P17 was observed with a higher inlet concentration because the retained bacteria could enhance the attraction between sequent bacteria and collector grains. However, Phenrat et al. (2008) suggested that the concentration of poly (styrene sulfonate) modified RNIP from 1

g/L to 6 g/L had no effect on particle deposition. Yet, they did not consider the concentration effect at higher dilutions.

Knowledge of the interaction between stabilized ZVI nanoparticles and natural organic matter (NOM) is of importance for understanding the transport behavior of ZVI, because NOM is widely present in the ecosystem. It is well known that natural organic matter could bind to clay minerals via ligand exchange, hydrogen binding or surface complexation (Murphy et al., 1994; Schlautman and Morgan, 1994), resulting in a negative surface charge of the porous media (Abudalo et al., 2010; Franchi and O'Melia, 2003). Such processes could also enhance the stability of colloidal particles. Mylon et al. (2004) observed that the critical coagulation concentration of Hematite colloids in NaCl solutions increased by more than 3 times after pre-adsorption of 15.2 mg C/g Suwannee River humic acid. Domingos et al. (2009) reported less aggregation of 1 mg/L TiO_2 nanoparticles when adding 1 mg C/L Suwannee River fulvic acid, which is attributed to the enhanced steric repulsion between nanoparticles. Pelley and Tufenkji (2008) suggested that the presence of 5 mg/L humic acid will decrease the attachment of polystyrene latex colloids on quartz sand columns as a result of electrosteric stabilization. Therefore, modification of the physicochemical properties of both colloids and collectors in the presence of NOM would alter the transport and deposition behavior of these nanoparticles.

The overall goal of this study was to investigate the transport behavior of stabilized ZVI nanoparticles in saturated porous media under varied solution and surface chemical conditions. Transport experiments of CMC-stabilized ZVI nanoparticles were conducted in glass columns packed with quartz sand, aluminum oxide-coated sand and

iron oxide-coated sand. Batch adsorption experiments were performed to estimate the ZVI adsorption rate. The contribution of adsorption and filtration effects on the removal of ZVI nanoparticles was evaluated via mathematical modeling. The effects of polymer stabilizer, ZVI concentration, ionic strength and natural organic matter were determined on the deposition and transport of ZVI nanoparticles.

3.2 Material and Methods

3. 2.1 Chemicals

All chemicals in this study were used as received: $FeSO_4 \cdot 7H_2O$ (Acros Organics, Morris Plains, NJ); sodium carboxymethyl cellulose (NaCMC or CMC, mean M.W. = 90,000, Acros Organics); $NaBH_4$ (ICN Biomedicals, Aurora, OH); sodium chloride (Fisher, Fair Lawn, NJ); $NaHCO_3$ (Fisher); $Na_2S_2O_4$ (laboratory grade, Fisher); H_2O_2 (Fisher); KBr (Fisher), and hydrochloric acid (Fisher), $CaCl_2$ (Fisher), starch (For electrophoresis, Sigma-Aldrich, St. Louis, MO), $AlCl_3$ (Fisher), $Fe(NO)_3$ (Fisher), NaOH (Fisher) .

Deionized (DI) water was produced by an ELGA Ultrapure system (ELGA, IL, USA). The natural soil soluble organic matter was obtained from the extraction of one potting soil (HYPONEX®, OH, USA) purchased from the local Walmart store. 30mL of DI water was mixed with 36 g of the potting soil for 7 days and after centrifugation, the supernatant was filtered with a 0.45 μm membrane to removed large colloidal particles and stored in a refrigerator at 4°C. The soluble soil organic matter was quantified as dissolved organic carbon (TOC) by a UV-persulfate TOC analyzer (Tekmar-Dohrmann Phoenix 8000, Mason, OH, USA). Bromide concentrations in the tracer tests were

measured with an ion chromatograph (DX-120, Dionex, Sunnyvale, CA, USA) using an AS14 analytical column.

3.2.2 Preparation of stabilized ZVI nanoparticles

In this study, 1.0 g/L zero valent iron nanoparticles were synthesized via the liquid reduction method using sodium borohydride at room temperature. Two polysaccharide stabilizers were employed: carboxymethyl cellulose and starch. The synthesis procedure followed the same procedure described in previous papers by He et al. (He and Zhao, 2005; He et al., 2007). The obtained 1.0 g/L ZVI nanoparticles were then diluted using deoxygenated DI water to 0.2 g/L immediately after synthesis. Particles sizes determined from dynamic light scattering (DLS) experiments and ζ-potentials of stabilized ZVI nanoparticles were obtained using a Zetasizer Nano instrument (Malvern, Southborough, MA). The total iron concentration in the sample was determined with an inductively coupled plasma ICP-AES apparatus (Liberty-Series II, Varian, Palo Alto, CA) after acid digestion with the concentrated hydrochloric acid at a volume ratio of 1:4.

3.2.3 Preparation of Porous Media

Uniform quartz sand (Accusand 40/60) was used for all experiments, purchased from Unimin Corporation (Le Sueur, MN, USA). Prior to the experiments, the sand grains were cleaned thoroughly: rinsed with DI water for 1 hour, immersed in a 0.1 M sodium dithionite solution for 2 hours in order to eliminate metal impurities on the sand surface, soaked in 5% hydrogen peroxide for 2 hours to remove organic impurities, washed in DI water again and rinsed in 12 N hydrochloric acid overnight, finally soaked

with DI water again until the pH become neutral. The sand was air-dried and stored for use.

IOCS (iron oxide coated sand) was prepared based on a modified precipitation method (Bailey et al., 1992; Xu and Axe, 2005). 150 g of clean sand were first mixed with 80 ml of 2.1 M $Fe(NO_3)_3$. The pH of the slurry was increased to 12 by drop-wise adding a 10 M NaOH solution and then dried in an oven at 110 °C for 14 hours. Upon cooling, the resultant coated sands were repeatedly washed with DI water and dried at 110 °C for 3 hours followed by 21 hours at room temperature, until no more iron rinsed off from the sand. The AOCS (aluminum oxide coated sand) was prepared based on the method by Kuan et al. (1998). 150 g of the cleaned quartz sand was soaked with a 1 M of $AlCl_3$ solution. 4.0 M NaOH was added drop-wise to reduce the pH of the slurry to 11. After mixing for 15 min, the suspension was dried at 70°C for 2 days. The sand was then washed with DI water and heated repeatedly until the rinse-off was clean. The average size and distribution of sand grains were not changed significantly based on the sieving method. The total amount of iron and alumina loaded on the sand were measured on a ICP-IEA instrument after acid digestion with the EPA method 3050b.

3.2.4 Transport experiments

ZVI nanoparticles transport experiments were performed in a glass chromatography column with dimensions of 1 cm inner diameter and 25 cm length (Omnifit USA, Cambridge, England). A piece of glass wool with a thickness of 0.3 cm was placed at the bottom of the column. Quartz sand with a porosity of 0.36 was wet-packed using the deoxygenated background electrolyte (0.84 mM NaCl + 0.16 mM $NaHCO_3$, pH 7.5). A HPLC pump was used to introduce the background solution and

nanoparticles suspension into the column at a constant pore velocity of 0.0353 cm/s. Column effluent was collected continuously with an Eldex fraction collector (Eldex, CA, USA).

Prior to each column test, the packed column was pre-equilibrated with about 15 pore volumes of the background electrolyte to remove background turbidity. Afterwards, a tracer test was conducted to investigate the hydrodynamic properties of this column. ~8 pore volumes (PVs) of 30 mg/L potassium bromide (KBr) solution as a conservative tracer was introduced into the column in the up-flow mode under the same condition as the nanoparticles breakthrough test. The effluent concentration of bromide was recorded and fitted to a one-dimensional form of the convective-dispersive reactive (CDR) transport equation using the Hydrus-1D software to evaluate the flow hydrodynamic conditions. Lastly, another ~8 PVs of the background electrolyte was pumped into the column to thoroughly elute the bromide. Duplicate or triplicate transport tests have been done but only the representative results are presented for comparison.

After the system was equilibrated with the background electrolyte, a ~7.5 PVs of 0.2 g/L stabilized ZVI nanoparticles was introduced under certain experimental conditions. The Fe concentration history in the effluent was monitored. After each ZVI transport test, the column was flushed with another ~8 PVs of background electrolyte. The elution with the background electrolyte was trying to reduce the ionic strength in the aqueous phase back to the background level, to evaluate the total amount of nanoparticles released from the column, which can be calculated by numerically integrating the area under the elution curve. At the end of the transport experiments, the sand column was divided into 3 cm increments. The retained ZVI nanoparticles on sand could be washed

off by acid digestion using the EPA method 3050b and the total iron concentration was analyzed on an ICP-IEA instrument.

3.2.5 Stabilized ZVI nanoparticle adsorption kinetic and isotherm tests

Batch tests were conducted in 43 mL borosilicate glass vials (Fisher) to investigate the adsorption kinetics and isotherms of stabilized ZVI nanoparticles in both quartz sands, IOCS and AOCS. The septa were wrapped with Al foil because precipitation of CMC-ZVI nanoparticles on Teflon-lined septa was observed (data not shown). A certain amount of dry sand (3 g, 8 g or 12 g) was added into each vial containing 43 mL of stabilized ZVI colloids at different concentrations ranging from 0.05 g/L to 0.4 g/L. These glass vials were shaken on a rotator in an incubator at 21±1 °C. At the selected time points, an aliquot (1 mL) of supernatant was used to measure the concentration of suspended iron in the aqueous phase. The adsorption process was observed to reach equilibrium in 2 days. The amount of ZVI adsorbed on sands was calculated by subtracting the iron left in the aqueous phase from the total iron added. Control tests were conducted with stabilized ZVI nanoparticles in the absence of sand. The iron concentration in the aqueous phase varied slightly from 95% to 106%, indicating no loss of ZVI during the control test.

3.2.6 Mathematical modeling

The transport and retention of ZVI nanoparticles was modeled using a modified one-dimensional convection-dispersion equation (Wang et al., 2008),

$$\frac{\partial C}{\partial t} + \frac{\rho_b}{\theta_w}\frac{\partial S}{\partial t} = D_H \frac{\partial^2 C}{\partial x^2} - v_p \frac{\partial C}{\partial x} \quad (3\text{-}1)$$

where C is the ZVI concentration in the aqueous phase, S is the ZVI concentration in the solid phase, x is the distance along the column from the inlet, t is the time, D_H is the

hydrodynamic dispersion coefficient, v_p is the pore velocity, ρ_b is the bulk density and θ_w is the water content, which is equal to porosity under saturated conditions. The kinetics of ZVI nanoparticles retention was expressed as follows:

$$\frac{\rho_b}{\theta_w}\frac{\partial S}{\partial t} = k_{ads}\psi C + k_{flt}C - \frac{\rho_b}{\theta_w}k_{det}S \quad (3\text{-}2)$$

k_{ads} is the first-order adsorption coefficient of ZVI nanoparticles, k_{flt} is the first-order filtration coefficient of ZVI nanoparticles which is governed by the interception, gravitational sedimentation and Brownian diffusion and k_{det} is the first-order detachment coefficient.

Under our experimental conditions, a sharp decrease of ZVI concentration after elution with the background solution without any significant tailing indicated that the release of ZVI from the sand grains was negligible and the detachment coefficient k_{det} approached zero (Wang et al., 2008). Therefore Eq. 3-2 could be written as

$$\frac{\rho_b}{\theta_w}\frac{\partial S}{\partial t} = k_{ads}\psi C + k_{flt}C \quad (3\text{-}3)$$

Ψ is a blocking function to describe the available attachment sites on the collectors, which is described by:

$$\psi = \frac{S_{max}-S}{S_{max}} \quad (3\text{-}4)$$

where S_{max} is the maximum solid concentration. The value of S_{max} is determined through a ZVI sorption isotherm study as the adsorbed amount of ZVI which is in equilibrium with the ZVI effluent concentration. A kinetics analysis of batch adsorption tests is performed to determine the rate constant of ZVI nanoparticles adsorption k_{ads} using the modified Eq. 3-3 as follows:

$$M\frac{\partial S}{\partial t} = k_{ads}\frac{S_{max}-S}{S_{max}}CV \quad (3\text{-}5)$$

where M is the total mass of sand in the batch tests, V is the volume of the CMC-ZVI suspension. The Hydrus-1D code was then used to fit the experimental breakthrough curves obtained in this study to obtain the attachment coefficient k_{flt}.

3.3 Results and Discussion

3.3.1 Transport and deposition of CMC-stabilized ZVI nanoparticles

Previous studies have shown that CMC could effectively prevent zero valent iron nanoparticles from agglomeration and facilitate the in-situ mobility of ZVI through the porous media (He et al., 2007; He et al., 2010). **Figure 3-1** presents the effluent breakthrough curves of CMC-stabilized ZVI nanoparticles through saturated columns packed with quartz sand, iron oxide coated sand and aluminum oxide coated sand. Iron and aluminum oxide were selected because they are the common impurities on the sand matrix and the main sources of surface charge heterogeneity. The symmetrical shape of the breakthrough curves for bromide tracer in each column suggested that there was no stagnant region in the saturated columns and no physical non-equilibrium was involved (Wang et al., 2008). The almost identical breakthrough curves of tracer tests with bromide in these 3 columns suggested no significant change in the dispersive properties of the porous medium after coating.

CMC-stabilized ZVI nanoparticles displayed superior mobility through the saturated sand columns, while their non-stabilized counterparts were unable to migrate through the sand columns due to rapid aggregation. **Figure 3-1**indicates that the breakthrough concentration of CMC-stabilized ZVI followed the order of pure sand > AOCS ≈ IOCS. The corresponding elution efficiency of ZVI nanoparticles was 93%, 80% and 78%, respectively. The higher retention of ZVI nanoparticles on IOCS and

AOCS can be attributed to the presence of positively-charged or weakly negatively-charged metal oxides on the sand, which thereby resulted in the elimination of electrostatic repulsion between ZVI nanoparticles and the porous media. Due to the presence of carboxylate and hydroxyl groups, CMC-stabilized ZVI nanoparticles carried a large negative charge under the experimental conditions, with a ζ-potential of -160 mV. As for the sands, the point of zero net charge (pznc) of the synthesized iron oxide and alumina in this study was measured to be 7.53 and 8.65, respectively, which are consistent with reported values (Atkinson et al., 1967; Kuan et al., 1998). The pznc of clean quartz sand was reported to be ~2 (Bueno et al., 1998). Therefore, under the experimental pH (7.5 ~ 8.3), both iron oxide and aluminum oxide carried a weaker negative or even slightly positive charge, as compared to a large negative charge of pure sand. Consequently, the overall surface charge, i.e. ζ-potential, of the colloidal-sized clean quartz sand at a pH of 8 and in 0.01M KCl solutions decreased from -60.5 mV to -42.3 mV and -44.5 mV after coating with iron oxide and alumina oxide, respectively.

Another possible reason would be the formation of CMC-metal chelates on the oxide-sand surface, thereby enhancing the adsorption of iron nanoparticles. It is known that CMC could be strongly bonded to an iron surface via bidentate bridging with carboxylate groups and hydrogen bonding with hydroxyl groups (He et al., 2007). In this manner, iron oxide or alumina oxide could form chelating complexes with the carboxylate groups of the CMC-stabilized ZVI nanoparticles (Joo et al., 2009), inhibiting the diffusion of the iron nanoparticles.

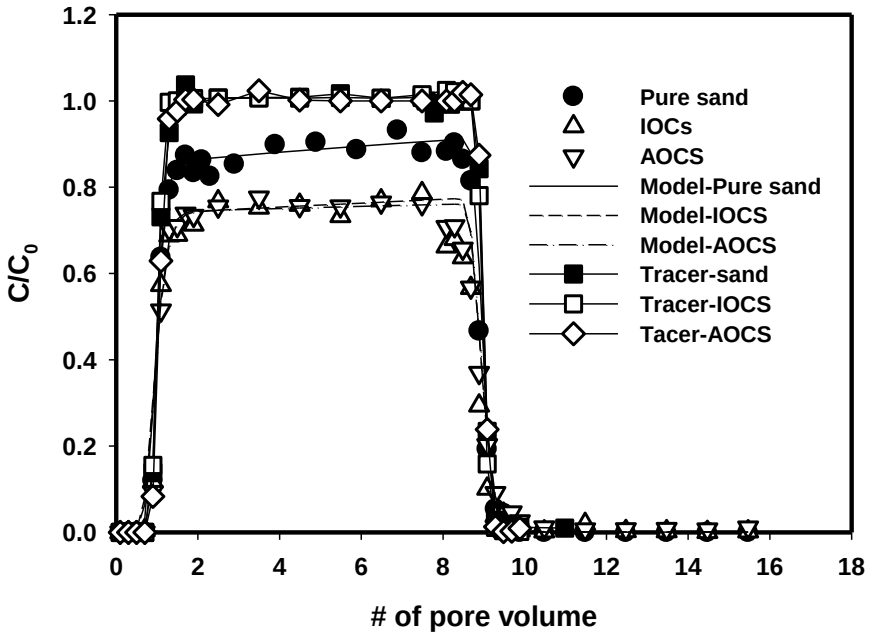

Figure 3- 1. Breakthrough curves of 0.2g/L CMC-stabilized ZVI nanoparticles in pure sand, IOCS and AOCS column. Data plotted as mean of duplicates.

It is noteworthy that the total amount of iron oxide and aluminum oxide loaded on the sand is 4.14 mg/g sand and 3.6 mg/g sand, respectively. The corresponding molar solid concentration is 0.074 mmol/g sand and 0.13 mmol/g sand. However, the deposition efficiency was almost the same. As observed, both IOCS and AOCS are not completely coated. Assuming that there is only one layer of metal oxide on the sand surface, it can be concluded that iron oxide is more effective than aluminum oxide to retain CMC-stabilized ZVI. A possible reason may be the slightly less negative charge of the iron oxide than that of the aluminum oxide under the identical conditions. Another possible explanation is that iron oxide forms stronger carboxylate chelates than those formed by aluminum oxide (Joo et al., 2009).

To further investigate the contribution of adsorption and filtration in the nanoparticles transport, additional batch tests of CMC-stabilized ZVI adsorption on different sands were performed. The resulting sorption isotherm and kinetics are shown in **Figure 3-2** and **Figure 3-3**, respectively. All sets of the CMC-ZVI nanoparticles sorption equilibrium data were analyzed in accordance with the Langmuir model using a nonlinear least-squares regression analysis according to:

$$q = \frac{bQC}{1+bC} \tag{3-6}$$

where q is the equilibrium ZVI concentration in the solid phase (in mg/g), C is the equilibrium ZVI concentration in the aqueous phase, Q is the Langmuir maximum capacity (mg/g), and b is the Langmuir affinity constant (L/mg). **Table 3-2** shows the maximum adsorption capacity (mg/g) and the affinity constant (L/mg) under the experimental conditions, i.e., with pure sand, IOCS and AOCS. As anticipated from the column results, adsorption of ZVI nanoparticles on IOCS was the highest, followed by

AOCS and then pure sand. For example, when the ZVI nanoparticles concentration stays at about 0.2 mg/L, of these 3 sands, the IOCS exhibited the greatest adsorption capacity, approaching 0.86 mg/g sand. The adsorption of ZVI nanoparticles by AOCS slightly decreased to a solid phase equilibrium concentration of 0.55 mg/g sand. The adsorption of ZVI on pure sand was considerably lower, yielding an equilibrium value of 0.119 mg/g sand.

Figure 3-3 shows the kinetics of CMC-ZVI adsorption onto the different sands. The plots represented the amounts of iron adsorbed onto the sand versus time, for an initial total iron concentration of 0.2 g/L. For pure sands, it is shown that the amount of iron sorbed per unit mass of sand decreased with an increase of the sand mass. Although the overall ZVI removal from the liquid phase increased with the mass of sands due to the more available surface area and sorption sites, the fast removal of ZVI resulted in a lower concentration in the liquid phase, yielding a decrease in the equilibrium amount of ZVI sorbed on unit weight of sands. (Nouri et al, 2007) The adsorption coefficient was determined by fitting the kinetic Eq. 3-5.

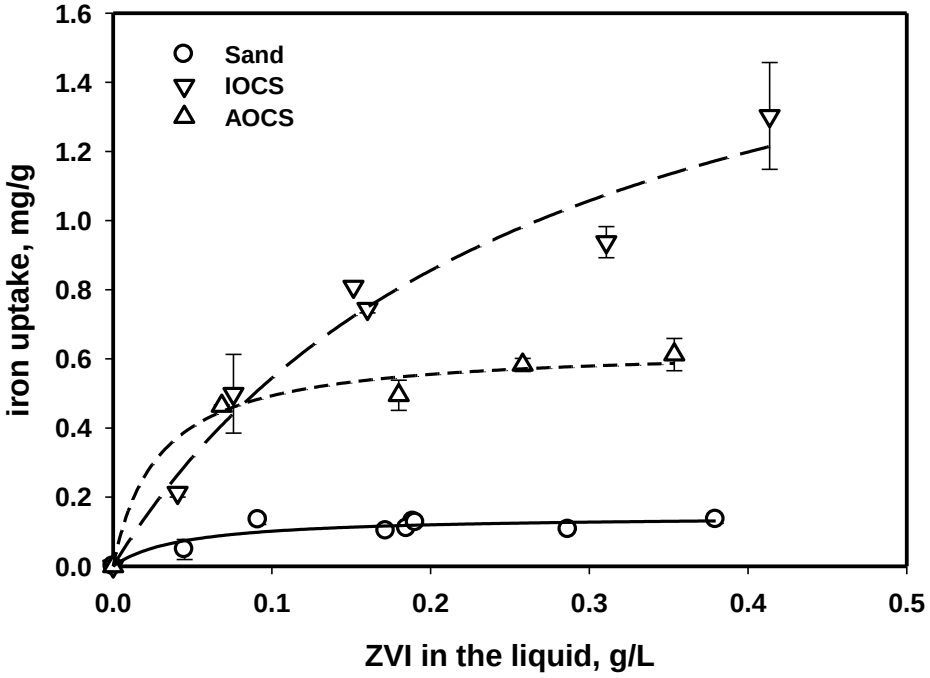

Figure 3- 2. The sorption isotherm curves of CMC-stabilized ZVI nanoparticles on pure sand, iron oxide coated sand and alumina oxide coated sand. Data plotted as mean of duplicates, error bars indicate standard deviation from the mean.

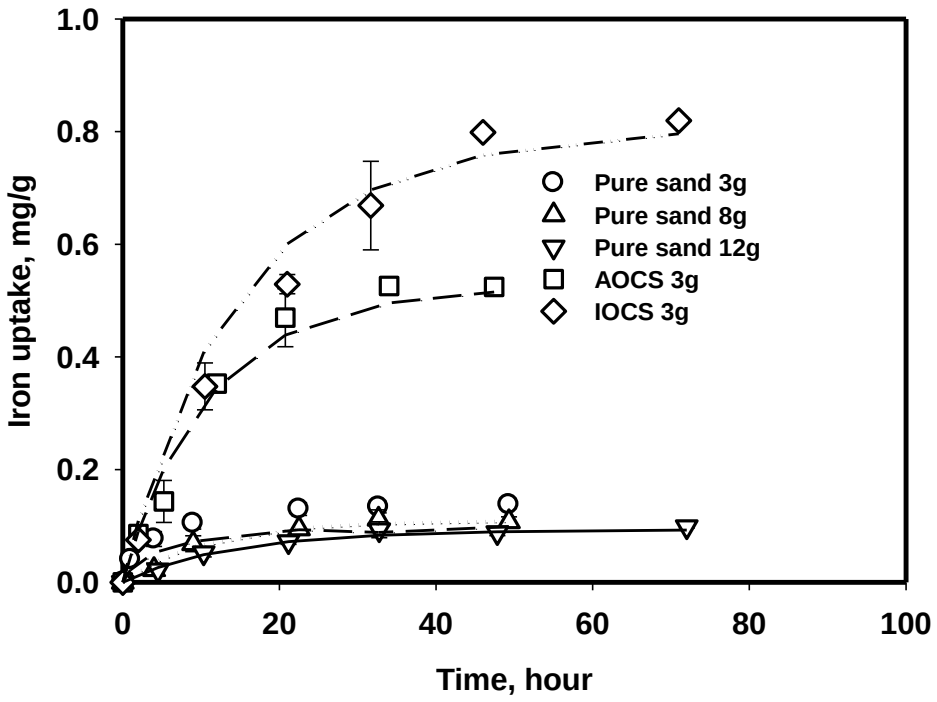

Figure 3- 3. Measured and stimulated curves of CMC-ZVI sorption kinetics with sand, iron oxide coated sand and aluminum oxide coated sand. Data plotted as mean of duplicates, error bars indicate standard deviation from the mean.

Table 3- 1. Parameters for the CMC-ZVI sorption isotherm and kinetics with different sands

Sand grains	Pore velocity, cm/s	Longtitual dispersivity, cm	Adsorption coefficient k_{ads}, h^{-1}	K_{fil}, h^{-1}
Pure sand	0.0353	0.17417	0.00953	0.647
	0.0353	0.17417	0.00942	
	0.0353	0.17417	0.00984	
	0.0706*	0.17417	0.00953	0.00036
IOCS	0.0353	0.17189	0.0168	1.69
AOCS	0.0353	0.17975	0.0154	1.69

*Data was taken from He et al. (2009b)

Table 3- 2. Parameters for the CMC-ZVI sorption isotherm and kinetics with different sands

Sand grains	Mass to liquid ratio	Langmuir maximum capacity, mg/g	Langmuir affinity constant, L/mg	Adsorption coefficient k_{ads}, h^{-1}
Pure sand	3g:43mL	0.1466	22.4	0.00953
	8g:43mL			0.00942
	12g:43mL			0.00984
IOCS	3g:43mL	1.999	3.74	0.0165
AOCS	3g:43mL	0.6345	34.9	0.0154

As shown in the **Table 3-1**, the kinetic rate of sorption was almost constant with varied sand to liquid ratios, resulting in an average value of 0.0096 ± 0.0002 h^{-1}. Thus, the sorption kinetic rate seems to be independent of the mass of sands and available surface area. Combined with the values of the adsorption coefficient obtained from the batch tests, a modified filtration model was used to evaluate the effect of filtration on ZVI breakthrough in the column experiments. In these simulations, the hydrodynamic dispersion coefficient, D_H, was obtained independently by fitting the measured breakthrough curve of tracer bromide to the classic one-dimensional convection-dispersion equation.

Table 3-2 gives the values of k_{abs} and k_{fil} for the different sand columns. Both the adsorption kinetics rate constant and the filtration rate constant increased with metal oxide coated sand. However, even though the adsorption kinetic rate constants increased from 0.0095 h^{-1} for pure sands to 0.0165 h^{-1} for IOCS due to higher affinity of CMC-ZVI to the iron oxides, the filtration removal rate constant k_{fil} was still about one-order-of-magnitude higher than the adsorption kinetics rate constant for IOCS. Therefore, it can be concluded that under our experimental conditions the filtration effect played a predominant role in the ZVI retention. However, it is noted that the role of adsorption would become more significant when the flow rate increased. When the flow rate is doubled to 0.0706 cm/s, the resultant filtration coefficient from the breakthrough curves is less than 0.0036 h^{-1}, which was more than one-order of-magnitude smaller than adsorption coefficient. Increasing the flow velocity would result in a larger "shadow zone" on the collector surface down-gradient of collector grains, yielding a reduced subsequent deposition during colloid filtration (Ko and Elimelech, 2000).

3.3.2 Effect of stabilized-ZVI nanoparticles using different polysaccharides

The effect of different polysaccharide stabilizers was determined on the ZVI nanoparticles transport. On addition to CMC, starch was chosen as another polysaccharide stabilizer for ZVI. Starch is a type of polysaccharide made of α-D-glucose monomers, with a molecular formula of $[C_6H_{10}O_5]_n$. Hydroxyl groups are attached to the five-carbon atoms in the glucose monomeric units. Carboxymethyl cellulose is a derivative from cellulose made of β-D-glucose by substituting some of hydroxyl groups with carboxymethyl groups.

Adsorption of CMC on the iron surface increased the measured ζ-potential to -160 mV, while the starch-ZVI has an almost neutral surface with a ζ-potential of -4 mV. The hydrodynamic particle diameter of CMC-ZVI was 155 nm including the adsorbed polymer layer whereas the starch-ZVI nanoparticles were significantly larger with a hydrodynamic particle diameter of 303 nm. Both of the stabilized-ZVI nanoparticles exhibited sizes in the optimal range of 0.1-1 μm for an efficient transport through soil, as suggested by Zhan et al. (2008). During the experimental period of 2 hours, the hydrodynamic particle size and ζ-potential remained constant for both stabilized ZVI nanoparticles and no significant aggregation or sedimentation were observed as shown in **Figure 3-4**. These results indicate that both stabilizers counteracted the strong attractive van der Waals and magnetic forces between particles, successfully preventing particle agglomeration.

Effluent breakthrough curves of CMC-stabilized ZVI nanoparticles and starch-stabilized ZVI nanoparticles through saturated columns packed with quartz sands were presented in the **Figure 3-5**. It was observed that the mass recovered from elution was

88% and 93% for starch-stabilized and CMC-stabilized ZVI nanoparticles, respectively. Relative to the limited mobility of bare ZVI nanoparticles, both of the polysaccharide-stabilized ZVI nanoparticles displayed improved mobility of ZVI nanoparticles through the sand columns, while CMC is more effective. The effluent concentration of CMC-stabilized ZVI is 10% higher than that of starch-stabilized ZVI nanoparticles after 3 PVs. The higher retention of starch-stabilized ZVI nanoparticles on quartz sands, implies that the adsorbed layer of polysaccharide stabilizers can modify the particle mobility.

The mobility of starch-stabilized ZVI nanoparticles is attributed to the steric repulsion between sands and ZVI nanoparticles introducted by starch, considering the almost neutral surface charge of starch-stabilized ZVI nanoparticles. Tong et al. (2005) reported that the extracellular polymers on the bacteria surface could decrease the number of collisions between bacteria and collectors via steric repulsion. Vecchia et al. (2009) suggested that a high viscosity of the polymer solution, such as xanthan gum, would resist strong flow drag forces to particle motion and keep particles suspended at the center of the pore space.

Attachment of CMC onto quartz sand is considered even less probable due to the strong negative surface charge of -160 mV. At the experimental pH of ~8, the surface potential of quartz sand is also negative according to its pzc of 2.The resultant electrostatic repulsion between CMC-ZVI nanoparticles and quartz sands will further minimize particle adhesion to the sand surface and provide an unfavorable condition for iron deposition and retention.

The retention profiles of stabilized ZVI nanoparticles are presented in **Figure 3-6** as a function of distance from the inlet. Consistent with the breakthrough curves, the

retention of CMC-stabilized ZVI nanoparticles is lower than that of starch. However, its deposition with increasing distance is rather uniform. Cantrell et al (1997) also reported an almost flat retention profile of microiron in the presence of 3 polymers in sand columns. The distribution of starch-stabilized ZVI nanoparticles is non-monotonic, increasing first and then decreasing as a function of transport distance. The maximum retained concentrations were located at around 4 and 16 cm down-gradient for ZVI stabilized with CMC and starch, respectively. Straining at small pore throats which are too narrow to allow particles to pass through is not assumed to be the major reason for ZVI nanoparticles deposition. The reason is that the ratio of CMC-stabilized and starch-stabilized ZVI nanoparticles to the sand collector is 3.8×10^{-4} and 9.0×10^{-4}, which is one order of magnitude lower than the reported threshold value for the size ratio of particle and collector grain of 0.005 for straining (Bradford et al., 2004). A similar deviation from a log-linear retention profile, predicted by clean bed filtration, was observed with carboxylate-modified polystyrene latex microspheres, suggesting a spatial variation in the deposition coefficient of colloids through the columns in the presence of unfavorable deposition conditions (Li and Johnson, 2005).

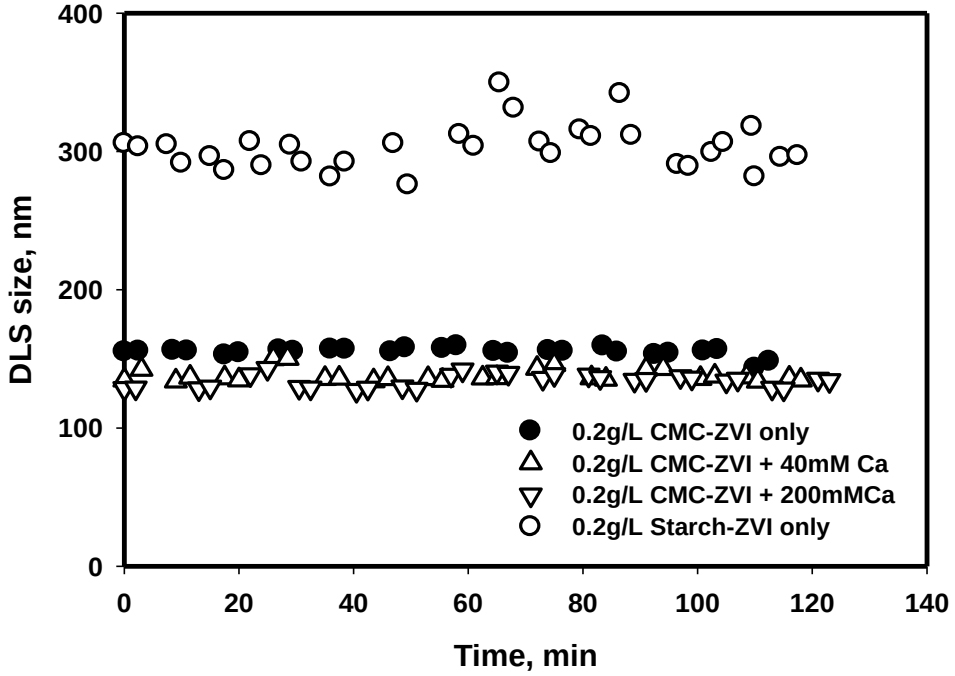

Figure 3- 4. The DLS size of starch-stabilized and CMC-stabilized ZVI as a function of time**.**

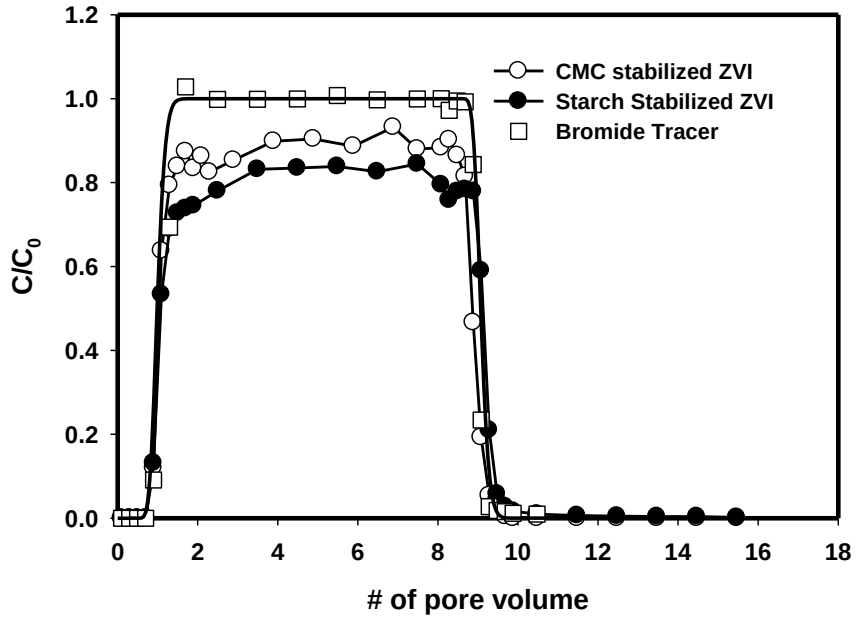

Figure 3- 5. Representative breakthrough curves for CMC-stabilized and starch-stabilized ZVI. Data plotted as mean of duplicates.

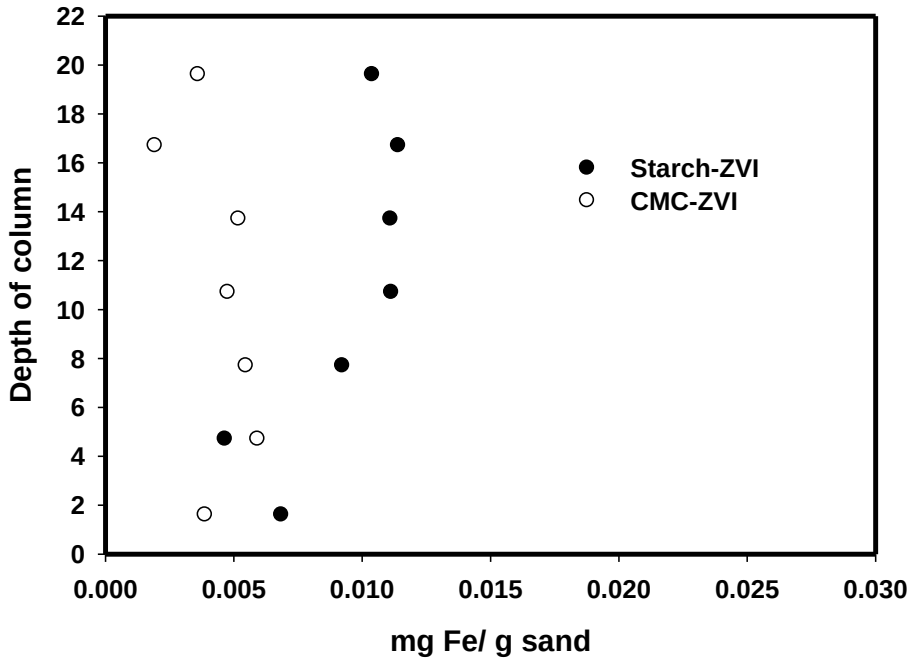

Figure 3- 6. Representative retention profiles for CMC-stabilized ZVI and starch-stabilized ZVI after background solution flush. Data plotted as mean of duplicates.

3.3.3 Effect of ZVI nanoparticles concentrations

Column experiments were conducted to investigate the effect of different concentrations on the mobility of CMC-stabilized ZVI nanoparticles, results are shown in **Figure 3-7**. The value of ZVI concentration was in a range of over one order of magnitude (from 0.05 g/L to 0.8 g/L). The effluent concentration is normalized to the input ZVI concentration to illustrate the concentration effect. It is noted that the normalized effluent concentration C/C_0 increased with the elevated inlet concentrations. At the end of ZVI injection at pore volume of 7.5, the normalized concentration of ZVI was 0.97, 0.89 and 0.83 for the initial injection concentration of 0.8 g/L, 0.2 g/L and 0.05 g/L, respectively. The traditional clean bed filtration theory did not include the concentration effect directly. This resultant diminished deposition efficiency with nanoparticles concentration might be attributed to the "blocking" effect due to a limited surface capacity of porous media for particle deposition (Bradford and Bettahar, 2006; Camesano and Logan, 1998; Tan et al., 1994). These deposited CMC-ZVI would might occupy the available surface area of the sand and subsequently block further deposition of CMC-ZVI nanoparticles due to the electrostatic repulsion. A higher concentration of ZVI would result in a more rapid surface coverage of nanoparticles on the sands and lead to a more significant "blocking" effect.

It is noted that under the experimental influent concentration from 0.05 g/L to 0.8 g/L, the effluent concentration did not stay at a constant plateau but slightly increase with time, which also indicates the occurrence of a declined deposition rate probably due to blocking. Phenrat et al. (2009) reported that under a high concentration of 1-6 g/L nanoiron stabilized by physisorption of poly(styrene sulfonate) the particle deposition

efficiency remained invariant with changing iron concentration, which apparently seems contradictory to our observations. However, it should be noted that in his study the iron nanoparticles were not well stabilized and agglomeration of ZVI nanoparticles was observed.

Previous studies have suggested that particle transport in porous media would be enhanced by changing the colloid concentration. Camesano et al. (1999) observed that the effluent concentration increased when injecting more than 10^9 fluorescent carboxylated latex microspheres through an Arizona soil column, along with an increase in the fraction of the surface covered by colloids. Bradford and Bettabar (2006) also demonstrated a higher mass recovery of fluorescent latex microspheres with an increase of inlet colloidal concentration and attributed it to the strong repulsive interactions at a high concentration between colloids in the solution and colloids retained on the collectors.

3.3.4 Effect of Ionic strength

Colloid suspensions used in this test were thermodynamically unstable but kinetically stable over the experiment time. With the addition of 40 mM, 100 mM and 200 mM $CaCl_2$, the zeta potential changed to -24.7 mV, -19.2 mV and -16.3 mV as compared to -160mV without $CaCl_2$. That is consistent with the prediction of the original Derjaguin-Landau-Verwev-Overbeek (DLVO) theory: a high ionic strength decreases the electrical double layer energy and reduces the surface charge. The particle size also decreased slightly from 155 nm to 130.5 nm with 40 mM $CaCl_2$, 127.5 nm with 100 mM $CaCl_2$ and 125.3 nm with 200 mM $CaCl_2$, which might be due to formation of calcium-dicarboxylate cross-links (Feng and Pelton, 2007; Konradi and Ruhe, 2005). The presence of divalent calcium ions could bridge carboxyl groups and decrease the swelling

of CMC molecules, which results in shrinkage of the swollen macromolecular layer on the ZVI nanoparticles surface (Konradi and Ruhe, 2005). However, there is no obvious aggregation formed in the presence of extra $CaCl_2$. As shown in **Figure 3-4**, the particle size barely changed within two hours even with the addition of 200 mM $CaCl_2$.The high stability of ZVI nanoparticles is attributed to the steric repulsive force due to the presence of an extended macromolecular layer of CMC on the surface of ZVI nanoparticles.

Addition of $CaCl_2$ did not yield significant differences in the breakthrough curves when comparing the effluent concentrations, as shown in **Figure 3-8**. Values of C/C_0 of 0.89 and 0.86 were obtained with 40 mM and 200 mM $CaCl_2$ at the pore volume of 7.5. Only a slightly decrease occurred for the effluent concentration. Despite the a significant decrease in electrostatic repulsion, the presence of CMC as the stabilizer maintained the stability of ZVI particles even under elevated ionic strengths due to steric repulsion forces. This result is consistent with other researches using steric stabilization. Jiang et al. (2009) reported that sterically stabilized quantum dots remained suspended even in a water solution of 0.15 M ionic strength. Kim et al. (2010) also suggested that steric repulsion as a result of the macromolecules on occyst surface could successfully decrease the bacteria retention in a sand column at the ionic strength of 100 mM, which is even supposed to be electrostatic favorable condition based on DLVO calculations. Sirk et al. (2009) reported that elevated ionic strengths from 1 mM to 50 mM had little effect on adhesion of a triblock copolymer-modified RNIP to silica.

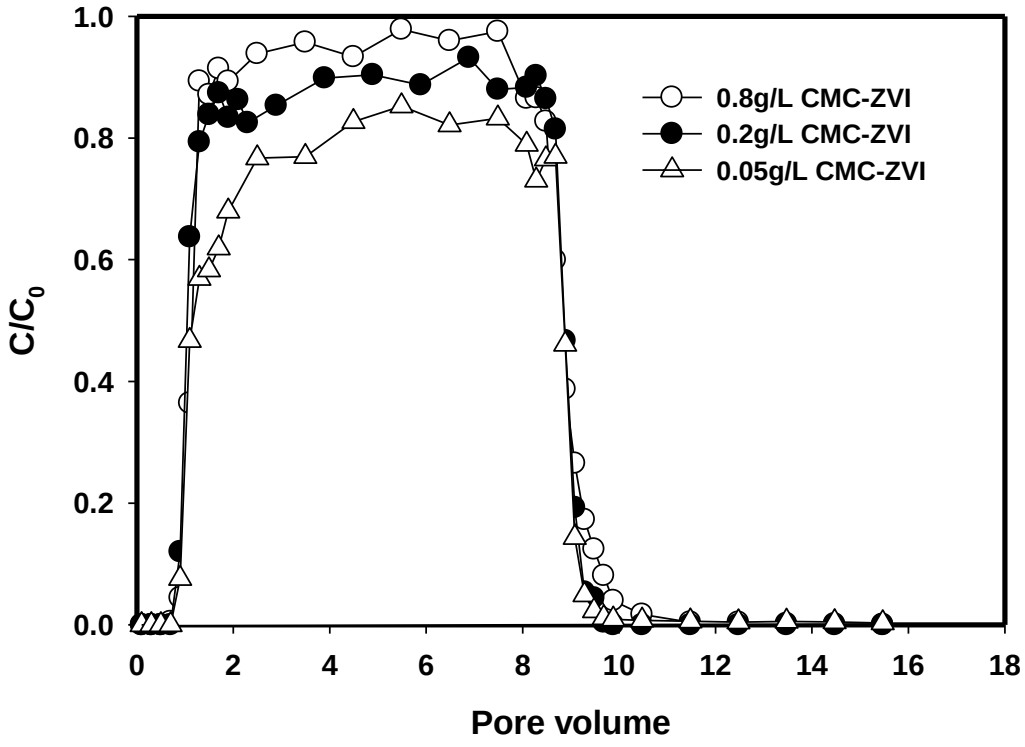

Figure 3- 7. Breakthrough curves of different concentrations of CMC-stabilized ZVI nanoparticles in sand columns. Data plotted as mean of duplicates.

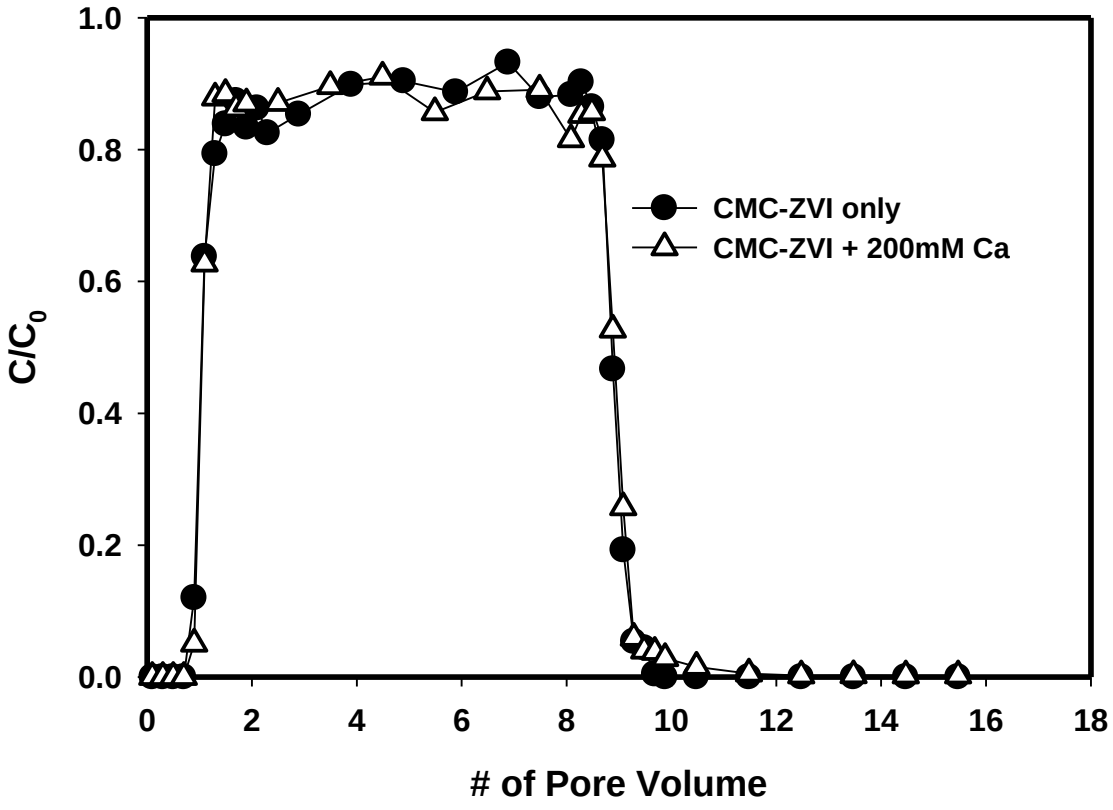

Figure 3- 8. Breakthrough curves of 0.2 g/L CMC-stabilized ZVI nanoparticles in sand columns without and with 200 mM $CaCl_2$. Data plotted as mean of duplicates.

3.3.5 Effect of natural organic matter

Natural organic matter obtained from extraction of a potting soil was used to investigate the NOM effect on the CMC-stabilized ZVI breakthrough behavior in quartz sand, as shown in **Figure 3-9**. The concentration of NOM is expressed in terms of the content of total organic carbon. It is observed that the effect of NOM on the transport of CMC-stabilized ZVI through sand columns was not pronounced. When the NOM concentration increased from 0 to 40 mg/L TOC, the breakthrough concentration C/C_0 of ZVI after 7.5 P.V. slightly decreased from 0.89 to 0.86. However, when the NOM concentration continued to increase to 80 mg/L TOC the C/C_0 rose up to 0.93.

Other researchers reported that NOM could enhance colloidal transport for hematite (Kretzschmar and Sticher, 1997), Titanium dioxide (Domingos et al., 2009) and latex particles (Davis et al., 2002; Pelley and Tufenkji, 2008) due to a surface modification. In their cases, negatively charged NOM was absorbed on the surface of colloids as a type of stabilizer or even on the porous media, and further decreasing colloid attachment due to electrostatic and steric repulsions. An improved mobility of RNIP, a commercial ZVI nanoparticles, was reported by Johnson et al. (2009) after the adsorption of NOM.

In this study, CMC-stabilized ZVI was used and there was a fairly dense layer of polyelectrolyte CMC on the surface of ZVI, whose ζ -potential is -160 mV. After adding NOM, the zeta potential decreased slightly to -150 mV and -151 mV with 40 mg/L TOC and 80 mg/L TOC. The molecules of NOM may approach the surface of ZVI nanoparticles through the loosely-adsorbed CMC layer and adsorb on the ZVI via surface

complexation, which subsequently altered the surface charge of iron (Giasuddin et al., 2007)

The decreasing electrostatic repulsion between ZVI particles and quartz sand is expected to result in an increase of ZVI attachment rate on sand.

When NOM further increased from 40 mg/L TOC and 80 mg/L TOC, it is noted that the ζ- potential did not change much, however, the breakthrough concentration increased from 0.86 to 0.93. This might be attributed to the competition for the attachment sites between NOM and CMC-stabilized ZVI. As measured, the ζ- potential of the macromolecules in a NOM solution is -20.1 mV. Adsorption of NOM on washed quartz sand was not expected because of electrostatic repulsions between the negative charged colloids and the negative-charged sands. However, the competitive adsorption of NOM on sands could occur via retention in secondary energy minimum wells. Particle deposition in a deep secondary energy minimum well is commonly suggested to control the transport of colloids and bacteria in porous media under an unfavorable electrostatic conditions (Bradford et al., 2009; Kim et al., 2010; Redman et al., 2004; Tufenkji and Elimelech, 2004) Based on the DLVO theory, the sum of van der Waals and electrostatic interactions between particles will result in primary or secondary minimum sections, where the attractive force dominates. Under unfavorable conditions, when colloids approach to the collector surface, they could be captured in the second minima before meet the repulsive barrier if the second minima is deep enough (Hahn and O'Melia, 2004; Shen et al., 2007a). Compared to CMC-stabilized ZVI nanoparticles, NOM molecules may be more accessible for secondary energy minimum disposition due to their small molecular size and overcome electrostatic repulsion.

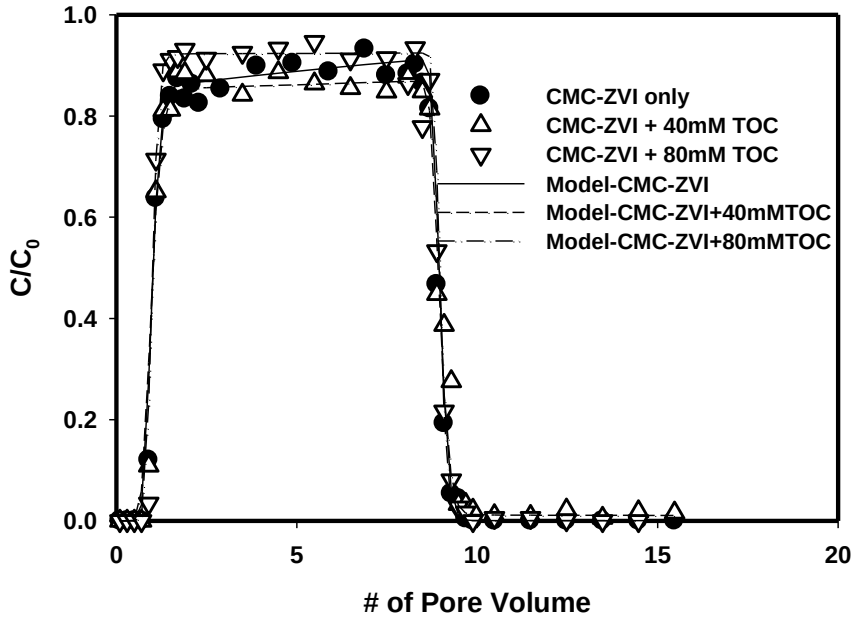

Figure 3- 9. Breakthrough curves of 0.2g/L CMC-stabilized ZVI nanoparticles in sand columns with various concentration of natural organic matter. Data plotted as mean of duplicates.

3. 4 Conclusions

The transport behavior of zero valent iron nanoparticles under various surface and solute conditions have great implications for their in-situ application on contaminant remediation. Our experimental results indicated that CMC would effectively facilitate the transport of ZVI nanoparticles through sand columns. The presence of mineral oxides such as iron oxide and aluminum oxide could increase the retention of ZVI. A mathematical model that incorporates non-equilibrium adsorption kinetics and filtration kinetics revealed that filtration played a substantial role in ZVI nanoparticles transport under a low flow velocity; however, at a high injection velocity adsorption would dominate the deposition behavior of CMC-ZVI nanoparticles. Another polysaccharide, starch, was used to stabilize ZVI nanoparticles and improved their deliverability with an elution rate of 88%. A lower retention of CMC-stabilized ZVI nanoparticles was observed when increasing the influent concentration from 0.05 g/L to 0.8 g/L. Ionic strength did not significantly alter the transport behavior of CMC-stabilized ZVI, even with 200 mM $CaCl_2$, indicating a robust stabilization. The deposition of CMC-stabilized ZVI changed slightly in the presence of 40 mg/L and 80 mg/L NOM as TOC.

These results indicate that ZVI nanoparticles could possess great mobility and deliverability via surface modification. Both surface modification and solution chemistry must be considered to accurately predict the ZVI transport behavior in the subsurface area.

CHAPTER 4. Catalytic Hydrodechlorination of Trichloroethylene in Water with Supported CMC-Stabilized Palladium Nanoparticles

4.1 Introduction

Contamination of water and soil by chlorinated solvents has been a major environmental problem worldwide for nearly a century (Doherty, 2000a; Doherty, 2000b; Orth and Gillham, 1995; Squillace et al., 2004). For example, TCE and PCE, both being potent carcinogens, have been identified in 405 and 320 sites designated by ATSDR in 2011, respectively (Agency for toxic substances and Disease Registry, 2007). To mitigate human exposure, the U.S. EPA has set a maximum contaminant level (MCL) of 5 μg/L for both TCE and PCE in drinking water (U.S. EPA, 2009).

Catalytic hydrodechlorination has been one of the most promising technologies for complete destruction and abatement of a wide range of chlorinated aliphatic and aromatic compounds in both gas and liquid phases (Marques et al., 1993). One of the most frequently used catalysts has been palladium (Pd), which is very active under ambient pressure and temperature (He et al., 2009a; Keane, 2004). Palladium is well known to facilitate C-Cl bond cleavage and reactive atomic hydrogen formation at the metal surface (Kulkarni et al., 1999; Sriwatanapongse et al., 2006). Lowry and Reinhard (1999) demonstrated that a commercial Pd-on-alumina (Pd/Al_2O_3) catalyst was able to catalyze the hydrodechlorination of TCE, resulting in direct conversion of TCE to ethane without intermediate products. Using in-situ surface-enhanced Raman spectroscopy, Heck et al. (2008) studied the hydrodechlorination of 1,1-dichloroethene catalyzed by Pd

particles loaded on Au nanoshells in water. They observed formation of Cl-Pd and C-Pd bonds and the appearance of vinyl/ethyl species on the metal surface with time, confirming that the degradation process was a sequence of dechlorination and hydrogenation.

Pd as a catalyst has also shown promising activity for in-situ remediation of contaminated groundwater and wastewater (Hildebrand et al., 2009). McNab et al. (2000) carried out a field demonstration study on the catalytic hydrodechlorination with commercial Pd/alumina beads. The researchers demonstrated that the catalyst used in a column configuration was able to effectively facilitate hydrodechlorination of various chlorinated hydrocarbons in groundwater for a test period of one year. Toxic intermediate products such as vinyl chloride, a common toxic intermediate product in biological dechlorination, were not observed. The catalytic activity of Pd was maintained over an extended time through periodic aeration to regenerate the catalysts.

Scaling down Pd particles to the nanoscale is an emerging method to enhance its catalytic property. Nanoscale Pd has been found to offer much greater catalytic activity than conventional Pd powders. Such activity enhancement has been attributed to a number of factors, including: 1) much greater specific surface area of the nanoparticles (Huang et al., 2008; Roucoux et al., 2002), 2) weaker adsorption of reactants to the catalytic sites (Zhou et al., 2010), and 3) greater fraction of more active Pd atoms on the catalyst surface (Li et al., 2002).

However, nanoscale Pd particles are thermodynamically unstable in solution and tend to aggregate into larger particles. Consequently, a stabilizer or a supporting template is often required to acquire stable and discrete Pd particles. To this end, various

stabilizers and templates such as carboxymethyl cellulose (CMC) (He et al., 2009a), polyvinylpyrrolidone (PVP) (Li et al., 2002), dendrimers (Scott et al., 2004), surfactants (Pal et al., 1997), and microgels (Mei et al., 2007) have been tested. However, for practical applications (e.g., for treatment of contaminated water), the stabilized Pd nanoparticles, once dispersed in water, are difficult to separate from the aqueous phase. To overcome this drawback, Pd nanoparticles are often immobilized on a catalyst carrier.

In industrial catalysis, various materials have been used as catalyst carriers, such as alumina, silica, titania, and activated carbon (Bond, 1991). A catalyst carrier not only serves as a supporting template to disperse the catalyst particles against aggregation, but also enhances the reactivity of the catalyst metal (Zheng et al., 2011). Judai et al. (2003) reported that a single Pd atom on MgO support can catalyze acetylene polymerization, while an ensemble of seven Pd atoms would be needed with unsupported single-crystals for the reaction to occur. The researchers attributed the elevated activity of MgO-supported Pd atoms to an increased electron density induced by the MgO substrate.

Deposition of nanoparticles on supports can better control the structure and size of the catalysts. Scott et al. (2004) prepared titania-supported Au-Pd bimetallic nanoparticles, where dendrimer-encapsulated Au-Pd nanoparticles were prepared first and then loaded on the oxide support via the wet impregnation method. Chou et al. (2004) prepared supported Au nanoparticles using TiO_2 and ZnO supports for CO oxidation and propylene hydrogenation. The researchers observed that in the presence of a polymer stabilizer, the nanoparticles are well separated and dispersed on the supports. To avoid causing additional diffusion resistance through the polymer network (Mei et al.,

2007), the stabilizer is usually removed through thermal calcination (Scott et al., 2004) or oxidation treatment (Crespo-Quesada et al., 2011) upon particle immobilization.

It has been known that the catalytic activity of Pd can be inhibited by competing electron acceptors (nitrite, DO, carbonate) in groundwater and/or via blockage of active sites by sulfur and sulfide (Lowry and Reinhard, 2000; Lowry and Reinhard, 2001; Munakata and Reinhard, 2007). For example, Lowry and Reinhard (2000) reported that the presence of 87 mg/L SO_3^{2-} or 0.4 mg/L HS^- can rapidly deactivate a Pd-on-γ-Al_2O_3 catalyst. However, the effect of natural organic matter (NOM) on catalytic TCE dechlorination has not been well investigated. Chaplin et al. (2006) reported that humic acid at a concentration of 3.3 mg/L as carbon decreased the NO_3^- reduction rate by 83% due to humic acid adsorption on an alumina supported Pd-Cu catalyst .

In our previous work, He et al. (2009a) and Liu et al. (2008) developed an approach for preparing stabilized Pd nanoparticles using CMC as a stabilizer. The resultant Pd particles exhibited a mean particle size of 2.4 nm. When applied for the hydrodechlorination of TCE in water, the water dispersed nanoparticles demonstrated an extraordinary catalytic activity with an observed pseudo-first order rate constant (k_{obs}) of 828 L/g/min, as compared to 0.42 L/g/min for bulk Pd (Nutt et al., 2005). However, the application of these highly reactive nanoparticles for water treatment would be limited due to the difficulty in separating the dispersed nanoparticles from the solution phase.

To utilize the unique reactivity of the stabilized Pd nanoparticles for water treatment uses, we prepared a new class of supported Pd catalysts by immobilizing CMC-stabilized Pd nanoparticles onto various representative carrier materials, including alumina, a carbonaceous resin Ambersorb 572 and a titanium-silicalite zeolite (TS-1).

While detailed material characterization has been reported elsewhere (Bacik et al., 2012), this current study aimed to: 1) characterize the catalytic activity of the immobilized CMC-stabilized Pd nanoparticles for hydrodechlorination of TCE in water; 2) test the effect of Pd particle size on the particle reactivity; 3) examine the effect of the physical properties (especially hydrophobicity) of the carrier materials on the reactivity; and 4) evaluate the effect of dissolved natural organic matter (DOM) on the catalytic activity.

4.2 Experimental section

4.2.1 Materials

Sodium tetrachloropalladate (II) trihydrate ($Na_2PdCl_4 \cdot 3H_2O$, 99%) was purchased from Strem Chemicals (Newburyport, MA, USA). Sodium carboxymethyl cellulose (NaCMC, M.W. = 90,000, SLR Grade) and trichloroethylene of spectrophotometric grade (>99%) were obtained from Acros Organics (Fair Lawn, NJ, USA) and Aldrich Chemical Company (Milwaukee, WI, USA), respectively. Hexanes (pesticide grade) and methanol (ACS grade) were purchased from Fisher Scientific (Fairlawn, NJ, USA). UHP grade hydrogen gas was acquired from Airgas South (Opelika, AL, USA). γ-alumina (1/8") and titanium silicalite zeolite (TS-1) (O.D.=1/16", Length=1/16"~1/4") were received as pellets from Alfa Aesar (Ward Hill, MA, USA) and Sud-Chemie (Louisville, KY, USA), respectively. Prior to use, the pellets were ground and sieved to a final size range of 212-355 μm. A carbonaceous resin (Ambersorb 572) with surface area of 1100 m^2/g was used as received from Rohm & Haas (Midland, MI, USA). Lab-produced deionized (DI) water was for preparing all solutions. Dissolved NOM was obtained by extracting a natural potting soil (HYPONEX®, OH, USA) purchased from a local Wal-Mart store (Auburn, AL, USA). The extraction was performed by mixing 500 g of the

soil with 0.5 L DI water for 2 weeks. Then, the slurry was centrifuged at 400 G-Force for 20 min, and the resultant supernatant was then filtered through a 0.45 μm membrane. The dissolved NOM was quantified by measuring the total organic carbon (TOC) with a Shimadzu TOC-VCPN analyzer (Columbia, MD, USA).

4.2.2 Preparation of supported CMC-stabilized Pd nanoparticles

The CMC-stabilized Pd nanoparticles were first prepared following the method by He and his coworkers (He et al., 2009a). In brief, 100 mL of a CMC solution was prepared in each batch at room temperature. Then 1 mL of a 0.05 M $Na_2PdCl_4 \cdot 3H_2O$ solution was added into the 100 mL CMC solution, and mixed for 10 min under continuous magnetic stirring. Next, 3.6 mL of a 0.05 M sodium borohydride solution was added dropwise into the Pd-CMC solution under magnetic stirring at 700 rpm. A dark color indicates formation of CMC-stabilized Pd nanoparticles, which were allowed to grow for 24 hours. The mature CMC-stabilized nanoparticle suspension was then concentrated by a factor of 21 to ~5 mL with a rotary evaporator (Rotavapor RE 121, Buchi Labortechnik AG, Flawil, Switzeland).

Alumina, Ambersorb 572 and TS-1 were used as the Pd supports. The concentrated nanoparticle suspension was first added dropwise onto each of the support materials until the volume approached that of one pore volume. Then the mixture was dried in an oven at 80 ^oC for 24 hours under air. The loading process was repeated 8~12 times until a desired Pd loading was achieved. For the alumina support, the dried catalysts were further calcined at 500 ^oC for 5 hours in air and then reduced by H_2 at 400 ^oC for 4 hours before being used for TCE degradation tests. For the Ambersorb 572 resin, the catalyst was calcined at 300 ^oC for 4 hours under air and H_2-reduced at 300 ^oC for 3 hours prior to

use. For TS-1, Pd nanoparticles were prepared by loading 5mL of 0.01 M Na_2PdCl_4 as the precursor onto 1.6 g of TS-1, following the same calcination and reduction procedure as for the alumina supported Pd. The total Pd loading was about 0.33 wt% in all cases.

4.2.3 Physical characterization

The morphology and size distribution of CMC-stabilized Pd nanoparticles in the aqueous suspension were determined on a Zeiss ME 10 TEM (Carl Zeiss, Oberkochen, Germany) with an operating voltage of 60 kV. Fourier Transform Infrared (FTIR) spectroscopy was carried out using a PerkinElmer Spectrum 2000 spectrometer (PerkinElmer, Waltham, MA, USA) equipped with a liquid-nitrogen-cooled mercury cadmium telluride (MCT) detector. Infrared spectra were recorded at 4.0 cm^{-1} resolution in the transmission mode accumulating 500 scans. For FTIR analysis, an aliquot (1~2 mL) of the aqueous nanoparticle suspension (Pd = 0.053 mg/L, CMC=0.15 wt%) was first calcined on an aluminum pan under atmospheric environment for one hour at various temperature levels, i.e., 80 ^oC, 120 ^oC, 320 ^oC and 500 ^oC, to estimate the effect of calcination temperature on the removal of CMC adsorbed on the Pd nanoparticles. Then the samples were re-dispersed in 1~2 mL of DI water through sonicating for 5 minutes. Lastly, a drop of the resultant Pd suspensions was deposited onto an attenuated total reflection (ATR) element made from of Zinc Selenide crystals and dried at 80^oC under nitrogen gas prior to analysis. More detailed characterization of the alumina-supported CMC-stabilized Pd nanoparticles was provided by Bacik et al.(2012).

4.2.4 Hydrodechlorination of TCE

Batch tests were conducted to evaluate the effectiveness of the supported Pd nanoparticles for catalytic hydrodechlorination of TCE. First, 0.1 g of the alumina-

supported catalyst was mixed with 100 mL DI water in a 127 mL serum bottles (in duplicate) equipped with an open-top screw cap and PTFE-lined septa. Then, hydrogen gas was purged into the mixture for 20 min to saturate the aqueous phase and fill up the headspace before the reactors were capped. TCE hydrodechlorination was then initiated by injecting 25 μL of a TCE stock solution each of the reactors, yielding an initial TCE concentration of ~50 mg/L. The mixtures were then constantly stirred using a magnetic stirrer at room temperature and sampled at predetermined times by transferring 100 μL sample of the solution with a gas-tight syringe into 1 mL of hexane. TCE and potential degradation by-products in hexane were then analyzed with an HP 6890 Gas Chromatograph (Hewlett Packard, Palo Alto, CA, USA) equipped with an electron capture detector (ECD) following the method by He et al.(2009a). Control experiments were conducted using the same amount of alumina without Pd and under the same hydrogen conditions. Chloride concentration in the aqueous phase was analyzed using a Ion chromatograph DX-120 (Dionex, Sunnyvale, CA, USA) equipped with an AS14 column and a suppressed conductivity detector.

To compare the effect of the supporting materials, the degradation experiments were also carried out in a similar manner using Pd particles loaded on the Ambersorb 572 resin and TS-1 support. In these cases, TCE in both the aqueous phase and the solid phase was analyzed because of TCE adsorption on these hydrophobic supports (Note: no TCE adsorption was observed for the alumina template). At each sampling time, duplicate samples were centrifuged at 160 g-force for 3 minutes. TCE in the liquid phase was hexane-extracted and analyzed following the same GC-ECD procedure described previously. TCE sorbed on the solid phase was first extracted using 50 mL methanol in a

hot water bath at 70°C for 24 h, and then analyzed following the GC-ECD method. Separate mass balance tests indicated that TCE sorbed on these supports could be completely recovered through the one batch hot-methanol extraction.

4.2.5 Catalyst lifetime

In order to estimate the lifetime and reusability of the catalyst, the same alumina supported Pd catalyst was repeatedly used in 6 consecutive cycles of TCE hydrodechlorination. Each cycle of batch tests was conducted in the same manner as described above with a 100 mL solution, and TCE degradation kinetics was monitored for 30 min in each batch test. After each test cycle, both samples used in the duplicate experiments were centrifuged at 160 g-force for 3 minutes to separate the catalyst from the aqueous phase. Then, ~ 93 mL of the solution in each reactor was replaced with the same volume of fresh DI water. Upon hydrogen purging, a new cycle of TCE hydrodechlorination was started by injecting the same mass of TCE into the reactor. To determine any possible Pd bleeding or dissolution during the tests, aqueous samples were acidified and analyzed for Pd using an Inductively Coupled Plasma-Optical Emission Spectrometry instrument (Varian 710-ES, Varian, Walnut Creek, CA, USA).

4.3 Results and discussion

4.3.1 Catalyst characterization

To prevent particle aggregation, 0.053 g/L Pd nanoparticles were synthesized in the presence of 0.005 wt%, 0.05 wt % and 0.15 wt % of CMC, respectively. **Figure 4-1** shows the TEM images of the CMC-stabilized Pd nanoparticles. Based on analysis of ~5000 Pd nanoparticles, the size of the stabilized Pd nanoparticles was determined to be 4.3 ± 1.6 nm (mean ± SD), 2.8 ± 0.9 nm, and 2.7 ± 0.8 nm for the three CMC levels,

respectively. Evidently, the nanoparticles prepared with higher CMC concentration are smaller and of narrower size distribution.

The alumina supported CMC-stabilized Pd nanoparticles were subjected to calcination and reduction to remove CMC and enhance Pd particle immobilization. To optimize the calcination temperature, we examined band changes of FTIR spectra for CMC-stabilized Pd nanoparticles calcined at 80 ^{o}C, 120 ^{o}C, 320 ^{o}C and 500 ^{o}C, respectively. Previous studies of CMC-stabilized Pd nanoparticles revealed that CMC interacts with the Pd nanoparticles via its carboxylate (-COO^-) and hydroxyl (-OH^-) groups (Liu et al., 2008). **Figure 4-2a** shows the FTIR spectra of CMC-Pd nanoparticles calcined at 80°C. Two bands at 1416 cm^{-1} and 1599 cm^{-1} were observed, corresponding to the symmetric $\nu_s(COO^-)$ and asymmetric $\nu_{as}(COO^-)$ stretches due to the presence of carboxylate groups on the surface of Pd nanoparticles. The wave number separation of these two bands was about 183 cm^{-1}, confirming the bidentate bridging mode between the carboxylate group and Pd. The absorption peak at 3332 cm^{-1} is ascribed to the –OH stretching vibration, which suggests the existence of hydrogen bonding between the CMC molecules and Pd particle surface. When the calcination temperature was increased to 120 °C, the stretching bands for both carboxylate and hydroxyl groups remained nearly the same (**Figure 4-2b**) as at 80°C. However, upon calcination at 320°C, the hydroxyl stretch was almost flattened (**Figure 4-2c**). Meanwhile, the absorption bands of the carboxylate group were markedly weakened and shifted from 1416 cm^{-1} to 1404 cm^{-1} for the symmetric stretch and 1599 cm^{-1} to 1584 cm^{-1} for the asymmetric stretch, indicating a much diminished interaction between carboxylate groups and Pd. When calcined at 500 °C, the peak for asymmetric carboxylate stretch completely vanished and a boarder peak

at 3380 cm^{-1} became evident and new peaks arose in the range of 650 ~ 1500 cm^{-1}, suggesting that decomposition of CMC had occurred. Thermogravimetric analysis (TGA) of CMC decomposition under air indicated that at 500 °C approximately 44 % of CMC weight remained in the sample (Nadagouda and Varma, 2007), indicating the presence of carbonaceous products from the CMC decomposition. The three absorption bands observed at 1380, 938 and 688 can be assigned to the $-CH_2$ scissoring mode (Biswal and Singh, 2004), $-CH_2$ rocking vibration (Schmelz et al., 1959), ring stretching and ring deformation of α-D-(1-4) and α-D-(1-6) linkages (Wang and Somasundaran, 2005). The calcination temperature of CMC for alumina-supported Pd catalysts in this study was set to be 500 °C, considering that CMC is decomposed at this temperature. Baker et al. (2005) reported that even when pyrolyzed at 900 °C in 10 % oxygen in nitrogen, 16% of the CMC original weight still remained. Calcination at extremely high temperatures and complete removal of CMC is not desired in this study to avoid the risk of losing the Pd catalytic activity due to particle sintering and growth (Carter et al., 1966).

The BET surface area for the bare alumina support was measured to be 92.1 m^2/g after calcinations at 500 °C. This value agrees with the value of ~100 m^2/g provided by the manufacturer for virgin alumina pellets. However, after calcination the BET surface area decreased to 82, 85 and 78 m^2/g upon loading of Pd nanoparticles stabilized with 0.005, 0.05 and 0.15 wt% CMC, respectively. Apparently, the stabilized Pd nanoparticles were able to diffuse into the mesopores of the alumina support and block some internal pores (Babu et al., 2007). TEM images of the alumina supported catalyst did not reveal Pd clusters on the alumina surface, suggesting a high dispersion of Pd nanoparticles on the support surface and inside the pores.

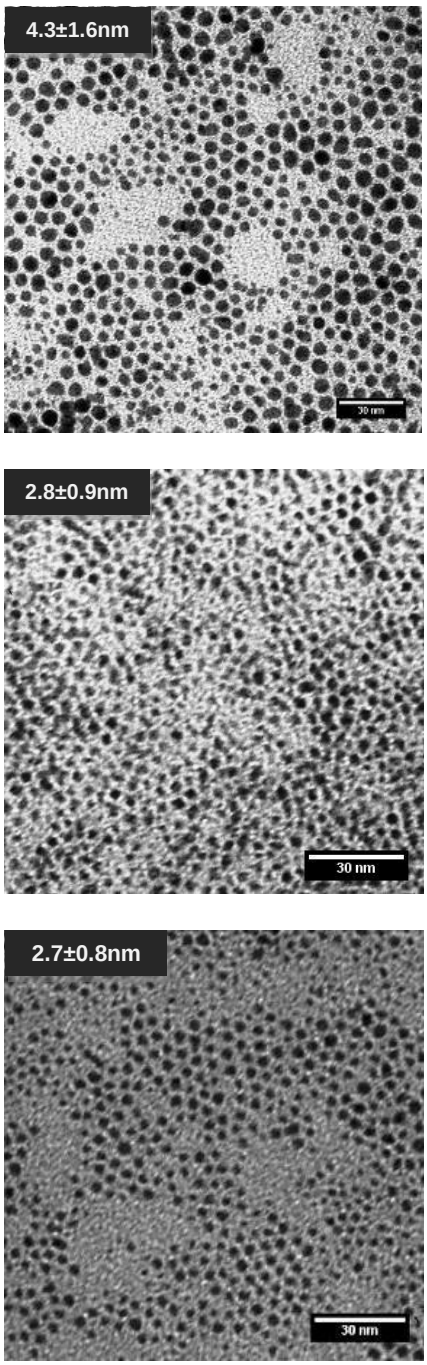

Figure 4-1. TEM images of Pd nanoparticles synthesized using (a) 0.005 wt% CMC, (b) 0.05 wt% CMC and (c) 0.15 wt% CMC in the aqueous phase at 23^{o}C. Catalyst preparation and characterization were performed by Deborah Bacik (A collaborative paper was submitted).

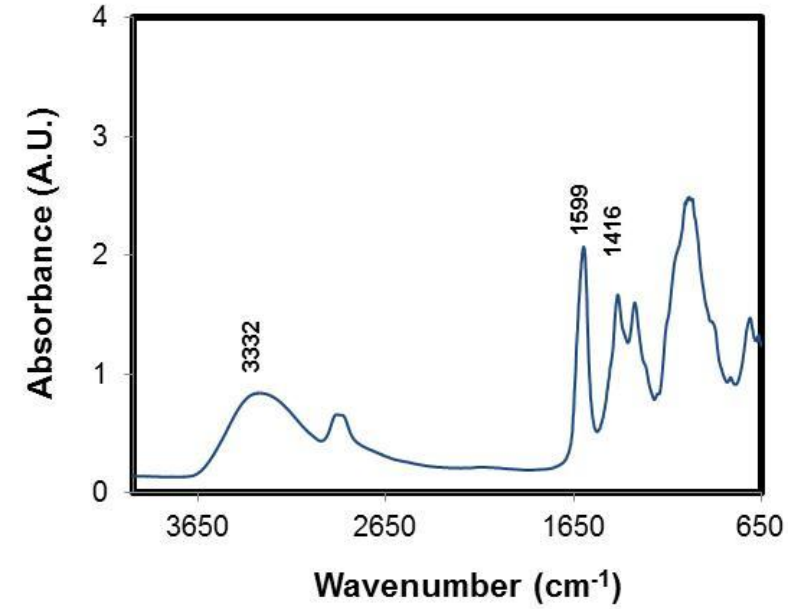
Absorbance (A.U.)
Wavenumber (cm-1)
3332
1599
1416
0
1
2
3
4
3650
2650
1650
650

(a)

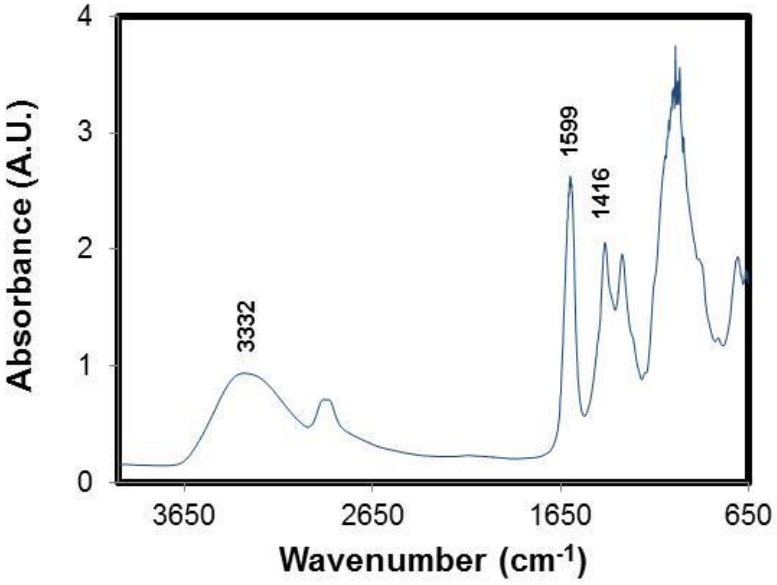
Absorbance (A.U.)
Wavenumber (cm-1)
3332
1599
1416
0
1
2
3
4
3650
2650
1650
650

(b)

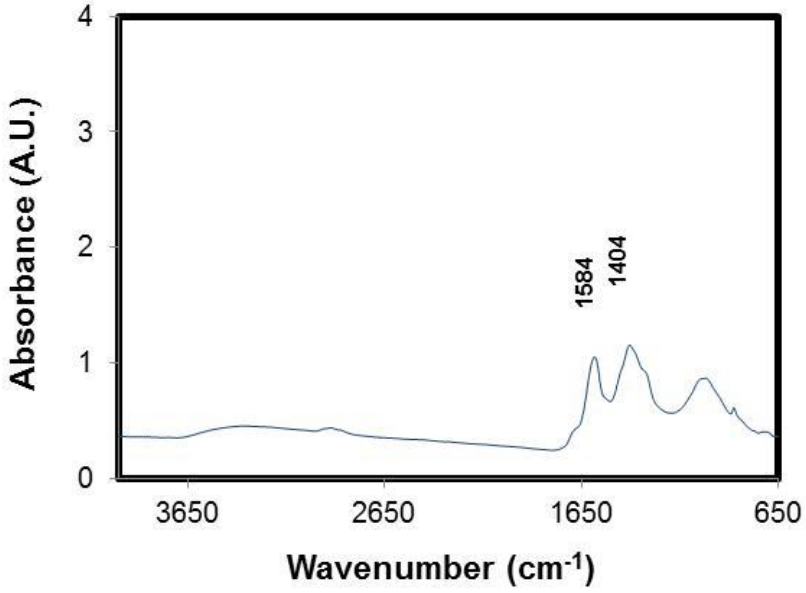

(c)

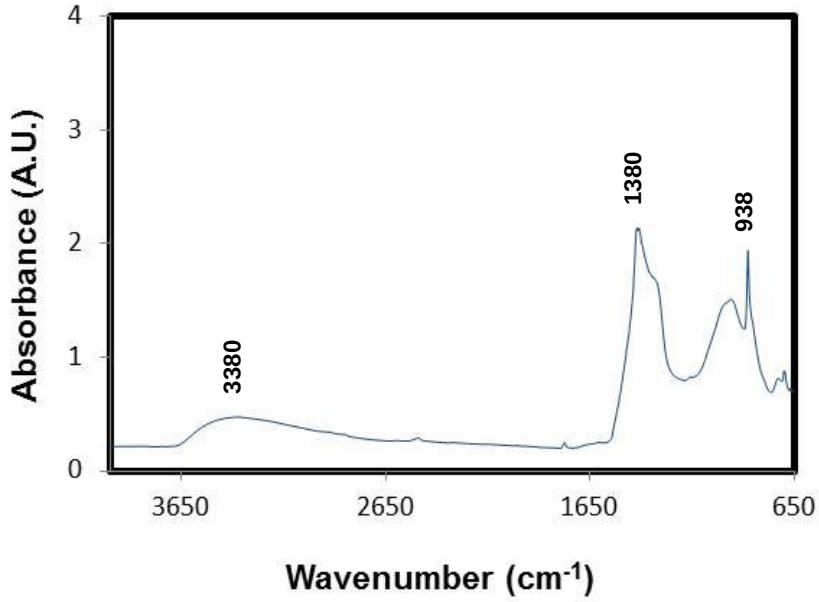

(d)

Figure 4-2. Change of FRIR spectra of 0.15% CMC-stabilized Pd nanoparticles calcined at: **(a)** 80°C, **(b)** 120°C, **(c)** 320°C, and **(d)** 500°C. Catalyst preparation and characterization were performed by Deborah Bacik (A collaborative paper was submitted).

4.3.2 Catalytic activity of alumina supported CMC-stabilized Pd nanoparticles

Batch kinetic tests of TCE hydrodechlorination were carried out under various conditions. **Figure 4-3** shows the rates of TCE hydrodechlorination and chloride production with the alumina supported Pd nanoparticles and in the presence of hydrogen. The TCE hydrodechlorination can be represented by Eq. 4-1:

$$C_2HCl_3 + 4H_2 \xrightarrow{Pd} C_2H_6 + 3H^+ + 3Cl^- \quad (4\text{-}1)$$

In all cases, the H_2 supplied to the system was ~10 times the stoichiometric demand (i.e., H_2 in the solution phase remained nearly constant at its solubility level for the duration of the test). Furthermore, mass transfer of H_2 across the stagnant water film surrounding the catalyst pellets was not rate limiting, i.e., the H_2 supply at the reaction sites was abundant in comparison with TCE. This can be justified by comparing the hydrogen and TCE diffusion fluxes through the film, namely, $[C_{H2} \times D_{H2}]/[C_{TCE}/D_{TCE}] = [0.8\ mM \times 4.8 \times 10^{-5}\ cm^2/s]/ [0.38\ mM \times 1.04 \times 10^{-5}\ cm^2/s]) \approx 10$ (where C_{H2} and C_{TCE} are the solubility of H_2 and the initial concentration of TCE, and D_{H2} and D_{TCE} are the molecular diffusion coefficients of H_2 and TCE in water, respectively. The 10 times greater diffusion flux of H_2 assures abundant H_2 supply at the catalyst surface (Hildebrand et al., 2009; Nutt et al., 2006).

Figure 4-3 shows that the TCE reduction is nearly stoichiometrically coupled with production of chloride; no chlorinated intermediates such as vinyl chloride, cis- or trans-dichloroethene (DCE) were detected during the TCE degradation. These observations indicate that the supported Pd nanoparticles were able to facilitate rapid and complete TCE hydrodechlorination.

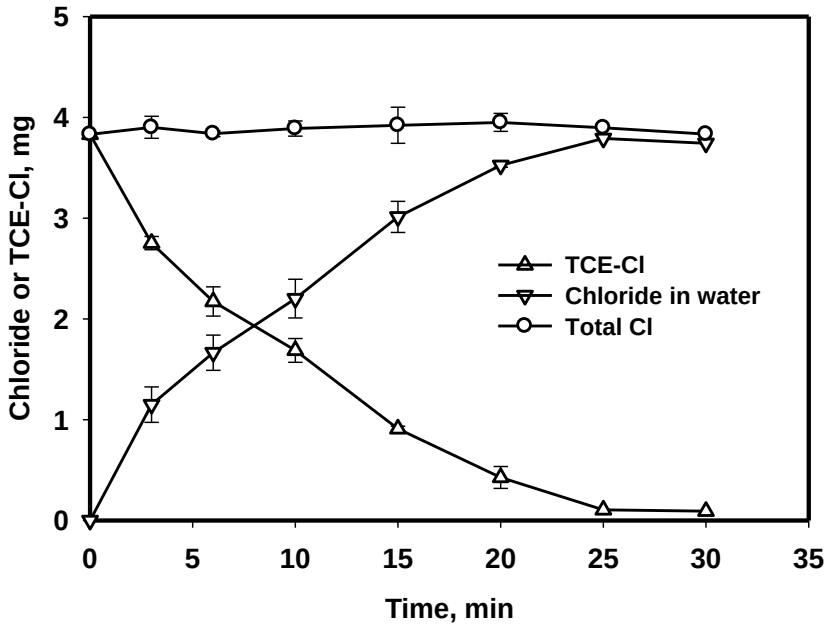

Figure 4-3. Concentration histories of chloride and TCE (expressed as TCE-bonded Cl or TCE-Cl) during hydrodechlorination of TCE using alumina supported Pd nanoparticles (Initial TCE=50mg/L, alumina = 1g/L, Pd = 0.33 wt% of alumina, CMC-stabilized Pd was prepared at 0.05 g/L Pd and 0.15 wt% CMC). Data plotted as mean of duplicates, error bars indicate deviation from the mean.

Figure 4-4 compares the catalytic activity of alumina supported and unsupported CMC-stabilized Pd nanoparticles. In both cases, the total mass of Pd in the systems was kept identical. To test the effect of CMC stabilizer, Pd nanoparticles prepared with 0.005, 0.05, and 0.15 wt% of CMC were compared. Control tests indicated that the alumina template and H_2 without Pd nanoparticles did not degrade any TCE. **Figure 4-5** plots the kinetic data in accord with the linearized pseudo first order rate law:

$$-\frac{dC_{TCE}}{dt} = k_{app}C_{TCE} = k_{obs}C_{pd}C_{TCE} \quad (4\text{-}2)$$

where k_{app} is the apparent rate constant, k_{obs} is the observed rate constant normalized to Pd concentration (C_{Pd}) and C_{TCE} is the aqueous concentration of TCE.

On an equal mass basis, the catalytic activity of unsupported, CMC-stabilized Pd nanoparticles far exceeded that of the supported counterparts, although both types of Pd catalysts were highly effective for the hydrodechlorination of TCE. From **Figure 4-5**, the observed pseudo first order rate constant for unsupported Pd was estimated to be 470, 606 and 632 L/min/g at a CMC concentration of 0.005, 0.05, and 0.15 wt%, respectively, compared to 28, 63, 109 L/min/g for the supported Pd nanoparticles. The activity drop of the supported Pd nanoparticles can be attributed to: a) loss in surface area of the supported nanoparticles, b) increased mass transfer resistance for TCE and H_2 to reach the Pd nanoparticles impregnate inside the alumina pellets (i.e., the intraparticle diffusion in the alumina pellets may slow down the overall rate), and c) loss in Pd activity due to calcination.

Immobilization of the CMC-stabilized Pd nanoparticles on alumina can decrease the available surface area of the catalyst due to the agglomeration of Pd on the alumina surface. This is true even for the uncalcined alumina supported Pd. As shown in **Figure**

4-4, the TCE degradation rate constant (k_{obs}) decreased from 470 L/g/min for unsupported Pd (CMC = 0.005 wt%) to 57 L/g/min when the same nanoparticles were loaded onto the alumina support and no calcination was performed.

Figure 4-4b reveals that calcination and reduction treatment of supported Pd resulted in further loss of the catalytic activity, with the rate constant being further reduced to 28 L/g/min. Particle sintering and the associated morphological change can account for the activity loss (Carter et al., 1966; Rupprechter and Freund, 2001). Sun and Crooks (2002) observed aggregation of Pd nanoparticles on a mica surface via surface diffusion during calcination with oxygen at 630°C. Boccuzzi et al.(2001) reported that the fraction of small gold nanoparticles (1-2 nm) on a TiO_2 support decreased when the calcination temperature increased from 473K to 873K and suggested that agglomeration of the finer particles took place. In our case, the calcination and reduction treatment increased the size of supported Pd nanoparticles to 14 ± 3 nm (Bacik et al., 2012), as compared to 4.3 ± 1.6 nm for the unsupported counterparts. Increases in the Pd particle size not only reduces the specific surface area, but also decreases the fraction of more reactive surface Pd atoms such as the edge and vertex sites, leading to a much diminished overall activity (Liu et al., 2008). Gomez-Quero et al. (2008) reported that in the size range of 1.9-13.1 nm, the finer Pd nanoparticles would possess more electron-deficient sites to promote hydrodechlorination of 2, 4-dichlorophenol. Furthermore, during calcination the original morphology of the Pd nanoparticles can be altered, thereby losing some catalytic activity. Lee et al. (2008) observed that Pt nanoparticles supported on a porous silica xerogel deformed upon calcination at 575 K. Grass et al. (2009) reported that while no particle aggregation was observed during the calcination process,

uncalcined Rh nanoparticles on a SBA15 support exhibited higher catalytic reactivity for CO oxidation than the calcined counterparts. The researcher attributed the phenomenon to the loss of CO adsorption sites on the Rh surface upon calcination.

Figure 4-5 also shows that the smaller nanoparticles prepared at a higher CMC concentration are more reactive and the size effect becames more discernible for the supported nanoparticles. This is reasonable because, the smaller nanoparticles not only offer greater specific surface area, but can also diffuse deeper into pores of the alumina support and become more evenly dispersed on the alumina surface.

Figure 4-4b also reveals a two-phase reaction kinetic profile, i.e., a slower first phase followed by a faster second phase, with both phases conforming to the pseudo first order rate law. The slower initial period, known as "the induction period", has been often observed in many catalytic processes. For examples, Hildebrand et al. (2009) observed a similar two-stage kinetic profile during hydrodechlorination of TCE with magnetite supported Pd. Wunder et al. (Wunder et al., 2011; Wunder et al., 2010) reported an induction stage in the reduction of p-nitrophenol (Nip) by sodium borohydride catalyzed by supported gold nanoparticles on cationic polyelectrolyte brushes. They attributed the phenomenon to the so-called surface restructuring of the clean gold nanoparticles induced by adsorption of Nip, i.e., the bond-breaking and rearrangement of the metal atoms on the surface. Mei et al. (2005) pointed out that such induced restructuring is a onetime process, i.e., when the restructured catalyst is reused, no more induction time would be expected. In our case, however, when the same alumina supported catalyst was repeatedly used for six times, the two-phase kinetic profile was repetitively observed (data in **Figure 4-6**). Therefore, the surface restructuring mechanism is precluded for the

alumina supported Pd. Furthermore, Zhou et al. (2010) reported that such induced surface restructuring is size-dependent and more likely to occur for smaller particles due to their high surface energy. However, the induction time shown in **Figure 4-5b** was about the same despite the 1.6 times difference in particle size, which backs the assertion that the induced restructuring is absent in our case.

Consequently, the presence of induction period can be attributed to the slow diffusion of TCE in the alumina pores to reach the Pd nanoparticles. Signori et al. (2010) observed a time lag of 2-16 min when tested silver nanoparticles loaded on branched polyethyleneimine derivatives for p-nitrophenol reduction by borohydride; and Gao et al. (2007) reported an "activation" time of 1~6 min in studying Pd and Au nanoparticles embedded within alginate nanocapsules. The researchers attributed the time lag to the slow diffusion of the reactants. As for our alumina-supported Pd catalyst, it is plausible that a great fraction of the Pd nanoparticles are located deep in the micro and meso-pores of alumina support, whereas a small fraction of the nanoparticles are located in relatively shallow and more easily accessible sites. Therefore, the initial slow reaction is facilitated by the easily accessible Pd nanoparticles, while the following fast reaction is attributed to the Pd nanoparticles in the deeper pores.

Based on the Pd-normalized rate constant (k_{obs}) values, the catalytic activity of our alumina supported CMC-stabilized Pd nanoparticles is 7.3 and 538 times, respectively, greater than those of commercial alumina supported non-stabilized Pd reported by Nutt et al. (2005) and Munakata and Reinhard (2007).

4.3.3 Catalyst lifetime

The lifetime and reusability of the alumina supported catalyst were tested in a series of six TCE hydrodechlorination tests where the same catalyst was repeatedly used without any treatment. **Figure 4-6** shows kinetic profiles of TCE hydrodechlorination in Runs 1, 3 and 6 (data for Runs 2, 4, 5 are not shown for clarity). The k_{obs} values for the six consecutive runs were determined to be 109, 101, 100, 94, 97 and 95 L/g/min, respectively. In the first three runs, a small amount (≤6%) of Pd bleeding was observed. As a result, the catalytic activity decreased by ~9%. However, no further Pd bleeding was detected and the reaction rate remained constant in the subsequent runs, indicating that no significant catalyst deactivation was evident. For the uncalcined alumina supported Pd (**Figure 4-4**), about 3.3 % of the Pd was detected in the solution after the first batch tests. When the same catalyst was reused for six times, about 10% Pd was lost with less Pd loss being observed in later runs. This observation suggests that the CMC coating can serve as a binding agent and facilitate immobilization of the Pd nanoparticles on alumina.

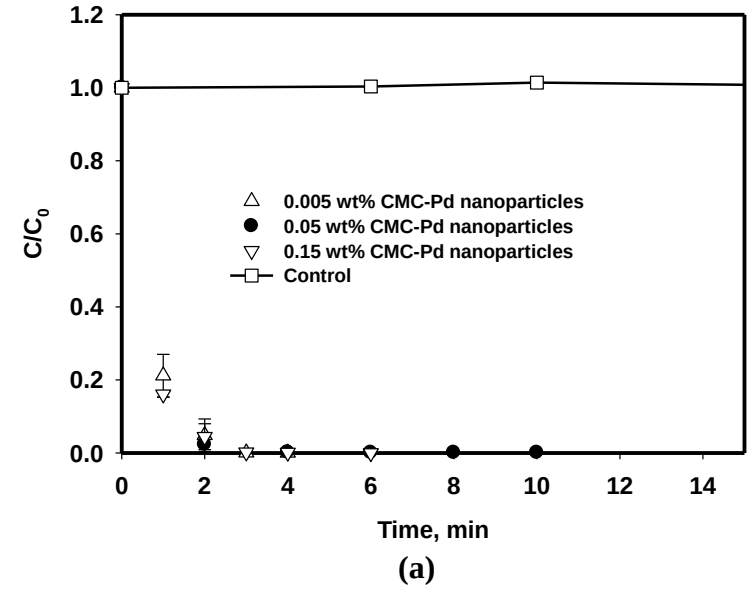

(a)

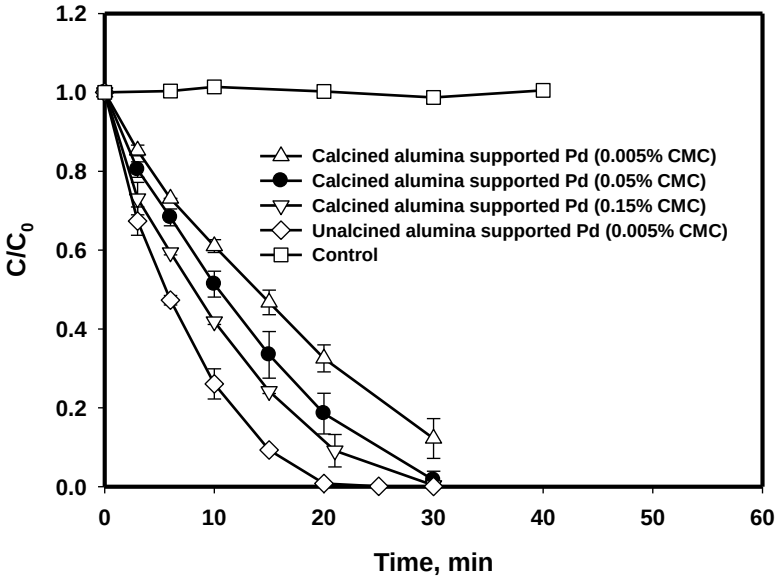

(b)

Figure 4-4. Kinetics of TCE hydrodechlorination in the presence of: **(a)** unsupported CMC-Pd nanoparticles and **(b)** alumina-supported Pd nanoparticles (Initial TCE = 50mg/L, alumina = 1 g/L, Pd = 0.33 wt% of alumina, CMC-stabilized Pd was prepared at 0.05 g/L Pd and 0.005, 0.05 and 0.15 wt% CMC, respectively). Data plotted as mean of duplicates, error bars indicate deviation from the mean.

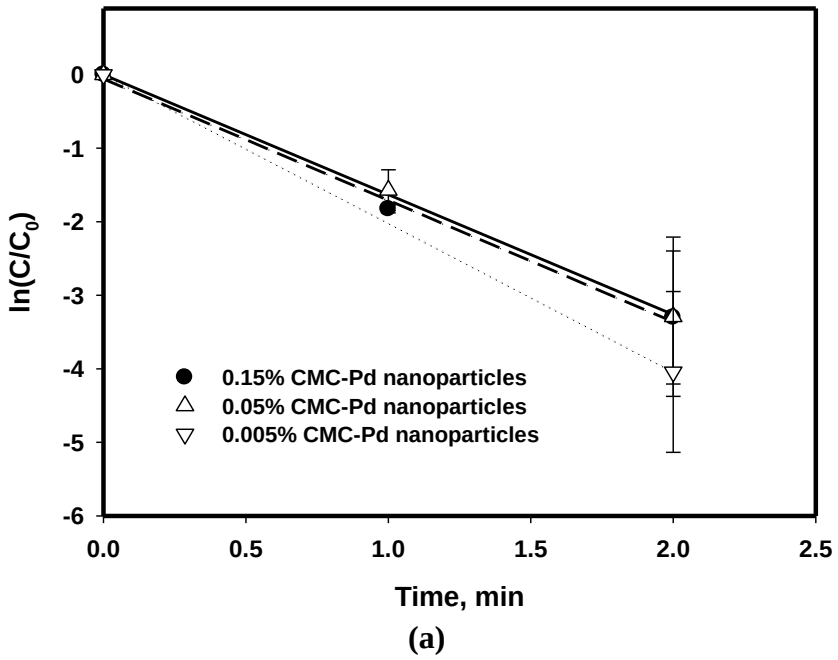

(a)

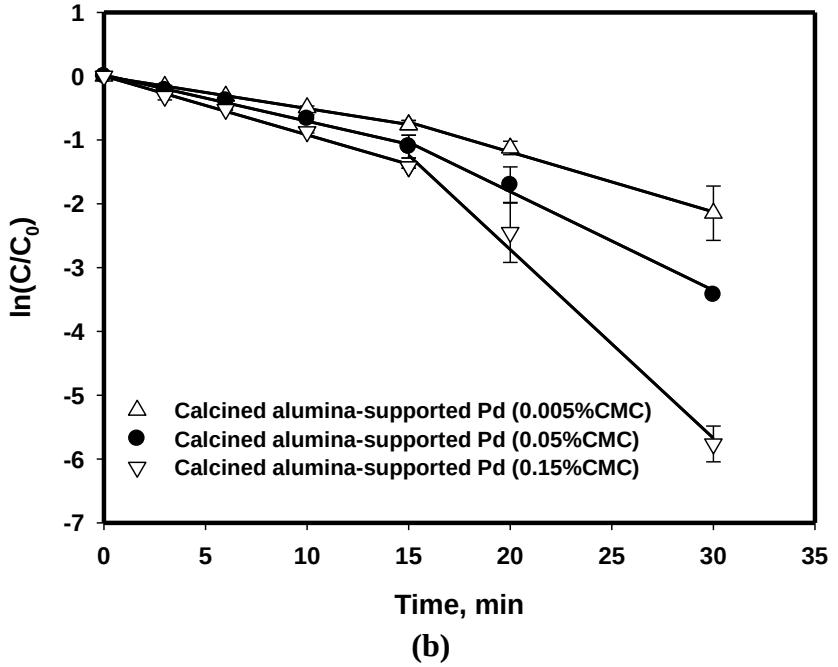

(b)

Figure 4-5. Linearized plots of the TCE hydrodechlorination kinetic data of Figure 4-4: **(a)** unsupported CMC-Pd nanoparticles and **(b)** alumina-supported Pd nanoparticles.

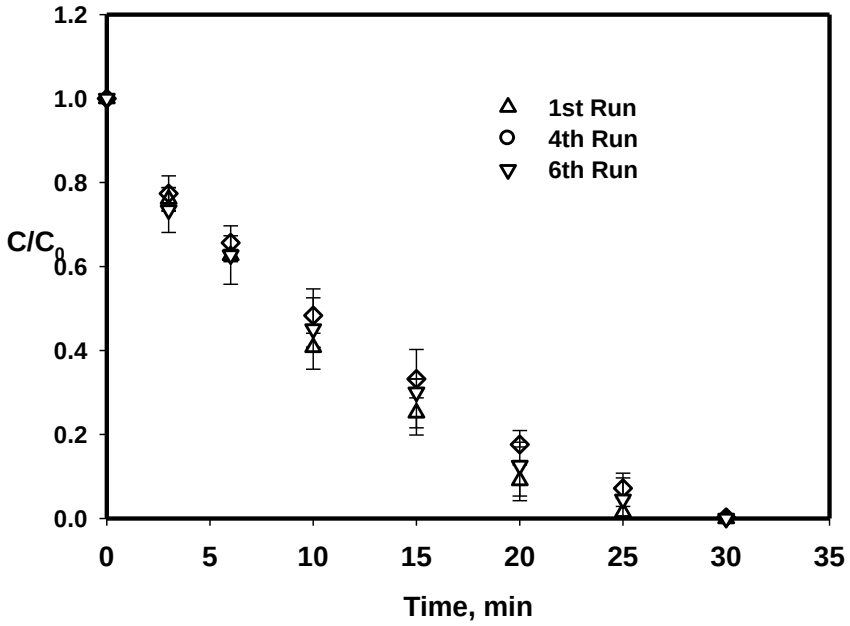

Figure 4-6. Kinetic profiles of TCE hydrodechlorination in six consecutive batch tests where the same alumina supported CMC-stabilized Pd nanoparticles were repeatedly used (Initial TCE = 50 mg/L, alumina = 1g/L, Pd = 0.33wt% of alumina). Data plotted as mean of duplicates, error bars indicate deviation from the mean. For visual clarity, only data of Runs 1, 3 and 6 are plotted.

4.3.4 Effect of dissolved organic matter

DOM is ubiquitous in natural waters, especially in surface wasters. **Figure 4-7** shows kinetics of TCE hydrodechlorination with the supported Pd nanoparticles at various concentrations of DOM measured as total organic carbon (TOC). At a TOC concentration of 2 mg/L, no significant impact was evident on the reaction rate. Increasing the TOC concentration to 10 mg/L decreased the k_{obs} value from 109 L/g/min to 106 L/g/min. At a TOC concentration of 30 mg/L, the k_{obs} was reduced abruptly to 17 L/g/min.

While DOM may serve as soluble electron carriers to facilitate reductive dechlorination (Dunnivant et al., 1992), DOM can inhibit the reaction due to competitive sorption of DOM onto the catalyst surface sites. Doong and Lai (2005) observed that the presence of 50 mg/L of Aldrich humic acid lowered the PCE dechlorination rate with palladized iron by ~20 times. Chaplin et al. (2006) reported that the observed reaction rate constant for nitrate reduction by hydrogen gas with an alumina-supported Pd-Cu catalyst decreased by 83% in the presence of 3.3 mg/L as DOC of humic acid. Adsorption of humic acid on the catalysts was observed in the reaction. Ambonguilat et al. (2006) found that the hydrogenation rate of nitrate using an alumina supported Pd-Sn catalyst was reduced by ~98% in the presence of 20 mg/L as TOC of natural organic matter, and they observed strong adsorption of DOM on the catalyst at about 15 mg TOC/g.

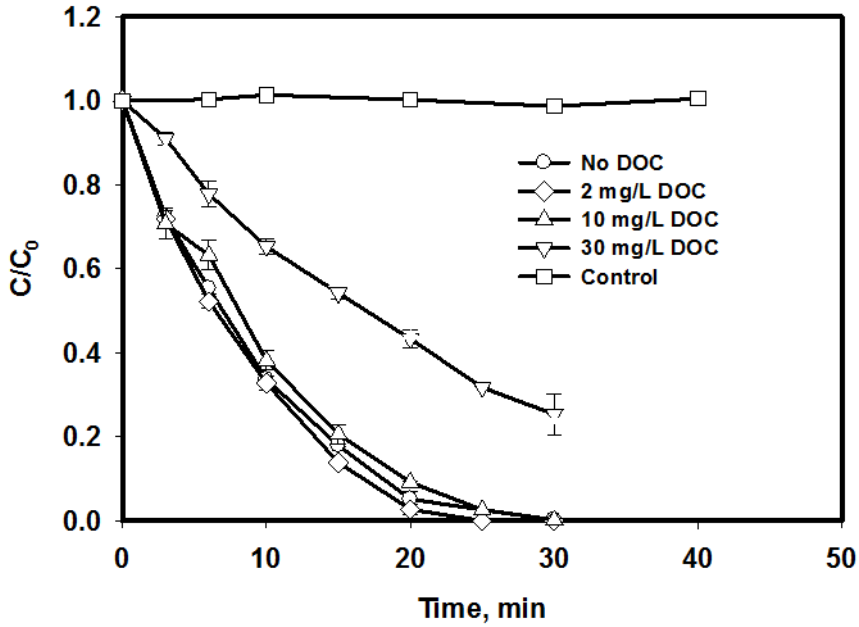

Figure 4-7. TCE hydrodechlorination using alumina-supported CMC-stabilized Pd nanoparticles (CMC=0.15 wt%) in the presence of various concentrations of dissolved organic carbon (TCE = 50 mg/L, alumina = 1 g/L, Pd = 0.33 wt% of alumina). Data plotted as mean of duplicates, error bars indicate deviation from the mean.

In our case, DOM sorption tests (data not shown) indicated that the alumina support adsorbed ~59% in 5 min and 63% in 30 min of the 30 mg/L DOM, and the loading of Pd nanoparticles did not change DOM adsorption due to the low surface coverage (0.17%). Our results are consistent with the reported assertion that adsorption DOM on the catalyst surface is, at least in part, responsible for the diminished reaction rate.

4.3.5 Effect of supporting material hydrophobicity

Given the hydrophobic nature of TCE, it could be an intuitive perception that a hydrophobic support such as a carbonaceous sorbent would offer a more favorable environment for TCE hydrodechlorination than a hydrophilic support like alumina. Researchers (Diaz et al., 2011; Gomez-Sainero et al., 2000) reported that activated carbon supported metal (including Pd) catalysts can effectively facilitate hydrodechlorination due to the surface adsorption of a target hydrocarbon. For example, Gomez-Sainero et al. (2000) reported that carbon supported Pd provided a more active and selective performance towards chloroform dechlorination as compared to other inorganic supports such as SiO_2 and sepiolite. To examine the effects of the supporting material hydrophobicity on TCE degradation, a carbonaceous resin (Ambersorb-572) and a widely used catalyst (TS-1) were tested as a support for the CMC-stabilized nanoparticles. **Figure 4-8** shows TCE adsorption rates for the two sorbents, confirming the hydrophobic nature of the materials. At equilibrium, Ambersorb-572 offered 1.5 times greater TCE uptake than TS-1 on a mass basis, indicating its stronger adsorption capacity. Mass balance analysis indicated that both types of the materials without Pd did not show any hydrodechlorination of TCE (data not shown).

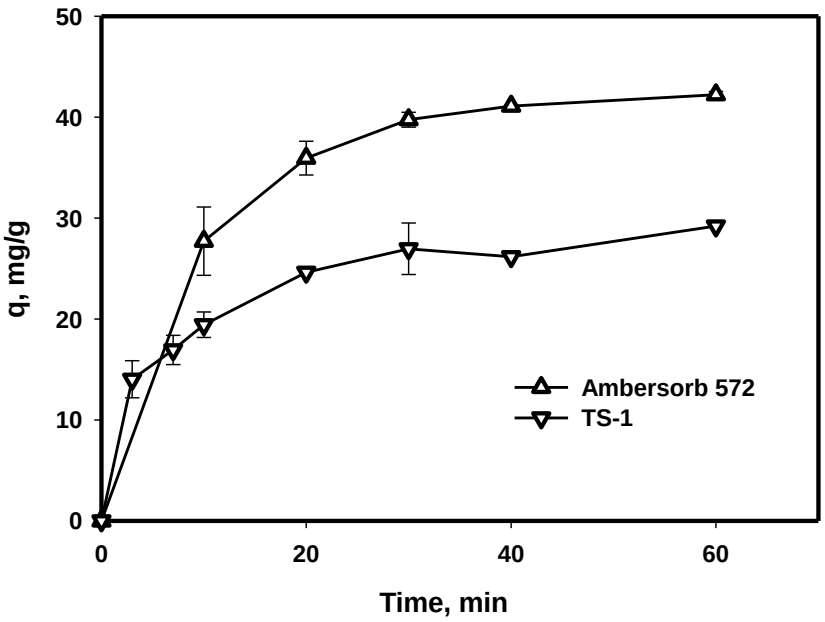

Figure 4-8. TCE adsorption kinetics on Ambersorb 572 and TS-1 supports (Initial TCE= 50 mg/L, Ambersorb 572 = 1 g/L, TS-1 = 1 g/L). q refers to solid phase TCE concentration. Data plotted as mean of duplicates, error bars indicate deviation from the mean.

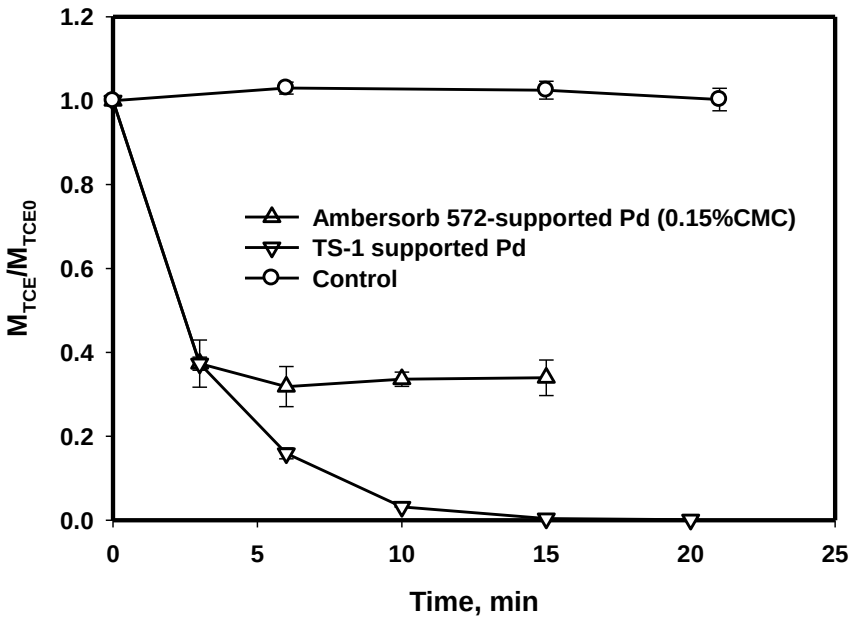

Figure 4-9. TCE hydrodechlorination using Ambersorb supported Pd nanoparticles (stabilized with 0.15 wt% CMC) and TS-1-supported Pd nanoparticles (Initial TCE=50 mg/L, Ambersorb 572 = 1 g/L, TS-1 = 1 g/L, Pd = 0.33 wt% of Ambersorb 572/TS-1). M_{TCE} and M_{TCE0} are total TCE mass remaining in the system at time t and 0, respectively. Data plotted as mean of duplicates, error bars indicate deviation from the mean.

Figure 4-9 shows TCE hydrodechlorination rate using Ambersorb and TS-1 supported Pd nanoparticles under otherwise identical conditions as for alumina supported Pd. Evidently, the Ambersorb supported Pd offered a faster initial reaction rate, with an equilibrium time of ~6 min and a k_{obs} value of 279 L/g/min (as compared to ~ 30 min and a k_{obs} value of 109 L/g/min for alumina supported Pd). However, the rapid initial reaction rate was virtually halted after 6 min, with ~33% of the initial TCE adsorbed on the resin without further degradation. This observation indicates that the use of a hydrophobic support such as Ambersorb-572 can result in two opposing effects. On the one hand, rapid accumulation of TCE at the reactive Pd sites accelerates TCE hydrodechlorination. On the other hand, strong adsorption of TCE may render it less available for Pd due to the retarded surface diffusion rate. Such an adsorption limitation on reaction rate could be more profound when the surface density of Pd nanoparticles is low (the surface coverage of Pd on Ambersorb was <0.02%). In addition, the observed reduction in the TCE hydrodechlorination can be attributed to surface contamination of Pd by carbon atoms upon the calcination of the carbonaceous support (Neri et al., 2001). Krishnankutty and Vannice (1995) observed a suppressed (>85%) hydrogen chemisorption on Pd on a carbon catalyst support, along with an expanded Pd lattice due to the presence of interstitial carbon in the Pd crystallites. The reduced reaction was ascribed to partial encapsulation of the Pd surface by the migration of carbon atoms from the support onto or into the Pd lattice at the elevated temperature.

While minimal Pd leaching was observed with the alumina supported Pd, ~40% of Pd initially loaded on Ambersorb-572 was leached out, indicating a rather weak binding of the CMC-stabilized Pd on the carbon surface. As a result, TCE degradation

was decreased from 67% in run 1 to 17% when the Ambersorb supported Pd was reused in the second batch. Similar high leachability of Pd from carbon supported Pd catalysts was also reported by others. For example, Forni et al. (1997) observed a 20% Pd leaching with activated carbon supported Pd used for degradation of polychlorinated biphenyls. Yuan and Keane (2004) compared alumina and carbon supported Pd, and observed a 13% leaching of Pd from a carbon catalyst. The researchers attributed the high leachability of carbon supported Pd to the weak Pd-carbon interaction and suggested that the alumina support is more resistant to leaching.

In contrast, **Figure 4-9** shows that the TS-1 supported Pd nanoparticles displayed a superior catalytic performance than the Ambersorb supported counterpart. Complete degradation of TCE was achieved within 15 min, as compared to 30 min for alumina supported Pd (**Figure 4-4**). TS-1 offers much greater hydrophobicity due to the much lower surface acidity (strong acid and hydrogen bonding) than alumina (Drago et al., 1998), although TS-1 is less hydrophobic than Ambersorb-572. At the end of each batch test, samples of the TS-1 supported catalysts were collected and exhaustively extracted for TCE. Yet, no TCE was detected in the solid phase, indicating that adsorption of TCE was not limiting the reaction as was the case for Ambersorb-572. Considering that the particle size of Pd on TS-1 is in the range of 2.2 to 10 nm, as reported by Chen et al. (2008) who prepared silica-alumina supported Pd nanoparticles in a similar manner, the surface coverage of Pd on the TS-1 is estimated to be 0.01%~0.06 %. Therefore, as is the case for Ambersorb-572, the Pd loading should not alter the surface hydrophobicity of TS-1. The results in Figure 9 indicate that TS-1 is able to create a more favorable hydrophobic surface than alumina for TCE degradation, and yet, the mildly hydrophobic

surface of TS-1 does not render strong TCE adsorption that may inhibit the mass transfer of TCE as is the case for Ambersorb-572. Furthermore, TS-1 does not seem to contaminate the Pd nanoparticles as Ambersorb does. The leachability of Pd loaded on TS-1 was less than ~4% Pd.

While the TCE degradation kinetics catalyzed by TS-1 supported Pd also follows pseudo-first-order kinetics, no induction time was evident as was the case for alumina supported Pd. This observation indicates that the reactive Pd nanoparticles on TS-1 are more easily accessible than those on alumina. Despite the superior technical performance of TS-1, the cost of TS-1 ($45/g) is about 115 times higher than for alumina, which may prohibit its broad industrial applications.

4.4 Conclusions

A new class of supported pre-stabilized Pd catalyst was developed by immobilizing CMC-stabilized Pd nanoparticles onto alumina, Ambersorb-572 and TS-1. At a Pd mass loading of 0.33%, the alumina and TS-1 supported Pd nanoparticles were able to effectively catalyze a rapid and complete hydrodechlorination of TCE. For the alumina supported Pd, the observed pseudo first order reaction rate constant, $k_{obs,}$ increased from 28 to 109 L/min/g when the Pd nanoparticle size was reduced from 4.8 nm to 2.7 nm. Calcination of alumina supported Pd at 500 °C reduced the catalytic activity, but resulted in much reduced Pd bleeding and the catalysts remained 7.3 to 538 times more effective than reported supported Pd nanoparticles. A two-phase kinetic profile was observed for the supported catalyst with an induction time of ~15 min. The supported Pd can function well in the presence of DOM at 10 mg/L as TOC without activity loss; elevated TOC levels (e.g., 30 mg/L) may inhibit the catalytic activity (by a factor of 7). The highly

hydrophobic carbonaceous support (Ambersorb-572) does not offer advantage in terms of TCE hydrodechlorination because of strong adsorption effect and carbon contamination upon calcination. Bearing prohibitively high cost, the moderately hydrophobic support TS-1 displayed superior catalytic performance, indicating that an ideal Pd support should incorporate moderate hydrophobicity, tolerance of high temperature calcination, and low mass transfer resistance. The findings indicate that alumina supported CMC-stabilized Pd nanoparticles may serve as a promising catalyst to facilitate hydrodechlorination or other catalytic reactions in water treatment.

CHAPTER 5. Field Demonstration of CMC-stabilized Iron Nanoparticles for In-situ Chlorinated Solvents Remediation

5.1 Introduction

As an emerging technology for in-situ remediation of soil contaminants, zero valent iron has stimulated significant interest in the past decades for its high effectiveness on immobilization and/or transformation of contaminants into less toxic products. Laboratory and field studies have demonstrated its application to remove varieties of organic or inorganic contaminants, such as chlorinated solvents, heavy metals, anions, radio-nuclides, and etc. (Alowitz and Scherer, 2002; Gillham and Ohannesin, 1994; Morrison et al., 2001; Shokes and Moller, 1999; Su and Puls, 2001). Due to its low cost and ready availability, granular ZVI has been used widely as the reactive component in permeable reactive barrier system for in-situ groundwater remediation, where the contaminant plume is intercepted in its flow path and transformed into environmentally acceptable forms when passing through the reactive media (Powell et al., 1998; Scherer et al., 2000). Contrary to the traditional pump-and-treat system, which extracts the groundwater contaminants by pumping and then removes the contaminants with aboveground facilities, abiotic reductive degradation of contaminants with zero valent iron offers significant environmental and economic advantages (Higgins and Olson, 2009). However, these permeable reactive barriers are restricted to shallow plumes and work in a passive way (U.S. EPA, 1997).

With the prospective application of nanotechnology, nanoscale zero valent iron materials have drawn increasing attention among environmental researchers due to its extremely small particle size, high specific surface area and stronger tendency to interact and react with contaminants (Li et al., 2006a). Wang and Zhang (1997) reported that the ZVI nanoparticles (1-100 nm) prepared with a borohydride reduction method would offer 10-100 times higher surface-area-normalized rate constants for TCE degradation than those of commercially available iron particles. Considering the small size of ZVI nanoparticles, it is hypothesized that they would migrate readily along with the groundwater flow in the soil matrix just like other natural colloids and be able to travel into the subsurface contaminant source zone, even in deeper areas where an excavation is not applicable. Elliott and Zhang (2001) proved this concept in a field study by injecting the nanoscale iron nanoparticles into the soil of a manufacturing facility in New Jersey. Up to 96% of TCE was reduced over a 4-week monitoring period after 1.7 kg of the nanoparticles were injected in the test area. However, detailed laboratory studies found that the bare zero valent iron nanoparticles would easily form large aggregates rapidly and then lose their ability to migrate through the soil matrix (He et al., 2007; Saleh et al., 2007).

To improve the particle deliverability and reactivity, Auburn University has developed a new class of highly dispersible Fe-Pd bimetallic nanoparticles using low-cost and biodegradable polysaccharides such as starch and carboxymethyl cellulose as stabilizers (He and Zhao, 2005; He et al., 2007). Laboratory tests have shown that these stabilized nanoparticles possessed greater dechlorination reactivity, improved stability against aggregation and enhanced mobility in soil columns (He et al., 2009b). Successful

field tests in California and Alabama have yielded promising results using CMC-stabilized Fe-Pd nanoparticles for in-situ dechlorination (Bennett et al., 2010; He et al., 2010). These iron nanoparticles were successfully injected into the tested sandy aquifers. Under the natural hydraulic gradient, the iron nanoparticles that moved five feet down-gradient from the injection well were about 37% of that for the tracer Bromide. The mobility of iron particles would be enhanced under higher pressure (He et al., 2010). Rapid abiotic dechlorination of chlorinated solvents was observed after injection of iron nanoparticles, and a long-term in-situ biological dechlorination was also boosted in the subsurface using CMC as the carbon source and hydrogen gas, which isproduced from the iron corrosion, as electron donor for microbial degradation.

Other field tests were conducted using different strategies to deliver zero iron nanoparticles into the subsurface for source treatment. Quinn et al. (2005) conducted a field test in Florida to evaluate the performance of one type of zero-valent iron nanoparticles, which is emulsified by a food-grade surfactant, a biodegradable vegetable oil and water, for the in-situ dechlorination of TCE DNAPLs. Sixteen months after the ZVI injection, 57%-100% decreases of the TCE concentration in groundwater were reported in the 16-24 ft bgs. Wei et al. (2010) prepared the zero valent iron nanoparticles stabilized by a nonionic surfactant on site for in-situ groundwater remediation in Taiwan. Those surfactant-stabilized iron nanoparticles were reported to travel at least three meters in a coarse sand aquifer via gravity. 50%-99% of vinyl chloride in the monitoring area was degraded.

In this study, we conducted a field demonstration to evaluate the performance of the CMC-stabilized iron nanoparticles for chlorinated solvents remediation in a source

zone area. The primary objective of the demonstration was to test the feasibility of using the stabilized nanoparticles for in-situ degradation of chlorinated solvents in a test area of low permeability. The transport behavior of the nanoparticles and the evolution of TCE concentration in the soil and groundwater were assessed. The field environmental conditions such as pH, dissolved oxygen, oxidation and reduction potential, ionic strength and dissolved organic matter in the test area were monitored to understand the impact of the injected zero valent iron on groundwater geochemistry.

5.2 Site description and methods

5.2.1 Site description

The site selected for the pilot test is located at Hill Air Force Base in Utah, USA. The test area was about 20 ft long by 5 ft wide. The soil mainly consisted of silty clay with thin sand seems. **Figure 5-1** presents a sectional view of the aquifer elevation and locations of five testing wells, including one injection well (IW-1), three monitoring wells (MW-1, MW-2, MW-3) along the groundwater flow direction and one monitoring well (MW-4) in the up-gradient of the injection well. MW-1, MW-2 and MW-3 were 5 ft, 10 ft and 15 ft down-gradient from the injection well IW-1, and MW-4 was 5 ft up-gradient. IW-1, MW-1, MW-2 and MW-3 were installed to a total depth of 26 feet bgs (below ground surface) and screened from 20 to 25 ft bgs, while the screen interval of the pre-existing MW-4 was from 19 to 39 ft g bgs. The hydraulic conductivity (k) of the test zone was determined to approximately 0.01 feet per day based on slug tests conducted in the groundwater monitoring wells.

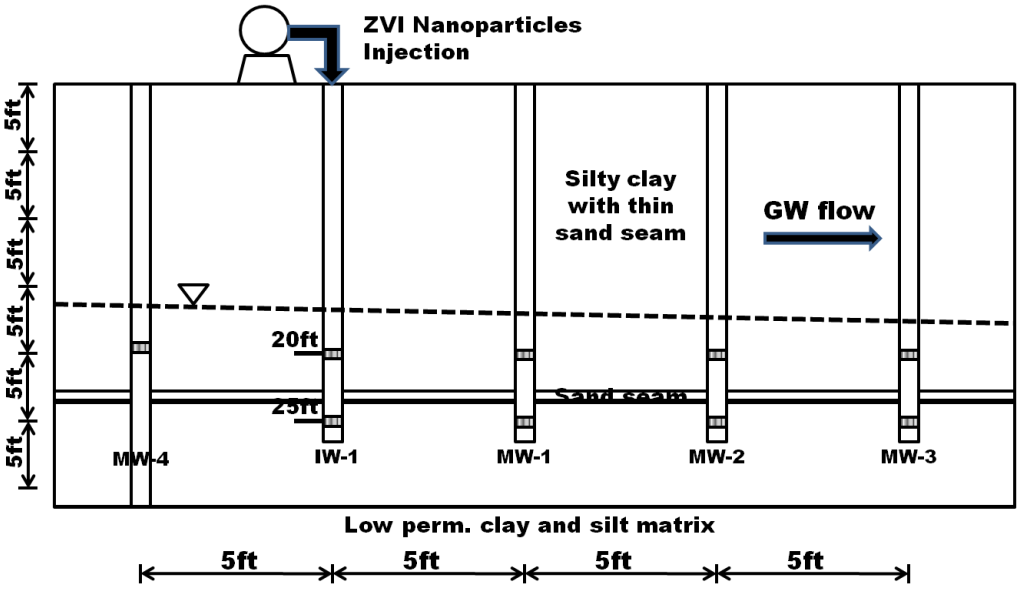

Figure 5- 1. A sectional view of the aquifer at the testing site and schematic of the in situ injection of CMC-stabilized Fe–Pd nanoparticles

5.2.2 Groundwater quality in the test area

To determine the field environmental conditions, groundwater samples were collected from the existing monitoring well MW-4 and analyzed prior to the field test. Several chlorinated ethenes including TCE and PCE have been detected in the groundwater. TCE, which was the primary chlorinated solvent contaminant in the test zone, was detected at a concentration of 14.7 mg/L in a baseline sample. PCE was detected at a concentration of 0.06 mg/L in the groundwater. The pH was slightly basic, about 7.81. The measured total organic carbon, alkalinity and electrical conductivity in the groundwater were 123.7 mg/L, 711 mg/L and 1.2 mmhos/cm, respectively.

5.2.3 Laboratory feasibility studies

Batch tests were conducted in the laboratory using the site groundwater samples to evaluate the effectiveness of the CMC-stabilized Fe-Pd nanoparticles for the TCE degradation. 1.0 g/L CMC-stabilized Fe-Pd nanoparticles were prepared following the method described by He et al. (He et al., 2007). TCE degradation tests were initiated by mixing 14.3 mL of 1.0 g Fe/L stabilized Fe-Pd nanoparticles with 28.6 mL groundwater obtained from MW-4 in a 43 mL glass vial sealed with Teflon-lined septa, yielding an initial TCE concentration of 9.5 mg/L. The glass vials were placed on a rotary shaker at 60 rpm for continuous reactions. Liquid samples were withdrawn at selected time intervals using a 100 μL gas-tight syringe for analysis. Control tests were conducted by adding deoxygenated DI water to groundwater to evaluate the potential loss of TCE by biodegradation.

5.2.4 Field preparation of CMC-stabilized nanoparticles

The CMC-stabilized Fe-Pd nanoparticles were prepared via the sodium borohydride reduction of aqueous ferrous sulfate in the presence of sodium carboxymethyl cellulose (CMC) as a stabilizer. The nanoparticle suspension was prepared right before each injection. Thirty to forty US gallons of tap water were added into a 55-gallon polyethylene reactor and purged with nitrogen gas to evacuate dissolved oxygen. To prepare 1 g/L iron nanoparticles, approximately 946 g CMC powder (Acros Organics, Morris Plains, NJ, U.S.A.) were slowly added into the water to yield a 0.5% (by weight) solution. The reactor was mixed with a 1/3 horsepower motorized impeller until the CMC was completely dissolved. Next, approximately 943 g $FeSO_4 \cdot 7H_2O$ (Acros Organics) were dissolved in two gallons of tap water and added into the reactor. Nitrogen purging continued for another 10~15 minutes. Approximately 257 g of sodium borohydride (Acros Organics) were dissolved in one gallon of tap water and then added into the reactor at a rate of approximately 0.5 L/min with a peristaltic pump. The mixture in the reactor quickly became inky black, indicating the formation of zero valent iron. After ~15 min, 50 mL of 12.4 g/L $Na_2PdCl_4 \cdot 3H_2O$ were added into the ZVI suspension to yield the desirable Pd loading of 0.1 % (by weight) on Fe. The added Pd^{2+} was reduced to Pd^0 by zero valent iron to produce Fe-Pd bimetallic nanoparticles (He et al., 2007). Approximately 28 g of a conservative tracer (potassium bromide, KBr) were added into each batch of 50 gal of the nanoparticles suspension to evaluate the transport behavior of bimetallic Fe-Pd nanoparticles.

5.2.5 Iron injection and groundwater monitoring

Two rounds of zero valent iron nanoparticles injection were performed on 3/30/2011~4/1/2011 and 5/9/2011~5/11/2011. For the first injection, two batches of 50 gallons of 1g/L Fe-Pd were prepared with 0.5 wt % CMC and then diluted using deoxygenated tap water to ~ 100 gallons at an iron concentration of 0.5g/L before injection. Another 105 gallons of 1g/L Fe-Pd stabilized using 0.5% CMC were injected without dilution. For the second injection, 320 gallons of 1.0g/L Fe-Pd stabilized using 0.5% CMC were prepared and injected into the subsurface.

Considering the very low permeability of the test site, a pressure injection system was set up on the injection well. The wellhead of IW-1 was sealed and a pressure gauge was installed to monitor the wellhead pressure. The prepared Fe-Pd nanoparticles were delivered into the injection well through a pipe with a peristaltic pump and then pushed through the screened intervals of the well into the subsurface area. The wellhead pressure was measured to be less than 8 psi during the field test. The injection flow rate was kept at 0.5~1.0 gallons/min and each batch injection lasted about 1.6 h. Groundwater samples were collected from five wells before and after injection using low-flow purging techniques. A peristaltic pump was used to extract groundwater samples from each well. A multi-parameter probe (YSI) with a flow-through cell was used to monitor pH, conductivity, oxidation-reduction potential (ORP), DO and temperature on site.

Soil samples were collected about 16 months (11/18/2009) before the first nanoparticles injection and approximately 36 days (6/16/2011) after the second nanoparticles injection, to examine any change in the concentration of chlorinated solvents in soil. For the pre-test sampling, three soil borings (SB-1 through SB-3) to a

total depth of 40 ft bgs were drilled in the test area. SB-1, SB-2 and SB-3 were approximately 5, 15 and 20 ft northeast of MW-4, respectively. Soil cores were obtained using a 2-inch Geoprobe dual-tube system and soil samples were collected at 6-inch intervals at soil borings using ESS Lock N' Load handle and syringes (Environmental sampling supply, Oakland, California) following the EPA method 5035 for analysis of volatile organic compounds (VOCs). For the post-test sampling, four soil borings (SB-4 through SB-7) were advanced to a total depth of 30 ft bgs. Soil samples were collected at one-foot intervals from 15 feet to 20 ft bgs, at 6-inch intervals from 20 ft to 25 ft bgs and at one-foot intervals from 25 ft to 30 ft bgs.

5.2.6 Chemical analyses

The collected groundwater and soil samples from the field were sent to the environmental laboratory at Auburn University for chemical analyses. To determine chlorinated solvents concentration such as TCE and PCE, 100 µL of water samples were taken using a gas-tight syringe and mixed with 1 mL of hexanes for organic contaminant extraction. The resultant extract was analyzed on an HP 6890GC equipped with a 0.32 mm ID ×32 m RTX-624 capillary column (Restek Co., Bellefonte, PA, USA) and a µECD detector. Selected samples were also sent to Microseeps, Inc. in Pittsburg, Pennsylvania for analysis of methane, ethene and ethane using method AM20GAX and to ALS Group USA, Corp. in Salt Lake City, Utah for analysis of VOCs using EPA method 8060B.

Total iron was measured as an indicator of the concentration of Fe-Pd nanoparticles. In order to assure the nanoparticles were completely dissolved, 1 mL of groundwater samples was mixed with 4 mL of the concentrated hydrochloric acid. The

mixture was further diluted by 15 mL DI water before being analyzed on a flame atomic-absorption spectrophotometer AAS (220FS, Varian, Palo Alto, CA, USA). Cations, such as calcium and magnesium, were analyzed by Inductively Coupled Plasma (ICP) Atomic Emission Spectrometry using a Varian Vista-MPX Axial Spectrometer. Anions were analyzed using a Dionex ion chromatograph (DX-120) equipped with a suppressed conductivity detector. The nitrate-nitrogen was measured colorimetrically with a thermospectronic Genesis 20 Sepctrophotometer after being digested with phenoldisulfonic acid. The alkalinity was determined using the standard sulfuric acid titration method. The electrical conductivity was analyzed using YSI Model 31 Conductivity Bridge. Total organic carbon was measured with a Shimadzu TOC-VCPN analyzer.

Field soil samples were preserved with 10 ml methanol in 43mL glass EPA vials capped with Teflon-lined septa, following the method of EPA 5035A. These methanol-preserved soil samples were shipped on ice to the laboratory and stored at 4°C in a refrigerator, prior to analysis. After arrival, soil samples were sonicated until being well suspended in methanol for a two-day extraction. Prior to analysis, the sample vials were centrifuged using a Fisher Marathon 21K/R Centrifuge (Fisher Scientific) at 160 g-force for 10 minutes in order to obtain clean supernatants. The analyses were completed within 14 days as required in the method 5035.

5.3 Results and discussion

5.3.1 Laboratory tests of Fe-Pd nanoparticles for TCE degradation

Figure 5-2 showed batch kinetic data of TCE degradation in the field groundwater and compared with that in DI water. The initial TCE concentration was 9.5

mg/L. Experimental results indicated that TCE degradation followed a pseudo-first-order reaction kinetics. With 0.33g/L freshly prepared Fe-Pd nanoparticles, TCE could be completely degraded in groundwater within 4 hours with an observed pseudo-first-order reaction rate constant of 6.9 L/h/g Fe. However, TCE degradation in the deoxygenated DI water was about 18 times faster, with a reaction rate constant of 122.8 L/h/g Fe. The slower degradation in groundwater can be attributed to the presence of dissolved organic matter, which was detected at 123.7 mg/L as TOC. Previous study have shown that soil organic matter could inhibit the TCE dechlorination using Fe-Pd nanoparticles (Zhang et al., 2011). The presence of nitrate at a concentration of 2.7 mg/L was also reported to consume some reducing equivalents of zero valent iron nanoparticles (Su and Puls, 2004). Other chlorinated contaminants in the groundwater such as cis-DCE (0.19mg/L), although their concentrations are very low, could compete with TCE for available electrons as well and thereby decrease the dechlorination rate of TCE.

5.3.2 Fe-Pd nanoparticles preparation in the field

To avoid the potential loss of particle reactivity due to iron corrosion with water, the CMC stabilized Fe-Pd nanoparticles were prepared on site freshly before injection, at a concentration of 1.0 g Fe/L with 0.5 wt% NaCMC. The nanoparticles samples taken from the field has shown a hydrodynamic size of 178 nm with an average zeta potential of -40.7 mV. To evaluate the particle size of prepared Fe-Pd nanoparticles in a simply and fast way, the nanoparticle suspension was filtered on sit through 0.45 μm syringe filter and about 85% of the total iron would readily pass through.

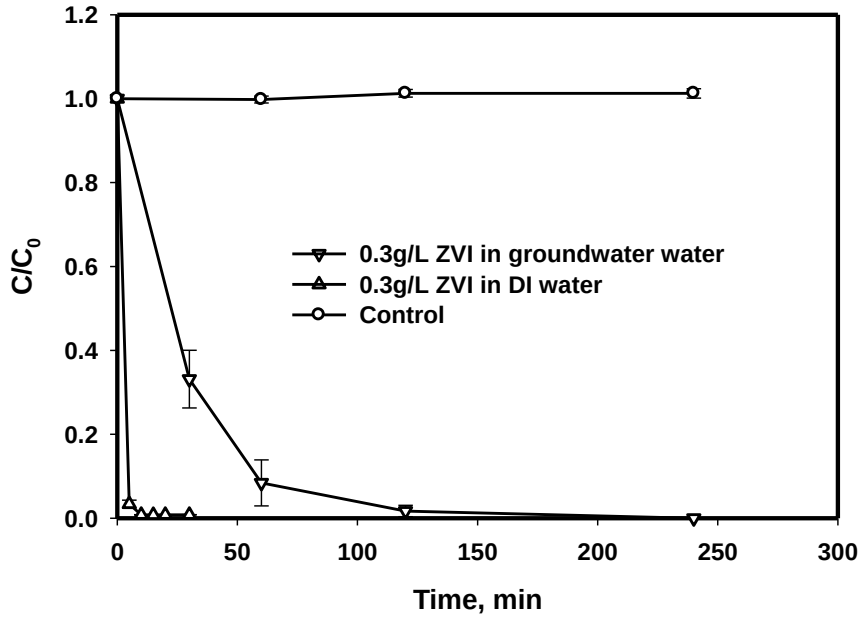

Figure 5- 2. Reduction of TCE in a field groundwater and DI water using CMC-stabilized Fe-Pd nanoparticles. Fe = 0.33g/L, Pd = 0.1 wt % as Fe, NaCMC = 0.27 wt%, TCE = 9.5 mg/L. Data plotted as mean of duplicates, error bars indicate deviation from the mean.

5.3.3 Transport of CMC-stabilized Fe-Pd nanoparticles

The inorganic anion bromide, which is commonly considered "conservative" or nonreactive under most of the field conditions, was injected into the test area with the Fe-Pd nanoparticles to provide insight into the direction and mobility of injected fluid. The concentration history of the bromide and the total iron in the monitoring wells after injection #2 is shown in **Figure 5-3**. The baseline concentration of bromide in the groundwater was 0.3 mg/L, which is two orders of magnitude lower than that in the injected fluid. A substantial amount of the bromide and total iron was found in the monitoring well MW-1, which is located about five feet down-gradient from the injection well. However, the concentration of bromide and the total iron remained around the pre-injection level in the downstream monitoring well MW-2 to MW-3 and the upstream monitoring well MW-4 even two months after injection. The absence of bromide in the monitoring wells MW-2 and MW-3 may indicate that after leaving the first monitoring well MW-1, the injected fluid followed a different pathway, rather than the predetermined groundwater flow direction as the other monitoring wells were installed. The change of injected fluid pathway might be attributed to seasonal variation of groundwater flow pattern around the lake area (Anderson and Munter, 1981), considering that the test site was located near the Great Salt Lake . Williams (1968) observed that the direction of groundwater flow in the vicinity of two basins in the northeastern Illinois could even be reversed during wet and dry seasons. It is also noted that on the third day of the second injection, a fraction of Fe-Pd nanoparticles was forced out of the ground surface under pressure in the vicinity of MW-1, instead of moving horizontally down-gradient. The upward migration of the Fe-Pd nanoparticles can be attributed to excessive

buildup of hydrostatic pressure during the nanoparticles injection. The remedial injection of Fe-Pd nanoparticles was applied in an uppermost shallow unconfined aquifer where the water table was only 16.4 ft bgs. The soil permeability in this aquifer was found very low, with a hydraulic conductivity of only 0.01 ft/day. It is plausible that a the buildup of hydrostatic pressure by the injection of non-compressible Fe-Pd nanoparticles occurred, resulting in soil fracturing in the subsurface and ultimately leading the injection fluid to the surface along a path of least resistance. Therefore, proper design of the injection program is needed for injection into the unconfined shallow aquifer with very low hydraulic conductivity.

The normalized concentration (C/C_0) of the total iron in MW-1 was compared with that of the bromide to determine the mobility of the Fe-Pd nanoparticles in the subsurface aquifer, as indicated in **Figure 5-4**. The iron breakthrough and peak concentration arrival time agreed very well with that of the conservative tracer, which is consistent with our previous lab studies (He et al., 2009b). It is noted that during the second injection, the normalized peak concentration to the initial injection concentration for bromide ion in MW-1 is about 0.92, as compared to the normalized peak concentration of the iron at 0.58. A mass recovery of tracer lower than 100% might be due to a poor hydraulic connection between adjacent wells (Sanford et al., 2006) or the effect of groundwater dilution and dispersion. Therefore, a direct comparison of the normalized peak concentration (C/C_0) of tracer and the total iron is not sound to evaluate the Fe-Pd nanoparticles mobility. The percentage of the injected iron which was transported to MW-1 (the area under the normalized concentration curves versus time) was compared to that of tracer, as an indicator of the nanoparticles deliverability. In this

manner, the amount of Fe-Pd nanoparticles transported to MW-1 is about 19% of that for bromide. The recovery of the total iron in this test is lower than that reported by He et al. (2010) for a sandy aquifer, where the iron transported to 5 ft down-gradient from the injection well could amount to 37.4% and 70% of that for the tracer. The injected Fe-Pd nanoparticles could be absorbed on the soil grains (Zhang et al., 2011) or intercepted via filtration effect (He et al., 2009b) when migrating through the soil matrix.

The low recovery of total iron in this test indicated a significant retention of Fe-Pd nanoparticles in the vicinity of the injection well. Although the mobility of iron nanoparticles is limited under the test condition, the retained Fe-Pd nanoparticles in this test area could still serve as a reactive permeably barrier in the subsurface for degradation of chlorinated solvents when they flow through along with the groundwater.

.

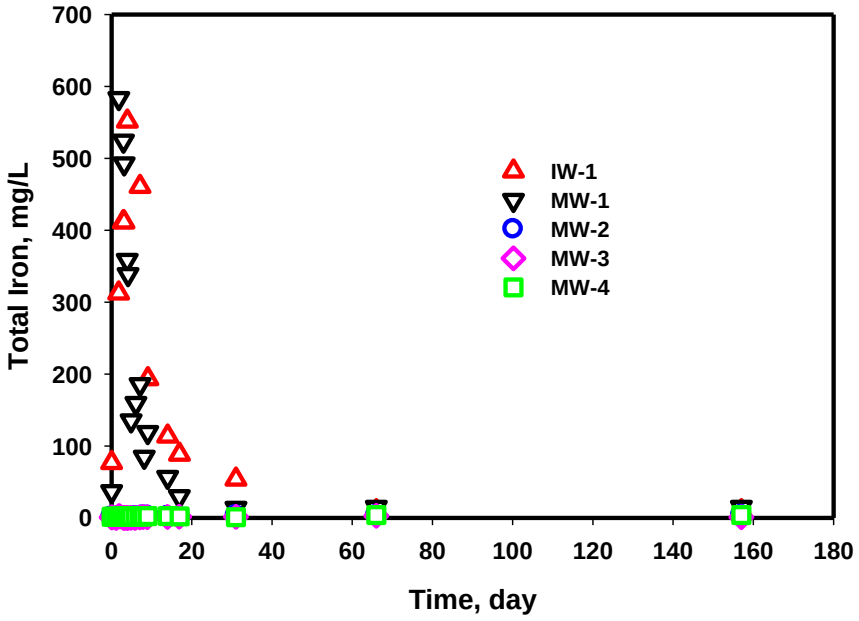

(a)

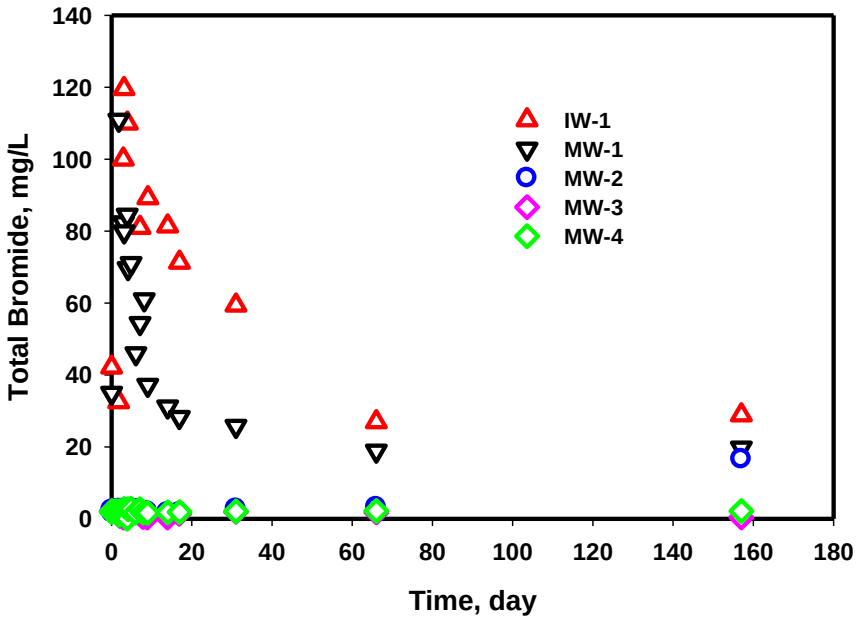

(b)

Figure 5- 3. The concentration histories of the total iron **(a)** and the tracer Bromide **(b)** in the groundwater from the monitoring wells.

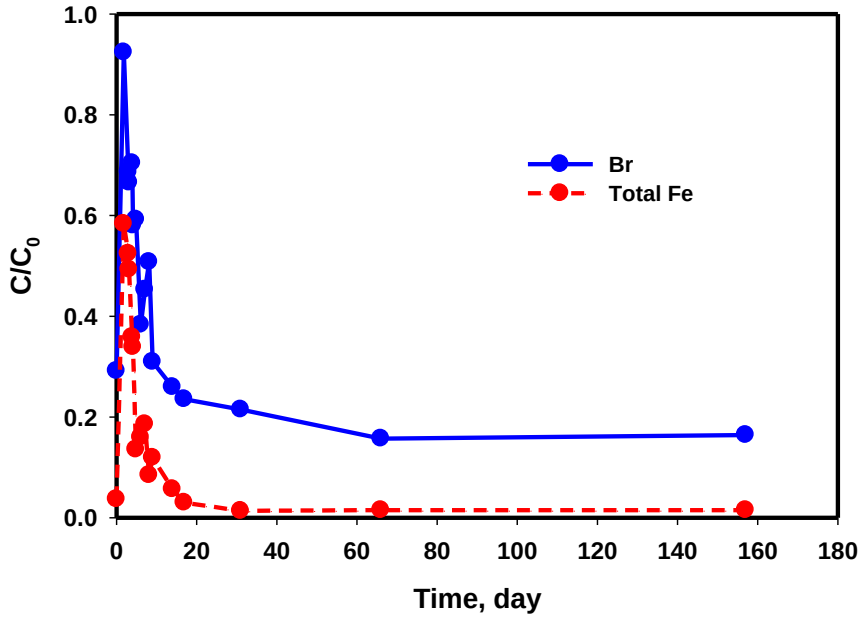

Figure 5- 4. The normalized breakthrough concentration (C/C_0) for the tracer Bromide and the total iron monitored in the MW-1.

5.3.4 Effects of nanoparticle injection on groundwater chemistry

The injection of Fe-Pd nanoparticles into the subsurface would break the prevailing chemical equilibrium state in the groundwater and alter the groundwater chemical conditions, such as the oxidation/reduction potential (ORP), dissolved oxygen (DO), and total organic carbon (TOC).

The ORP is known as an indicator of the ability of one substance to accept or lose electrons. It has been widely adopted in the field test of iron to monitor the changes in groundwater chemistry (Elliott and Zhang, 2001; He et al., 2010; Wei et al., 2010).

Typically, positive values of ORP indicate oxidizing conditions, while negative values of ORP represent reducing conditions, which are desirable for reductive dechlorination process. The baseline ORP of groundwater sampled from IW-1, MW-1, MW-2, MW-3, MW-4 was 173, 111, 123, 151 and 168 mV, respectively, indicating an oxidizing condition predominated in the test area before injection. After the first injection, the ORP values in groundwater decreased rapidly to negative in all four monitoring wells, as shown in **Figure 5-5**. At the end of the first Fe-Pd injection, the ORP of the down-gradient monitoring wells MW-1, MW-2, MW-3 and MW-4 reduced to -526, -143, -94 and -99 mV, respectively, indicating that a strongly reducing condition was established throughout the test area. That may be attributed to the production of hydrogen gas due to the iron corrosion or the consumption of dissolved oxygen (DO) and other oxidizing agents by Fe-Pd nanoparticles. The DO in MW-1, MW-2, MW-3 and MW-4 decreased from the baseline value of 4.5, 4.1, 4.8 and 5.8 mg/L to 0.02, 1.5, 0.45 and 2.18 mg/L, respectively. At the beginning of the second injection (38 days after the first injection), the ORP values in the IW-1 and MW-1 remained at -606 mV and -265

mV, respectively. However, a slightly oxidizing condition (-6.4 ~18.1mV) appeared in wells MW-2 through MW-4. Along with the second injection of Fe-Pd nanoparticles, the ORP values quickly dropped in IW-1, MW-1 and MW-2 to the bottom value of -548, -516 and -103 mV on the 3rd day and then gradually bounced back to -198, -269 and -104mV on the 66th days, respectively. The subsequent rise in ORP was attributed to the consumption of the reducing capacity of Fe-Pd nanoparticles. However, different from the first injection, the ORP values stayed positive in MW-3 and MW-4 most of the time during and after the second injection. These results are in agreement with the observation that no significant amounts of Fe-Pd nanoparticles were observed in MW-3 and MW-4, as shown in **Figure 5-3**.

The polysaccharide stabilizer CMC is known to act as a carbon source that supports the growth of bacteria during the reductive degradation of chlorate under anaerobic conditions (van Ginkel et al., 1995). Therefore, the presence of CMC could hold promise to promote bacteria growth for in-situ biodegradation. The TOC concentration in the groundwater was selected as an indicator to monitor the transport of CMC. The baseline TOC concentration in IW-1, MW-1, MW-2, MW-3 and MW-4 was only 4.1, 20.6, 3.9, 3.3 and 3.2 mg/L, respectively.

At the beginning of the second injection, the TOC concentration in IW-1 and MW-1 was observed at 520 mg/L and 402 mg/L, respectively. The high TOC concentration was attributed to the presence of some residual CMC-stabilized particles in these two monitoring wells from the first injection. The groundwater samples extracted from IW-1 and MW-1 indicated about 76.7 mg/L and 36.7 mg/L of Fe still existed prior to the second injection. Interestingly, the TOC concentration in the monitoring wells

agreed well with the observed total iron concentration. As shown in **Figure 5-6**, after the second injection, the TOC concentration in wells IW-1 and MW-1 increased rapidly from 520 mg/L and 402 mg/L to 1843 mg/L and 1451 mg/L, respectively, on the 3rd days. On the same day, the total iron concentration in wells IW-1 and MW-1 also reached their peak values, as shown in **Figure 5-3**. The similar behavior of TOC and total iron concentration implied that CMC was primarily adsorbed on the surface of Fe-Pd nanoparticles and migrated following the same pathway as the nanoparticles in the subsurface aquifer.

However, it is also noted that although there was no discernable change of the total iron concentration in the monitoring wells MW-2, MW-3 and MW-4, TOC was observed to increase slightly from the 9.1, 2.7 and 20.2 mg/L to 40, 25 and 89 mg/L, respectively, on the 31^{th} day after the second injection. These results indicated that some of the CMC on the nanoparticles could be released into the groundwater along with the consumption of Fe-Pd and become more accessible for microorganisms in water.

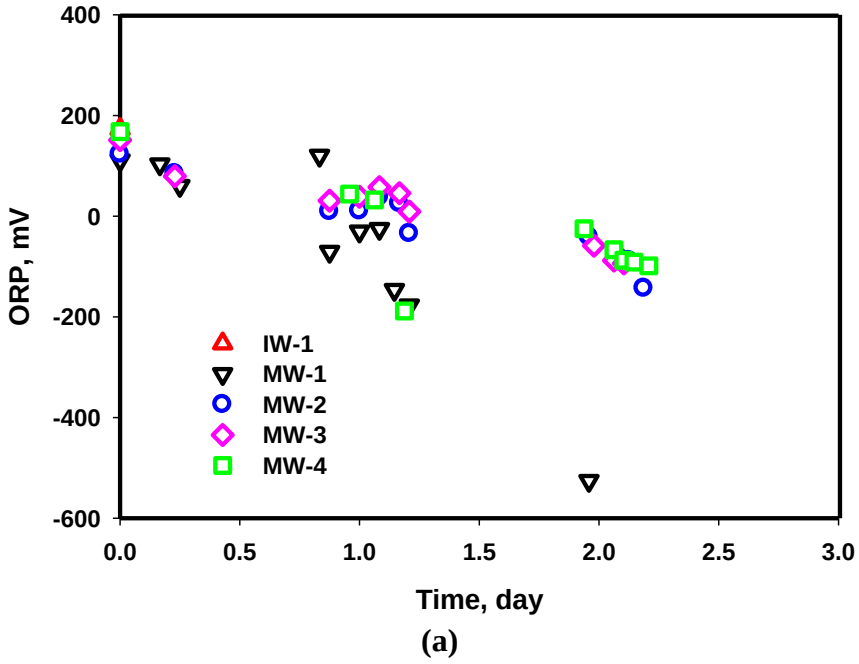

(a)

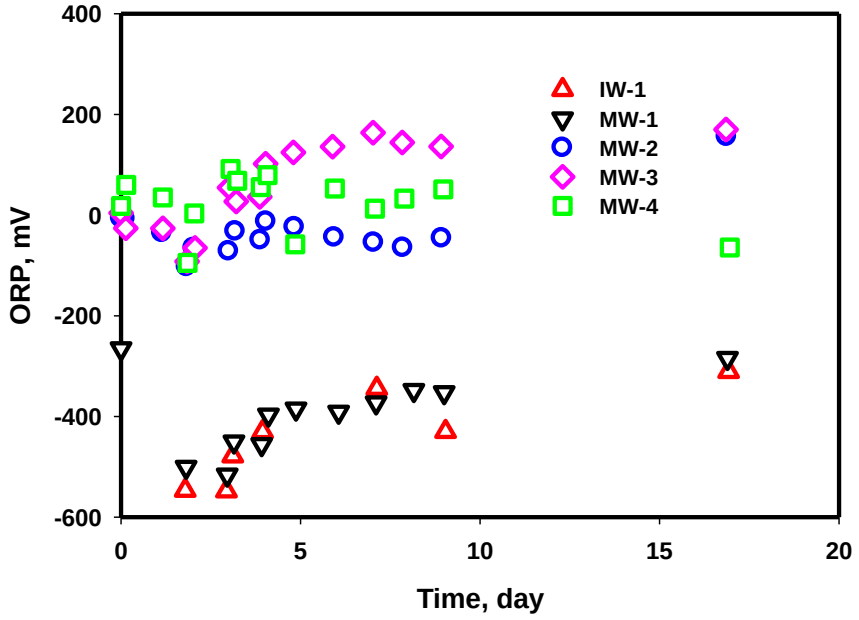

(b)

Figure 5- 5. Change of oxidation and reductive potential in monitoring wells during **(a)** the first injection and **(b)** the second injection.

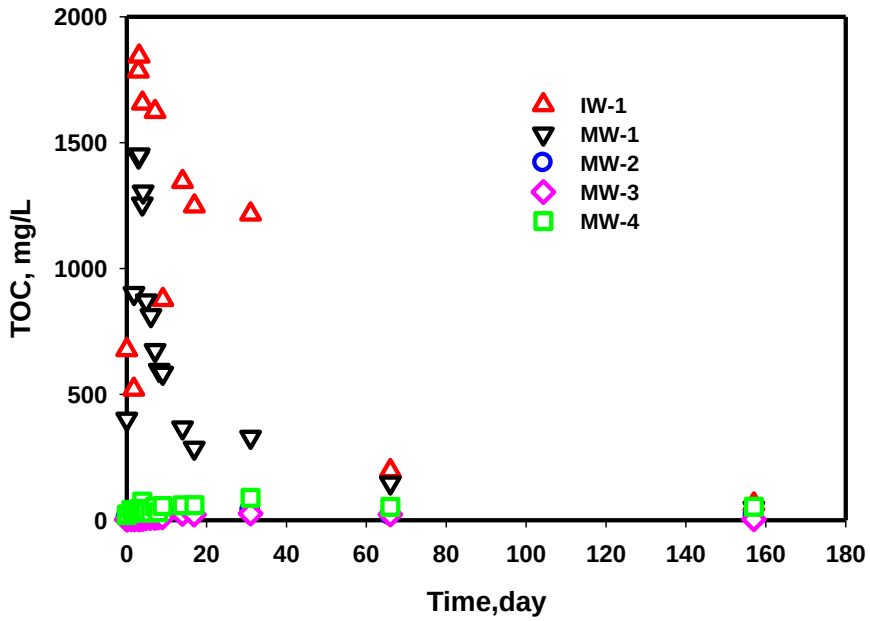

Figure 5- 6. Change of total organic carbon in the monitoring wells after the second injection

5.3.5 Degradation of Chlorinated solvents

The normalized concentration history of TCE in the groundwater after the second injection is illustrated in **Figure 5-7**. In the IW-1, the TCE concentration rapidly decreased to below the detection limit immediately after injection and remained under 0.2 mg/L until the 14^{th} days. On the 17^{th} days after the second injection, the TCE concentration started gradually increasing to 32% of the pre-injection concentration on the 66^{th} day, which indicated a slow exhaustion of the reactivity of Fe-Pd nanoparticles. Rapid degradation of TCE was also observed in the well MW-1. The TCE concentration remained at a low concentration of only about 10% of the pre-injection level in the first two days after injection. However, after five days the TCE concentration started to bounce back until the 17^{th} day and stayed at 75% -85% of the pre-injection level from then on. The TCE concentration in the following monitoring well MW-2 also decreased to 63% of the baseline concentration within ten days after the second injection. This might be attributed to the dilution from the up-gradient groundwater in which most TCE was removed as a result of a rapid abiotic reductive dechlorination.

It is noted that after 31 days, the TCE concentration in wells MW-1 and MW-2 gradually decreased again. At the 157^{th} days, TCE concentration in MW-1 and MW-2 was only 16.5 and 19.1mg/L, respectively, which was only 50.6% and 68.6% of the pre-injection concentration. It might be due to the prolonged reduction of TCE by the Fe-Pd nanoparticles retained in the soil pores or intercepted in the soil matrix, and/or reductive biodegradation of chlorinated solvents enhanced by the injection of Fe-Pd nanoparticles where CMC serves as the carbon source for bacteria growth and the hydrogen gas produced from iron corrosion acts as the electron donor.(He et al., 2010)

Ethane and ethene are the primary reaction products of abiotic reductive dechlorination of TCE by zero valent iron (Liu et al., 2005). Concentrations of ethane and ethene in the groundwater from the monitoring wells were monitored and shown in **Figure 5-8**. Ethane concentration was observed to increase up to three orders of magnitude after Fe-Pd nanoparticles injections. Thirty-eight days after the first injection, a significant increase of the ethane concentration in IW-1, MW-1, MW-2, MW-3 and MW-4 was observed from the baseline concentration of 1.0, 1.6, 0.6, 0.4 and 0.05 mg/L to 380, 680, 58, 2.3 and 35 mg/L, respectively. About 31 days after the second injection, the ethane concentration further rose up to 690, 1100, 53, 1.6 and 95 mg/L, respectively. Similar trends were observed for the ethene concentrations. As shown in **Figure 5-8 (b)**, the ethene concentration in IW-1, MW-1, MW-2, MW-3 and MW-4 increased from the baseline concentrations of 0.9, 4.3, 1.9, 0.8 and 0.09 mg/L to 140, 180, 4.1, 2.3 and 0.4 mg/L, respectively. Thirty-one days after the second injection, the ethane concentration was detected up to 220, 120, 7.7, 2.9 and 6.3 mg/L, respectively. A significant production of ethane and ethene indicated an effective abiotic dechlorination of TCE and other chlorinated compounds occurred right after Fe-Pd nanoparticles injections at the site.

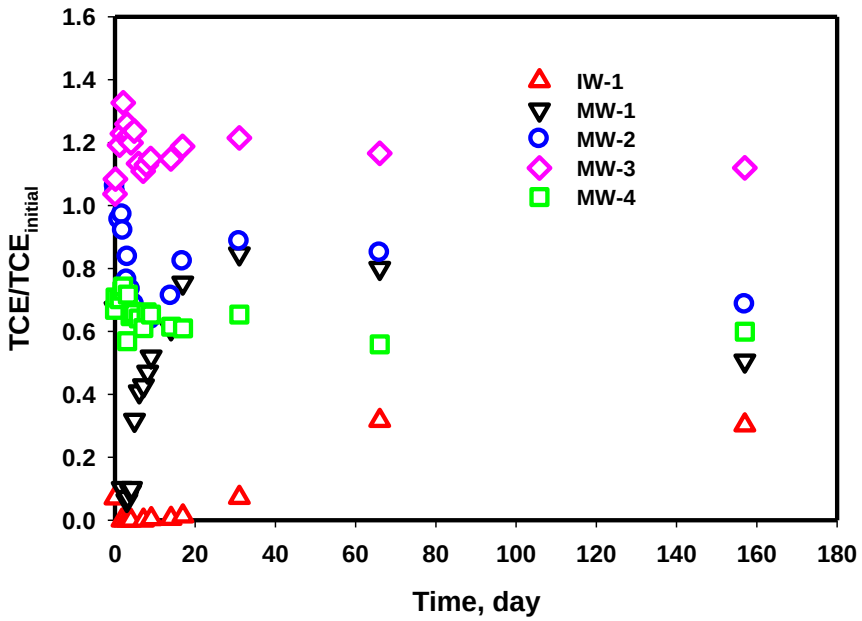

Figure 5- 7. Normalized concentration histories of TCE in groundwater from the installed 5 wells following injection #2. The pre-injection concentration of TCE is IW-1, MW-1, MW-2, MW-3 and MW-4 was 47.4, 32.7, 27.9, 9.77 and 10.8 mg/L, respectively.

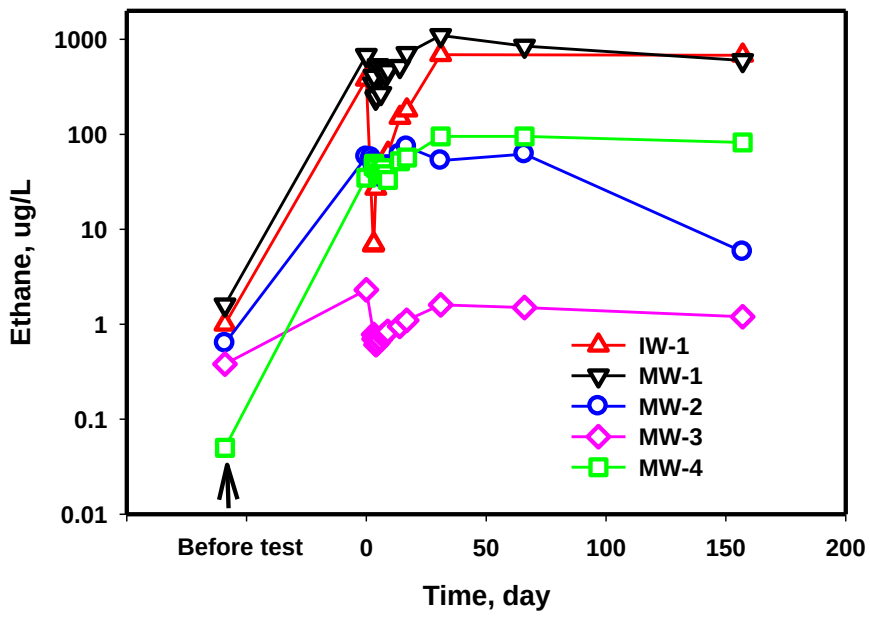

(a)

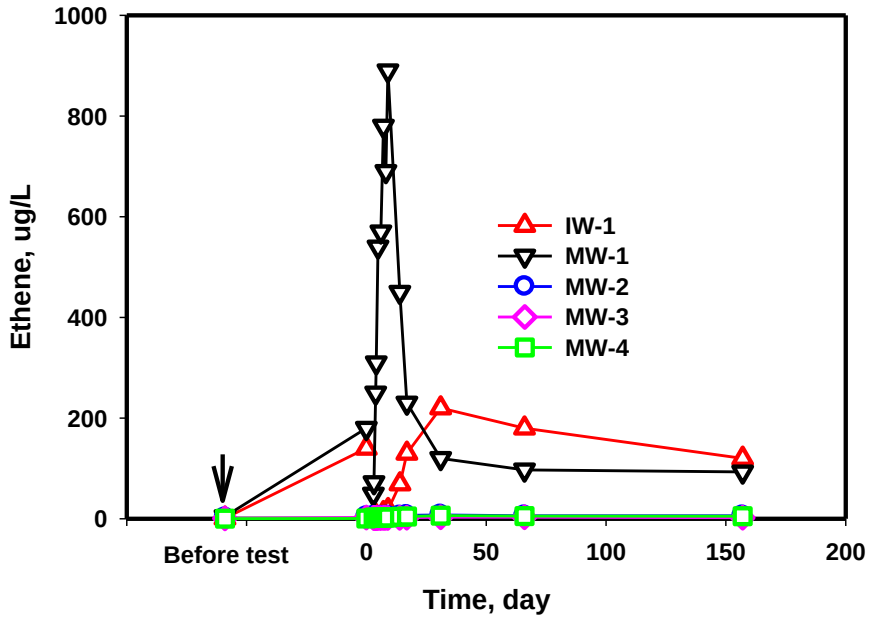

(b)

Figure 5- 8. Evolution of ethane (a) and ethene (b) after Fe-Pd nanoparticles injection.

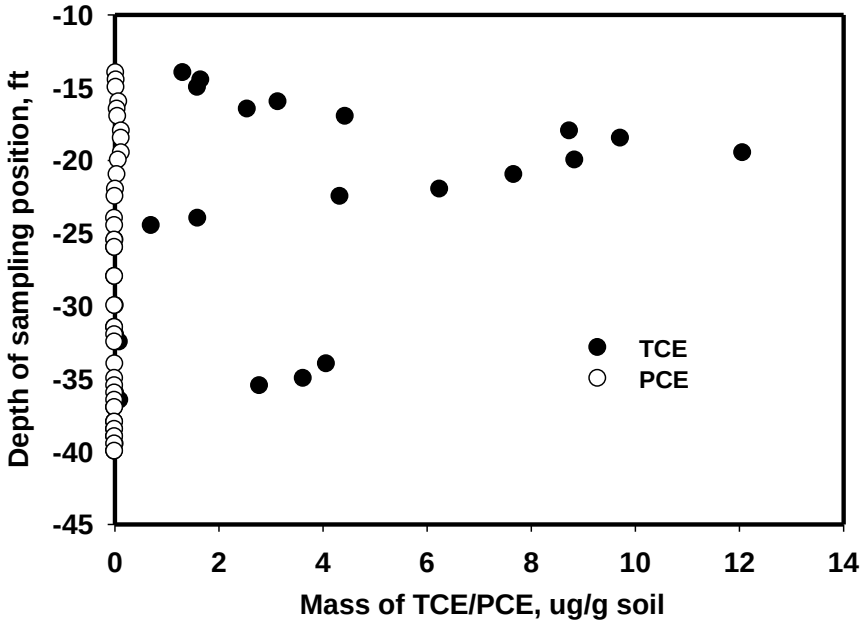
-10
-15
-20
-25
-30
-35
-40
-45
Depth of sampling position, ft
0
2
4
6
8
10
12
14
Mass of TCE/PCE, ug/g soil
TCE
PCE

(a)

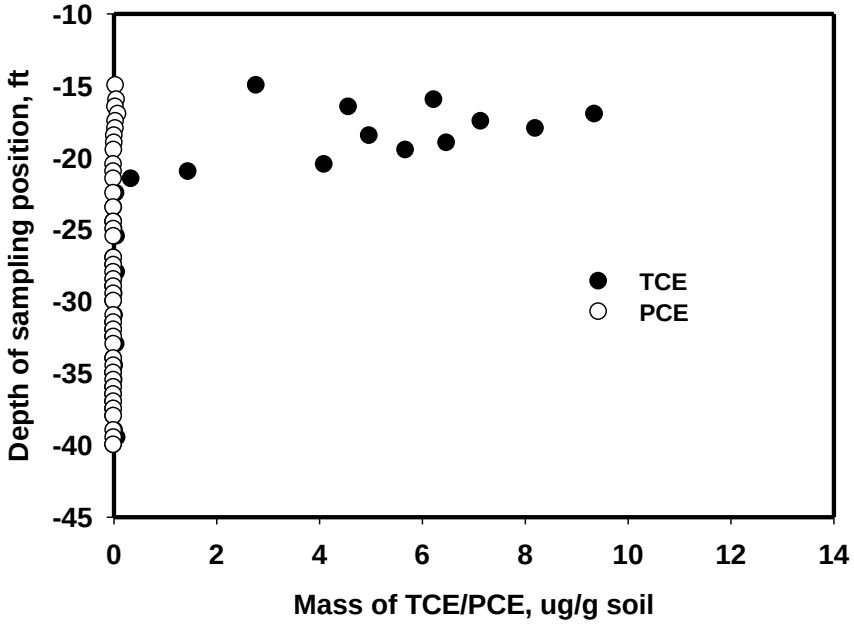
-10
-15
-20
-25
-30
-35
-40
-45
Depth of sampling position, ft
0
2
4
6
8
10
12
14
Mass of TCE/PCE, ug/g soil
TCE
PCE

(b)

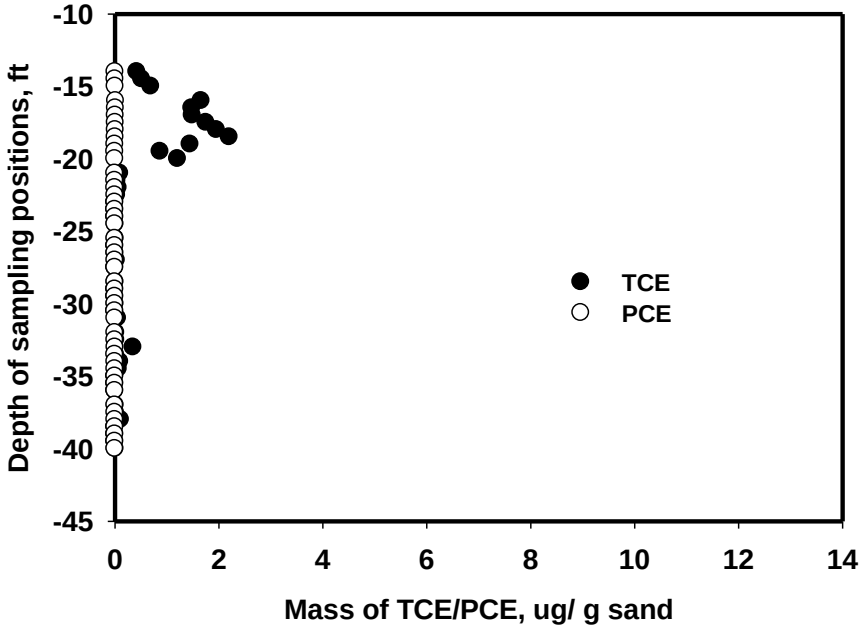

(c)

Figure 5- 9. TCE/PCE concentration distributions in the soil samples from **(a)** SB-1, **(b)** SB-2 and **(c)** SB-3 before Fe-Pd nanoparticles injections

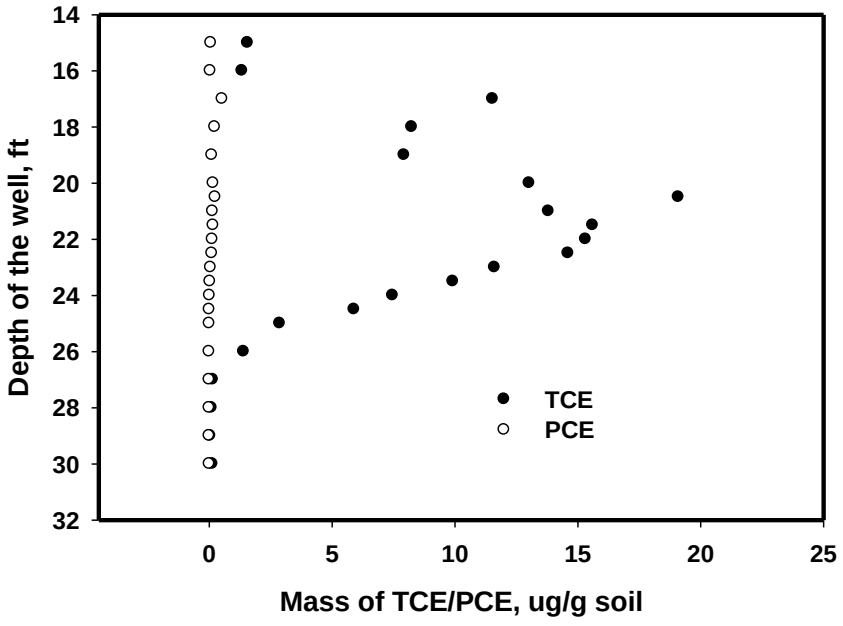
Depth of the well, ft
14
16
18
20
22
24
26
28
30
32
0
5
10
15
20
25
Mass of TCE/PCE, ug/g soil
TCE
PCE

(a)

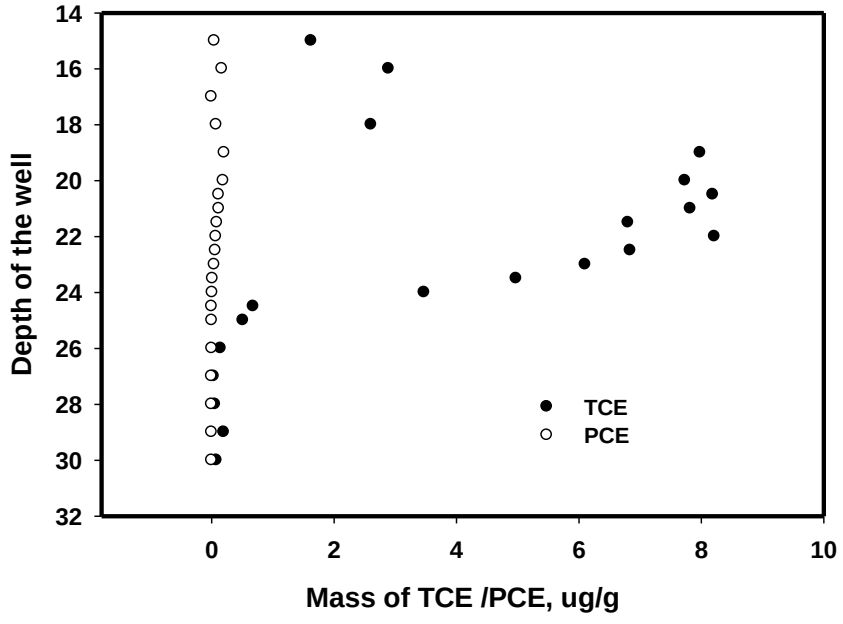
Depth of the well
14
16
18
20
22
24
26
28
30
32
0
2
4
6
8
10
Mass of TCE /PCE, ug/g
TCE
PCE

(b)

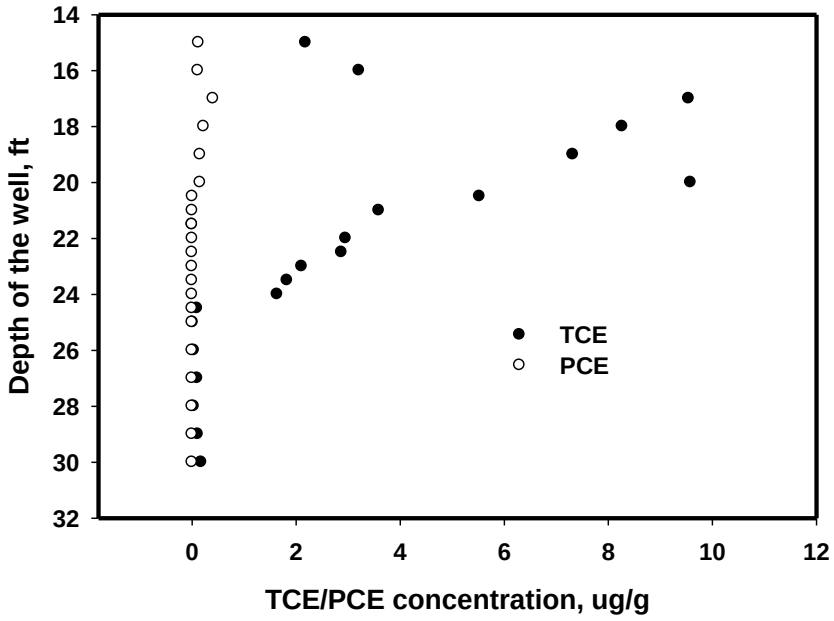

(c)

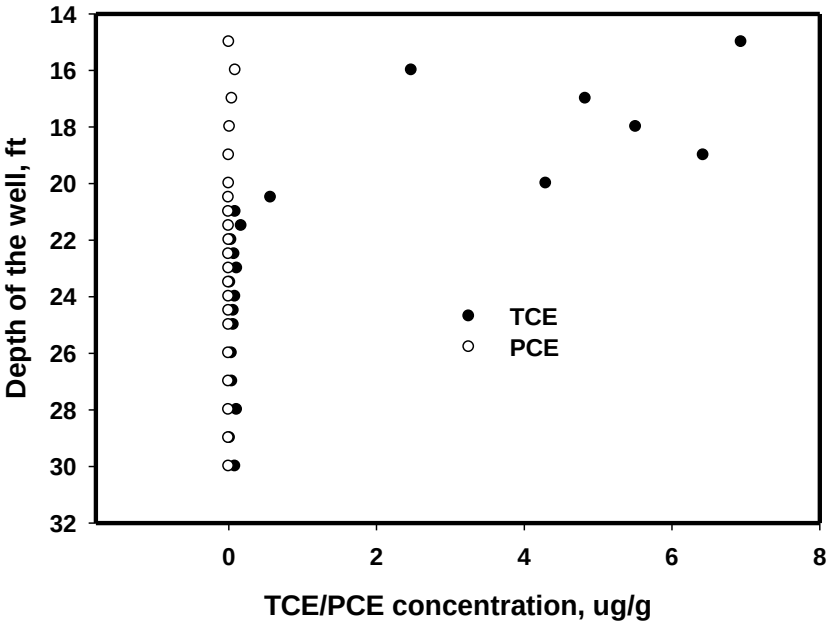

(d)

Figure 5- 10. TCE/PCE concentration distributions in the soil samples from **(a)** SB-4, **(b)** SB-5, **(c)** SB-6 and **(d)** SB-7 two months after Fe-Pd nanoparticles injection

Soil samples from the tested area were obtained and analyzed before and after Fe-Pd injections to evaluate the change of chlorinated solvent concentrations in soil. The TCE and PCE concentrations in the soil samples from three boreholes (SB-1, SB-2, SB-3) from the interval (15-40 ft) before the field test were shown in the **Figure 5-9**. TCE is the predominant contaminant in the soil phase. In all of these three cores, the TCE concentration gradually increased with depth from 15ft bgs to about 20 ft bgs and then progressively decreased to less than 0.1μg/g soil from the interval of 20- 25 ft bgs. Among these cores, TCE is the most concentrated in the SB-1, with a peak value of 12.1 μg/g at the depth of 19.5 ft bgs. PCE is also detectable; however, its concentration is no higher than 0.13 μg/g soil in the sample area.

Approximately two months after the second injection of Fe-Pd nanoparticles, soil samples were collected in the vicinity of the injection area. The TCE and PCE concentration distribution in four soil boreholes were shown in **Figure 5-9**. Although there was a remarkable decrease of TCE in the groundwater, no significant decrease in TCE concentration was observed in soil phase. In the borehole SB-4, the peak concentration of 19.1 μg/g is found at the depth of 20.5 ft bgs. This even higher than the baseline values in TCE concentration is most likely due to the spatial variability in contaminant concentration in the soil phase.

The lower than anticipated degradation of TCE in the soil is probably due to the limited mobility of Fe-Pd nanoparticles in this test area. As discussed earlier, the majority of the Fe-Pd nanoparticles injected was intercepted and immobilized near the injection well and MW-1. Therefore, the primary treatment mechanisms would be the destruction of chlorinated solvents by these immobilized iron nanoparticles as the reactive permeable

barriers for destruction of chlorinated ethenes. They are more effective to reduce the mobile contaminants which would move through the reactive immobilization area of Fe-Pd with groundwater, than those strongly sorbed in the soil which is considered "immobile", resulting in an inappreciable change of chlorinated solvents in the soil phase even two months after Fe-Pd injection.

5.4 Conclusion

The field testing results indicated that CMC-stabilized iron nanoparticles will hold promise for in situ destruction of chlorinated solvents in soil and groundwater. These stabilized Fe-Pd nanoparticles were readily delivered into the contaminant source area via pumping and migrated to at least five- feet down-gradient of the injection well, even in a low-permeability area. Rapid abiotic dechlorination of chlorinated solvents was observed sooner after the Fe-Pd nanoparticles injection, along with a significant increase of abiotic dechlorination products, i.e., ethane and ethene. Biodegradation might be boosted considering a further decrease of TCE concentration in MW-1 and MW-2 66 days after the Fe-Pd injections, but long-term monitoring data will be needed to assess if appreciable contaminant removal occurred, which would support a contribution due to biological activity. When injecting the nanoparticles into a shallow, unconfined aquifer with low permeability, a proper design of the injection program is required to avoid excessive pressure buildup in the subsurface.

CHAPTER 6. Conclusions and Recommendations for Future Research

6.1 Summary and Conclusions

Zero valent iron nanoparticles have proved to be an effective technology for in situ destruction of various chlorinated solvents in water in both laboratory and field tests, however, little is known about the effectiveness for degrading soil-sorbed contaminants. This work investagated reductive dechlorination of trichloroethylene (TCE) sorbed in two model soils using CMC stabilized Fe-Pd bimetallic nanoparticles. Experimental results showed that these nanoparticles can effectively degrade soil-sorbed TCE. However, the TCE degradation rate can be strongly limited by desorption kinetics, especially for soil of higher SOM content, such as a potting soil (sandy loam) which has an organic content of 8.2%. Under otherwise identical conditions, ~44% of TCE sorbed in the potting soil was degraded in 30 h, while ~82% of sorbed TCE could be destructed in a loam soil (organic matter content= 0.7%). DOM from the potting soil could inhibit TCE degradation. The presence of the soil exudates at 40 mg/L and 350 mg/L as TOC reduced the TCE degradation rate by 34% and 67%, respectively. Four prototype surfactants were tested for their effects on TCE desorption and degradation rates in soil, including two anionic surfactants known as SDS (sodium dodecyl sulfate) and SDBS (sodium dodecyl benzene sulfonate), a cationic surfactant hexadecyltrimethylammonium (HDTMA) bromide, and a nonionic surfactant Tween 80. All four surfactants were observed to enhance TCE desorption at concentrations below or above the critical micelle concentration, with SDS being most effective. Based on the pseudo-first-order reaction rate law, the presence of 1

x cmc SDS also could increase the TCE degradation rate by a factor of 1.7 when the nanoparticles were used in a water solution. However, effect of SDS on TCE degradation in the potting soil was more complex. The presence of SDS at sub-cmc concentrations decreased TCE degradation by 5%; however, when the SDS dosage was raised to 5 x cmc, the degradation rate was increased by 5%. The opposing effects were attributed to combined effects of SDS on TCE desorption and degradation, release of soil organic matter and nanoparticle aggregation.

The fate and transport behavior of CMC-stabilized ZVI nanoparticles in the subsurface aquifers have been of great interest for in-situ application of the technology. A systematic investigation of the transport behavior of stabilized ZVI nanoparticles in sand columns was carried out under various surface properties of the sand medium and solution chemistries. CMC-stabilized ZVI nanoparticles displayed superior mobility in the quartz sand and the maximum breakthrough concentration reached about 93% of the influent CMC-ZVI level. More deposition of the nanoparticles was observed when the sand surface was coated with iron oxide or aluminum oxide. A revised transport model was proposed and tested. The new model distinguishes adsorption and filtration removals of the nanoparticles in the porous medium, with the adsorption arte being determined through independent batch adsorption kinetic tests. The simulation results indicated that at a low pore velocity of 0.0353 cm/s, the filtration effect predominated the transport of ZVI nanoparticles in sands, while the contribution of particle adsorption on the retention of ZVI became more significant when the pore velocity doubled. When a water soluble starch was used to stabilize the ZVI nanoparticles, the maximum breakthrough concentration (C/C_0) of starch-ZVI reached 0.83. Relatively less particle deposition of

CMC-ZVI in the effluent was observed when the influent concentration of ZVI increased from 0.05 g/L to 0.8 g/L, while the presence of 40 ~ 80 mg/L DOM as TOC had insignificant impact on the breakthrough profiles of the nanoparticles. It is noteworthy that the attachment of CMC-stabilized ZVI nanoparticles was insensitive to change in ionic strength. Increasing Ca^{2+} concentration to 200 mM led to no difference in the effluence concentration of ZVI. Our findings indicated that the presence of stabilizers would modify the original surface properties of bare ZVI nanoparticles and effectively facilitate the deliverability of nanoparticles in the subsurface.

A field test was performed at the Hill Air Force Base in Utah to demonstrate the performance of CMC-stabilized Fe-Pd nanoparticles for in situ destruction of chlorinated solvents in groundwater and soil. CMC-stabilized Fe-Pd nanoparticles were freshly prepared on site right before each injection. Approximately 2.7 kg of nanoparticles as iron were injected into the test area which mainly consists of silty clay with some thin sand seams. The delivered Fe-Pd nanoparticles were observed in a five-feet downgradient monitoring well. Results from this field demonstration confirmed the effectiveness of stabilized Fe-Pd nanoparticles for in situ destruction of chlorinated solvents. TCE concentrations declined rapidly to below the detection limit (5 µg/L) in the injection well IW-1 following the injection. Accordingly, the concentration of final degradation products, i.e. ehane and ethene, increased by up to three orders of magnitude in the injection well IW-1 and monitoring wells MW-1. However, the further transport of the iron nanoparticles to MW-2 and MW-3 was impeded due to the low permeability of subsurface formation, suggesting that a proper design of the injection system is needed for successful remediation in shallow, unconfined aquifers with low permeability.

To facilitate hydrodechlorination of TCE in the liquid phase under ambient conditions, a new class of supported Pd catalyst was prepared and tested by depositing CMC-stabilized Pd nanoparticles on three support materials (alumina, Ambersorb 572 and TS-1). The alumina supported Pd nanoparticles catalyzed the rapid hydrodechlorination of TCE, with no production of chlorinated intermediates. Under the Pd loading of 0.33% of the support weight, the catalytic activity (k_{obs}) of the alumina-supported Pd increased from 28 to 109 L/min/g, when the size of the precursor CMC-stabilized Pd nanoparticles decreased from 4.8±1.6 nm to 2.7±0.8 nm. DOM from a sandy loam soil did not retard the TCE hydrodechlorination rate at a concentration of 10 mg/L as TOC. A weaker and incomplete catalytic activity was observed when the highly hydrophobic carbonaceous resin Ambersorb 572 was used as a support, which was attributed to carbon contamination of Pd during calcination and the strong adsorption and the retarded mass transfer of TCE on support. TS-1 offered superior catalytic performance over alumina, suggesting that a support of modest hydrophobicity would favor the hydrodechlorination process.

6.2 Recommendations for future research

While this work demonstrated that CMC-stabilized Fe-Pd nanoparticles were able to degrade chlorinated solvents sorbed in the soil phase, this technology bears with several key limitations when used for in situ remediation. First, it has to overcome the inhibitive effect of DOM at elevated concentrations; second, it has to overcome desorption limitation, and thus, it more suitable for soils of low-SOM content; third, while the use of carboxymethyl cellulose as a stabilizer improves the soil deliverability and reactivity of iron nanoparticles, the hydrophilic nature of CMC will limit the partition

of iron nanoparticles into the bulk TCE through the water/NAPL interface. Consequently, it is desirable to develop a strategy to improve the partition of stabilized Fe-Pd nanoparticles into the organic phase for DNAPL remediation. To this end, Zhan et al. (2009) proposed the idea of depositing CMC stabilized Fe-Pd nanoparticles onto carbon microsphere to enhance the partition of iron nanoparticles to the organic phase. However, our study on the bleeding of Ambersorb-572 supported Pd catalysts revealed that approximately 40% of Pd nanoparticles was leached out from the carbonaceous resin. Therefore, the stability and bleeding of iron nanoparticles on the carbon support would be of concern.

Column studies have confirmed the iron nanoparticles could be delivered into porous media under various groundwater chemical conditions. However, experimental studies are usually conducted with uncontaminated "idealized" porous media. However, it is known that the morphology and physical-chemical properties of iron nanoparticles will change after long-term aging or reacting with contaminants, which may subsequently alter the particle transport behavior. Therefore, column tests with contaminated real soil or even NAPL plumes would be of interest to predict the reactive transport behavior of iron under real environmental conditions. A transport model coupled with reductive dechlorination process will provide an better insight into nanoparticles transport under field conditions.

To prepare more effective supported Pd catalysts, a support of modest hydrophobicity is needed. This support should offer similar characteristics to TS-1, but should be less costly.

Appendix. Reactivity of Metal Nanoparticles towards Hydrodechlorination of Chlorinated Solvents: Influence of Catalyst Metals and Organochlorinated Compounds

7.1 Introduction

Catalytic hydrodechlorination using hydrogen gas and a noble metal has been successfully used for effective destruction of a broad range of chlorinated environmental contaminants such as chlorinated aliphatics, olefins and aromatics, under mild conditions. Concentrations of only a few parts per billion (ppb) of these potential carcinogens in drinking water are enforced by US EPA. Nobel metals such as Pd, Pt and Ni have been shown to effectively catalyze the hydrodechlorination reaction in either water or gas phase. Lowry and Reinhard (1999) reported that alumina supported Pd catalyst could facilitate rapid destruction of tetrachloroethylene (PCE), trichloroethylene (TCE), cis-, trans-, 1,1-dichloroethylene (DCE), carbon tetrachloride and 1,2-dibromo-3-chloropropane by hydrogen at ambient conditions without forming harmful chlorinated intermediates. Supported Pt on alumina/activated carbon was used for hydrodechlorination of carbon tetrachloride (Bae et al., 2003), chlorobenzenes (Hashimoto et al., 2005), and chlorinated ethanes and ethenes (Ordonez et al., 2000). Gold has been considered less active towards dechlorination process (Andersin and Honkala, 2011), however, Cwiertny et al.(2007) reported the presence of Au would enhance the reductive dechlorination of cis-DCE by zero valent iron nanoparticles.

The reaction rate of catalytic hydrodechlorination would depend on the nature of the noble metals. For example, the reaction activity of carbon-supported catalysts followed the order of Pd/C>>Pt/C>Rh/C>Ru/C>Ni/C during the hydrodechlorination of carbon tetrachloride carried out in the liquid phase (Gomez-Sainero et al., 2000). The structure of chlorinated compounds also plays an important role in controlling reaction rates. Under identical conditions over a commercial Pd/Al_2O_3 catalyst, the hydrodechlorination rate of carbon tetrachloride was 14.5 times faster than that of chloroform (Lowry and Reinhard, 1999).

Although there are a growing number of studies on the catalysis of hydrodechlorination, there exists a challenge to systematically compare the reactivity of different noble metals towards different halogenated compounds using the results from the literature. This is because the operation conditions in these studies differed, i.e. the size and mass loading of active metals, the reaction temperature, the reaction media, the catalyst supports and etc. To this end, Mackenzie et al. (2006) conducted a systematic study on the dechlorination reactivity of a wide range of halogenated hydrocarbons in water with a commercial alumina-supported Pd catalyst. Yet, information is still needed to explain the different behavior of different noble metal catalysts.

To enhance the catalytic activity of noble metals for hydrodechlorination, one strategy has been employed is developing unsupported, nano-scale metal catalysts by utilizing its greater specific surface area and size-dependent catalytic activity. It is generally accepted that the catalytic hydrodechlorination is mediated over the surface of catalyst metals. Decreasing the particle size to the nano-scale will render a higher percentage of active atoms on the surface, thereby enhancing the reaction rate. For

example, the small Pd nanoparticles (3.6 nm) prepared using sodium carboxymethyl cellulose (CMC) as a capping agent was found to be 1647 times more reactive than Pd black (He et al., 2009a). It is also expected that the catalytic reactivity of other noble metals will be greatly enhanced when their particle sizes are reduced to nanoscale although their performance on hydrodechlorination of chlorinated solvents have not been explored.

The overall objective of this research was to evaluate the catalytic hydrodechlorination reactivity of three air stable metal nanoparticles towards both vinyl polyhalides and alkyl polyhalides, and use this information to probe the reaction mechanism of catalyzed hydrodechlorination. A green and low-cost polymer, CMC, is used as the capping agent to prepare highly dispersed metal nanoparticles. The CMC-stabilized metal nanoparticles were employed as catalysts to eliminate the potential effect of catalyst support on the reaction rate. The specific objectives were to 1) prepare various highly-dispersed metal nanoparticles using a green stabilizer CMC in aqueous phase; 2) evaluate the catalytic reactivity of the as-synthesized metal nanoparticles toward both vinyl and alkyl polyhalides; and 3) explore the reaction mechanisms of vinyl and alkyl polyhalide reduction catalyzed by metal nanoparticles.

7.2 Materials and experimental methods

7.2.1 Materials

$Na_2PdCl_4 \cdot 3H_2O$ was purchased from Strem Chemicals (Newburyport, MA, USA). $H_2PtCl_6 \cdot 6H_2O$ precursor was purchased from Acros Organics (Morris Plains, NJ, USA). $HAuCl_4 \cdot 3H_2O$, Carboxymethyl cellulose (CMC) sodium salt (average *MW:* ~ 90 000),TCE and PCE of spectrophotometric grade (>99%), PCE, 1,1,1-TCA and 1,1,1,2-

TeCA of analytical standard, were obtained from Sigma-Aldrich (St. Louis, MO, USA). Hexane (pesticide grade) was obtained from Fisher Scientific (Fair Lawn, NJ, USA).

7.2.2 Preparation of stabilized noble metal nanoparticles catalyst

Pd, Pt and Au nanoparticles were prepared by liquid reduction of the corresponding metal salt by sodium borohydride with CMC as a stabilizer. Briefly, a metal salt solution was prepared by diluting 1mL of 0.05M metal salt solution in 250mL of 0.15% CMC solution. Noble metal nanoparticles were then formed via reduction using 3.5mL of a 0.05mM borohydride solution. The resultant suspension was stirred at 300rpm under room temperature for 24 hours prior to use. For TEM analysis, three droplets of the nanoparticles suspension were casted onto a copper grid and air-dried overnight under ambient conditions. The TEM images were obtained on a Zeiss EM 10 transmission electron microscope at an operating voltage of 60 kV.

7.2.3 Liquid-phase hydrodechlorination of Trichloroethylene

Batch degradation tests were carried out using 127mL amber Boston Round bottles with open-top screw caps and PTFT-lined septa. Before the experiments, 4.5mL of a metal nanoparticle suspension was mixed with 85mL of deionized water before sparged with hydrogen gas for 30 min to displace dissolved oxygen in water and fill the headspace with a hydrogen atmosphere. Then the serum bottle was immediately sealed with a magnetic stir bar, and 25 µL of a contaminant (i.e, TCE, PCE, TCA, or 1,1,1,2-TeCA) stock solution (1.36 M in methanol) was spiked into the solution to initiate the reaction. The catalytic reactions were conducted at room temperature under constant magnetic stirring. At selected time intervals, 100 µL aliquot of aqueous solution was taken and extracted using 1mL hexane followed by GC analysis on an HP 6890 GC

equipped with an electron capture detector (ECD). The detailed analysis methods can be found in He and Zhao (2005).

As H_2 in the system far exceeded the stoichiometric demand for the complete TCE transformation (i.e. the H_2 concentration in the suspension phase remained constant), the TCE degradation kinetics in can be interpreted using a pseudo-first-order kinetic model (Lowry and Reinhard, 1999).

$$-\frac{dC_{polyhalide}}{dt} = k_{app} \cdot C_{polyhalide} = k_{obs} \cdot C_{metal} \cdot C_{polyhalide} = k_{SA} \cdot \alpha_s \cdot C_{metal} \cdot C_{polyhalide} \quad (7\text{-}1)$$

where the k_{app} is the apparent reaction rate constant, C_{metal} is the concentration of metal nanoparticles, and $C_{polyhalide}$ is the concentration of chlorinated contaminants during the reaction. k_{app} is normalized by the catalyst concentration to yield the observed reaction rate constant, k_{obs}. k_{obs} is further normalized by specific surface area of the nanoparticles to yield k_{SA}.

7.3 Results

Figure 7-1 shows representative TEM images of the 0.15%CMC stabilized Pd, Pt and Au nanoparticles after synthesis. The size of stabilized Pd, Pt and Au nanoparticles was measured to be 2.4±0.5 nm, 3.9±0.5 nm and 3.1±0.9 nm, respectively. CMC molecules exhibited effective capping performance for the synthesis and stabilization of uniform catalyst nanoparticles with small size and narrow distribution. To estimate the surface area of Pd, Pt and Au nanoparticles, Eq. 7-2 is used (Liu et al., 2008)

$$r = 3\ (\rho\alpha_s)\text{-}1 \quad (7\text{-}2)$$

where r is the particle radius (m), ρ is the density of the particles (assuming identical to the density of bulk metal), and α_s is the specific surface area of the nanoparticles (m^2/g).

Based on the mean particle radii of metal nanoparticles from TEM analysis, the α_s values of all the metal nanoparticles were calculated and summarized in **Table 7-1**.

The metal nanoparticles were first used for hydrodechlorination of TCE, one of the most important contaminants in U.S. groundwater. **Figure 7-2** presents the TCE reduction kinetics by hydrogen in the presence of 0.01 mM Pd, Pt, Ru, and Au nanoparticles stabilized by 0.15 wt% CMC. Control test in the absence of metal catalysts indicated no appreciable conversion for TCE, PCE, 1,1,1-TCA and 1,1,1,2-TeCA occurred with hydrogen gas only. An exponential decay of TCE concentration versus time was observed for all the case as shown in **Figure 7-2**, through which the reaction rate constant k_{app}, k_{obs} and k_{sa} for all metal nanoparticles were obtained and summarized in Table 1. All metal catalysts enhanced the rate of TCE reduction, following the trend Pd > Pt >> Au. Pd nanoparticles are most reactive with a k_{SA} of 3.5 L/min/m^2, where a near-complete reduction of TCE occurred within 6 minutes. Rate of TCE reduction by Pt nanoparticles was slightly slower with a k_{SA} of 2.4 L/min/m^2, followed by Au nanoparticles with a k_{SA} of only 0.07 L/min/m^2.

The hydrodechloration of another important vinyl polyhalide contaminant, PCE, were also performed. As shown in **Figure 7-3**, PCE can be effectively reduced by hydrogen gas with these three metal nanoparticles and the reduction follows a pseudo-first-order reaction kinetics. A similar trend of catalytic reactivity of the metal nanoparticles was observed for hydrodechlorination of TCE and PCE (i.e., Pd > Pt >> Au). However, while Pt nanoparticles exhibited only 1.5 times lower reactivity than Pd nanoparticles towards TCE, its reactivity towards PCE was 7 times lower. The surface

area-normalized rate constant k_{SA} for PCE hydrodechlorination was determined to be 1.48, 0.22 and 0.01 L/min/m^2 for Pd, Pt and Au nanoparticles, respectively.

The hydrodechlorination reactivity of the metal nanoparticles was further tested for alkyl polyhalide contaminants. **Figure 7-4** and 7-**5** present the catalytic hydrodechlorination of 1,1,1-TCA and 1,1,1,2-TeCA with metal nanoparticles as a function of reaction time. The degradation kinetics could also be described by a pseudo-first-order model for all the cases. The same reactivity trend of metal nanoparticles was observed as Pd>Pt>Au. From the degradation tests, it is also apparent that the rate enhancement provided by metal nanoparticles are generally larger for 1,1,1,2-TecA than 1,1,1-TCA. For example, the surface area normalized reaction rate constant K_{SA} for 1,1,1-TCA was only 0.06, 0.005 and 0.003 L/min/m^2 for Pd, Pt and Au nanoparticles, respectively, while the k_{SA} for 1,1,1,2-TeCA was up to 0.95, 0.11 and 0.03 L/min/m^2 for Pd, Pt and Au nanoparticles. Our experimental results clearly suggested that palladium was much more effective in promoting the dechlorination reaction than platinum and gold nanoparticles, and the catalytic activity of metal nanoparticles can vary towards different organochlorinated compounds. Furthermore, the nano-scale metal particles could significantly enhanced the dechlorination rate. Mackenzie et al.(2006) investigated the hydrodechlorination in water with a commercial 0.5% Pd/Al_2O_3 catalyst and the observed reaction rate constant for trichloroethene, tetrachloroethene, 1,1,1-trichloroethane and 1,1,1,2-tetrachloroethane was reported to be 420, 210, 15 and 100 L/g/min, respectively. In our study, using Pd nanoparticles of 2.4 nm, the observed reaction rate constant was considerably increased to 728, 308, 13 and 197 L/g/min, respectively.

Table 7- 1. Properties of metal nanoparticles and their pseudo-first-order reaction rate constants

Metal NP	D, (nm)	P, (kg/m^3)	as, (m^2/g)	k_{app}, (1/min)				K_{SA}, ($L/min/m^2$)			
				TCE	PCE	1,1,1-TCA	1,1,1,2-TeCA	TCE	PCE	1,1,1-TCA	1,1,1,2-TeCA
Pd	2.4±0.5	12023	207.9	0.7750	0.3280	0.0134	0.2090	3.520	1.480	0.060	0.950
Pt	3.9±0.5	21450	71.7	0.3330	0.0310	0.0007	0.0154	2.380	0.220	0.005	0.110
Au	3.1±0.9	19320	100.2	0.0130	0.0012	0.0005	0.0058	0.066	0.010	0.003	0.030

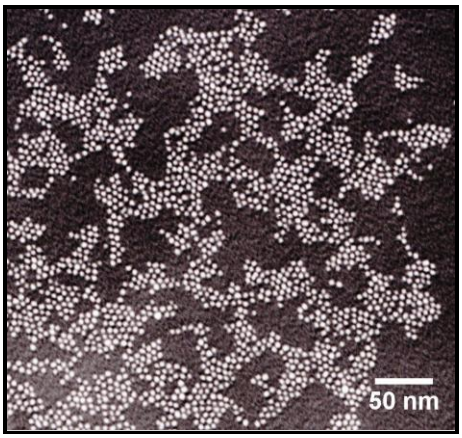

(a)

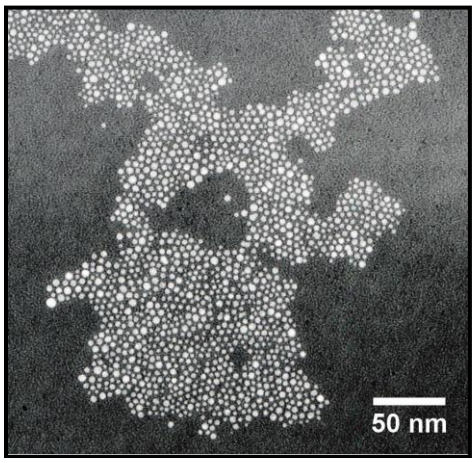

(b)

Figure 7- 1. TEM images of **(a)** Pd nanoparticles and **(b)** Au nanoparticles (stabilized using 0.15 wt% CMC in aqueous phase.

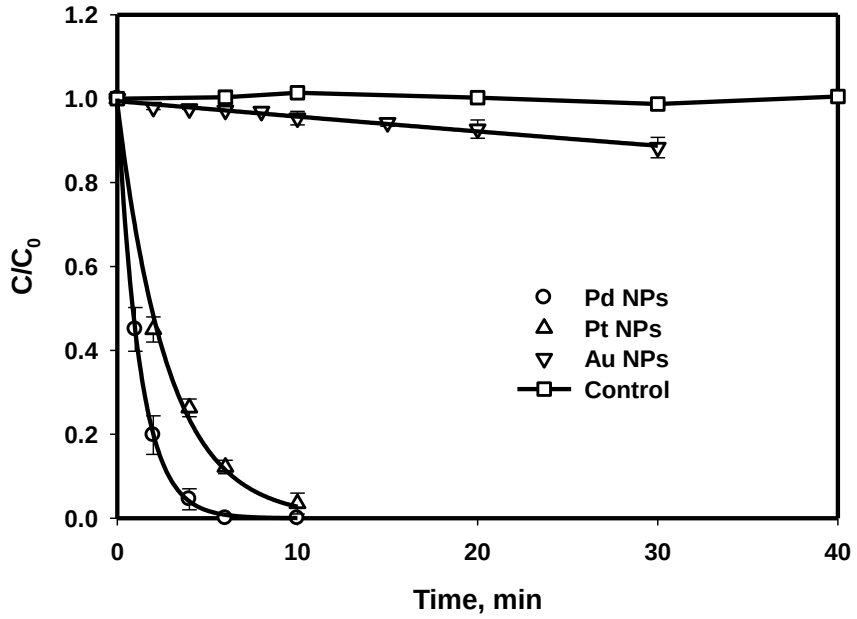

Figure 7- 2. Catalytic hydrodechlorination of TCE over time. Pd = 0.01 mM, Pt = 0.01 mM, Au = 0.01 mM, TCE = 50 mg/L. Data plotted as mean of duplicates, and error bars represent deviation from mean of duplicates.

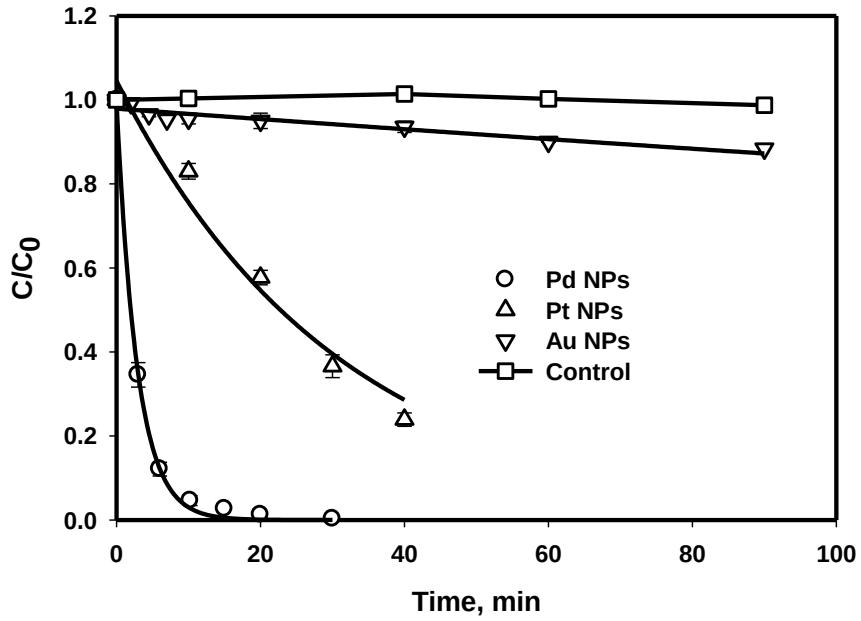

Figure 7- 3. Catalytic hydrodechlorination of PCE over time. Pd = 0.01 mM, Pt = 0.01 mM, Au = 0.01 mM, PCE =50 mg/L. Data plotted as mean of duplicates, and error bars represent deviation from mean of duplicates.

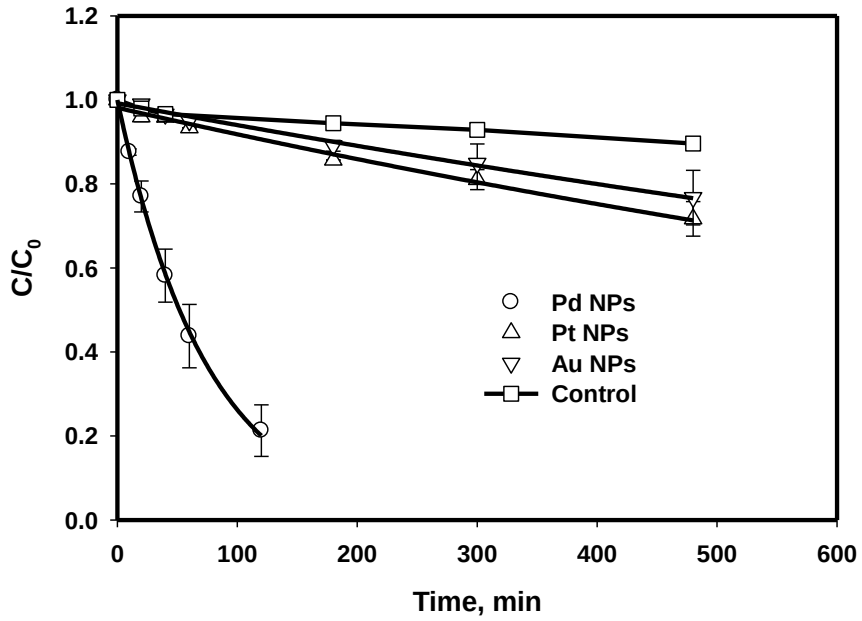

Figure 7- 4. Catalytic hydrodechlorination of 1,1,1-TCA over time. Pd = 0.01 mM, Pt = 0.01 mM, Au = 0.01 mM, 1,1,1-TCA = 50 mg/L. Data plotted as mean of duplicates, and error bars represent deviation from mean of duplicates.

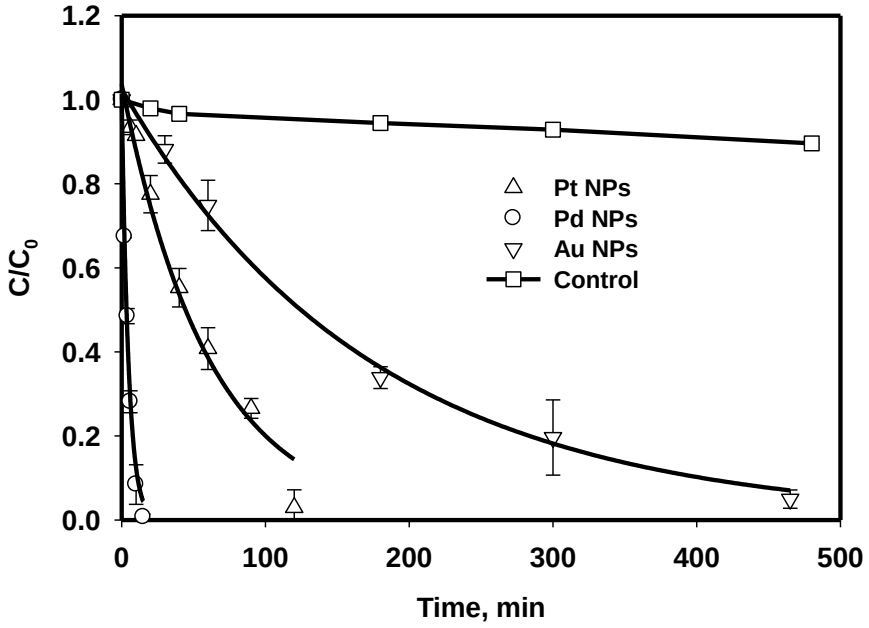

Figure 7- 5. Catalytic hydrodechlorination of 1,1,1,2-TeCA over time. Pd = 0.01 mM, Pt = 0.01 mM, Au = 0.01 mM, 1,1,1,2-TeCA = 50 mg/L. Data plotted as mean of duplicates, and error bars represent deviation from mean of duplicates.

7.4 Discussion

7.4.1 Catalytic activity of Pd, Pt and Au nanoparticles

Similar to other catalytic reactions (Nørskov et al., 2002), the catalytic hydrodechlorination reaction often involves multiple kinetic steps, including dissociative or molecular adsorption of organochlorinated compounds and hydrogen on catalyst surface, hydrogenolysis or hydrogenation between reactive species, and release of the reaction products to the bulk liquid (Chen et al., 2002). In a multi-step reaction, the overall reaction rate is always governed by the slowest step, i.e., the rate-limiting step. Therefore, the overall reaction rate constant obtained from our experiments is considered to be a reliable measurement for the rate-limiting process.

A generalized reactivity trend towards chlorinated solvents degradation was observed in our study as follows: Pd> Pt > Au. The different behavior of three metals can be attributed to their intrinsic electronic structure, i.e. the local density of unoccupied state at the Fermi level ($N(E_F)$), which inherently controls the reactant adsorption on the metal surface. The density of unoccupied state at the Fermi level characterizes the electron donor-acceptor capacity of the metal. The lower density of unoccupied state suggests the metal should possess a higher affinity towards electronegative chloride group of chlorinated reactants (Shin et al., 2008) for adsorption on the metal surface. Studies have shown that the catalytic reactivity of transition metals is correlated with its $N(E_F)$ values, for hydrogenolysis and hydrogenation processes (Arcoya et al., 1991; Vaarkamp et al., 1993). Gomez-Sainero et al. (2000) observed that Pd, which has the highest unoccupied density of state, displayed the greatest reactivity by promoting the adsorption of carbon tetrachloride when investigating the hydrodechlorination activity of

five carbon-supported metal catalysts in liquid phase. The magnetic susceptibility of the metals was used to describe the magnitude of $N(E_F)$ because it is easily available. In our study, because the particle size of metal nanoparticles are higher than 2 nm, it is assumed that the average electronic properties agreed with those of bulk material (Arcoya et al., 1991; Gomez-Sainero et al., 2000). The magnetic susceptibility was reported to be 5.231×10^{-6} cgs, 0.9712×10^{-6} cgs, 0.1430×10^{-6} cgs for palladium, platinum and gold at room temperature, respectively (Albert and Rubin, 1971; Garber et al., 1960). A strong correlation between surface arear normalized reaction rate constant k_{SA} and the magnetic susceptibility of these metals was observed for TCE (r^2=0.85), PCE (r^2=0.98), 1,1,1-TCA (r^2=0.85) and 1,1,1,2-TeCA (r^2=0.97). The strength of this correlation indicates that no matter for vinyl or alkyl polyhalides, the adsorption of organochlorinated compounds onto the metal surface governs the catalytic activities for hydrodechlorination.

This observation concords with the result of other studies on the reaction mechanism of catalytic hydrodechlorination. Weiss et al.(1971) suggested that the dissociative adsorption of carbon tetrachloride on Pt surface alone is the rate-limiting step when investigating the hydrodechlorination kinetics over an alumina-supported Pt catalyst. For vinyl polyhalides, Gonzalez and de Correa (2010) also observed the hydrodechlorination kinetics of tetrachloroethylene over 0.8% Pd/TiO_2 corresponds well to the model where the adsorption of PCE is considered as the rate-limiting step.

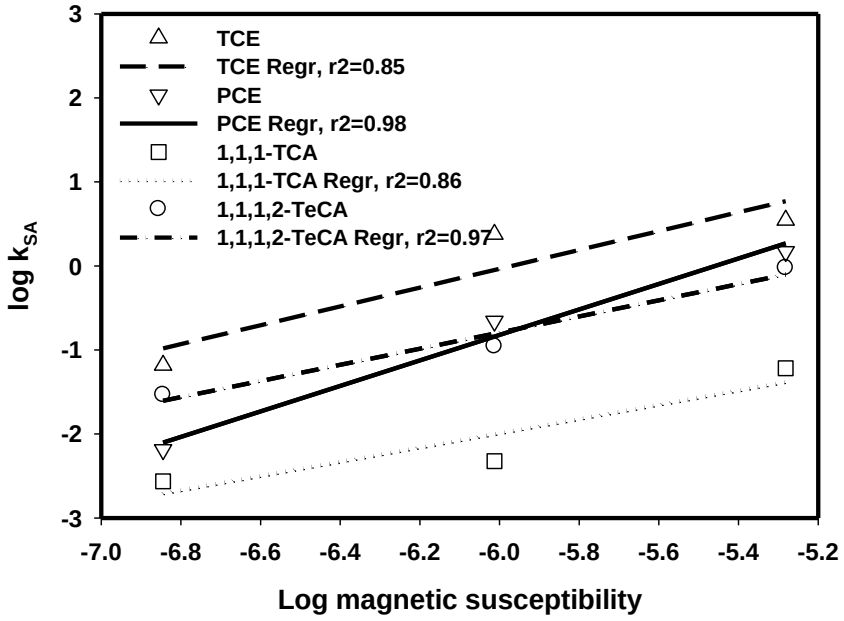

Figure 7- 6. Correlation between log(k_{SA}) for TCE, PCE, 1,1,1-TCA and 1,1,1,2-TeCA reduction and logarithm value of the magnetic susceptibility of the metals. Solid lines represent least-squares linear regression fits to the experimental data.

7.4.2 Hydrodechlorination reactivity of organohalides

As illustrated in **Figures 7-5** , the rate of catalytic hydrodechlorination also depended on the nature of organohalides compounds. TCE was the most reactive compounds with all of three metal catalysts, following by PCE, 1,1,1-TeCA and 1,1,1-TCA which was the least reactive. For examples, with Pd nanoparticles, the surface normalized reaction rate constant k_{SA} for TCE was 3.5 L/min/m^2, about 2.3, 3.7 and 58 times higher than that of PCE, 1,1,1,2-TeCA and 1,1,1-TCA, respectively. Considering the reactant adsorption is the rate-limiting process during the hydrodechlorination, the different behavior of organochlorinated compounds could be attributed to the ease of reactant sorption on the metal surface.

For alkyl polyhalides such as 1,1,1-TCA and 1,1,1,2-TeCA, Thompson et al. (1999) proposed that the hydrodechlorination process starts with dissociative adsorption of reactants on the metal catalyst, involving the scission of the C-Cl bond and the formation of σ-bond between metal atoms with the carbon atom in the fragmented chlorinated compounds. Lee et al. (2004) studied the hydrodechlorination of 1,1,1-trichloroethane over Pt surface at 150K using Fast X-ray photoelectron spectroscopy and also reported decomposition occur via sequential cleavage of C-Cl bonds. Yang et al. (1997) found that dissociation of the first C-Cl bond in the chlorinated compounds controlled the reaction rate during the hydrodechlorination of chlorinated ethanes on clean Cu(100) surface. Therefore, the breakage of C-Cl bond is considered as the key step for dissociative adsorption of alkyl polyhalides, and further controls the hydrodechlorination rate. The C-Cl bond strength of 1,1,1-TCA and 1,1,1,2-TeCA is reported to be 309 kJ/mol and 295 kJ/mol, respectively (Mackenzie et al., 2006). The

higher hydrodechlorination reactivity of 1,1,1,2-TeCA over 1,1,1-CA agreed well with its lower energy demand for C-Cl bond scission, and therefore facilitated the reactant sorption on the metals.

For vinyl polyhalides such as TCE and PCE, Gonzalez and de Correa (2010) suggested the chloroethylene adsorption (dissociative or molecular) on the catalytic metals is the rate-limiting step for hydrodechlorination based on their fitting results for kinetic models. The researchers did not provide further discussion on the adsorption mechanism. If we assume the same dissociative adsorption mechanism with C-Cl bond cleavage for vinyl polyhalides, PCE would be most facile for hydrodechlorination than TCE considering the C-Cl bond strength of PCE (382 kJ/mol) is lower than that of TCE (392 kJ/mol) (Mackenzie et al., 2006). However, our experimental data showed the opposite way. The reduction of PCE was slower than that of TCE under the identical experimental conditions, which is also reported by other studies (Ordonez et al., 2000). Therefore, the adsorption mechanisms for alkyl and vinyl polyhalides are different. The C-Cl bond cleavage is clearly not the main step controlling the adsorption of vinyl polyhalides. Either molecular adsorption or the adsorption of fragmented chlorinated compounds after breaking one C-Cl bond is more likely the rate-limiting process. Mackenzie et al.(2006) suggested that the hydrodechlorination rate of vinyl halides is inversely correlated with the number of Cl attached on the double bond. The substituted chlorine atoms would adsorb electron density from the π bond of the carbon double bond and therefore decrease the interaction between vinyl polyhalide reactants and the metallic surfaces of the catalysts.

.

7.4.3 Kinetics of catalytic hydrodechlorination by Pd nanoparticles

Further studies were conducted with TCE, PCE, 1,1,1-TCA and 1,1,1,2-TeCA at varied concentrations of Pd nanoparticles to investigate the reaction order of the catalyst. The change of hydrodechlorination reactivity as a function of catalyst concentration was presented as the logarithmic plot of pseudo-first-order rate constant k_{app} and the amount of catalyst in **Figure 7-7**. Pd nanoparticles were selected because of its great reactivity.

Interestingly, the apparent rate constant k_{app} increased linearly as a function of catalyst concentrations as illustrated in **Figure 7-7**. The change in log k_{SA} with the catalyst concentration was almost equivalent for all of the selected contaminants. The slope of the linear regression for TCE (r^2=0.998), PCE (r^2=0.975), 1,1,1-TCA (r^2=0.998) and 1,1,1,2-TeCA(r^2=0.979) were 1.27, 1.1, 1.04 and 1.07, respectively. Thereby, the reaction order for the Pd catalysts during the catalytic hydrodechlorination towards both vinyl and alkyl polyhalides was determined to be one (Kong et al., 2004), although the adsorption mechanism for vinyl and alkyl polyhalides are different.

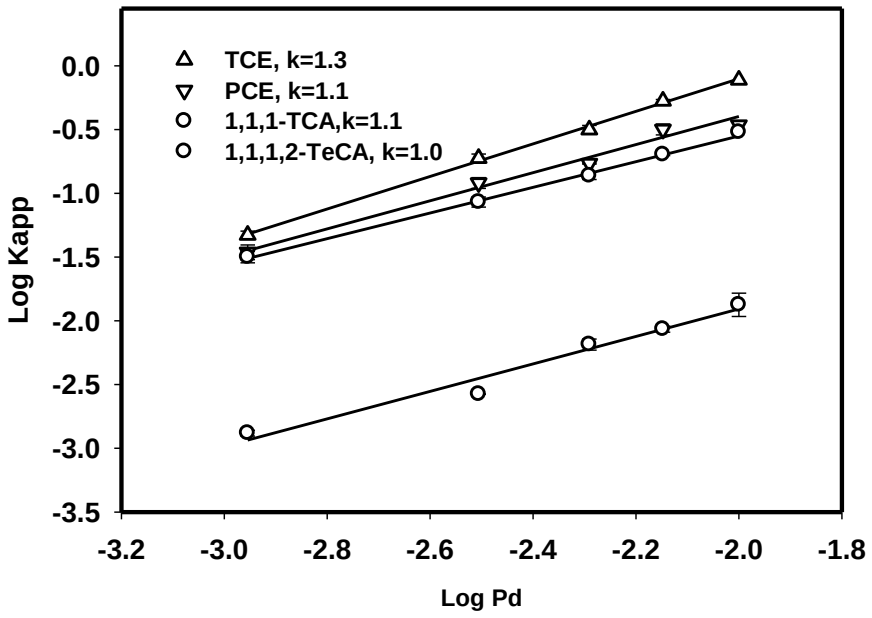

Figure 7- 7. Plot of logk_{SA} versus log[Pd] for TCE, PCE, 1,1,1-TCA and 1,1,1,2-TeCA in Pd nanoparticles systems. Solid lines represent least-squares linear regression fits to the experimental data.

7. 5 Conclusion

In this work, highly stable Pd, Pt and Au nanoparticles were prepared in the aqueous phase with CMC as a stabilizer. The nanoparticles were tested as catalysts to explore the reaction mechanism of catalytic hydrodechlorination towards organochlorinated compounds. Four chlorinated contaminants including TCE, PCE,1,1,1-TCA and 1,1,1,2-TeCA were tested. Palladium nanoparticles exhibited superior reactivity towards all contaminants. The catalytic reactivity of these catalyst metals followed Pd>Pt>Au. The order correlated with the adsorption affinity of chlorinated compounds on each metal, suggesting that the adsorption of chlorinated solvents onto the catalyst metals is the rate-limiting process during hydrodechlorination reaction. Further examination on the reactivity of four chlorinated compounds revealed that the adsorption mechanism are also different for alkyl and vinyl polyhalides. For the alkyl polyhalides, the C-Cl bond cleavage, which is the first step of dissociative adsorption, controls the overall reaction rate. However, for the vinyl polyhalides, molecular adsorption or fragment chlorinated compounds adsorption is rate-limiting. Interestingly, even though the adsorption mechanism for alkyl and vinyl polyhalides are different, the reaction order of palladium nanoparticles in the hydrodechlorination process is identical, equal to one for all four chlorinated compounds.

References

Abudalo, R.A. et al., 2005. Effect of ferric oxyhydroxide grain coatings on the transport of bacteriophage PRD1 and Cryptosporidium parvum oocysts in saturated porous media. Environmental Science & Technology, 39(17): 6412-6419.

Abudalo, R.A., Ryan, J.N., Harvey, R.W., Metge, D.W. and Landkamer, L., 2010. Influence of organic matter on the transport of Cryptosporidium parvum oocysts in a ferric oxyhydroxide-coated quartz sand saturated porous medium. Water Research, 44(4): 1104-1113.

Adamczyk, Z., Siwek, B. and Musial, E., 2003. Latex particle adsorption at heterogeneous surfaces. Colloids and Surfaces A:Physicochemical and Engineering Aspects, 214(1-3): 219-229.

Agency for toxic substances and Disease Registry, 2007. 2007 ATSDR Completed Exposure Pathway Site Count Report, http://www.atsdr.cdc.gov/cep/archive/.

Agency for toxic substances and Disease Registry, 2011a. 2011 ATSDR Completed Exposure Pathway Site Count Report, http://www.atsdr.cdc.gov/cep/archive/.

Agency for toxic substances and Disease Registry, 2011b. ATSDR 2011 substance priority list, http://www.atsdr.cdc.gov/SPL/index.html.

Alowitz, M.J. and Scherer, M.M., 2002. Kinetics of nitrate, nitrite, and Cr(VI) reduction by iron metal. Environmental Science & Technology, 36(3): 299-306.

Amarante, D., 2000. Applying in situ chemical oxidation. Pollution Engineering, 32(2).

Ambonguilat, S., Gallard, H., Garron, A., Epron, F. and Croue, J.P., 2006. Evaluation of the catalytic reduction of nitrate for the determination of dissolved organic nitrogen in natural waters. Water Research, 40(4): 675-682.

Andersin, J. and Honkala, K., 2011. First principles investigations of Pd-on-Au nanostructures for trichloroethene catalytic removal from groundwater. Physical Chemistry Chemical Physics, 13(4): 1386-1394.

Anderson, M.P. and Munter, J.A., 1981. Seasonal reversals of groundwater-flow around lakes and the relevance to stagnation points and lake budgets. Water Resources Research, 17(4): 1139-1150.

Arcoya, A., Cortes, A., Fierro, J.L.G. and Seoane, X.L., 1991. Comparative study of the deactivation of Group VIII metal catalysts by thiophene poisoning in ethylbenzene hydrogenation. Studies in Surface Science and Catalysis, 68: 557-564.

Arnold, W.A. and Roberts, A.L., 2000. Pathways and kinetics of chlorinated ethylene and chlorinated acetylene reaction with Fe(O) particles. Environmental Science & Technology, 34(9): 1794-1805.

Atkinson, R.J., Posner, A.M. and Quirk, J.P., 1967. Adsorption of potential-determining ions at the ferric oxide-aqueous electrolyte interface. The Journal of Physical Chemistry, 71(3): 550-558.

Ayoub, S.R.A., Uchiyama, H., Iwasaki, K., Doi, T. and Inaba, K., 2008. Effects of several surfactants and high-molecular-weight organic compounds on decomposition of trichloroethylene with zerovalent iron powder. Environmental Technology, 29(4): 363-373.

Babu, N.S., Lingaiah, N., Gopinath, R., Reddy, P.S.S. and Prasad, P.S.S., 2007. Characterization and reactivity of alumina-supported Pd catalysts for the room-temperature hydrodechlorination of chlorobenzene. Journal of Physical Chemistry C, 111(17): 6447-6453.

Bacik, D.B. et al., 2012. Synthesis and characterization of supported polysugar-stabilized palladium nanoparticle catalysts for enhanced hydrodechlorination of trichloroethylene. Nanotechnology, In press.

Bae, J.W., Kim, I.G., Lee, J.S., Lee, K.H. and Jang, E.J., 2003. Hydrodechlorination of CCl_4 over Pt/Al_2O_3: effects of platinum particle size on product distribution. Applied Catalysis A: General, 240(1-2): 129-142.

Bailey, R.P., Bennett, T. and Benjamin, M.M., 1992. Sorption onto and recovery of Cr (VI) using iron-oxide-coated sand. Water Science and Technology, 26(5-6): 1239-1244.

Baker, R. and Heron, G., 2004. In-situ delivery of heat by thermal conduction and steam injection for improved DNAPL remediation, Proceedings of the 4th International conference on remediation of chlorinated and recalcitrant compounds. Battelle press, Monterey, CA.

Baker, R.R., Coburn, S., Liu, C. and Tetteh, J., 2005. Pyrolysis of saccharide tobacco ingredients: A TGA–FTIR investigation. Journal of Analytical and Applied Pyrolysis, 74(1–2): 171-180.

Barrabés, N. et al., 2010. Pretreatment effect on Pt/CeO_2 catalyst in the selective hydrodechlorination of trichloroethylene. The Journal of Physical Chemistry C, 114(41): 17675-17682.

Bartsch, H., Malaveille, C., Barbin, A. and Planche, G., 1979. Mutagenic and alkylating metabolites of halo-ethylenes, chlorobutadienes and dichlorobutenes produced by rodent or human liver tissues. Archives of Toxicology, 41(4): 249-277.

Baston, D.P., Falta, R.W. and Kueper, B.H., 2010. Numerical modeling of thermal conductive heating in fractured bedrock. Ground Water, 48(6): 836-843.

Bennett, P., He, F., Zhao, D.Y., Aiken, B. and Feldman, L., 2010. In situ testing of metallic iron nanoparticle mobility and reactivity in a shallow granular aquifer. Journal of Contaminant Hydrology, 116(1-4): 35-46.

Biswal, D.R. and Singh, R.P., 2004. Characterisation of carboxymethyl cellulose and polyacrylamide graft copolymer. Carbohydrate Polymers, 57(4): 379-387.

Block, P.A., Brown, R.A. and Robinson, D., 2004. Novel activation technologies for sodium persulfate in situ chemical oxidation, Proceedings of the Fourth International Conference on the Remediation of Chlorinated and Recalcitrant Compounds. Battelle Press, Monterey, CA.

Boccuzzi, F. et al., 2001. Au/TiO_2 nanosized samples: a Catalytic, TEM, and FTIR study of the effect of calcination temperature on the CO oxidation. Journal of Catalysis, 202(2): 256-267.

Bond, G.C., 1991. Supported metal catalysts:some unsolved problems. Chemical Society Reviews, 20(4): 441-475.

Bouwer, E.J., Rittmann, B.E. and McCarty, P.L., 1981. Anaerobic degradation of halogenated 1-carbon and 2-carbon organic compounds. Environmental Science & Technology, 15(5): 596-599.

Boving, T.B. and Brusseau, M.L., 2000. Solubilization and removal of residual trichloroethene from porous media: comparison of several solubilization agents. Journal of Contaminant Hydrology, 42(1): 51-67.

Bradford, S.A. and Bettahar, M., 2006. Concentration dependent transport of colloids in saturated porous media. Journal of Contaminant Hydrology, 82(1-2): 99-117.

Bradford, S.A., Bettahar, M., Simunek, J. and van Genuchten, M.T., 2004. Straining and attachment of colloids in physically heterogeneous porous media. Vadose Zone Journal, 3(2): 384-394.

Bradford, S.A., Kim, H.N., Haznedaroglu, B.Z., Torkzaban, S. and Walker, S.L., 2009. Coupled factors influencing concentration-dependent colloid transport and retention in saturated porous media. Environmental Science & Technology, 43(18): 6996-7002.

Bradley, P.M., 2003. History and ecology of chloroethene biodegradation: a review. Bioremediation Journal, 7(2): 81-109.

Bueno, M., Astruc, A., Astruc, M. and Behra, P., 1998. Dynamic sorptive behavior of tributyltin on quartz sand at low concentration levels: Effect of pH, flow rate, and monovalent cations. Environmental Science & Technology, 32(24): 3919-3925.

Burris, D.R., Campbell, T.J. and Manoranjan, V.S., 1995. Sorption of trichloroethylene and tetrachloroethylene in a batch reactive metallic iron-water system. Environmental Science & Technology, 29(11): 2850-2855.

Butler, E.C. and Hayes, K.F., 1999. Kinetics of the transformation of trichloroethylene and tetrachloroethylene by iron sulfide. Environmental Science & Technology, 33(12): 2021-2027.

Butler, E.C. and Hayes, K.F., 2000. Kinetics of the transformation of halogenated aliphatic compounds by iron sulfide. Environmental Science & Technology, 34(3): 422-429.

Butler, E.C. and Hayes, K.F., 2001. Factors influencing rates and products in the transformation of trichloroethylene by iron sulfide and iron metal. Environmental Science & Technology, 35(19): 3884-3891.

Buyuksonmez, F., Hess, T.F., Crawford, R.L., Paszczynski, A. and Watts, R.J., 1999. Optimization of simultaneous chemical and biological mineralization of perchloroethylene. Applied and Environmental Microbiology, 65(6): 2784-2788.

Camesano, T.A. and Logan, B.E., 1998. Influence of fluid velocity and cell concentration on the transport of motile and nonmotile bacteria in porous media. Environmental Science & Technology, 32(11): 1699-1708.

Camesano, T.A., Unice, K.M. and Logan, B.E., 1999. Blocking and ripening of colloids in porous media and their implications for bacterial transport. Colloids and Surfaces A: Physicochemical and Engineering Aspects, 160(3): 291-308.

Carter, J.L., Cusumano, J.A. and Sinfelt, J.H., 1966. Catalysis over supported metals. V. The effect of crystallite size on the catalytic activity of nickel. The Journal of Physical Chemistry, 70(7): 2257-2263.

Chaplin, B.P., Roundy, E., Guy, K.A., Shapley, J.R. and Werth, C.J., 2006. Effects of natural water ions and humic acid on catalytic nitrate reduction kinetics using an alumina supported Pd-Cu catalyst. Environmental Science & Technology, 40(9): 3075-3081.

Chen, J., Zhang, Q., Wang, Y. and Wan, H., 2008. Size-dependent catalytic activity of supported palladium nanoparticles for aerobic oxidation of alcohols. Advanced Synthesis & Catalysis, 350(3): 453-464.

Chen, N., Rioux, R.M. and Ribeiro, F.H., 2002. Investigation of reaction steps for the hydrodechlorination of chlorine-containing organic compounds on Pd catalysts. Journal of Catalysis, 211(1): 192-197.

Cheng, I.F., Muftikian, R., Fernando, Q. and Korte, N., 1997. Reduction of nitrate to ammonia by zero-valent iron. Chemosphere, 35(11): 2689-2695.

Childs, J. et al., 2006. Field demonstration of surfactant-enhanced solubilization of DNAPL at Dover Air Force Base, Delaware. Journal of Contaminant Hydrology, 82(1-2): 1-22.

Chiou, C.T., Peters, L.J. and Freed, V.H., 1979. A physical concept of soil-water equilibria for nonionic organic compounds. Science, 206(4420): 831-832.

Chou, J., Franklin, N.R., Baeck, S.H., Jaramillo, T.F. and McFarland, E.W., 2004. Gas-phase catalysis by micelle derived Au nanoparticles on oxide supports. Catalysis Letters, 95(3-4): 107-111.

Clancy, P.B., Armstrong, J., Couture, M., Lussky, R. and Wheeler, K., 1996. Treatment of chlorinated ethenes in groundwater with ozone and hydrogen peroxide. Environmental Progress, 15(3): 187-193.

Cohen, R.M., Vincent, A.H., Mercer, J.M., Faust, C.R. and Spalding, C.P., 1994. Methods for monitoring pump-and-treat performance. EPA/600/R-94/123. U.S. EPA, Ada, OK.

Coq, B. and Figueras, F., 2001. Bimetallic palladium catalysts: influence of the co-metal on the catalyst performance. Journal of Molecular Catalysis A: Chemical, 173(1-2): 117-134.

Crespo-Quesada, M. et al., 2011. UV-Ozone cleaning of supported poly(vinylpyrrolidone)-stabilized palladium nanocubes: effect of stabilizer removal on morphology and catalytic behavior. Langmuir, 27(12): 7909-7916.

Cupples, A.M., Spormann, A.M. and McCarty, P.L., 2003. Growth of a Dehalococcoides-like microorganism on vinyl chloride and cis-dichloroethene as electron acceptors as determined by competitive PCR. Applied and Environmental Microbiology, 69(2): 953-959.

Cupples, A.M., Spormann, A.M. and McCarty, P.L., 2004. Comparative evaluation of chloroethene dechlorination to ethene by Dehalococcoides-like microorganisms. Environmental Science & Technology, 38(18): 4768-4774.

Curtis, G.P. and Reinhard, M., 1994. Reductive dehalogenation of hexachloroethane, carbon tetrachloride, and bromoform by anthrahydroquinone disulfonate and humic acid. Environmental Science & Technology, 28(13): 2393-2401.

Cushing, B.L., Kolesnichenko, V.L. and O'Connor, C.J., 2004. Recent advances in the liquid-phase syntheses of inorganic nanoparticles. Chemical Reviews, 104(9): 3893-3946.

Cwiertny, D.M., Bransfield, S.J. and Roberts, A.L., 2007. Influence of the Oxidizing Species on the Reactivity of Iron-Based Bimetallic Reductants. Environmental Science & Technology, 41(10): 3734-3740.

Dahmani, M.A., Huang, K. and Hoag, G., 2006. Sodium persulfate oxidation for the remediation of chlorinated solvents (USEPA superfund innovative technology evaluation program). Water, Air, & Soil Pollution: Focus, 6(1-2): 127-141.

Dalla Vecchia, E., Luna, M. and Sethi, R., 2009. Transport in porous media of highly concentrated iron micro- and nanoparticles in the presence of Xanthan Gum. Environmental Science & Technology, 43(23): 8942-8947.

Davis, C.J., Eschenazi, E. and Papadopoulos, K.D., 2002. Combined effects of Ca^{2+} and humic acid on colloid transport through porous media. Colloid & Polymer Science(1): 52-58.

Davis, E.L., 1997. How heat can enhance in-situ soil and aquifer remediation: important chemical properties and guidance on choosing the appropriate technique. EPA/540/S-97/502. U.S. EPA, Ada, OK.

Debruin, W.P., Kotterman, M.J.J., Posthumus, M.A., Schraa, G. and Zehnder, A.J.B., 1992. Complete biological reductive transformation of tetrachloroethene to ethane. Applied and Environmental Microbiology, 58(6): 1996-2000.

Deshpande, S., Shiau, B.J., Wade, D., Sabatini, D.A. and Harwell, J.H., 1999. Surfactant selection for enhancing ex situ soil washing. Water Research, 33(2): 351-360.

Diaz, E., Faba, L. and Ordonez, S., 2011. Effect of carbonaceous supports on the Pd-catalyzed aqueous-phase trichloroethylene hydrodechlorination. Applied Catalysis B: Environmental, 104(3-4): 415-417.

Dobrev, I.D., Andersen, M.E. and Yang, R.S., 2002. In silico toxicology: simulating interaction thresholds for human exposure to mixtures of trichloroethylene,

tetrachloroethylene, and 1,1,1-trichloroethane. Environ Health Perspect, 110(10): 1031-9.

Doherty, R.E., 2000a. A history of the production and use of carbon tetrachloride, tetrachloroethylene, trichloroethylene and 1,1,1-trichloroethane in the United States: Part 1 - Historical background; Carbon tetrachloride and tetrachloroethylene. Environmental Forensics, 1(2): 69-81.

Doherty, R.E., 2000b. A history of the production and use of carbon tetrachloride, tetrachloroethylene, trichloroethylene and 1,1,1-trichloroethane in the United States: Part 2 - Trichloroethylene and 1,1,1-trichloroethane. Environmental Forensics, 1(2): 83-93.

Domingos, R.F., Tufenkji, N. and Wilkinson, K.J., 2009. Aggregation of titanium dioxide nanoparticles: role of a fulvic acid. Environmental Science & Technology, 43(5): 1282-1286.

Doong, R.A. and Lai, Y.J., 2005. Dechlorination of tetrachloroethylene by palladized iron in the presence of humic acid. Water Research, 39(11): 2309-2318.

Dowideit, P. and von Sonntag, C., 1998. Reaction of ozone with ethene and its methyl- and chlorine-substituted derivatives in aqueous solution. Environmental Science & Technology, 32(8): 1112-1119.

Drago, R.S., Dias, S.C., McGilvray, J.M. and Mateus, A.L.M.L., 1998. Acidity and hydrophobicity of TS-1. the Journal of Physical Chemistry B, 102(9): 1508-1514.

Dunnivant, F.M., Schwarzenbach, R.P. and Macalady, D.L., 1992. Reduction of substituted nitrobenzenes in aqueous solutions containing natural organic matter. Environmental Science & Technology, 26(11): 2133-2141.

Dwarakanath, V., Kostarelos, K., Pope, G.A., Shotts, D. and Wade, W.H., 1999. Anionic surfactant remediation of soil columns contaminated by nonaqueous phase liquids. Journal of Contaminant Hydrology, 38(4): 465-488.

Elliott, D.W. and Zhang, W.X., 2001. Field assessment of nanoscale biometallic particles for groundwater treatment. Environmental Science & Technology, 35(24): 4922-4926.

Fathepure, B.Z. and Boyd, S.A., 1988. Dependence of tetrachlorethylene dechlorination on methanogenic susbtrate consumption by methanosarcina sp strain DCM. Applied and Environmental Microbiology, 54(12): 2976-2980.

Fauvarque, J., 1996. The chlorine industry. Pure and Applied Chemistry, 68(9): 1713-1720.

Feng, J., Zhu, B.W. and Lim, T.T., 2008. Reduction of chlorinated methanes with nano-scale Fe particles: effects of amphiphiles on the dechlorination reaction and two-parameter regression for kinetic prediction. Chemosphere, 73(11): 1817-1823.

Feng, X.H. and Pelton, R., 2007. Carboxymethyl cellulose: Polyvinylamine complex hydrogel swelling. Macromolecules, 40(5): 1624-1630.

Fillipi, B.R., Brant, L.W., Scamehorn, J.F. and Christian, S.D., 1999. Use of micellar-enhanced ultrafiltration at low surfactant concentrations and with anionic-nonionic surfactant mixtures. Journal of Colloid and Interface Science, 213(1): 68-80.

Forni, P., Prati, L. and Rossi, M., 1997. Catalytic dehydrohalogenation of polychlorinated biphenyls Part II: Studies on a continuous process. Applied Catalysis B: Environmental, 14(1-2): 49-53.

Fountain, J.C., Klimek, A., Beikirch, M.G. and Middleton, T.M., 1991. The use of surfactants for insitu extraction of organic pollutants from a contaminated aquifer. Journal of Hazardous Materials, 28(3): 295-311.

Franchi, A. and O'Melia, C.R., 2003. Effects of natural organic matter and solution chemistry on the deposition and reentrainment of colloids in porous media. Environmental Science & Technology, 37(6): 1122-1129.

Gantzer, C.J. and Wackett, L.P., 1991. Reductive dechlorination catalyzed by bacterial transition metal coenzymes. Environmental Science & Technology, 25(4): 715-722.

Gao, Y.Y., Ding, X.B., Zheng, Z.H., Xu, C. and Peng, Y.X., 2007. Template-free method to prepare polymer nanocapsules embedded with noble metal nanoparticles. Chemical Communications(36): 3720-3722.

Gardner, K. and Mayer, J., 1995. Understanding C-H bond oxidations: H. and H- transfer in the oxidation of toluene by permanganate. Science, 269(5232): 1849-1851.

Gates, D.D. and Siegrist, R.L., 1995. In-situ chemical oxidation of trichloroethylene using hydrogen peroxide. Journal of Environmental Engineering, 121(9): 639-644.

Gerritse, J. et al., 1999. Influence of different electron donors and accepters on dehalorespiration of tetrachloroethene by Desulfitobacterium frappieri TCE1. Applied and Environmental Microbiology, 65(12): 5212-5221.

Giasuddin, A.B.M., Kanel, S.R. and Choi, H., 2007. Adsorption of humic acid onto nanoscale zerovalent iron and its effect on arsenic removal. Environmental Science & Technology, 41(6): 2022-2027.

Gillham, R.W. and Ohannesin, S.F., 1994. Enhanced degradation of halogenated aliphatics by zero valent iron. Ground Water, 32(6): 958-967.

Glaze, W.H. and Kang, J.W., 1988. Advanced oxidation processes for treating groundwater contaminated with TCE and PCE-labratory studies. Journal American Water Works Association, 80(5): 57-63.

Gomez-Quero, S., Cardenas-Lizana, F. and Keane, M.A., 2008. Effect of metal dispersion on the liquid-phase hydrodechlorination of 2,4-dichlorophenol over Pd/Al_2O_3. Industrial & Engineering Chemistry Research, 47(18): 6841-6853.

Gomez-Sainero, L.M., Cortes, A., Seoane, X.L. and Arcoya, A., 2000. Hydrodechlorination of carbon tetrachloride to chloroform in the liquid phase with metal-supported catalysts: Effect of the catalyst components. Industrial & Engineering Chemistry Research, 39(8): 2849-2854.

Gonzalez, C.A. and de Correa, C.M., 2010. Catalytic hydrodechlorination of tetrachloroethylene over Pd/TiO_2 minimonoliths. Industrial & Engineering Chemistry Research, 49(2): 490-497.

Grass, M.E., Joo, S.H., Zhang, Y.W. and Somorjai, G.A., 2009. Colloidally synthesized monodisperse Rh nanoparticles supported on SBA-15 for size- and pretreatment-dependent studies of CO oxidation. Journal of Physical Chemistry C, 113(20): 8616-8623.

Grasso, D., Subramaniam, K., Pignatello, J.J., Yang, Y. and Ratte, D., 2001. Micellar desorption of polynuclear aromatic hydrocarbons from contaminated soil. Colloids and Surfaces A:Physicochemical and Engineering Aspects, 194(1-3): 65-74.

Hahn, M.W. and O'Melia, C.R., 2004. Deposition and reentrainment of Brownian particles in porous media under unfavorable chemical conditions: Some concepts and applications. Environmental Science & Technology, 38(1): 210-220.

Harvey, C.F., Haggerty, R. and Gorelick, S.M., 1994. Aquifer remediation: A method for estimating mass-transfer rate coefficients and an evaluation of pulsed pumping. Water Resources Research, 30(7): 1979-1991.

Hashimoto, Y., Uemichi, Y. and Ayame, A., 2005. Low-temperature hydrodechlorination mechanism of chlorobenzenes over platinum-supported and palladium-supported alumina catalysts. Applied Catalysis A: General, 287(1): 89-97.

Haston, Z.C. and McCarty, P.L., 1999. Chlorinated ethene half-velocity coefficients (Ks) for reductive dehalogenation. Environmental Science & Technology, 33(2): 223-226.

He, F., Liu, J., Roberts, C.B. and Zhao, D., 2009a. One-step "green" synthesis of Pd nanoparticles of controlled size and their catalytic activity for trichloroethene hydrodechlorination. Industrial & Engineering Chemistry Research, 48(14): 6550-6557.

He, F., Zhang, M., Qian, T.W. and Zhao, D.Y., 2009b. Transport of carboxymethyl cellulose stabilized iron nanoparticles in porous media: Column experiments and modeling. Journal of Colloid and Interface Science, 334(1): 96-102.

He, F. and Zhao, D., 2008. Hydrodechlorination of trichloroethene using stabilized Fe-Pd nanoparticles: Reaction mechanism and effects of stabilizers, catalysts and reaction conditions. Applied Catalysis B: Environmental, 84(3–4): 533-540.

He, F. and Zhao, D.Y., 2005. Preparation and characterization of a new class of starch-stabilized bimetallic nanoparticles for degradation of chlorinated hydrocarbons in water. Environmental Science & Technology, 39(9): 3314-3320.

He, F., Zhao, D.Y., Liu, J.C. and Roberts, C.B., 2007. Stabilization of Fe-Pd nanoparticles with sodium carboxymethyl cellulose for enhanced transport and dechlorination of trichloroethylene in soil and groundwater. Industrial & Engineering Chemistry Research, 46(1): 29-34.

He, F., Zhao, D.Y. and Paul, C., 2010. Field assessment of carboxymethyl cellulose stabilized iron nanoparticles for in situ destruction of chlorinated solvents in source zones. Water Research, 44(7): 2360-2370.

He, J.Z., Ritalahti, K.M., Yang, K.L., Koenigsberg, S.S. and Loffler, F.E., 2003. Detoxification of vinyl chloride to ethene coupled to growth of an anaerobic bacterium. Nature, 424(6944): 62-65.

Heck, K.N., Janesko, B.G., Scuseria, G.E., Halas, N.J. and Wong, M.S., 2008. Observing metal-catalyzed chemical reactions in situ using surface-enhanced raman spectroscopy on Pd-Au nanoshells. Journal of the American Chemical Society, 130(49): 16592-16600.

Heron, G., Carroll, S. and Sowers, H., 2000. Steam stripping/hydrous pyrolysis oxidation for in-situ remediation of a TCE DNAPL spill, In proceedings of the 2000 Battelle Conference on Chlorinated and Recalcitrant Compounds. Battelle Press, Monterey, CA, pp. 149-156.

Heron, G., Van Zutphen, M., Christensen, T.H. and Enfield, C.G., 1998. Soil heating for enhanced remediation of chlorinated solvents: A laboratory study on resistive

heating and vapor extraction in a silty, low-permeable soil contaminated with trichloroethylene. Environmental Science & Technology, 32(10): 1474-1481.

Higgins, M.R. and Olson, T.M., 2009. Life-cycle case study comparison of permeable reactive barrier versus pump-and-treat remediation. Environmental Science & Technology, 43(24): 9432-9438.

Hildebrand, H., Mackenzie, K. and Kopinke, F.D., 2009. Highly Active Pd-on-Magnetite Nanocatalysts for Aqueous Phase Hydrodechlorination Reactions. Environmental Science & Technology, 43(9): 3254-3259.

Holliger, C., Schraa, G., Stams, A.J.M. and Zehnder, A.J.B., 1993. A highly purified enrichment culture couples the reductive dechlorination of tetrachloroethene to growth. Applied and Environmental Microbiology, 59(9): 2991-2997.

Hong, Y.S., Honda, R.J., Myung, N.V. and Walker, S.L., 2009. Transport of iron-based nanoparticles: role of magnetic properties. Environmental Science & Technology, 43(23): 8834-8839.

Hrapovic, L., Sleep, B.E., Major, D.J. and Hood, E.D., 2005. Laboratory study of treatment of trichloroethene by chemical oxidation followed by bioremediation. Environmental Science & Technology, 39(8): 2888-2897.

Huang, K.C., Hoag, G.E., Chheda, P., Woody, B.A. and Dobbs, G.M., 2002. Chemical oxidation of trichloroethylene with potassium permanganate in a porous medium. Advances in Environmental Research, 7(1): 217-229.

Huang, W. et al., 2008. Dendrimer templated synthesis of one nanometer Rh and Pt particles supported on mesoporous silica: Catalytic activity for ethylene and pyrrole hydrogenation. Nano Letters, 8(7): 2027-2034.

Hunt, J.R., Sitar, N. and Udell, K.S., 1988. Nonaqueous phase liquid transport and cleanup 1. analysis of mechanism. Water Resources Research, 24(8): 1247-1258.

Ilinitch, O.M. et al., 2000. Catalytic reduction of nitrate and nitrite ions by hydrogen: investigation of the reaction mechanism over Pd and Pd-Cu catalysts. Journal of Molecular Catalysis A:Chemical, 158(1): 237-249.

Imlay, J., Chin, S. and Linn, S., 1988. Toxic DNA damage by hydrogen peroxide through the Fenton reaction in vivo and in vitro. Science, 240(4852): 640-642.

Interstate Technology and Regulatory Cooperation, 2001. Technical and regulatory guidance for in situ chemical oxidation of contaminated soil and groundwater, ITRC.

Jackson, R.E., 1998. The migration, dissolution, and fate of chlorinated solvents in the urbanized alluvial valleys of the southwestern USA. Hydrogeology Journal, 6(1): 144-155.

Jiang, J.K., Oberdorster, G. and Biswas, P., 2009. Characterization of size, surface charge, and agglomeration state of nanoparticle dispersions for toxicological studies. Journal of Nanoparticle Research, 11(1): 77-89.

Johnson, P.R., Sun, N. and Elimelech, M., 1996. Colloid transport in geochemically heterogeneous porous media: Modeling and measurements. Environmental Science & Technology, 30(11): 3284-3293.

Johnson, R.L., Johnson, G.O., Nurmi, J.T. and Tratnyek, P.G., 2009. Natural organic matter enhanced mobility of nano zerovalent iron. Environmental Science & Technology, 43(14): 5455-5460.

Joo, S.H., Al-Abed, S.R. and Luxton, T., 2009. Influence of carboxymethyl cellulose for the transport of titanium dioxide nanoparticles in clean silica and mineral-coated sands. Environmental Science & Technology, 43(13): 4954-4959.

Joo, S.H. and Zhao, D., 2008. Destruction of lindane and atrazine using stabilized iron nanoparticles under aerobic and anaerobic conditions: Effects of catalyst and stabilizer. Chemosphere, 70(3): 418-425.

Judai, K. et al., 2003. Acetylene polymerization on supported transition metal clusters. Journal of Molecular Catalysis A: Chemical, 199(1-2): 103-113.

Jujjuri, S., Ding, E., Hommel, E.L., Shore, S.G. and Keane, M.A., 2006. Synthesis and characterization of novel silica-supported Pd/Yb bimetallic catalysts: Application in gas-phase hydrodechlorination and hydrogenation. Journal of Catalysis, 239(2): 486-500.

Kanel, S.R., Goswami, R.R., Clement, T.P., Barnett, M.O. and Zhao, D., 2008. Two dimensional transport characteristics of surface stabilized zero-valent iron nanoparticles in porous media. Environmental Science & Technology, 42(3): 896-900.

Karapanagioti, H.K., Sabatini, D.A. and Bowman, R.S., 2005. Partitioning of hydrophobic organic chemicals (HOC) into anionic and cationic surfactant-modified sorbents. Water Research, 39(4): 699-709.

Keane, M.A., 2004. Hydrodehalogenation of haloarenes over silica supported Pd and Ni: A consideration of catalytic activity/selectivity and haloarene reactivity. Applied Catalysis A:General, 271(1-2): 109-118.

Kim, D.I. and Allen, D.T., 1997. Catalytic hydroprocessing of chlorinated olefins. Industrial & Engineering Chemistry Research, 36(8): 3019-3026.

Kim, H., Phenrat, T., Tilton, R.D. and Lowry, G.V., 2009. Fe^0 nanoparticles remain mobile in porous media after aging due to slow desorption of polymeric surface modifiers. Environmental Science & Technology, 43(10): 3824-3830.

Kim, H.N., Walker, S.L. and Bradford, S.A., 2010. Coupled factors influencing the transport and retention of Cryptosporidium parvum oocysts in saturated porous media. Water Research, 44(4): 1213-1223.

Kim, S.B., Park, S.J., Lee, C.G. and Kim, H.C., 2008. Transport and retention of Escherichia coli in a mixture of quartz, Al-coated and Fe-coated sands. Hydrological Processes, 22(18): 3856-3863.

Klausen, J. et al., 2003. Longevity of granular iron in groundwater treatment processes: Solution composition effects on reduction of organohalides and nitroaromatic compounds. Environmental Science & Technology, 37(6): 1208-1218.

Knauss, K.G., Copenhaver, S.C. and Aines, R.D., 2000. Hydrous pyrolysis/oxidation process for in situ destruction of chlorinated hydrocarbon and fuel hydrocarbon contaminants in water and soil. The Regents of the University of California, United States.

Knox, R.C. et al., 1997. Surfactant remediation field demonstration using a vertical circulation well. Ground Water, 35(6): 948-953.

Ko, C.H. and Elimelech, M., 2000. The "shadow effect" in colloid transport and deposition dynamics in granular porous media: Measurements and mechanisms. Environmental Science & Technology, 34(17): 3681-3689.

Ko, S.O., Schlautman, M.A. and Carraway, E.R., 1998. Partitioning of hydrophobic organic compounds to sorbed surfactants. 1. Experimental studies. Environmental Science & Technology, 32(18): 2769-2775.

Kong, L.Y., Li, G. and Wang, X.S., 2004. Kinetics and mechanism of liquid-phase oxidation of thiophene over TS-1 using H_2O_2 under mild conditions. Catalysis Letters, 92(3-4): 163-167.

Konradi, R. and Ruhe, J., 2005. Interaction of poly(methacrylic acid) brushes with metal ions: Swelling properties. Macromolecules, 38(10): 4345-4354.

Kretzschmar, R. and Sticher, H., 1997. Transport of humic-coated iron oxide colloids in a sandy soil: Influence of Ca^{2+} and trace metals. Environmental Science & Technology, 31(12): 3497-3504.

Kriegman-King, M.R. and Reinhard, M., 1994. Transformation of carbon tetrachloride by pyrite in aqueous solution. Environmental Science & Technology, 28(4): 692-700.

Kriegmanking, M.R. and Reinhard, M., 1992. Transformation of carbon tetrachloride in the presence of sulfide, biotite, and vermiculite. Environmental Science & Technology, 26(11): 2198-2206.

Krishnankutty, N. and Vannice, M.A., 1995. The effect of pretreatment on Pd/C catalysts. 1. adsorption and absorption properties. Journal of Catalysis, 155(2): 312-326.

Kuan, W.H., Lo, S.L., Wang, M.K. and Lin, C.F., 1998. Removal of Se(IV) and Se(VI) from water by aluminum-oxide-coated sand. Water Research, 32(3): 915-923.

Kulkarni, P.P., Deshmukh, S.S., Kovalchuk, V.I. and d'Itri, J.L., 1999. Hydrodechlorination of dichlorodifluoromethane on carbon-supported Group VIII noble metal catalysts. Catalysis Letters, 61(3-4): 161-166.

Lee, A.F., Carr, P. and Wilson, K., 2004. Direct Observation of Extremely Low Temperature Catalytic Dehydrochlorination of 1,1,1-Trichloroethane over Platinum. The Journal of Physical Chemistry B, 108(39): 14811-14814.

Lee, E.S., Seol, Y., Fang, Y.C. and Schwartz, F.W., 2003. Destruction efficiencies and dynamics of reaction fronts associated with the permanganate oxidation of trichloroethylene. Environmental Science & Technology, 37(11): 2540-2546.

Lee, I., Morales, R., Albiter, M.A. and Zaera, F., 2008. Synthesis of heterogeneous catalysts with well shaped platinum particles to control reaction selectivity. Proceedings of the National Academy of Sciences of the United States of America, 105(40): 15241-15246.

Lee, W. and Batchelor, B., 2002a. Abiotic reductive dechlorination of chlorinated ethylenes by iron-bearing soil minerals. 1. Pyrite and magnetite. Environmental Science & Technology, 36(23): 5147-5154.

Lee, W. and Batchelor, B., 2002b. Abiotic, reductive dechlorination of chlorinated ethylenes by iron-bearing soil minerals. 2. Green rust. Environmental Science & Technology, 36(24): 5348-5354.

Li, J.H., Zhou, B.X. and Cai, W.M., 2007. The solubility behavior of bisphenol A in the presence of surfactants. Journal of Chemical and Engineering Data, 52(6): 2511-2513.

Li, X.Q., Elliott, D.W. and Zhang, W.X., 2006a. Zero-valent iron nanoparticles for abatement of environmental pollutants: Materials and engineering aspects. Critical Reviews in Solid State and Materials Sciences, 31(4): 111-122.

Li, X.Q. and Johnson, W.P., 2005. Nonmonotonic variations in deposition rate coefficients of microspheres in porous media under unfavorable deposition conditions. Environmental Science & Technology, 39(6): 1658-1665.

Li, X.Q. and Zhang, W.X., 2007. Sequestration of metal cations with zerovalent iron nanoparticles - A study with high resolution X-ray photoelectron spectroscopy (HR-XPS). Journal of Physical Chemistry C, 111(19): 6939-6946.

Li, Y., Boone, E. and El-Sayed, M.A., 2002. Size effects of PVP-Pd nanoparticles on the catalytic Suzuki reactions in aqueous solution. Langmuir, 18(12): 4921-4925.

Li, Z.H., 2004. Surfactant-enhanced oxidation of trichloroethylene by permanganate - proof concept. Chemosphere, 54(3): 419-423.

Li, Z.H., Willms, C., Alley, J., Zhang, P.F. and Bowman, R.S., 2006b. A shift in pathway of iron-mediated perchloroethylene reduction in the presence of sorbed surfactant - A column study. Water Research, 40(20): 3811-3819.

Liang, C., Lee, I.L., Hsu, I.Y., Liang, C.P. and Lin, Y.L., 2008. Persulfate oxidation of trichloroethylene with and without iron activation in porous media. Chemosphere, 70(3): 426-435.

Liang, C.J., Wang, Z.S. and Bruell, C.J., 2007. Influence of pH on persulfate oxidation of TCE at ambient temperatures. Chemosphere, 66(1): 106-113.

Lien, H.L. and Zhang, W.X., 2005. Hydrodechlorination of chlorinated ethanes by nanoscale Pd/Fe bimetallic particles. Journal of Environmental Engineering, 131(1): 4-10.

Lin, Y.H., Tseng, H.H., Wey, M.Y. and Lin, M.D., 2010. Characteristics of two types of stabilized nano zero-valent iron and transport in porous media. Science of the Total Environment, 408(10): 2260-2267.

Liu, D.L., Johnson, P.R. and Elimelech, M., 1995. Colloid deposition dynamics in flow through porous media: Role of electrolyte concentration. Environmental Science & Technology, 29(12): 2963-2973.

Liu, J.C., He, F., Durham, E., Zhao, D.Y. and Roberts, C.B., 2008. Polysugar-stabilized Pd nanoparticles exhibiting high catalytic activities for hydrodechlorination of environmentally deleterious trichloroethylene. Langmuir, 24(1): 328-336.

Liu, Y. and Lowry, G.V., 2006. Effect of particle age (Fe^0 Content) and solution pH on NZVI reactivity: H_2 evolution and TCE dechlorination. Environmental Science & Technology, 40(19): 6085-6090.

Liu, Y., Phenrat, T. and Lowry, G.V., 2007. Effect of TCE concentration and dissolved groundwater solutes on nZVI-promoted TCE dechlorination and H_2 evolution. Environmental Science & Technology, 41(22): 7881-7887.

Liu, Y.Q., Majetich, S.A., Tilton, R.D., Sholl, D.S. and Lowry, G.V., 2005. TCE dechlorination rates, pathways, and efficiency of nanoscale iron particles with different properties. Environmental Science & Technology, 39(5): 1338-1345.

Liu, Z.B., Edwards, D.A. and Luthy, R.G., 1992. Sorption of non-ionic surfactants onto soils. Water Research, 26(10): 1337-1345.

Loraine, G.A., 2001. Effects of alcohols, anionic and nonionic surfactants on the reduction of PCE and TCE by zero-valent iron. Water Research, 35(6): 1453-1460.

Lowry, G.V. and Johnson, K.M., 2004. Congener-specific dechlorination of dissolved PCBs by microscale and nanoscale zerovalent iron in a water/methanol solution. Environmental Science & Technology, 38(19): 5208-5216.

Lowry, G.V. and Reinhard, M., 1999. Hydrodehalogenation of 1-to 3-carbon halogenated organic compounds in water using a palladium catalyst and hydrogen gas. Environmental Science & Technology, 33(11): 1905-1910.

Lowry, G.V. and Reinhard, M., 2000. Pd-catalyzed TCE dechlorination in groundwater: Solute effects, biological control, and oxidative catalyst regeneration. Environmental Science & Technology, 34(15): 3217-3223.

Lowry, G.V. and Reinhard, M., 2001. Pd-catalyzed TCE dechlorination in water: effect of $[H_2](aq)$ and H_2-utilizing competitive solutes on the TCE dechlorination rate and product distribution. Environmental Science & Technology, 35(4): 696-702.

Lyne, F.A. and McLachlan, T., 1949. Contamination of water by trichloroethylene. Analyst, 74(882): 513-513.

Ma, J. and Graham, N.J.D., 2000. Degradation of atrazine by manganese-catalysed ozonation - Influence of radical scavengers. Water Research, 34(15): 3822-3828.

Mackay, D.M. and Cherry, J.A., 1989. Groundwater contamination: pump-and-treat remediation. Environmental Science & Technology, 23(6): 630-636.

Mackay, D.M. et al., 2000. A controlled field evaluation of continuous vs. pulsed pump-and-treat remediation of a VOC-contaminated aquifer: site characterization, experimental setup, and overview of results. Journal of Contaminant Hydrology, 41(1-2): 81-131.

Mackenzie, K., Frenzel, H. and Kopinke, F.-D., 2006. Hydrodehalogenation of halogenated hydrocarbons in water with Pd catalysts: Reaction rates and surface competition. Applied Catalysis B: Environmental, 63(3–4): 161-167.

Magnuson, J.K., Stern, R.V., Gossett, J.M., Zinder, S.H. and Burris, D.R., 1998. Reductive dechlorination of tetrachloroethene to ethene by two-component enzyme pathway. Applied and Environmental Microbiology, 64(4): 1270-1275.

Major, D.W. et al., 2002. Field demonstration of successful bioaugmentation to achieve dechlorination of tetrachloroethene to ethene. Environmental Science & Technology, 36(23): 5106-5116.

Marques, C.A., Selva, M. and Tundo, P., 1993. Facile hydrodechlorination with hydrogen and Pd/C catalyst under multiphase conditions. Journal of Organic Chemistry, 58(19): 5256-5260.

Martin, J.E. et al., 2008. Determination of the oxide layer thickness in core-shell zerovalent iron nanoparticles. Langmuir, 24(8): 4329-4334.

Mata-Sandoval, J.C., Karns, J. and Torrents, A., 2002. Influence of rhamnolipids and Triton X-100 on the desorption of pesticides from soils. Environmental Science & Technology, 36(21): 4669-4675.

Matheson, L.J. and Tratnyek, P.G., 1994. Reductive dehalogenation of chlorinated methanes by iron metal. Environmental Science & Technology, 28(12): 2045-2053.

Mayer, P., Fernqvist, M.M., Christensen, P.S., Karlson, U. and Trapp, S., 2007. Enhanced diffusion of polycyclic aromatic hydrocarhons in artificial and natural aqueous solutions. Environmental Science & Technology, 41(17): 6148-6155.

Maymo-Gatell, X., Anguish, T. and Zinder, S.H., 1999. Reductive dechlorination of chlorinated ethenes and 1,2-dichloroethane by "Dehalococcoides ethenogenes" 195. Applied and Environmental Microbiology, 65(7): 3108-3113.

MaymoGatell, X., Chien, Y.T., Gossett, J.M. and Zinder, S.H., 1997. Isolation of a bacterium that reductively dechlorinates tetrachloroethene to ethene. Science, 276(5318): 1568-1571.

McCarty, P.L., 1997. Microbiology - Breathing with chlorinated solvents. Science, 276(5318): 1521-1522.

McNab, W.W., Ruiz, R. and Reinhard, M., 2000. In-situ destruction of chlorinated hydrocarbons in groundwater using catalytic reductive dehalogenation in a reactive well: Testing and operational experiences. Environmental Science & Technology, 34(1): 149-153.

Mecozzi, R., Di Palma, L. and Merli, C., 2006. Experimental in situ chemical peroxidation of atrazine in contaminated soil. Chemosphere, 62(9): 1481-1489.

Mei, Y., Lu, Y., Polzer, F., Ballauff, M. and Drechsler, M., 2007. Catalytic activity of palladium nanoparticles encapsulated in spherical polyelectrolyte brushes and core-shell microgels. Chemistry of Materials, 19(5): 1062-1069.

Mei, Y. et al., 2005. High catalytic activity of platinum nanoparticles immobilized on spherical polyelectrolyte brushes. Langmuir, 21(26): 12229-12234.

Mohammad, O.I. and Kibbey, T.C.G., 2005. Dissolution-induced contact angle modification in dense nonaqueous phase liquid/water systems. Environmental Science & Technology, 39(6): 1698-1706.

Moran, M.J., Zogorski, J.S. and Squillace, P.J., 2007. Chlorinated solvents in groundwater of the United States. Environmental Science & Technology, 41(1): 74-81.

Morrison, S.J., Metzler, D.R. and Carpenter, C.E., 2001. Uranium precipitation in a permeable reactive barrier by progressive irreversible dissolution of zerovalent iron. Environmental Science & Technology, 35(2): 385-390.

Muller, J.A. et al., 2004. Molecular identification of the catabolic vinyl chloride reductase from Dehalococcoides sp strain VS and its environmental distribution. Applied and Environmental Microbiology, 70(8): 4880-4888.

Munakata, N. and Reinhard, M., 2007. Palladium-catalyzed aqueous hydrodehalogenation in column reactors: Modeling of deactivation kinetics with sulfide and comparison of regenerants. Applied Catalysis B: Environmental, 75(1-2): 1-10.

Muroi, Y., Kurawaki, J., Hayakawa, K., Takisawa, N. and Miyajima, T., 2009. Fluorescence spectroscopy of fulvic acids' interaction with surfactants. Colloid & Polymer Science, 287(1).

Murphy, E.M., Zachara, J.M., Smith, S.C., Phillips, J.L. and Wietsma, T.W., 1994. Interaction of hydrophobic organic compounds with mineral-bound humic substance. Environmental Science & Technology, 28(7): 1291-1299.

Mylon, S.E., Chen, K.L. and Elimelech, M., 2004. Influence of natural organic matter and ionic composition on the kinetics and structure of hematite colloid aggregation: Implications to iron depletion in estuaries. Langmuir, 20(21): 9000-9006.

Nadagouda, M.N. and Varma, R.S., 2007. Synthesis of thermally stable carboxymethyl cellulose/metal biodegradable nanocomposites for potential biological applications. Biomacromolecules, 8(9): 2762-2767.

National Research Council, 1994. Alternatives for ground water cleanup. National Academy Press, Washington DC.

Neri, G., Musolino, M.G., Milone, C., Pietropaolo, D. and Galvagno, S., 2001. Particle size effect in the catalytic hydrogenation of 2,4-dinitrotoluene over Pd/C catalysts. Applied Catalysis A: General, 208(1-2): 307-316.

Newmark, R., Aines, R., Leif, R. and Knauss, K., 1999. Thermal cleanups using dynamic underground stripping and hydrous pyrolysis oxidation. UCRL-JC-134080, Lawrence Livermore National Lab.

Niven, R.K., 2006. Force stability of pore-scale fluid bridges and ganglia in axisymmetric and non-axisymmetric configurations. Journal of Petroleum Science and Engineering, 52(1-4): 1-18.

Nutt, M.O., Heck, K.N., Alvarez, P. and Wong, M.S., 2006. Improved Pd-on-Au bimetallic nanoparticle catalysts for aqueous-phase trichloroethene hydrodechlorination. Applied Catalysis B: Environmental, 69(1-2): 115-125.

Nutt, M.O., Hughes, J.B. and Wong, M.S., 2005. Designing Pd-on-Au bimetallic nanoparticle catalysts for trichloroethene hydrodechlorination. Environmental Science & Technology, 39(5): 1346-1353.

Nyer, E.K. and Morello, B., 1993. Trichloroethylene treatment and remediation. Ground Water Monitoring and Remediation, 13(2): 98-103.

Nørskov, J.K. et al., 2002. Universality in heterogeneous catalysis. Journal of Catalysis, 209(2): 275-278.

Ong, S.K. and Lion, L.W., 1991. Effects of soil properties and moisture on the sorption of trichloroethylene vapor. Water Research, 25(1): 29-36.

Ordonez, S., Sastre, H. and Dez, F.V., 2000. Hydrodechlorination of aliphatic organochlorinated compounds over commercial hydrogenation catalysts. Applied Catalysis B: Environmental, 25(1): 49-58.

Orth, W.S. and Gillham, R.W., 1995. Dechlorination of trichloroethene in aqueous solution Using Fe^0. Environmental Science & Technology, 30(1): 66-71.

Otto, W.H., Britten, D.J. and Larive, C.K., 2003. NMR diffusion analysis of surfactant-humic substance interactions. Journal of Colloid and Interface Science, 261(2): 508-513.

Ozdemir, O., Cinar, M., Sabah, E., Arslan, F. and Cefik, M.S., 2007. Adsorption of anionic surfactants onto sepiolite. Journal of Hazardous Materials, 147(1-2): 625-632.

Page, N.P. and Arthur, J.L., 1978. Special occupational hazard review of trichloroethylene. NIOSH publication No. 78-130. National Institute for Occupational Safety and Health, Rockville, MD.

Pal, T., Sau, T.K. and Jana, N.R., 1997. Reversible formation and dissolution of silver nanoparticles in aqueous surfactant media. Langmuir, 13(6): 1481-1485.

Park, S.K. and Bielefeldt, A.R., 2005. Non-ionic surfactant flushing of pentachlorophenol from NAPL-contaminated soil. Water Research, 39(7): 1388-1396.

Pavlostathis, S.G. and Mathavan, G.N., 1992. Desorption kinetics of selected volatile organic compounds from field contaminated soils. Environmental Science & Technology, 26(3): 532-538.

Pelley, A.J. and Tufenkji, N., 2008. Effect of particle size and natural organic matter on the migration of nano-and microscale latex particles in saturated porous media. Journal of Colloid and Interface Science, 321(1): 74-83.

Pennell, K.D., Jin, M.Q., Abriola, L.M. and Pope, G.A., 1994. Surfactant enhanced remediation of soil columns contaminated by residual tetrachloroethylene. Journal of Contaminant Hydrology, 16(1): 35-53.

Peyton, G.R., Huang, F.Y., Burleson, J.L. and Glaze, W.H., 1982. Destruction of pollutants in water with ozone in combination with ultraviolet radiation. 1. General principles and oxidation of tetrachloroethylene. Environmental Science & Technology, 16(8): 448-453.

Phenrat, T. et al., 2009. Particle size distribution, concentration, and magnetic attraction affect transport of polymer-modified Fe^0 nanoparticles in sand columns. Environmental science & technology, 43(13): 5079-5085.

Phenrat, T. et al., 2008. Stabilization of aqueous nanoscale zerovalent iron dispersions by anionic polyelectrolytes: adsorbed anionic polyelectrolyte layer properties and their effect on aggregation and sedimentation. Journal of Nanoparticle Research, 10(5): 795-814.

Phenrat, T., Saleh, N., Sirk, K., Tilton, R.D. and Lowry, G.V., 2007. Aggregation and sedimentation of aqueous nanoscale zerovalent iron dispersions. Environmental Science & Technology, 41(1): 284-290.

Pignatello, J.J. and Xing, B.S., 1996. Mechanisms of slow sorption of organic chemicals to natural particles. Environmental Science & Technology, 30(1): 1-11.

Ponder, S.M. et al., 2001. Surface chemistry and electrochemistry of supported zerovalent iron nanoparticles in the remediation of aqueous metal contaminants. Chemistry of Materials, 13(2): 479-486.

Ponder, S.M., Darab, J.G. and Mallouk, T.E., 2000. Remediation of Cr(VI) and Pb(II) aqueous solutions using supported, nanoscale zero-valent iron. Environmental Science & Technology, 34(12): 2564-2569.

Powell, R.M. et al., 1998. Permeable reactive barrier technologies for contaminant remediation,EPA/600/R-98/125, US EPA, Washington DC.

Prengle, H.W., 1983. Experimental rate constant and reactor considerations for the destruction of micropollutants and trihalomethane precursors by ozone with ultraviolet radiation. Environmental Science & Technology, 17(12): 743-747.

Quinn, J. et al., 2005. Field demonstration of DNAPL dehalogenation using emulsified zero-valent iron. Environmental Science & Technology, 39(5): 1309-1318.

Ravikumar, J.X. and Gurol, M.D., 1994. Chemical oxidation of chlorinated organics by hydrogen peroxide in the presence of sand. Environmental Science & Technology, 28(3): 394-400.

Redman, J.A., Walker, S.L. and Elimelech, M., 2004. Bacterial adhesion and transport in porous media: Role of the secondary energy minimum. Environmental Science & Technology, 38(6): 1777-1785.

Rodriguez-Cruz, M.S., Sanchez-Martin, M.J. and Sanchez-Camazano, M., 2005. A comparative study of adsorption of an anionic and a non-ionic surfactant by soils

based on physicochemical and mineralogical properties of soils. Chemosphere, 61(1): 56-64.

Roucoux, A., Schulz, J. and Patin, H., 2002. Reduced transition metal colloids: A novel family of reusable catalysts? Chemical Reviews, 102(10): 3757-3778.

Rupprechter, G. and Freund, H.J., 2001. Adsorbate-induced restructuring and pressure-dependent adsorption on metal nanoparticles studied by electron microscopy and sum frequency generation spectroscopy. Topics in Catalysis, 14(1-4): 3-14.

Ryan, J.N., Elimelech, M., Rebecca, A., Harvey, R.W. and Johnson, P.R., 1999. Bacteriophage PRD1 and silica colloid transport and recovery in an iron oxide-coated sand aquifer. Environmental science & technology, 33(1): 63-73.

Sahoo, D. and Smith, J.A., 1997. Enhanced trichloroethene desorption from long term contaminated soil using Triton X-100 and pH increases. Environmental Science & Technology, 31(7): 1910-1915.

Saleh, N. et al., 2008. Ionic strength and composition affect the mobility of surface-modified Fe^0 nanoparticles in water-saturated sand columns. Environmental Science & Technology, 42(9): 3349-3355.

Saleh, N. et al., 2007. Surface modifications enhance nanoiron transport and NAPL targeting in saturated porous media. Environmental Engineering Science, 24(1): 45-57.

Sanchez-Camazano, M., Sanchez-Martin, M.J. and Rodriguez-Cruz, M.S., 2000. Sodium dodecyl sulphate-enhanced desorption of atrazine: Effect of surfactant concentration and of organic matter content of soils. Chemosphere, 41(8): 1301-1305.

Sanford, W.E., Cook, P.G., Robinson, N.I. and Weatherill, D., 2006. Tracer mass recovery in fractured aquifers estimated from multiple well tests. Ground Water, 44(4): 564-573.

Sayles, G.D., You, G.R., Wang, M.X. and Kupferle, M.J., 1997. DDT, DDD, and DDE dechlorination by zero-valent iron. Environmental Science & Technology, 31(12): 3448-3454.

Schaerlaekens, J., Vanderborght, J., Merckx, R. and Feyen, J., 2000. Surfactant enhanced solubilization of residual trichloroethene: An experimental and numerical analysis. Journal of Contaminant Hydrology, 46(1-2): 1-16.

Scherer, M.M., Richter, S., Valentine, R.L. and Alvarez, P.J.J., 2000. Chemistry and microbiology of permeable reactive barriers for in situ groundwater clean up. Critical Reviews in Microbiology, 26(4): 221-264.

Schlautman, M.A. and Morgan, J.J., 1994. Adsorption of aquatic humic substances on colloidal-size aluminum oxide particles: Influence of solution chemistry. Geochimica Et Cosmochimica Acta, 58(20): 4293-4303.

Schmelz, M.J., Nakagawa, I., Mizushima, S.-I. and Quagliano, J.V., 1959. Infrared absorption spectra of inorganic coördination complexes. XVIII. infrared studies of malonato metal complexes. Journal of the American Chemical Society, 81(2): 287-290.

Schreier, C.G. and Reinhard, M., 1994. Transformation of chlorinated organic compounds by iron and manganese powders in buffered water and in landfill leachate. Chemosphere, 29(8): 1743-1753.

Schreier, C.G. and Reinhard, M., 1995. Catalytic hydrodehalogenation of chlorinated ethylenes using palladium and hydrogen for the treatment of contaminated water. Chemosphere, 31(6): 3475-3487.

Schrick, B., Blough, J.L., Jones, A.D. and Mallouk, T.E., 2002. Hydrodechlorination of trichloroethylene to hydrocarbons using bimetallic nickel-iron nanoparticles. Chemistry of Materials, 14(12): 5140-5147.

Schrick, B., Hydutsky, B.W., Blough, J.L. and Mallouk, T.E., 2004. Delivery vehicles for zerovalent metal nanoparticles in soil and groundwater. Chemistry of Materials, 16(11): 2187-2193.

Schuth, C., Kummer, N.A., Weidenthaler, C. and Schad, H., 2004. Field application of a tailored catalyst for hydrodechlorinating chlorinated hydrocarbon contaminants in groundwater. Applied Catalysis B: Environmental, 52(3): 197-203.

Schuth, C. and Reinhard, M., 1998. Hydrodechlorination and hydrogenation of aromatic compounds over palladium on alumina in hydrogen-saturated water. Applied Catalysis B: Environmental, 18(3-4): 215-221.

Scott, R.W.J., Wilson, O.M. and Crooks, R.M., 2004. Titania-supported Au and Pd composites synthesized from dendrimer-encapsulated metal nanoparticle precursors. Chemistry of Materials, 16(26): 5682-5688.

Shen, C.Y., Li, B.G., Huang, Y.F. and Jin, Y., 2007a. Kinetics of coupled primary- and secondary-minimum deposition of colloids under unfavorable chemical conditions. Environmental Science & Technology, 41(20): 6976-6982.

Shen, X.Y. et al., 2007b. Effects of mixed surfactants on the volatilization of naphthalene from aqueous solutions. Journal of Hazardous Materials, 140(1-2): 187-193.

Shin, M.C., Choi, H.D., Kim, D.H. and Baek, K., 2008. Effect of surfactant on reductive dechlorination of trichloroethylene by zero-valent iron. Desalination, 223(1-3): 299-307.

Shokes, T.E. and Moller, G., 1999. Removal of dissolved heavy metals from acid rock drainage using iron metal. Environmental Science & Technology, 33(2): 282-287.

Signori, A.M. et al., 2010. Formation of catalytic silver nanoparticles supported on branched polyethyleneimine derivatives. Langmuir, 26(22): 17772-17779.

Sirk, K.M. et al., 2009. Effect of adsorbed polyelectrolytes on nanoscale zero valent iron particle attachment to soil surface models. Environmental Science & Technology, 43(10): 3803-3808.

Sorouradin, M.H., Hiraide, M., Kim, Y.S. and Kawaguchi, H., 1993. Quantitative desorption of humic substances from amberlite XAD resins with an alkaline solution of sodium dodecyl sulfate. Analytica Chimica Acta, 281(1): 191-195.

Squillace, P.J., Moran, M.J. and Price, C.V., 2004. VOCs in shallow groundwater in new residential/commercial areas of the United States. Environmental Science & Technology, 38(20): 5327-5338.

Sriwatanapongse, W., Reinhard, M. and Klug, C.A., 2006. Reductive hydrodechlorination of trichloroethylene by palladium-on-alumina catalyst: ^{13}C solid-state NMR study of surface reaction precursors. Langmuir, 22(9): 4158-4164.

Stellner, K.L. and Scamehorn, J.F., 1989. Hardness tolerance of anionic surfactant solutions 2. Effect of added nonionic surfactant. Langmuir, 5(1): 77-84.

Su, C.M. and Puls, R.W., 2001. Arsenate and arsenite removal by zerovalent iron: Kinetics, redox transformation, and implications for in situ groundwater remediation. Environmental Science & Technology, 35(7): 1487-1492.

Su, C.M. and Puls, R.W., 2004. Nitrate reduction by zerovalent iron: Effects of formate, oxalate, citrate, chloride, sulfate, borate, and phosphate. Environmental Science & Technology, 38(9): 2715-2720.

Sun, L. and Crooks, R.M., 2002. Dendrimer-mediated immobilization of catalytic nanoparticles on flat, solid supports. Langmuir, 18(21): 8231-8236.

Sunder, M. and Hempel, D.C., 1997. Oxidation of tri- and perchloroethene in aqueous solution with ozone and hydrogen peroxide in a tube reactor. Water Research, 31(1): 33-40.

Tan, Y., Gannon, J., Baveye, P. and Alexander, M., 1994. Transport of bacteria in an aquifer sand: Experiments and model simulations. Water resources research, 30(12): 3243-3252.

Thompson, C.D., Rioux, R.M., Chen, N. and Ribeiro, F.H., 1999. Turnover rate, reaction order, and elementary steps for the hydrodechlorination of chlorofluorocarbon compounds on palladium catalysts. The Journal of Physical Chemistry B, 104(14): 3067-3077.

Tong, M., Camesano, T.A. and Johnson, W.P., 2005. Spatial variation in deposition rate coefficients of an adhesion-deficient bacterial strain in quartz sand. Environmental Science & Technology, 39(10): 3679-3687.

Townsend, G.T. and Suflita, J.M., 1996. Characterization of chloroethylene dehalogenation by cell extracts of Desulfomonile tiedjei and its relationship to

chlorobenzoate dehalogenation. Applied and Environmental Microbiology, 62(8): 2850-2853.

Tratnyek, P.G., Scherer, M.M., Deng, B. and Hu, S., 2001. Effects of Natural Organic Matter, Anthropogenic Surfactants, and Model Quinones on the Reduction of Contaminants by Zero-Valent Iron. Water Research, 35(18): 4435-4443.

Travis, C.C. and Doty, C.B., 1990. Can contaminated aquifers at superfund sites by remediated? Environmental Science & Technology, 24(10): 1464-1466.

Tufenkji, N. and Elimelech, M., 2004. Deviation from the classical colloid filtration theory in the presence of repulsive DLVO interactions. Langmuir, 20(25): 10818-10828.

U.S. EPA, 1997. Permeable reactive subsurface barriers for the interception and remediation of chlorinated hydrocarbon and Chromium(VI) plumes in ground water. EPA/600/F-97/008, Ada, OK.

U.S. EPA, 2004. In situ thermal treatment of chlorinated solvents: fundamentals and field applications. EPA/542/R-04/010, Washington, DC.

U.S. EPA, 2008. Toxics Release Inventory (TRI) Basic Data, http://www.epa.gov/tri/tridata/current_data/index.html.

U.S. EPA, 2009. 2009 edition of the drinking water standards and health advisories. EPA/822/R-09/011, Washington, DC.

Vaarkamp, M., Miller, J.T., Modica, F.S., Lane, G.S. and Koningsberger, D.C., 1993. The relation between catalytic and electronic properties of supported platinum catalysts: The local density of states as determined by X-ray absorption spectroscopy. Studies in Surface Science and Catalysis, 75: 809-820.

van Aken, G.A., 2003. Competitive adsorption of protein and surfactants in highly concentrated emulsions: Effect on coalescence mechanisms. Colloids and Surfaces A: Physicochemical and Engineering Aspects, 213(2-3): 209-219.

van Ginkel, C.G., Plugge, C.M. and Stroo, C.A., 1995. Reduction of chlorate with various energy substrates and inocula under anaerobic conditions. Chemosphere, 31(9): 4057-4066.

Voudrias, E.A., 2001. Pump and treat remediation of groundwater contaminated by hazardous waste: Can it really be achieved? Global Network for Environmental Science and Technology, 3(1): 1-10.

Waldemer, R.H., Tratnyek, P.G., Johnson, R.L. and Nurmi, J.T., 2007. Oxidation of chlorinated ethenes by heat-activated persulfate: Kinetics and products. Environmental Science & Technology, 41(3): 1010-1015.

Wang, C.B. and Zhang, W.X., 1997. Synthesizing nanoscale iron particles for rapid and complete dechlorination of TCE and PCBs. Environmental Science & Technology, 31(7): 2154-2156.

Wang, J. and Somasundaran, P., 2005. Adsorption and conformation of carboxymethyl cellulose at solid–liquid interfaces using spectroscopic, AFM and allied techniques. Journal of Colloid and Interface Science, 291(1): 75-83.

Wang, Y. et al., 2008. Transport and retention of nanoscale C_{60} aggregates in water-saturated porous media. Environmental science & technology, 42(10): 3588-3594.

Watts, R.J., Udell, M.D., Rauch, P.A. and Leung, S.W., 1990. Treatment of pentachlorophenol-contaminated soils using Fentons reagent. Hazardous Waste & Hazardous Materials, 7(4): 335-345.

Wei, Y.T. et al., 2010. Influence of nanoscale zero-valent iron on geochemical properties of groundwater and vinyl chloride degradation: A field case study. Water Research, 44(1): 131-140.

Weiss, A.H., Gambhir, B.S. and Leon, R.B., 1971. Hydrodechlorination of carbon tetrachloride. Journal of Catalysis, 22(2): 245-254.

West, C.C. and Harwell, J.H., 1992. Surfactants and subsurface remediation. Environmental Science & Technology, 26(12): 2324-2330.

Williams, R.E., 1968. Flow of ground water adjacent to small closed basins in glacial till. Water Resources Research, 4(4): 777-&.

Wolfe, N.L. and Macalady, D.L., 1992. New perspectives in aquatic redox chemistry : abiotic transformations of pollutants in groundwater and sediments. Journal of Contaminant Hydrology, 9(1-2): 17-34.

Wu, C. and Schaum, J., 2000. Exposure assessment of trichloroethylene. Environmental Health Perspectives, 108: 359-363.

Wunder, S., Lu, Y., Albrecht, M. and Ballauff, M., 2011. Catalytic activity of faceted gold nanoparticles studied by a model reaction: Evidence for substrate-induced surface restructuring. ACS Catalysis, 1(8): 908-916.

Wunder, S., Polzer, F., Lu, Y., Mei, Y. and Ballauff, M., 2010. Kinetic analysis of catalytic reduction of 4-nitrophenol by metallic nanoparticles immobilized in spherical polyelectrolyte brushes. Journal of Physical Chemistry C, 114(19): 8814-8820.

Xu, Y. and Axe, L., 2005. Synthesis and characterization of iron oxide-coated silica and its effect on metal adsorption. Journal of Colloid and Interface Science, 282(1): 11-19.

Yan, Y.E. and Schwartz, F.W., 1999. Oxidative degradation and kinetics of chlorinated ethylenes by potassium permanganate. Journal of Contaminant Hydrology, 37(3-4): 343-365.

Yan, Y.E. and Schwartz, F.W., 2000. Kinetics and mechanisms for TCE oxidation by permanganate. Environmental Science & Technology, 34(12): 2535-2541.

Yang, K., Zhu, L.Z. and Xing, B.S., 2006. Enhanced soil washing of phenanthrene by mixed solutions of TX100 and SDBS. Environmental Science & Technology, 40(13): 4274-4280.

Yang, M.X., Sarkar, S., Bent, B.E., Bare, S.R. and Holbrook, M.T., 1997. Degradation of multiply-chlorinated hydrocarbons on Cu(100). Langmuir, 13(2): 229-242.

Yeh, C.K.J., Wu, H.M. and Chen, T.C., 2003. Chemical oxidation of chlorinated non-aqueous phase liquid by hydrogen peroxide in natural sand systems. Journal of Hazardous Materials, 96(1): 29-51.

Yeom, I.T., Ghosh, M.M., Cox, C.D. and Robinson, K.G., 1995. Micellar solubilization of polynuclear aromatic hydrocarbons in coal tar-contaminated soils. Environmental Science & Technology, 29(12): 3015-3021.

Yuan, S.H., Shu, Z., Wan, J.Z. and Lu, X.H., 2007. Enhanced desorption of hexachlorobenzene from kaolin by single and mixed surfactants. Journal of Colloid and Interface Science, 314(1): 167-175.

Zhan, J.J. et al., 2009. Multifunctional colloidal particles for in situ remediation of chlorinated hydrocarbons. Environmental Science & Technology, 43(22): 8616-8621.

Zhan, J.J. et al., 2008. Transport characteristics of nanoscale functional zerovalent iron/silica composites for in situ remediation of trichloroethylene. Environmental Science & Technology, 42(23): 8871-8876.

Zhang, C.L., Zheng, G. and Nichols, C.M., 2006. Micellar partitioning and its effects on Henry's law constants of chlorinated solvents in anionic and nonionic surfactant solutions. Environmental Science & Technology, 40(1): 208-214.

Zhang, M., He, F., Zhao, D.Y. and Hao, X.D., 2011. Degradation of soil-sorbed trichloroethylene by stabilized zero valent iron nanoparticles: Effects of sorption, surfactants, and natural organic matter. Water Research, 45(7): 2401-2414.

Zhao, B.W., Zhu, L.Z. and Yang, K., 2006. Solubilization of DNAPLs by mixed surfactant: Reduction in partitioning losses of nonionic surfactant. Chemosphere, 62(5): 772-779.

Zhao, D., Pignatello, J.J., White, J.C., Braida, W. and Ferrandino, F., 2001. Dual-mode modeling of competitive and concentration-dependent sorption and desorption kinetics of polycyclic aromatic hydrocarbons in soils. Water Resources Research, 37(8): 2205-2212.

Zheng, L.Q. et al., 2011. Catalytic hydrogenation of graphene films. Chemical Communications, 47(4): 1213-1215.

Zhou, X.C., Xu, W.L., Liu, G.K., Panda, D. and Chen, P., 2010. Size-dependent catalytic activity and dynamics of gold nanoparticles at the single-molecule level. Journal of the American Chemical Society, 132(1): 138-146.

Zhu, B.W., Lim, T.T. and Feng, J., 2008. Influences of amphiphiles on dechlorination of a trichlorobenzene by nanoscale Pd/Fe: Adsorption, reaction kinetics, and interfacial interactions. Environmental Science & Technology, 42(12): 4513-4519.

Zhuang, J. and Jin, Y., 2008. Interactions between viruses and goethite during saturated flow: Effects of solution pH, carbonate, and phosphate. Journal of Contaminant Hydrology, 98(1-2): 15-21.